

Attitude Transfer Assembly Design for MAGSAT

P.W. Collyer , N. P. Freund

**Barnes Engineering Company
30 Commerce Rd.
Stamford, Ct. 06904**

**October 1976
Final Technical Report**

Prepared for

**GODDARD SPACE FLIGHT CENTER
Greenbelt, Maryland 20771**



TECHNICAL REPORT STANDARD TITLE PAGE

1. Report No.		2. Government Accession No.		3. Recipient's Catalog No.	
4. Title and Subtitle ATTITUDE TRANSFER ASSEMBLY DESIGN FOR MAGSAT				5. Report Date 15 October 1976	
				6. Performing Organization Code 00430	
7. Author(s) P. W. Collyer, N. P. Freund				8. Performing Organization Report No. 2081 TR-001	
9. Performing Organization Name and Address Barnes Engineering Company 30 Commerce Road Stamford, Connecticut 06904				10. Work Unit No.	
				11. Contract or Grant No. NAS5-23598	
12. Sponsoring Agency Name and Address NASA/GSFC Greenbelt, Maryland 20771 Technical Officer: Mr. H. P. Scherer				13. Type of Report and Period Covered Final Technical Report June '76 to Sept. '76	
				14. Sponsoring Agency Code	
15. Supplementary Notes					
16. Abstract <p>A description is given of a design for an instrument system that will monitor the orientation of a boom-mounted vector magnetometer relative to the main spacecraft body. The attitude of the magnetometer is measured with respect to X and Z axes lateral to the boom length and also a twist axis around the boom center line. These measurements are made in a non-contact optical approach employing a three-axis autocollimator system mounted on the main body of the spacecraft with only passive elements (reflectors) located at the end of the 20-foot boom.</p> <p>In addition to a full discussion of the technical problem, the technical approach taken and design description, a discussion and analysis of system errors, cross coupling and system alignment to the spacecraft are included. A separate section is included discussing several tradeoffs and their effect on accuracy and other parameters.</p> <p align="right">(Continued)</p>					
17. Key Words (Selected by Author(s)) Autocollimator Twist Sensing Autocollimator Optical Alignment Instrument				18. Distribution Statement Unclassified and Unlimited	
19. Security Classif. (of this report) Unclassified		20. Security Classif. (of this page) Unclassified		21. No. of Pages 255	
				22. Price*	

Abstract (Continued)

Reliability calculations have shown that this system will have an MTBF of 11.75 years (mission life is anticipated to be 8 months), with a probability of success in excess of 94%.

Residual errors are calculated to be 0.3 arc-seconds in Y and Z axes, and 2.7 arc-seconds in twist, 1σ . These values can be further reduced through additional pre-flight calibration.

FOREWORD

This report describes the work performed under NASA Contract NAS5-23598 entitled Design Study of an Attitude Transfer Assembly for MAGSAT. The NASA Technical Officer is

Mr. H. Paul Scherer

Code 712 Room 116

Building 22

The contractor is Barnes Engineering Company, Stamford, Connecticut.

This report is submitted October 15, 1976 and covers the work performed from June 11, 1976 to September 15, 1976.

This document is Item of Article XV of the subject contract.

Significant contributions have been made by the following staff members in addition to the authors:

Robert F. Grudee:	Senior Mechanical Engineer Mechanical Design & Analysis
-------------------	---

Frank C. Demarest:	Electronics Engineer Electronic Design & Analysis
--------------------	---

Joseph A. Cianci:	Reliability Engineer Reliability Analysis
-------------------	--

TABLE OF CONTENTS

Page No.

FOREWORD

SUMMARY

1.0	INTRODUCTION	1 - 1
2.0	THEORY OF OPERATION	2 - 1
2.1	STATEMENT OF TECHNICAL PROBLEM	2 - 1
2.1.1	System Design Approach	2 - 2
2.2	MEASURING MODES	2 - 3
2.2.1	Y-Z Measuring System	2 - 3
2.2.2	X-axis Measuring System	2 - 7
2.3	SEARCH MODE	2 - 11
2.4	AUTOMATIC GAIN CONTROL	2 - 15
2.5	SYSTEM OUTPUTS	2 - 17
2.5.1	Analog Outputs	2 - 17
2.5.2	Digital Output	2 - 17
3.1	OPTICAL SYSTEM	3 - 1
3.1.1	Optical Head	3 - 1
3.1.1.1	Light Source	3 - 3
3.1.1.1.1	Calculation of Radiance	3 - 3
3.1.1.2	Detectors	3 - 4
3.1.1.2.1	Signal Amplitude	3 - 5
3.1.1.3	Objective Lens	3 - 9
3.1.1.3.1	Open Loop Linear Range	3 - 11
3.1.1.4	Vignetting	3 - 12
3.1.1.5	Micrometer Plate	3 - 15
3.1.2	Beam Deviation Wedges	3 - 16
3.1.2.1	Calculation of Wedge Apex Angle	3 - 19
3.1.2.2	Optical Wedge Specification	3 - 20
3.1.3	Reflectors	3 - 22
3.1.3.1	Remote Reflector Assembly	3 - 22
3.1.3.2	Calculation of Required Reflector Size	3 - 24
3.1.3.2.1	Y-Z System (Plane Mirror)	3 - 24
3.1.3.2.2	X System (Porro Reflectors)	3 - 25
3.1.3.2.2.1	Boom End or Twist Sensing Porro Reflector	3 - 25
3.1.3.2.2.2	Base Line Porro Reflector	3 - 26
3.1.3.3	Required Flatness of Reflectors	3 - 26
3.2	MECHANICAL SYSTEM	3 - 29
3.2.1	Autocollimator Assembly	3 - 30
3.2.1.1	Material Selection	3 - 30
3.2.1.2	Mounting of Optical Elements	3 - 33
3.2.1.3	Thermal/Vibration Characteristics	3 - 35
3.2.2	Deflection Wedge Assemblies	3 - 36
3.2.2.1	Structural Arrangements	3 - 36

TABLE OF CONTENTS
(Continued)

	<u>Page No.</u>
3.2.2.2 Mechanical Packaging	3 - 36
3.2.2.3 Encoder Mounting	3 - 37
3.2.2.4 Servo Drive	3 - 37
3.2.2.4.1 Motor	3 - 37
3.2.2.4.2 Gear Train	3 - 38
3.2.2.4.3 Bearings and Lubrication	3 - 40
3.2.2.5 Servo Performance	3 - 40
3.2.2.4.1 Gearing Reduction Ratio Optimization	3 - 40
3.2.2.5.2 Gear Train Accuracy and Backlash	3 - 42
3.3 ELECTRONICS	3 - 43
3.3.1 Electronics System Description	3 - 43
3.3.1.1 Power Consumption	3 - 43
3.3.1.2 Signal to Noise Calculations	3 - 45
3.3.1.2.1 Signal	3 - 45
3.3.1.2.2 Noise	3 - 45
3.3.1.2.3 Signal to Noise	3 - 47
3.3.1.3 AGC Loop Accuracy	3 - 47
3.3.2 Inputs and Outputs	3 - 48
3.3.2.1 Digital Outputs	3 - 49
3.3.2.2 Digital Inputs	3 - 51
3.3.2.3 Analog Outputs	3 - 51
3.3.3 Circuit Description	3 - 52
3.3.3.1 Preamplifier	3 - 53
3.3.3.2 Post Amplifiers	3 - 53
3.3.3.3 Synchronous Demodulator	3 - 53
3.3.3.4 Low Pass Filter	3 - 54
3.3.3.5 Sample and Hold	3 - 54
3.3.3.6 Comparators	3 - 54
3.3.3.7 Voltage Reference	3 - 55
3.3.3.8 Error Amplifier	3 - 55
3.3.3.9 Acquisition Detector	3 - 55
3.3.3.10 LED Driver	3 - 55
3.3.3.11 Digital Phase Shifter	3 - 56
3.3.3.12 Clock Generator	3 - 57
3.3.3.13 Encoders	3 - 57
3.3.3.14 Encoder Logic	3 - 58
3.3.3.15 Encoder Counters	3 - 59
3.3.3.16 Data Shift Registers	3 - 59
3.3.3.17 Spacecraft Data Interface	3 - 59
3.3.3.18 Motor Control Operation	3 - 60
3.3.3.19 State and Motor Sequencer	3 - 61

TABLE OF CONTENTS (Continued)

		<u>Page No.</u>
3.3.3.20	Mode Selector	3 - 61
3.3.3.21	Condition Latches	3 - 62
3.3.3.22	Logic Array	3 - 62
3.3.3.23	Motor Drive	3 - 62
3.3.3.24	Motors	3 - 62
3.3.3.25	Spacecraft Command Interface	3 - 63
3.3.3.26	Power Supply	3 - 63
3.4	WEIGHT AND POWER SUMMARY	3 - 64
4.0	TRADEOFF STUDIES	4 - 1
4.1	GIMBALLED BOOM MOUNT	4 - 1
4.2	SINGLE ENCODER IN Y AND Z AXES	4 - 4
5.0	RELIABILITY CONSIDERATIONS	5 - 1
6.0	SYSTEM ERROR ANALYSIS	6 - 1
6.1	CALIBRATED ACCURACY	6 - 8
6.2	RESOLUTION (NOISE EQUIVALENT ANGLE)	6 - 9
6.3	STABILITY OVER 5 MINUTES (TIME)	6 - 9
6.4	STABILITY THROUGH ENVIRONMENT	6 - 9
7.0	CROSS-COUPLING	7 - 1
7.1	MATHEMATICAL ANALYSIS	7 - 1
7.1.1	Y-Z System	7 - 1
7.1.2	X-Measuring System	7 - 8
8.0	SYSTEM ALIGNMENT	8 - 1
9.0	DISCUSSION AND CONCLUSIONS	9 - 1
APPENDIX A	PERFORMANCE REQUIREMENTS	
APPENDIX B	SYSTEM PARAMETERS	
APPENDIX C	LED DATA SHEET	
APPENDIX D	SCD FOR SILICON PLANAR DIFFUSED PHOTO DETECTOR	
APPENDIX E	PRELIMINARY GEAR TRAIN BACKLASH ANALYSIS	
APPENDIX F	ELECTRONIC SCHEMATICS	
APPENDIX G	RELIABILITY CONSIDERATIONS	

TABLES

		<u>After Page</u>
3.1	OPTICAL SYSTEM DATA SHEET	3 - 1
3.2	RADIOMETRIC SYSTEM PARAMETERS	3 - 9
6.1	ERROR BUDGET FOR THE ATTITUDE TRANSFER ASSEMBLY	6 - 8
9.1	ACHIEVED DESIGN VALUES VERSUS REQUIREMENTS	9 - 1

ILLUSTRATIONS

<u>Figure #</u>		<u>After Page</u>
2.1	Measuring System Arrangement	2 - 2
2.2A	The Null Condition }	
2.2B	Image Translation }	
2.2C	Linear Range }	2 - 4
2.2D	Acquisition Range }	
2.3A	Image Dimension & Detector Spacing }	
2.3B	Open-Loop Transfer Function }	2 - 5
2.4	Effects of Z-Axis Rotation In X-Axis System	2 - 9
2.5	X-Axis Image Formation	2 - 10
2.6	Erection Bias Deviation Mode	2 - 12
2.7	Circular Bending Deviation Mode	2 - 14
2.8	Worst Case Search Mode	2 - 14
2.9A	Detector Array in Y-Z Autocollimator }	
2.9B	Image Motion Resulting from Search Mode }	2 - 15
3.1A	Attitude Transfer Assembly Optical System Y-Z Channel	3 - 1
3.1B	Attitude Transfer Assembly Optical System X (Twist Sensing) Channel	3 - 1
3.2	Optical Schematic Autocollimator for MAGSAT	3 - 1
3.3	Error Detector Configuration	3 - 5
3.4	Spot Diagram	3 - 10
3.5	Spot Diagram - Best Focus	3 - 10
3.6	Knife Edge Plot - X Axis	3 - 11
3.7	Knife Edge Plot - Y Axis	3 - 11
3.8	Normalizing Vignetting Function for Autocollimator with Circular Aperture	3 - 14
3.9	Rotation & Deviation of Optical Wedges in the YZ Channel	3 - 19
3.10A	Deviation Wedge Drawing	3 - 21
3.10B, C	Measuring Ring for Wedges	3 - 21
3.11A	Remote Reflector Assembly	3 - 23

ILLUSTRATIONS
(Continued)

<u>Figure #</u>		<u>After Page</u>
3.11B	Base-Line Porro Reflector	3 - 23
3.12	Attitude Transfer Assembly: Autocollimator and Deflection Wedge Unit	3 - 30
3.13	MAGSAT Attitude Transfer Assembly Optical Head	3 - 30
3.14	MAGSAT Attitude Transfer Assembly: Deflection Wedge Assembly	3 - 36
3.15	Wedge Drive Unit	3 - 36
3.16	Deviation Wedges Gear Schematic	3 - 38
3.17	Block Diagram Power Supply and X Analog Signal Processing	3 - 43
3.18	Y & Z Analog Signal Processing Block Diagram	3 - 43
3.19	Encoder Digital Processing Block Diagram	3 - 43
3.20	Block Diagram - Motor Control and Digital Signal Processing	3 - 43
3.21	Electronic System Values	3 - 45
3.22	AGC Loop	3 - 47
3.23	Incremental Encoder Logic	3 - 58
3.24	State Diagram Overall Operation	3 - 60
3.25	State Diagram Mode 0	3 - 60
3.26	State Diagram Mode 1	3 - 60
3.27	State Diagram Mode 2	3 - 60
3.28	State Diagram Mode 3	3 - 60
4.1	Circular Bending with Resotation by Gimbal Rotation	4 - 2
7.1	Rotation About X Y' and Z''	7 - 2

SUMMARY

This report is the Final Report on the design study for an Attitude Transfer Assembly (ATA) for use with the MAGSAT magnetometer experiment. The Attitude Transfer Assembly has the function of measuring in essentially real time the variation in attitude of the magnetometer assembly, which is specified to be mounted at the outboard end of the SAS spacecraft.

Uncertainty in attitude of the magnetometer may result from two principal modes of departure from the nominal attitude. One results from the process of erection of the boom after reaching orbital altitude. The second is the cyclical bending of the boom due to unbalanced solar radiation which varies continuously through the orbital path.

A machined surface on the spacecraft approximately 30 x 12 inches will be used for mounting the inboard components of the ATA. This surface will serve as a reference surface for definition of the three orthogonal measuring axes; it also serves as a heat-sink controlled to $\pm 2^{\circ}\text{C}$.

The complement of equipment used for measuring angular deflections of the outer end of the boom includes one dual-axis autocollimator assembly aligned parallel to the nominal boom axis and responding to reflection of its projected beam from a 2.5-inch square mirror at the outer end of the boom. This sub-system measures angular deflections normal to the boom axis. Measurement accuracy and range are enhanced by the use of a servo-driven optical wedge assembly which keeps the projected beam normal to the mirror; the deviation of the wedges provides a coarse but accurate measure of boom deflection, and is supplemented by an open-loop error signal which serves as a fine-scale addendum.

The wedge position is derived from incremental encoders and the open-loop signal is digitized by the spacecraft system.

A second autocollimator is stationed 12 inches to the side of the first and is used to measure a 1/10th component of twist around the boom axis. Its beam is projected to a Porro reflector assembly at the end of the boom which, with a second Porro mounted at the spacecraft end, provides the sensitivity to twist. A separate electronics package houses power supplies and all circuitry except for the preamplifiers which are in the opto-mechanical housings.

This measuring system is firmly based on previously designed and built instrumentation for similar application. The basic angular deviation detection means has been used for fifteen years in other autocollimator systems, subject to periodic design improvements in the areas of LED sources, silicon detector arrays, and low-noise electronic amplifiers. Although previous wedge-deviation assemblies used resolvers to read out the wedge rotation, this design uses incremental encoders attached to each wedge for the same purpose.

The basic system design is fully documented by this report, but mechanical detail drawings remain to be prepared. Electronic design is complete, except that some individual component values in amplifier schematics do not reflect the final computations of required gain. The scope of this study did not permit generation of worst case analysis.

System power is an average of 12.3 watts. Weight is 21.8 lbs., including both autocollimators, reflectors, and the separate electronics package. MTBF is in excess of 102,800 hours.

Tradeoff studies include consideration of a gimballed boom, whereby the wedge assemblies would be

eliminated and the boom itself realigned in all but the twist axis by means of a two-axis gimbal at its base.

All performance goals have been met, as far as it is possible to determine pending completion of worst case analysis. The RSS value of all identifiable sources of error is 0.295 arc-seconds for the orthogonal deviation axes and 2.787 arc-seconds for twist, 1σ . A larger spread between the two autocollimators at the base of the boom would permit higher accuracy in the twist measurement if greater accuracy is desired.

1.0 INTRODUCTION

This document is the final report in the design study for an Attitude Transfer Assembly (ATA) for the MAGSAT spacecraft. The ATA is to monitor the orientation of a boom-mounted vector Magnetometer Experiment Package relative to the main spacecraft body. The attitude of the Experiment Package is measured in orthogonal Y and Z axes of lateral boom deviation and in a twist axis around the boom center line. These measurements are made in a non-contact optical approach employing a three axis autocollimator mounted on the main body of the spacecraft, with only passive optical components (reflectors) located at the boom end. The design concept presented here is not a novel or new one, but a complete revision of earlier work that resulted in the successful demonstration model. The approach incorporates the advances in electronics and data presentation and processing that have been made and implemented in other programs since the completion of the earlier work.

The objective of this effort is to carry out firm design activity within the constraints and performance requirements of the MAGSAT Spacecraft program, (these requirements are given in Appendix A.) leading to documentation defining all the basic characteristics of the three axis ATA. This report constitutes the work output of the study program and includes the following documentation:

- Opto mechanical layout drawings
- Optical specifications and schematic
- Preliminary mechanical packaging drawings
- Electronic schematic diagram
- Preliminary mechanical packaging drawings

The report begins with a description of the technical problem, description of autocollimator operation and the design approach taken to measure the orthogonal angular deviations and the twist about the boom in (Section 2). This section provides an introductory overall view of the ATA and its operation and leads into a detailed discussion of the various design concepts.

Section 3 provides the detailed description of the optical system, with all pertinent calculations performed within the text or, if too lengthy, in the Appendices. The mechanical system as well as electronic circuit descriptions are given in this Section.

It is felt that the tradeoffs to the design approach are important enough to be called out in a separate section. This is done in Section 4, where the impact of eliminating system redundancies is discussed. Another topic of discussion in this section is the constraint on the gimballed boom mount when used with the ATA.

The remaining sections deal with such things as preliminary reliability analysis, a discussion of system error, cross coupling and system alignment.

Especially noteworthy for consideration is Appendix B in which the various optical, electrical and mechanical parameters are tabulated for reference and system overview. Weight and power summary are included in Section 3.4.

This document is intended to be complete in itself and constitutes the Item of Article XV, "Type III Final Project Report" of the study program, "Design Study of an Attitude Transfer Assembly for MAGSAT", contract NAS 5-23598.

2.0 THEORY OF OPERATION

2.1 STATEMENT OF TECHNICAL PROBLEM

The MAGSAT experiment package includes a vector magnetometer capable of mapping three orthogonal components of the magnetic field traversed by the orbiting spacecraft. In order to relate these directional components to terrestrial coordinates it is necessary to be able to calculate the angular orientation of the magnetometer relative to reference surfaces on the spacecraft. This calculation must be derived in real time because the 20-foot boom which supports the magnetometer at its outboard end is subject to flexure, due particularly to orbital changes in solar heating.

In addition to the temporal changes in magnetometer orientation is the initial angular offset caused by uncertainty in attitude of the boom as a result of post-launch erection from its stowed position.

It has been determined that angular deflections of the end of the boom may have a magnitude up to ± 15 arc-minutes normal to the boom axis, and ± 5 arc-minutes around this axis. Since these deflections may occur simultaneously and in independently variable magnitudes around the three principal axes, it is essential that measurement of each rotation component be made without contamination by cross-coupling from other axes. Alternatively, if complete elimination of such cross-coupling is not possible or feasible, it must either be of an acceptably small magnitude or be removable by calibration and correction of data.

Not only must each angular measurement be independent of appreciable error due to coupling from other angular

deviations, but the translation of the end of the boom associated with these deflections must not frustrate, or compromise the accuracy of the angular measurements. It will be shown, for example, that the end of the boom may be expected to translate up to ± 0.5 inch in orthogonal directions due to solar heating and the resultant circular bending. This must be not only tolerated, but its implications for system error evaluated.

In addition to the implicit requirements of the measuring system stated above is the requirement that there be no magnetic field-generating equipment mounted close to the magnetometer. This clearly points toward an optical measuring system with only passive elements such as reflectors mounted at the end of the boom.

2.1.1 System Design Approach

For reference purposes a right-hand rectangular coordinate system will be defined as follows:

A mounting plane will be required on the spacecraft, and this plane will contain the X and Y axes. The central axis of the erected boom will be defined as the X axis and may also be referred to as the twist axis. The Y and Z axes normal to the boom length may also be referred to as the orthogonal axes.

Figure 2.1 shows the arrangement of measuring equipment relative to these axes. One autocollimator system is aligned parallel to X and cooperates with a plane mirror at the end of the boom for measuring angular deflections of the end of the boom about the Y and Z axes.

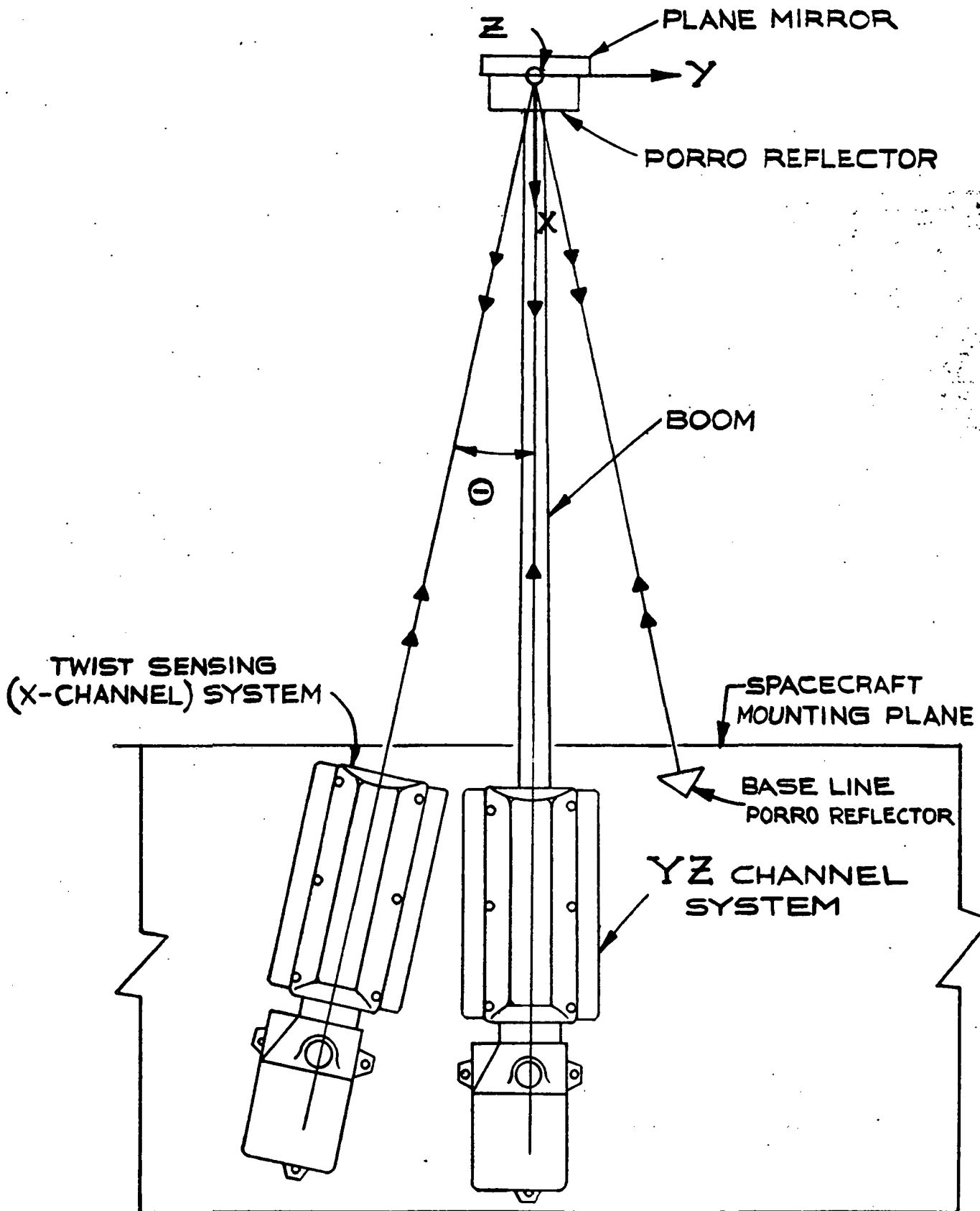
A second autocollimator system is mounted with its beam projected essentially in the X-Y plane but inclined at an angle θ from the X axis. Its beam impacts on the upper of a pair of two reflectors comprising a Porro reflector assembly at the end of the boom, and is then reflected to and from the lower reflector of this pair to a second Porro reflector assembly mounted on the spacecraft and on the opposite side of the X axis. From here it retraces its path to the remote pair of reflectors and back to the second autocollimator. This complement of equipment measures rotation about the X axis, or twist.

Rotation about the X, Y and Z axes respectively, will be referred to in this report as x-, y-, and z- rotation. It will be appreciated that a rotation of the remote plane mirror about the Y axis will produce a deviation of the reflected beam out of the X-Y plane, resulting in a projected component in the Z direction. The reader should be sensitive, therefore, to the distinction between an axis of rotation and the projected displacement in the focal plane of the autocollimator, which is in a direction orthogonal to the rotation axis. A unit vector parallel to the illuminating beam will have components, after reflection, parallel to X, Y, and Z axes and proportional to the direction cosines between the reflected ray and these axes.

2.2 MEASURING MODES

2.2.1 Y-Z Measuring System

The Y-Z measuring system consists of a dual-axis autocollimator and a beam-deflection unit, with the remote plane reflector. The autocollimator projects a collimated beam of pulsed energy from a gallium arsenide LED toward the remote



MEASURING SYSTEM ARRANGEMENT
FIGURE 2.1

reflector. When the latter is normal to the beam the reflected energy is refocused by the autocollimator into the plane of two separate pairs of silicon detectors. This is the null condition and is shown in Figure 2.2A.

As the reflector is rotated from the normal about one axis, the reticle image is translated onto a detector. In Figure 2.2B the image is shown translated by an amount δ onto detector B. The signal generated by this reflector rotation is proportional to the area of the image on the detector i.e. the area $h\delta$. Continued reflector rotation generates continued image translation, resulting in a linearly increasing signal up to the condition of Figure 2.2C that is, the end of the linear range. If there is further reflector rotation in the same direction, the image continues to translate until the end (or beginning) of the acquisition range is reached. This is shown in Figure 2.2d.

As mentioned above, the width of the image translated on the detector is δ . Image translation is related to the mirror rotation, y , by the equation

$$y = \frac{\delta}{2f} \quad (2-1)$$

where f = focal length of the objective. The factor of 2 is due to the law of incidence and reflection i.e. for a mirror rotation of angle y , the beam is deviated by an angle $2y$.

The detectors are connected with their polarities opposite. Movement of the image in one direction as in Figure 2.2B generates a signal essentially in phase with the light pulses; movement in the other direction generates a signal 180° out of phase. The detector pair supplies to the preamplifier an A-C signal whose phase is determined by mirror rotation and whose amplitude is determined by the magnitude of rotation. Electronic processing of the A-C signal is described in section 3.3.

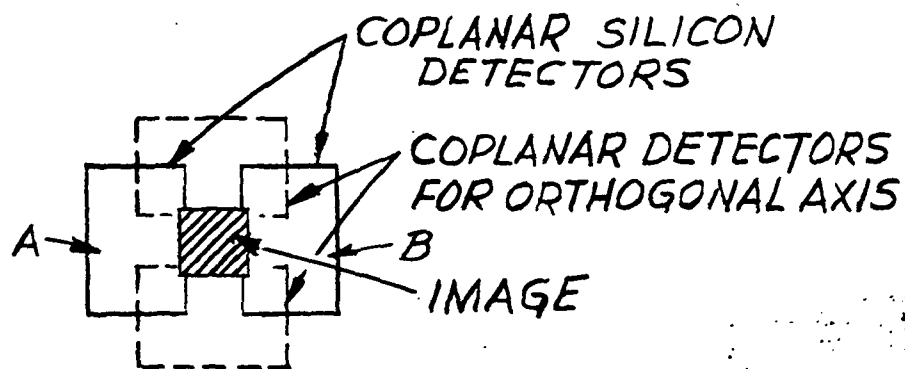


Fig. 2.2A THE NULL CONDITION

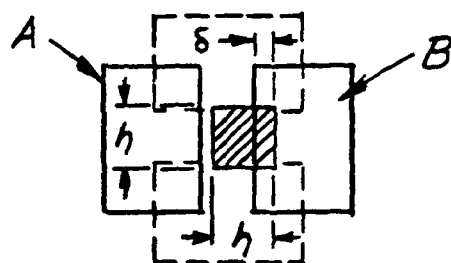


Fig. 2.2B IMAGE TRANSLATED BY AMOUNT δ

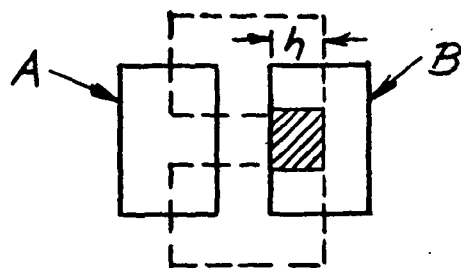


Fig 2.2C LINEAR RANGE: IMAGE TRANSLATED BY AMOUNT h

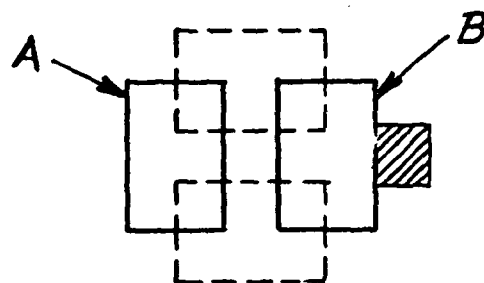


Fig. 2.2D ACQUISITION RANGE

The design for the ATA combines the advantages of an edge tracker, which is least susceptible to drift in the presence of temperature excursions, and that of a centroid tracker which provides a push-pull effect doubling the signal level in the presence of image motion. This is accomplished by making the gap between the detectors less than the nominal dimension of the source reticle. At null the overlap allows some energy to fall on each detector (see Figure 2.3A). Since the detectors are connected with the polarities opposite, the image portions on the two separate elements produce signal currents (proportional to image areas on detectors) of equal and opposite sign, resulting in zero output. As the image is translated onto detector B by an amount δ the image area on this detector increases by an amount δh and decreases by an amount δh on detector A. The net signal is thus proportional to $2\delta h$, which means that in the region of overlap of the image on the detectors the slope of the transfer function is twice the value of the slope in the region where there is no overlap, thereby providing the push-pull effect. The transfer function is illustrated in Figure 2.3B.

It has a scale factor of 100 mv per arc-second, is linear over a range of ± 20 arc-seconds, and is followed by a lesser slope over an additional ± 90 arc-seconds. The scale factor is held constant by means of Automatic Gain Control which compensates for changes in system transmittance, LED conversion efficiency, or detector responsivity.

The open-loop error signal from the detector is supplemented, however, by the action of the beam-deflection unit. Although conceptually a part of the autocollimator, it is housed separately for better thermal and structural stability.

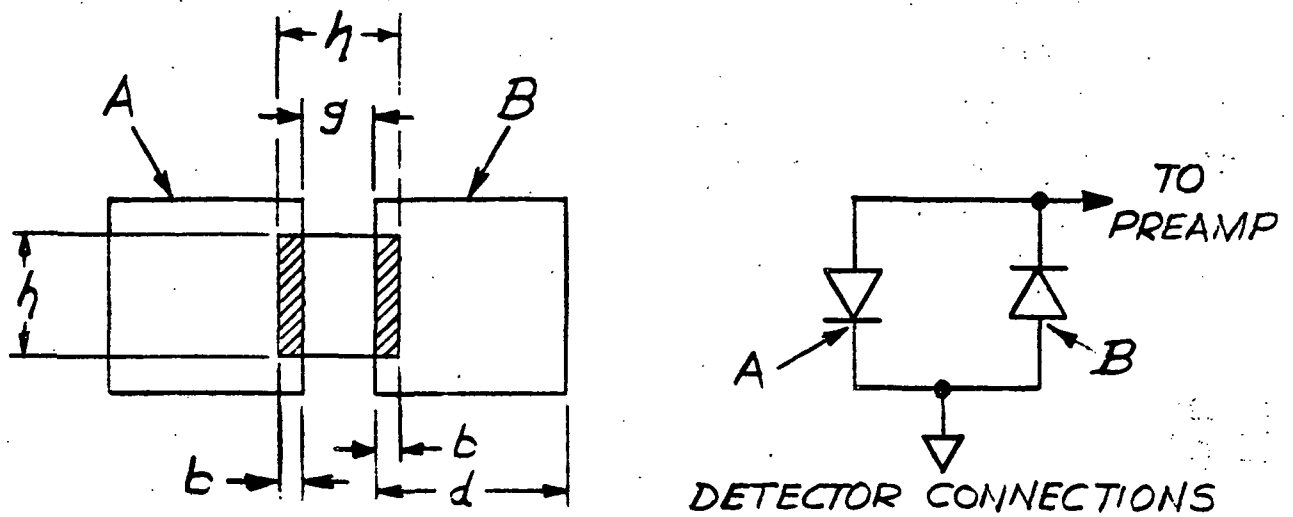


Fig. 2.3A IMAGE DIMENSION & DETECTOR SPACING

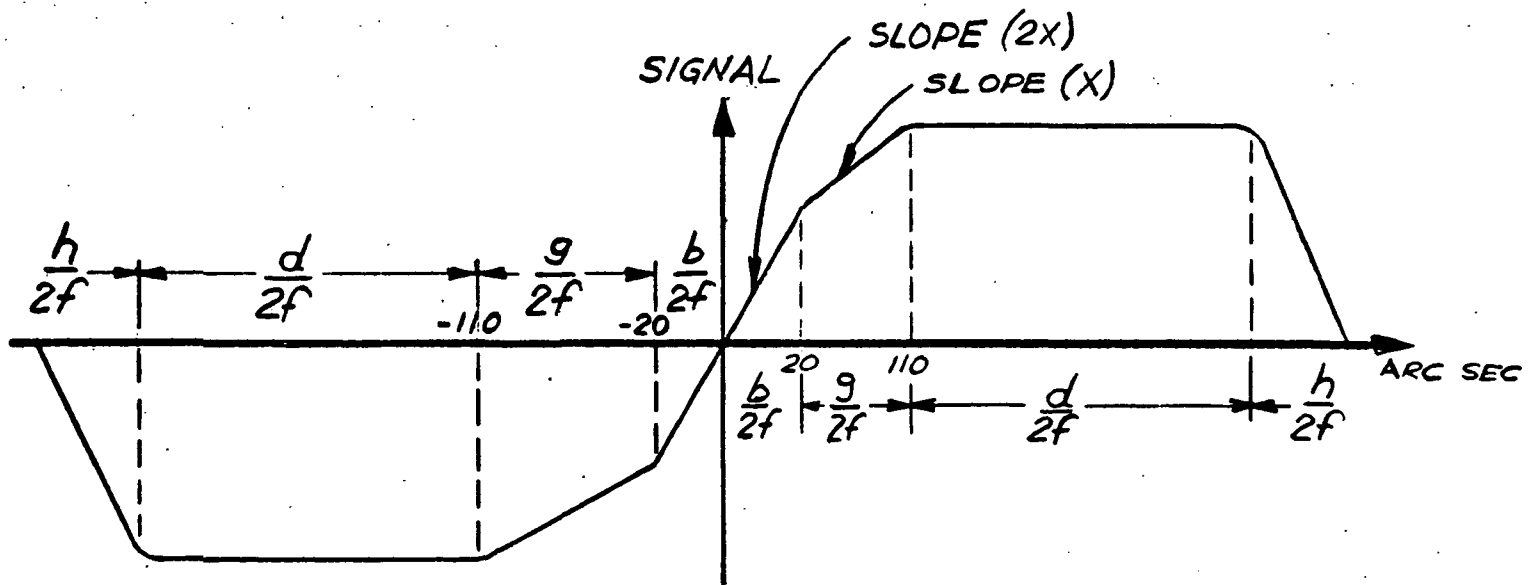


Fig. 2.3B OPEN-LOOP TRANSFER FUNCTION

It contains two independently operated pairs of contra-rotating glass wedges in optical series, through which the collimated beam is transmitted.

It is an obvious requirement that in order for the autocollimator to measure rotation of the remote reflector the projected beam must fall on the mirror, and that even with maximum angular deviation and translation, the reflected beam must reenter the autocollimator. To assure this result with an open-loop sensor would require an autocollimator of approximately 10-inch aperture diameter - an unacceptable requirement from the standpoint of weight and volume, as well as for other reasons.

The "tracking" effect of the wedge unit keeps the collimated beam incident on the mirror and also normal to it, so that the reflected beam returns along the same path, through the wedges and into the autocollimator. By measuring the deviation of the beam necessary to keep it normal to the reflector, the angular rotation of the mirror is inferred. Furthermore, an average optical reduction of 180:1 is achieved, which means that to measure the full $\pm 0.25^\circ$ angular excursion, the optical wedges rotate 45° . For a 1 arc-second deviation the wedge rotation averages 3 arc-minutes - easier to measure by more than two orders of magnitude.

The wedges are driven by a stepper motor. For deviations of less than 15 arc-seconds the wedges are not actuated, and the output is only the controlled transfer function from the detector amplifiers. When the signal exceeds the threshold corresponding to 15 arc-seconds (1.5 volts) a string of 16 motor pulses at a step rate of 60 Hz is

supplied to the wedges to cause them to rotate through 0.7° in a direction to reduce the error signal to null. Encoder discs mounted to the wedges provide a digital count of this rotation, and the measurement of boom deflection is then provided by the quantized sum of the encoder output and the residual open-loop or "raw" error signal.

The wedges have inherently high accuracy over a large measuring range as well as virtually perfect stability. The small residual errors which result principally from gear errors and encoder eccentricity are discussed in a later section. (This represents an advance over previous designs in which the wedge rotation was measured in analog fashion by means of resolvers.)

The angular deviation imparted by the wedges is actually a sine function of rotation, which must be rectified by a sine conversion of the encoder outputs. This is a trivial requirement at the current state of computer technology.

2.2.2 X-axis Measuring System

The X-axis system uses an autocollimator and deviation-wedge unit similar to the Y-Z system but with differences that will become apparent.

By way of introduction, consider a fictional, perfectly rigid boom mounted alongside the magnetometer boom, on the end of which is an autocollimator directed toward the magnetometer. If a plane mirror were mounted on the side of the latter facing the autocollimator, twist of the magnetometer boom would deviate the reflected autocollimator beam in an "elevation" direction relative to the autocollimator, and the twist would be directly measured.

At the opposite extreme, a beam projected along the boom axis toward a plane mirror would sense no component of twist about that axis. For intermediate "look angles" whereby the autocollimated beam makes an angle of θ relative to the boom axis, the measured deviation is proportional to $\sin \theta$. The two examples given represent $\sin \theta = 1$, and 0, respectively, and illustrates the previous statement without proving it. Proof of the principal and coupling terms is provided in Section 7.0.

We may then set up an autocollimator at an inclined angle θ as large as convenient, and sense a twist component. If the measured component is then divided by the constant $\sin \theta$, the true twist angle is derived.

If the reflector is a plane mirror, a serious interference arises in the presence of Y axis rotation (pitch in common terminology). The latter rotation would be reduced by $\cos \theta$, but for an offset angle θ of around 3° the measured pitch component would be about 20 times the twist for equal deviation angles. Even if the pitch component could be subtracted out by applying a correction from the Y measuring axis, the accuracy of twist would be seriously degraded by the overwhelming effect of the pitch component.

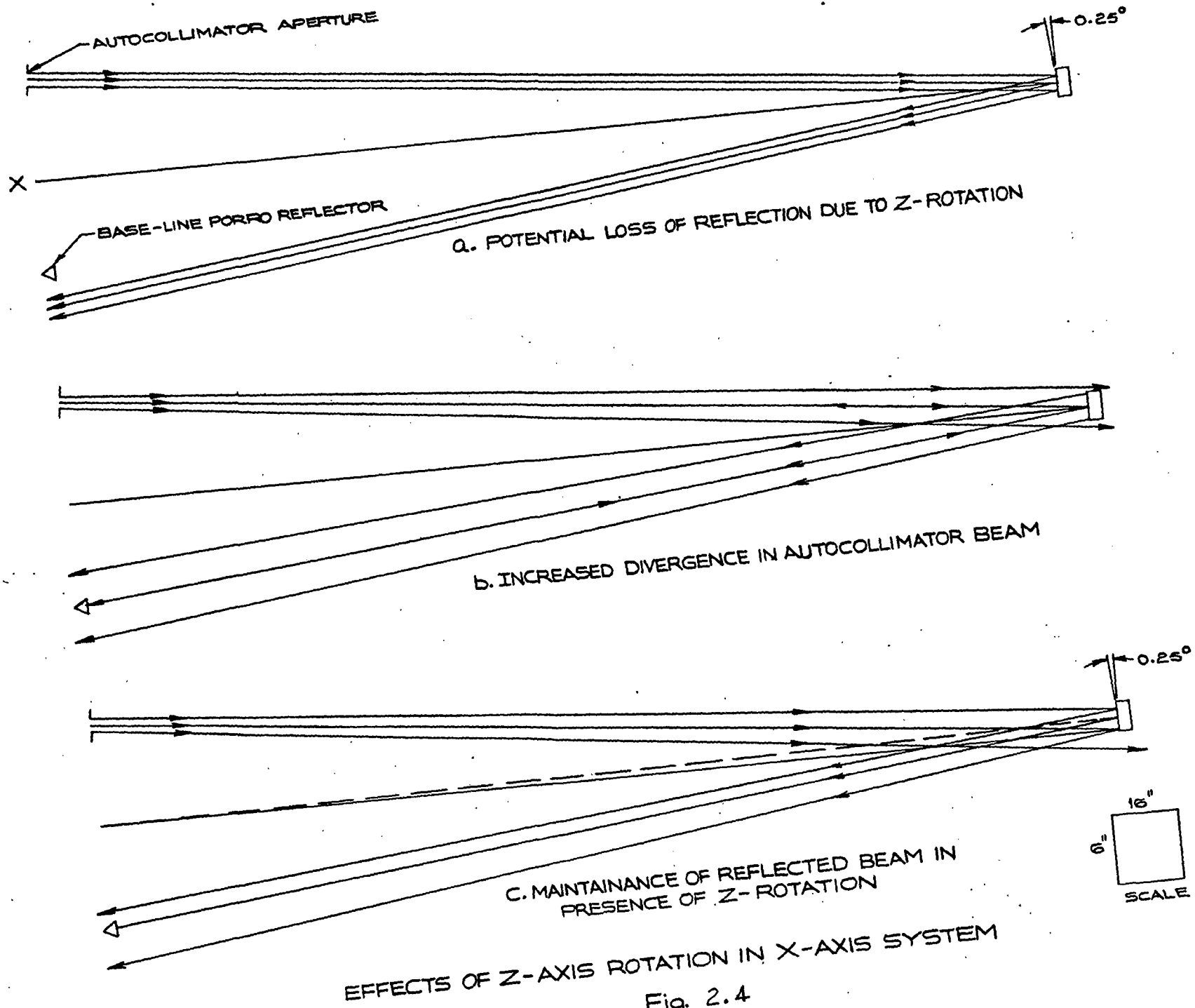
This potential problem is avoided by the use of a Porro reflector at the end of the boom. The Porro mirror assembly will have its roof edge parallel to the Y axis. Such a reflector has the property of rotating a reflected beam by twice the rotation angle, and it is this property which produces the component of X rotation which will be sensed and measured by the autocollimator and wedge unit.

The beam is reflected from the first (remote) Porro reflector to a second Porro on the opposite side of the X axis. This reflector has its roof edge parallel to the Z axis, and it returns the beam to the first reflector and then to the autocollimator. The "vertical" deviation (i.e., in the Z direction) imparted to the beam by its first encounter with the remote reflector in the presence of X rotation is doubled upon the return trip.

The final result is that the beam is deviated out of the X-Y plane by an angle $4 \times \sin \theta$ where x is the angular rotation about X. Since the beam reflected from any mirror is deviated by twice the mirror rotation, the difference between this term and normal mirror action is the factor $2 \sin \theta$.

Based on a moderate spread of the equipment, a value 0.05 has been selected for $\sin \theta$. This provides a center-to-center displacement between autocollimator and second Porro of 24 inches on the mounting surface. Therefore the system measures a one-tenth component of the true twist angle. As will be shown, this permits the measurement of X rotation with less accuracy than Y and Z, although not all sources of error are increased proportionately. In all discussion of errors which follow, the contributions are quantized in terms of true error in measuring x .

The design of the X autocollimator differs from the Y-Z instrument in another important respect. Whereas the Y-Z system requires a square source aperture in order to generate similar response functions in both axes, the X-axis system has no such limitation. Furthermore, the Z-axis rotation of the remote Porro reflector can cause the reflected beam to miss the base-line Porro, preventing measurement of the X-rotation. This is illustrated in Figure 2.4(a).



If the divergence of the beam in the XY plane is increased by use of a source aperture which is elongated in the Y direction, both the remote and base-line Porros are over-filled with the autocollimator beam, as shown in Figure 2.4(b). Then if the remote Porro rotates about Z and is also displaced in either stiff or curved boom modes, some portion of the beam will always be incident on the base-line Porro and be reflected via the remote Porro to the autocollimator.

The image formed between the detectors will be vignetted to a length determined by df/D where d is the autocollimator lens aperture diameter, f the focal length and D the distance to the base-line Porro:

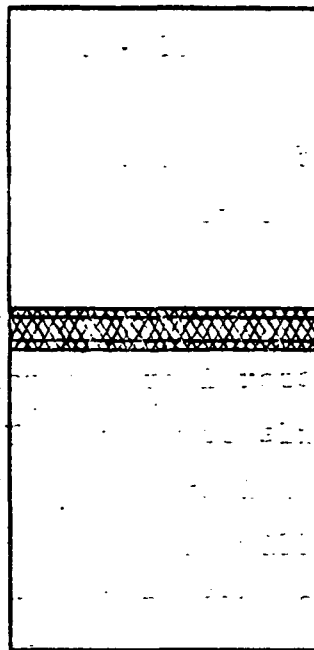
$$1.142 \times 4 / 480 = 0.0095 \text{ inches}$$

The image will then have an appearance relative to the detectors as shown in Figure 2.5. The source aperture will have dimensions 0.005×0.040 inches, so that with an unvignetted system the image length would be matched to the detectors as in 2.5(a). As calculated above the actual image length does not exceed 0.0095 inches, and the intensity falls off from the center outward as suggested by the non-uniformly spaced isorad circles in the image shown in 2.5(b).

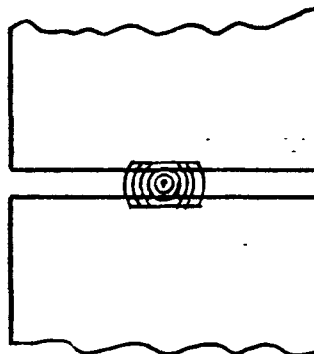
When the remote Porro has rotated through the angle $Z = 0.25^\circ$ it is not the center but the end of the potential image which actually finds its way back to the autocollimator detector plane, as shown in 2.5(c). The end of the image in

DETECTOR GAP
.0035 IN.

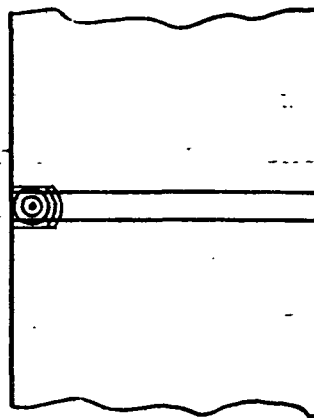
IMAGE WIDTH
.0050 IN.



a. FULL POTENTIAL IMAGE



b. VIGNETTED IMAGE
 $z=0$



c. VIGNETTED IMAGE
 $z=0.25^\circ$

Fig. 2.5 X-AXIS IMAGE FORMATION

the latter case is slightly clipped, but this small dropoff (about 15%) will be compensated by the AGC circuit. Of more concern, however, is the necessity to maintain the detector edges straight, parallel, and aligned parallel to the Y axis, so that the image motion due to Z rotation does not generate an X coupling error. They will be aligned to an optimum position as determined by calibration, and the residual coupling error after optimization will be supplied to the prime contractor upon delivery. Depending on magnitude of the residual errors, the calibration may be ignored or used for data correction.

2.3 SEARCH MODE

The possibility exists that when the Attitude Transfer Assembly (ATA) is turned on for the first time after launch or after subsequent shutdown, the reflected beam will not reenter the Y-Z autocollimator aperture. In this case a search mode will be instituted by means of the wedges to "find" the image. A preprogrammed search mode described in the next section is provided for this purpose, and the image will always be found in less than 70 seconds time.

In addition to the search mode to find the image it is also necessary to return to the encoder zeroes to start a measurement after power shutdown. A plan has been devised whereby the encoders will be "parked" close to their zero position before launch and whenever the ATA system is turned off. Thus when startup is instituted, the encoder zero is quickly found and the counting of encoder steps necessary to null the image position proceeds. This search for the encoder zero will normally take only 0.133 seconds time per axis, with

a maximum of 51 seconds. Thus the time required before accurate data is received from all three axes will be 17.5 seconds (1σ) after power turn-on, with an absolute (very improbable) maximum of 231 seconds.

Only one wedge motor will be actuated at any one time in order to limit peak power, and while the wedges are rotating, a clamp will be imposed on the output data. Normally, the system may be interrogated at the repetition rate of 8 per second providing "coarse" encoder output and "fine" open-loop output from each axis in essentially real time.

In order for a measurement of boom deflection to take place three conditions must be achieved: (1) the autocollimator beam must be incident on enough of the remote reflector for information on the orientation of the reflector to be imposed on the reflected beam, (2) the reflected beam must reenter the autocollimator aperture, and (3) the refocused image of the source reticle must fall on the detector arrays.

The two principal deviation modes (erection bias and circular bending) have been explored in order to determine the characteristics of a search mode adequate to acquire the image and institute the measurement function. Figure 2.6 illustrates a side view of the elements of the Y-Z system with the longitudinal distance compressed by a factor of 16 relative to the lateral dimensions. This compression also has the effect of scaling up angles by a factor of 16. (See the scale in lower right corner.)

In (a) the perfect alignment situation is illustrated. The slightly divergent beam from the autocollimator aperture

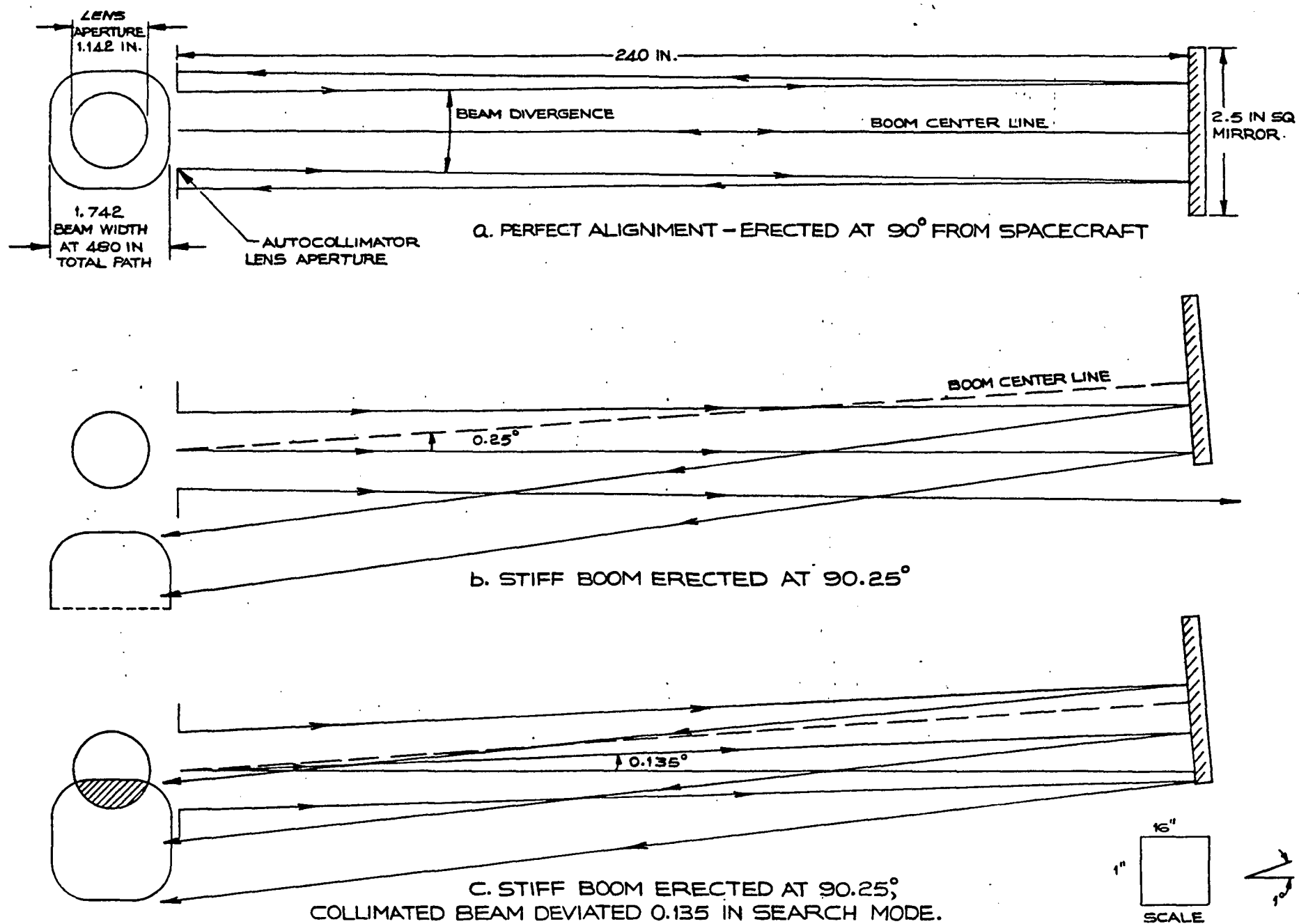


Fig. 2.6

(1.142 inch diameter) illuminates the 2.5-inch square mirror 240 inches distant. It is reflected back in the same direction because the mirror is normal to the beam.

The divergence causes further increase in beam cross-section on the return path. At the autocollimator aperture the effect of the square source reticle and circular lens aperture result in an essentially square reflected beam with rounded corners. This beam has a width of 1.742 inches at the autocollimator and only the central 1.142 diameter enters the autocollimator. The relative sizes and position are illustrated at the left edge of the figure.

In (b) the effect of a bias in the boom erection direction is shown. The boom center line is shown as straight, but rotated 0.25° from the nominal 90° direction relative to the spacecraft. Most of the autocollimator beam falls on the remote mirror, but is then reflected so that none of it reenters the autocollimator. The bottom of the beam is clipped by the mirror, so that the reflected pattern is not a complete square.

If the search mode drives the wedges so as to deviate the beam toward the mirror normal, the reflected beam will ultimately start to reenter the aperture. Figure 2.6c shows the beam after it has been deviated 0.135° (512 motor steps, 2048 encoder counts). Enough of the beam is now captured in the autocollimator aperture that a focused image of the source reticle falls on one detector and the system will switch from search to control mode.

The control mode will continue to drive the wedges until the autocollimator beam is within 15 arc-seconds of the mirror normal. The encoders will then provide an output

corresponding to approximately 885 arc-seconds and the open-loop residual error signal will provide the addendum corresponding to 900 arc-seconds. (Although the exact value of each output is not completely predictable, their sum will have all of the accuracy indicated by the error analysis.)

Figure 2.7 shows the case of circular bending of the boom, which produces a maximum rotation of 0.25° at the end of the boom, accompanied by a "droop" of 0.524 inches. Although the beam is still fully incident on the mirror, the reflected beam misses the autocollimator aperture as before. Again, a search mode of 0.135° in the correct direction is enough to acquire part of the reflected beam and switch to control mode.

In both Figures 2.6 and 2.7, deflection in a single axis is illustrated.

Figure 2.8 shows the worst-case combination of maximum Y and Z axis deviations, combined with the worst-case search pattern that might be required before recapture of the beam. The autocollimator aperture is shown with reflected beam displacement a maximum in both directions.

The first search action deviates the reflected beam from 0 to 1. It required 768 wedge motor steps or an encoder count of 3072 and a time of 8.53 seconds. The beam is still not acquired however, so an orthogonal excursion of the same magnitude is instituted. This happens to be in the wrong direction for the particular combination of deviation directions illustrated, so the beam is further from capture.

In step 3 the square search pattern is expanded by a factor of two, but not until step 5 does the beam find the autocollimator aperture. The total time required would not

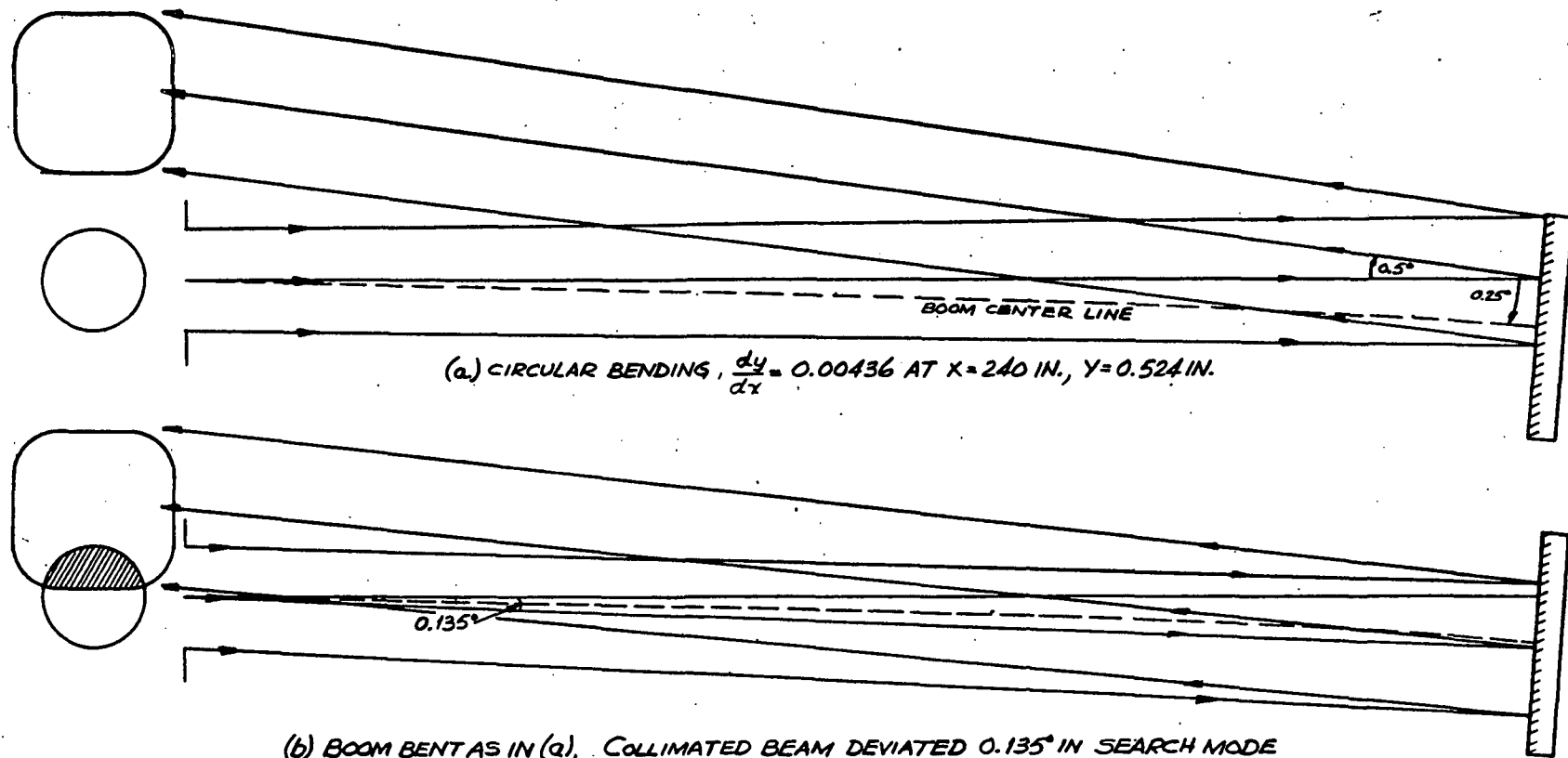
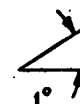
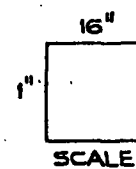


Figure 2.7



AUTOCOLLIMATOR APERTURE
REFLECTOR BEAM AT ENCODER
ZERO, 0.25° DEFLECTION IN Y & Z

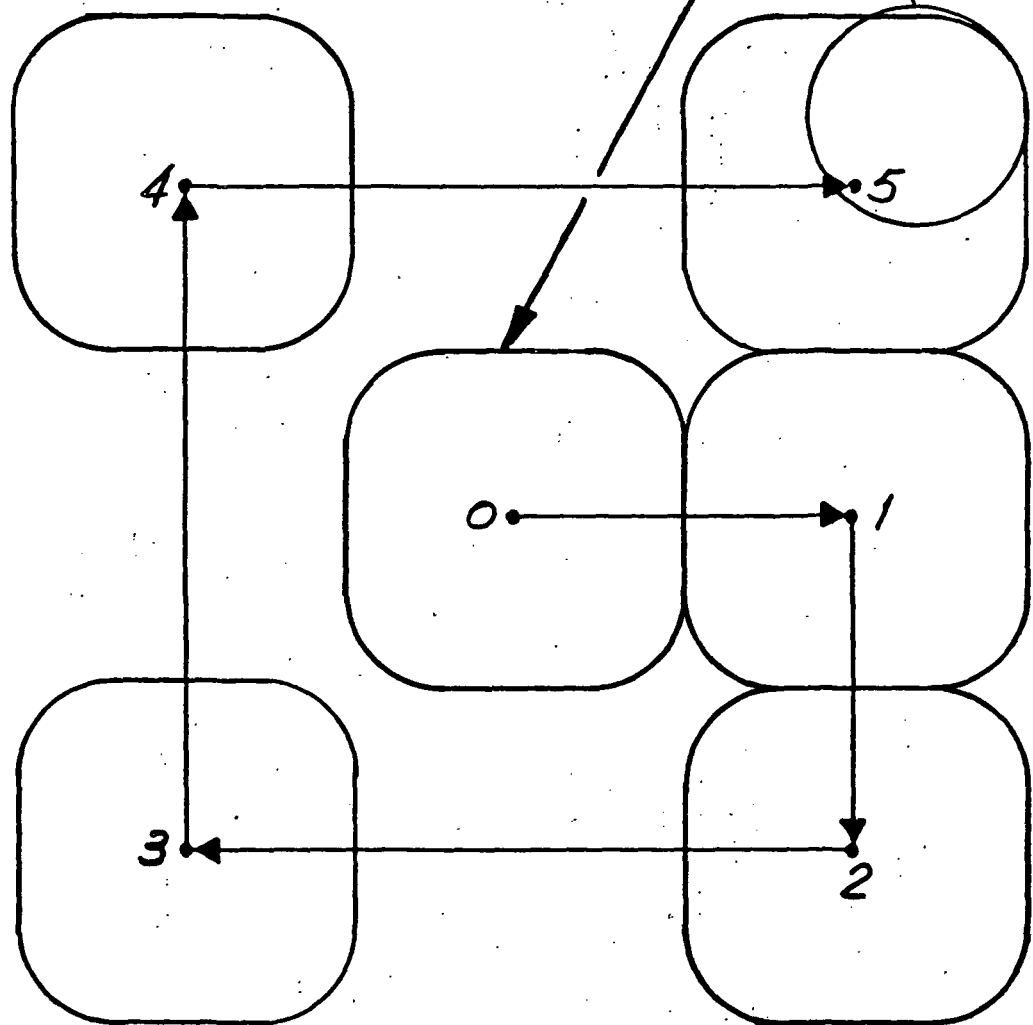


Fig. 2.8
REFLECTED BEAM DISPLACEMENT
RESULTING FROM SEARCH MODE

exceed 60 seconds. Clearly, if the original deviations were smaller or in any of the other three "corners" relative to the autocollimator aperture, capture would occur sooner.

As previously stated, the reflected beam must not only reenter the instrument aperture, but must be focused within the sensitive area of the detectors. Figure 2.9 shows the two sets of detectors superimposed on the same plane with the source reticle. In actuality they are, of course, separated by beamsplitters but effectively are coplanar.

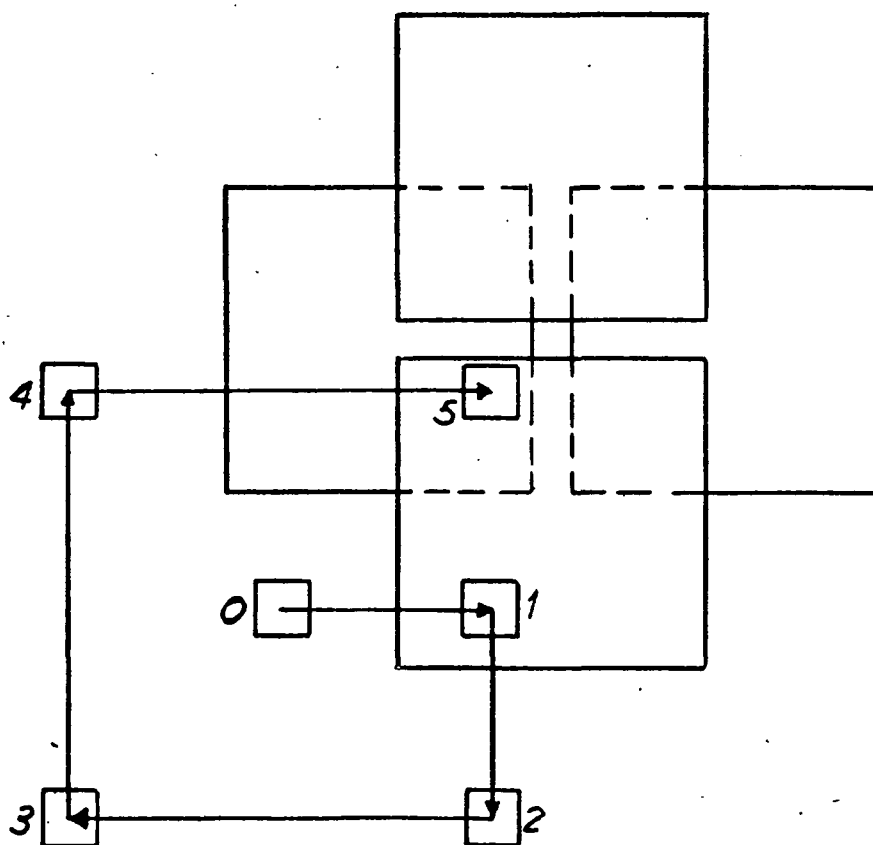
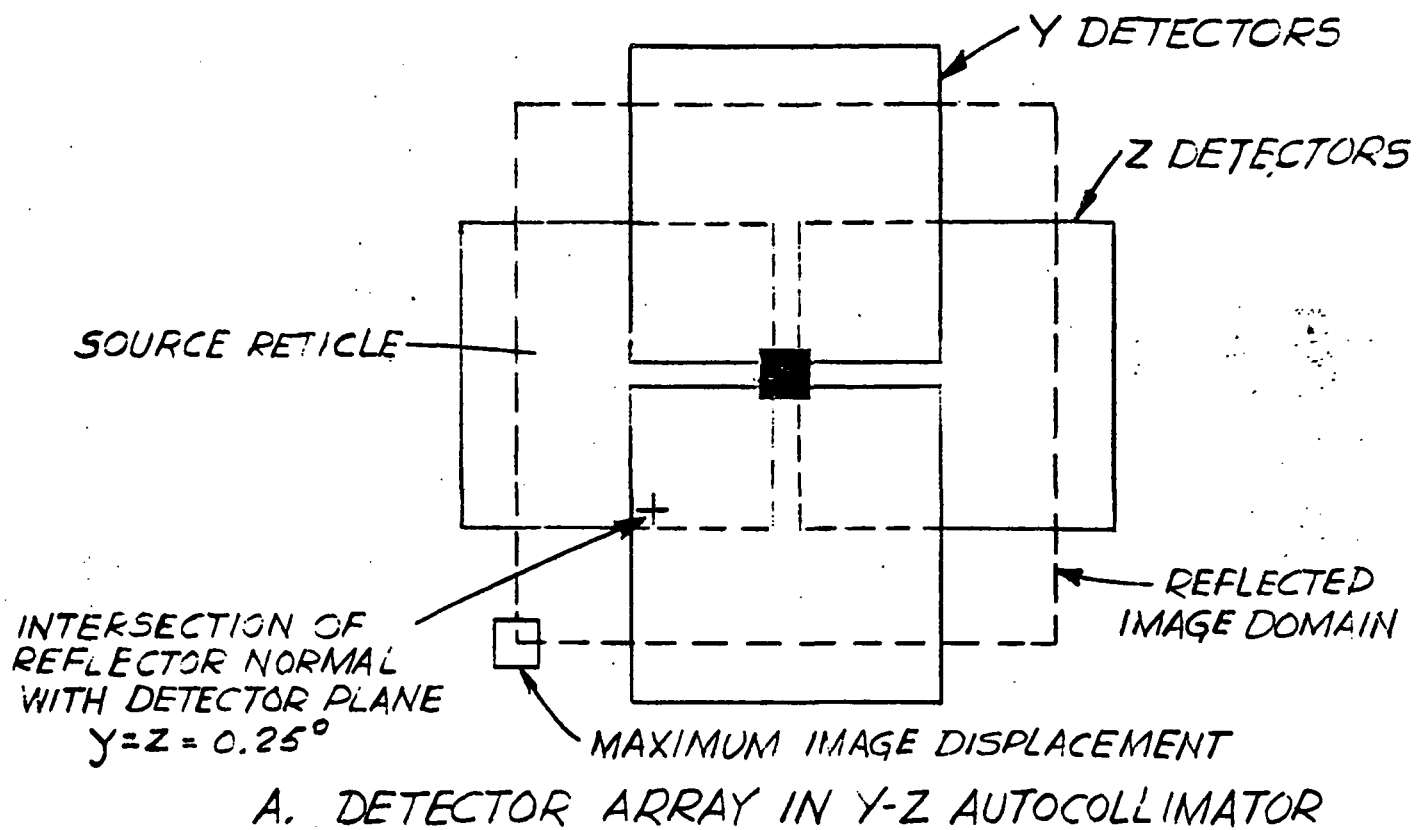
Figure 2.9 shows the outline of both pairs of error detectors and also the broken line square domain representing maximum displacement of the image from the center of the detectors. The small cross shows the intersection of the mirror normal with the detector plane. The image displacement is twice as great due to the law of reflection. It should be realized, however, that this image is only a potential image, since Figure 2.8 indicates that none of the reflected beam is captured by the lens aperture.

Similarly, although step #1 of the search mode shows the image on the detector, it is still dark, as shown in Figure 2.8. Not until step 5 of the search mode has been nearly completed are both conditions fulfilled: recapture of the beam and incidence on the detector.

No search mode is required of the X autocollimator, since the combination of Porro reflectors always returns the center of the reflected beam to the center of the aperture.

2.4 AUTOMATIC GAIN CONTROL

In order to maintain accuracy in the open-loop transfer function it is necessary to have automatic gain control to compensate for changes in external transmittance



B. IMAGE MOTION RESULTING FROM SEARCH MODE

Fig. 2.9

and/or reflectance, degradation of LED output efficiency with time and/or temperature, and changes in detector responsivity with time and/or temperature.

In order to accomplish this, a second detector (Acquisition or ACQ) receives a small portion of the beam which has been transmitted through the optical system to the external reflectors and back. The implicit assumption is made that changes with time and temperature will affect the ACQ and the error detectors equally, or at least that relative changes will be small compared with absolute changes.

The output from the ACQ detector is compared with a well-regulated reference voltage and the difference used to adjust the LED current and restore the ACQ detector output to the standard value. This automatically regulates the output of the error detectors and preserves the scale factor.

One additional detector further preserves the stability of the null by guarding against the effects of internal stray radiation. Although anti-reflection coatings, absorbing paints and other techniques are used to minimize scattered "light", there is always a possibility that some of the energy from the LED will irradiate the error and ACQ detectors. Furthermore, it may irradiate the two error detectors of a channel unequally, generating an offset signal which would require an angular offset of the remote mirror to achieve null.

As a precautionary measure, therefore, a compensation detector will also be provided to sample energy from the LED which has not traversed the external path. The output of this

detector will be attenuated and used to buck out any offset signal from the error detectors. This adjustment will be made with the external path blocked, and will be applied to the output of both the error detectors and of the ACQ detector.

2.5 SYSTEM OUTPUTS

2.5.1 Analog Output

Analog outputs from each channel will be bipolar dc, with scale factors of 100 mv/arc sec in Y and Z axes, and 200 mv/arc sec in X. All channels will have nominal dynamic ranges of ± 15 arc-seconds since the threshold for servo system actuation is set at that level.

2.5.2 Digital Output

Digital outputs will consist essentially of two numbers from each channel of the YZ sub-system, and one number from the X channel. These numbers are derived from the encoders, and their coding is described in the Electronics section of this report.

Because the deviation components of the wedges are trigonometric functions of their rotation angles, the raw encoder outputs must be converted to sines and cosines to provide (a) the primary output and (b) the cross-coupling correction from the orthogonal wedge pair.

A. Y-Z System

The 45° steps of the motors are reduced by factor of 1024 at the wedge/encoder assembly, or 158.2 arc-sec. Each step of the motor generates a count change of 4 in the encoder output, so that each count of the encoder represents a wedge rotation of $45^\circ/4096 = 39.5508$ arc-seconds. Beam

deviation B corresponding to rotation through N counts in the Y channel

$$= B_1 = D_{Y1} \sin (39.5508 N)$$

where

$$D_{Y1} = \text{wedge constant} = 636.4 \text{ arc-sec}$$

$$\text{For } N = 4096$$

$$\begin{aligned} B_1 &= 636.4 \sin (4096 \times 39.5508) \\ &= 636.4 \sin 45^\circ \\ &= 450 \text{ arc-sec} \end{aligned}$$

A second component B_2 is obtained from the second wedge, and if $D_{Y2} = 636.4 \text{ arc sec}$

$$\begin{aligned} B_1 + B_2 &= 1272.8 \sin 45^\circ \\ &= 900 \text{ arc-sec, which is the full} \end{aligned}$$

required measuring range.

Each count of the encoder represents a deviation of:

$$D = 2D_{Y1} \sin (39.5508 \text{ arc-sec}) \cos \phi$$

where ϕ is the displacement from the zero position, assuming $\phi = \phi_1 = \phi_2$.

When ϕ is in the vicinity of 0° ,

$$\begin{aligned} D &= 1272.8 \times 0.000192 \\ &= 0.244 \text{ arc-sec} \end{aligned}$$

When $\phi = 45^\circ$

$$\begin{aligned} D &= 1272.8 \times 0.000192 \times 0.70711 \\ &= 0.1725 \text{ arc-sec.} \end{aligned}$$

The string of 64 motor steps which is generated when the error signal exceeds 15-arc seconds equivalent thus produces a correction of 15.6 to 11.04 arc-seconds.

The difference in rotation angle between the two Z-measuring wedges produces an unmeasured deviation in the Y axis which must be added as a correction unless small enough to be ignored.

The correction

$$C_Y = D_Z \left[\cos (39.5508 N_{Z1}) - \cos (39.5508 N_{Z2}) \right]$$

Thus if $N_{Z1} = 0$ and $N_{Z2} = 4$, for example and $D_Z = 636.4$

$$\begin{aligned} C_Y &= 636.4 (1 - 0.9999998) \\ &= 1.3 \times 10^{-4} \text{ arc-sec} \end{aligned}$$

But if $N_{Z1} = 4092$ and $N_{Z2} = 4096$ (near the upper limit)

$$\begin{aligned} C_Y &= 636.4 (0.707649 - 0.707107) \\ &= 0.345 \text{ arc-sec.} \end{aligned}$$

A parallel situation governs the output from the Z channel, whereby the total output should be:

$$B_Z = D \left[\sin (RN_{Z1}) + \sin (RN_{Z2}) - \cos (RN_{Y1}) + \cos (RN_{Y2}) \right]$$

where R is the rotation angle corresponding to each count, or 39.5508 arc-sec.

In addition to the correction for disparity between the rotation angles of the two wedges in each pair, an additional correction must be made for rotation misalignment between the encoder zero and the wedge zero, although this will be reduced to a minimum during assembly.

If we call the zero correction associated with a certain wedge C_{0i} the new outputs become

$$\begin{aligned} B_Y = D \left[\sin \left[R (N_{Y1} - C_{0Y1}) \right] + \sin \left[R (N_{Y2} - C_{0Y2}) \right] \right. \\ \left. - \cos \left[R (N_{Z1} - C_{0Z1}) \right] + \cos \left[R (N_{Z2} - C_{0Z2}) \right] \right] \end{aligned}$$

$$B_Z = D \left[\sin \left[R(N_{Z1} - C_{OZ1}) \right] + \sin \left[R(N_{Z2} - C_{OZ2}) \right] \right. \\ \left. - \cos \left[R(N_{Y1} - C_{OY1}) \right] + \cos \left[R(N_{Y2} - C_{OY2}) \right] \right]$$

B. X-rotation Autocollimator

The deviation in the X-axis as sensed by the autocollimator is less than that in the Y and Z channels for two reasons:

1. The autocollimator senses only a $2 \sin \theta$ component of the true rotation. Since θ has been set at 0.05, this means that the autocollimator "sees" only 1/10th the true rotation.

2. The angular deviation range in the X channel has been set at 5 minutes compared with 15 minutes for the Y and Z channels.

Because of the reduced deviation range, and because the X-rotation autocollimator is a single-axis sensing instrument, we can eliminate one wedge and use a single wedge of

$$636.4/15 = 42.43 \text{ arc-sec deviation.}$$

The output equation from the encoder mounted to the twist-measuring wedge is therefore:

$$B_X = 10 \times 42.43 \sin(RN_X)$$

$$\text{For } N_X = 4096 \text{ and } R = 39.5508 \text{ arc-sec}$$

$B_X = 300 \text{ arc-sec}$, which represents maximum anticipated X-rotation.

C. Search Mode in Y-Z Autocollimator

The wedges will automatically return to a position slightly off encoder zero when a shutdown command is given. Thus a "stow" position is achieved, from which encoder zero may be acquired within a few steps, thus saving time when starting up.

Assuming that the stow position is at -8, for example, the sequence of commands after startup would be as shown in the table below. (Only one motor will be driven at a time.)

Procedure	Wedge Channel	Command	Time Required
1	Y	Step in + direction until both Y encoder zeroes have been acquired, and reset counters Y_1 and Y_2 at their respective zeroes. (If zeroes have not been acquired in 1024 steps, step in - direction until this is achieved.	Normally 0.133 sec. Max. 51.2 sec.
2	Z	Repeat above	Normally 0.133 sec. Max. 51.2 sec.
3	X	Repeat above	Normally 0.133 sec.
4	If signal has been achieved in either Y or Z channel, switch all channels to control mode. If there is no signal in any channel then,		
5	Y	Step to -3072 encoder counts in -Y direction until signal is acquired in either axis, then switch to control mode. If signal is not acquired proceed to step 6.	Up to 8.53 sec.

Procedure	Wedge Channel	Command	Time Required
6	Z	Step to 3072 in +Z direction. If signal is acquired proceed to step 5, if not proceed to step 7, etc.	8.53 sec.
7	Y	Step to 3072 in +Y direction.	17.06 sec.
8	Z	Step to 3072 in -Z direction.	17.06 sec.
9	Y	Step in -Y direction. Signal should be acquired before reaching count -3072.	17.06 sec.

No search mode is required for the X axis.

It will be seen that finding the encoder zero will normally be accomplished in all axes in one second of time because of the stowing procedure, and the search mode can be completed in not more than 77 seconds.

Each count represents 0.081 arc-sec of X-rotation at $\phi = 0^\circ$ and 0.0575 arc-sec at 45° .

The above-stated values of wedge constant (636.4 and 42.43 arc-seconds) are the nominal values designed to achieve the specified measuring range with exactly 45° rotation. A tolerance of 2 percent is specified for the YZ wedges, however, and 5 percent for the X wedge in order to avoid unnecessarily difficult fabrication. The deviation per step or per count will be proportionally increased or decreased, therefore, and the required range of wedge rotation decreased or increased, respectively. The exact calibration will be supplied with each instrument.

No stops are provided in the wedge drive, and the maximum measuring range of each channel is greater than that specified by about $\sqrt{2}$, the maximum being achieved by wedge rotation angles of $\pm 90^\circ$.

Step 1
direction

Step 2
direction

Step 3
Step 4
Step 5
Step 6

normal

beam

conductor

beam

at the end of

beam

at the end of

the beam

to the end of

and the end of

the beam

will be at the end of

the beam

return

each channel

3.1 OPTICAL SYSTEM

The optical system design for the ATA is not a new or novel one, but has been used and proven in various adaptations in many previous autocollimator systems. The optical system shown schematically in Figure 3.1A and 3.1B is conveniently divided into three major subassemblies: the optical head, the beam deviation wedges and the remote reflectors. A tabulation of system parameters is included in Appendix B.

3.1.1 Optical Head

The optical head, or autocollimator proper, is shown schematically in Figure 3.2 and specifications are given in Table 3.1. Figure 3.2 shows the Y-Z autocollimator. The twist sensing autocollimator or X-channel is the same, but has only one error detector pair, i.e. error detector pair number 1. The specifications are grouped into surfaces and distances to the next surface. The surface numbers appearing in Table 3.1 correspond to the numbering scheme in Figure 3.2. Each surface is specified by a radius of curvature and tolerance (∞ indicates that it is flat), whether concave (cc) or convex (cx) and the clear aperture at that surface. Distances between surfaces are given as a thickness and tolerance and the material composing the space between surfaces (i.e. whether air or glass). Specifications are also given on the allowable scratches and digs, i.e. surface code, on permissible departure from a spherical shape, i.e. surface irregularities, and optical coating type to be used on the surface.

A narrow bandpass filter is placed in front of each detector (used in single pass) and is selected for transmission only in the wavelength band of the source and provides

TABLE 3.1
OPTICAL SYSTEM DATA SHEET

SYSTEM DESCRIPTION: <u>ATA FOR MAGSAT: OBJECTIVE LENS TO SOURCE</u>										
PROJECT NO. <u>2081</u>										
SURF. NO.	mm. RADIUS & TOL In.	CC or CX	mm. CLEAR APER In.	mm. THK & TOL In.	MATERIAL	SURF. CODE	IRREG (fr.)	COATING		
								TYPE	THK	$\lambda(\mu)$
				∞	AIR					
1	54.428 $\pm .20$ mm	CX	29 mm			80-50	$\lambda/2$	**HEAR	$\lambda/4$	0.94
				8.06 $\pm .08$ mm	573 575 BAK-1					
2	40.031 ± 30 mm	CX CV	29 mm			80-50	$\lambda/2$	CEMENT		-
				2.5 $\pm .08$ mm	636 353 F6					
3	676.664 ± 1.3 mm	CX	29 mm			80-50	$\lambda/2$	HEAR	$\lambda/4$	0.94
				*85.45 mm NOM	AIR					
4A	∞	-	10 mm			80-50	$\lambda/4$	HEAR	$\lambda/4$	0.94
				10 mm NOM Cube 1	517 642 BK-7					
5a	∞	-	10 mm			40-20	$\lambda/4$	CEMENT		
				1 mm	Slide Glass					
6A	∞	YZ X	.127mm x .127mm (Source Ret)			40-20	$\lambda/4$	CEMENT		
			.127mm x 1.02 mm	1.27 $\pm .03$ mm	717 295 SF-1					
7A	1.27 $\pm .02$ mm	CX	0.6mm			60-40	$\lambda/2$	HEAR	$\lambda/4$.94
				to be determined	AIR					
8A	Source	-				-	-	-	-	-

REMARKS:

*The space between surface 3 and 4A contains 1mm thick beam splitter tilted @ 45° about y and 1.0 thick micrometer plate tilted @ 20° about y axis. Both are Glass Type 517 642 (BK-7) fine annealed with surface flatness $\lambda/4$ and HEAR** antireflection coating on all surfaces except beam splitting surface. **HEAR = high efficiency anti-reflection coating.

EFL = 101.6mm = 4 inches
BFL = 13.8mm BK-7 + 85.45 AIR
Clear Aperture = 29mm f/3.5

TABLE 3.1
OPTICAL SYSTEM DATA SHEET
(Continued)

SYSTEM DESCRIPTION: ATA FOR MAGSAT: OBJECTIVE LENS TO ERROR

PROJECT NO. 2081 DETECTOR

SURF. NO.	mm. RADIUS & TOL In.	CC or CX	mm. CLEAR APERTURE In.	mm. THK & TOL In.	MATERIAL	SURF. CODE	IRREG (fr.)	COATING		
								TYPE	THK	$\lambda(\mu)$
1-4B	Surfaces 1-1 to 4A	4B	The same as (Cube 2)			40-20	$\lambda/4$	*		
				1 mm	517-642 BK-7					
5B	∞	-	10 mm			40-20	$\lambda/4$	CEMENT		
				10 mm NOM Cube 2	517-642 BK-7					
6B	∞	-	10 mm			40-20	$\lambda/4$	HEAR $\lambda/4$.94
				ZERO (NOM.)	AIR					
7B	Detector	-	-			-	-	-	-	-

REMARKS:

Beam Splitter Coatings:

Cube 1 - Gold Metallic T = 80% \pm 5% @ 0.94 micron

Cube 2 - Dielectric R + T = 0.95 MIN @ 0.9 micron

R - T = 0.10 MIN @ 0.9 micron

Beam Splitter: Same as Cube 2, specified at 45° angle of incidence

Cubes are optical glass, fine annealed.

Cement is EPO-TEK 301

*Dielectric Multilayer: Transmission = 0.5 @ .940 micron

Bandwidth = 100 Å°

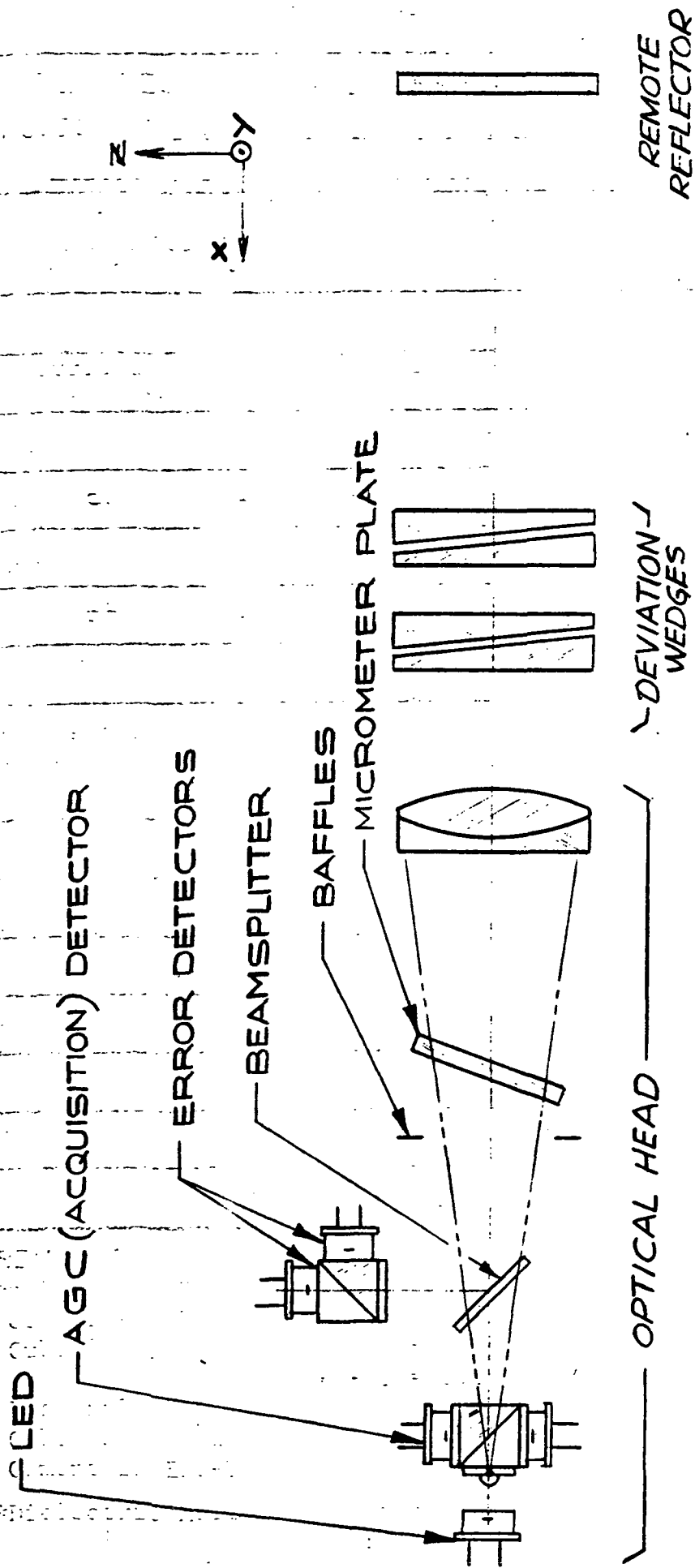


Figure 3.1A
ATTITUDE TRANSFER ASSEMBLY OPTICAL SYSTEMS
YZ CHANNEL

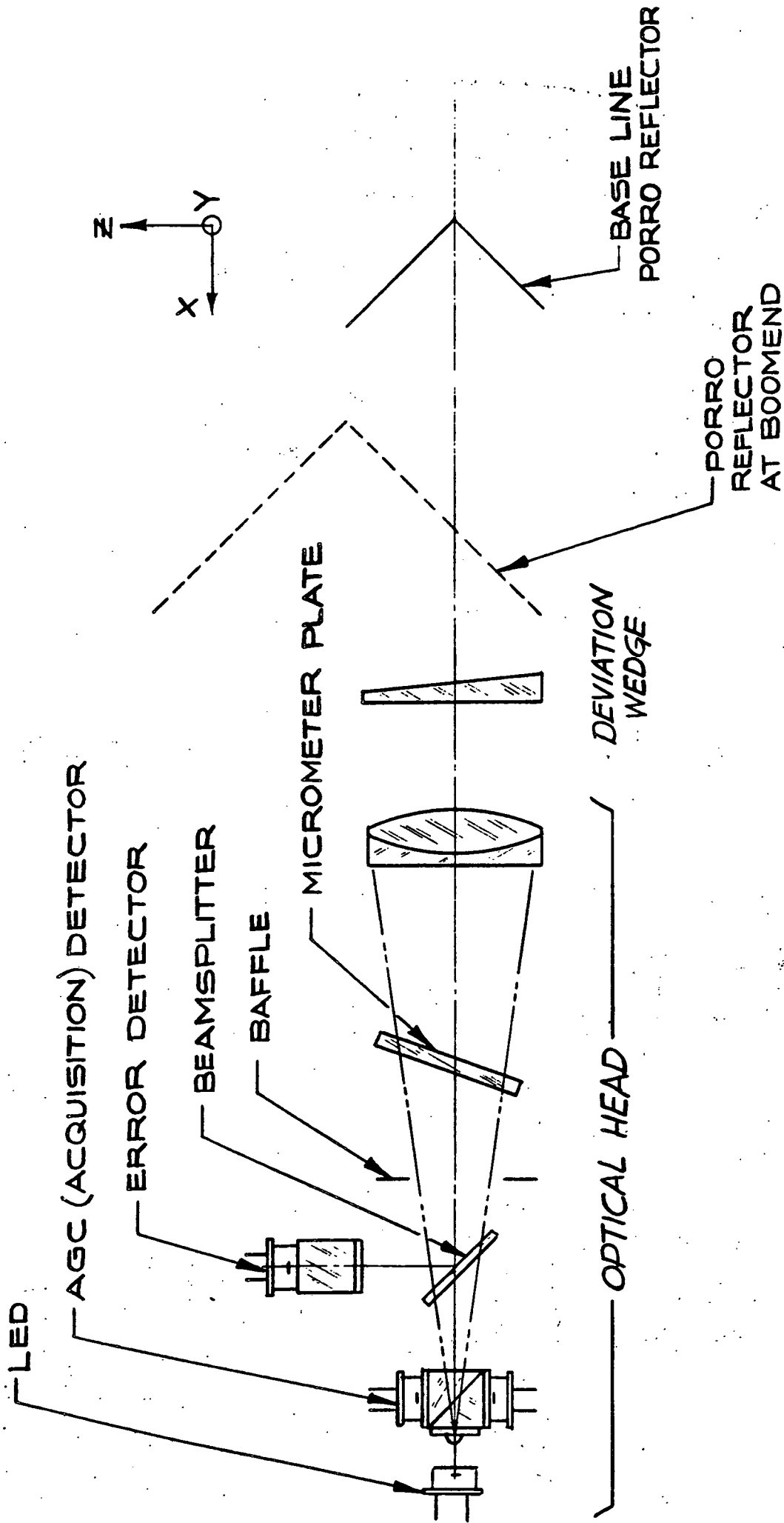


Fig. 3.1B
 ATTITUDE TRANSFER ASSEMBLY OPTICAL SYSTEM
 X (TWIST SENSING) CHANNEL

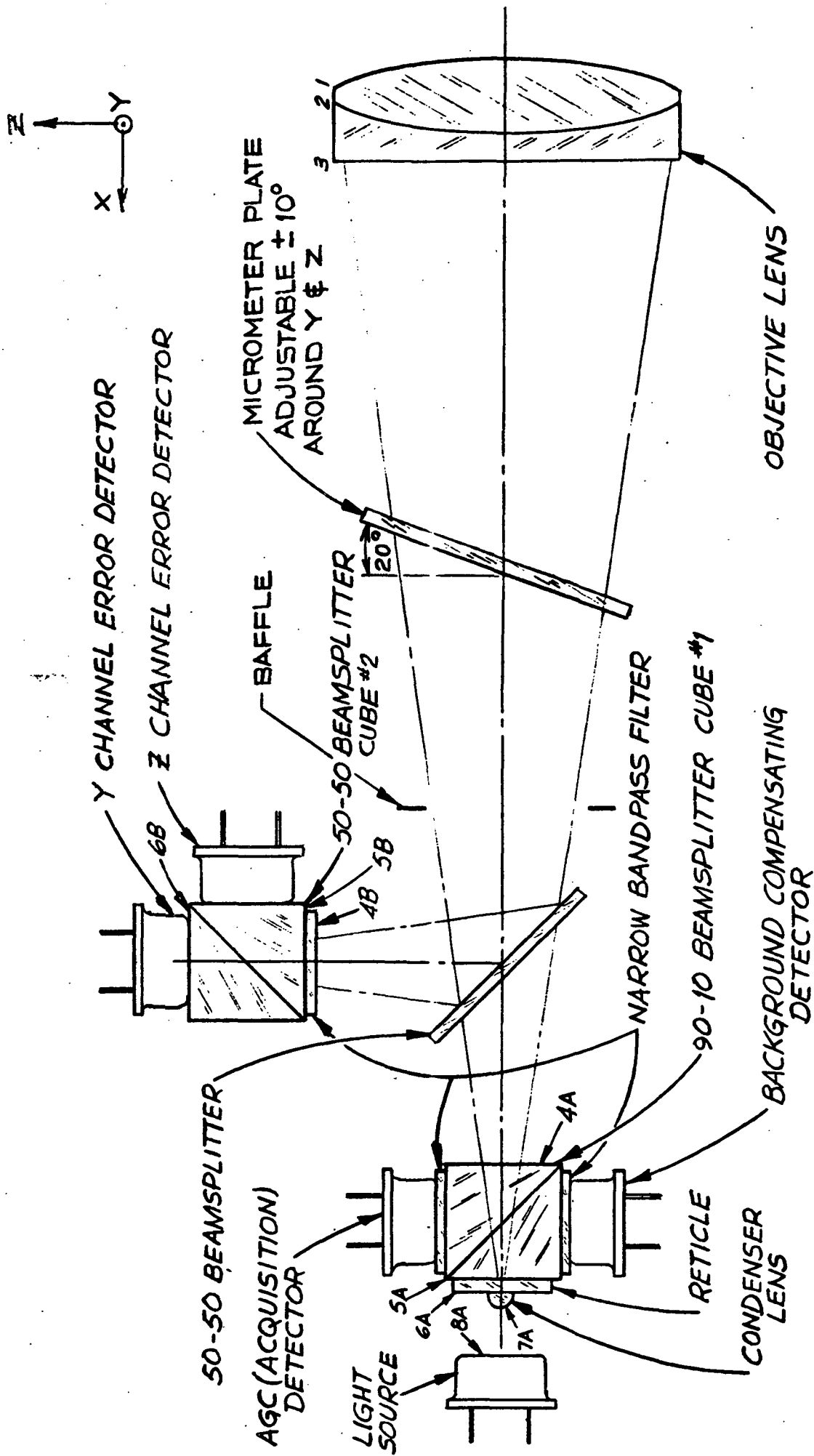


Fig. 3.2
OPTICAL SCHEMATIC
AUTOCOLLIMATOR FOR MAGSAT

an additional protection against stray sunlight which might enter the instrument. The optical coating will be a dielectric multilayer with a bandwidth of 100 Angstrom. The primary means of differentiation between sunlight and the autocollimated image is the pulsed mode of operation, followed by synchronous demodulation of the output signal. The narrow acceptance angle of 10×21 milliradians also helps provide protection against the intrusion of sunlight.

The beam splitting cubes form two major sub-assemblies of the optical head, see Figure 3.2. Each cube is fabricated by cementing two right angle prisms (10 mm per side) together. One prism in each cube has a beam splitter coating as specified in Table 3.1. All faces have HEAR (high efficiency anti-reflection) coatings. Associated with cube 1 are the AGC (acquisition) detector, the source reticle, the condenser lens and an additional detector to compensate for background radiation, which is due to light scattering and spurious reflections. With the addition of the compensating detector, the background signal level may be nulled out.

The source reticle is a slide glass with an opaque coating. The central area is a transparent square .127 mm (0.005 in.) on each side for the Y-Z channel. In the X channel the reticle is a rectangle .127 mm high by 1.02 mm (.040 in) long. The need for a rectangular reticle in the X channel is discussed in Section 2. This opaque surface lies in the focal plane of the system. The detectors and especially the error detectors are made to be coplanar with this surface. The source reticle may be considered to be the system source from which light emanates.

Cemented to the source reticle is the condenser lens which is used to image the LED surface onto the entrance pupil of the system (i.e. the aperture of the lens) so that the brightness of the projected reticle is maximized. It also provides uniform illumination of the source reticle.

3.1.1.1 Light Source

The light source, Texas Instrument LEDTIL 33, is located directly behind the condenser lens. This is a P-N Gallium Arsenide device operating at 0.94 microns, with an emitting surface 0.015 inch square. The data sheet is included in the Appendix, supplemented by additional information received from the manufacturer.

3.1.1.1.1 Calculation of Radiance

Using TI's data for this calculation of radiance, the maximum forward current at 25°C is 200 mA and derating this at 1.6 mA/°C*to 30°C gives 192 mA maximum continuous forward current. TI's data shows that the forward conduction characteristics (i.e. current versus voltage) follow a linear relationship which is written as

$$I = 0.385 (V - 1.3) + 0.050 \text{ amps} \quad (3-1)$$

and in terms of voltage

$$V = 2.6 (I + .450) \quad (3-2)$$

Then for $I = 192 \text{ mA}$,

$$V = 1.669 \text{ volts}$$

$$\text{and } P = I V = 320 \text{ mW (dissipated power)} \quad (3-3)$$

Derating this power by 65% as per NASA practice

$$P = 0.35 \times 320 = 112 \text{ mW} \quad (3-4)$$

Since the LED is to be driven with a 50% duty cycle, peak power is

$$P_{p-p} = 224 \text{ mW}$$

*This derating value differs from the presently-published TI data sheet, and was supplied as updated information by TI's Engineering Dept.

To find the current at this power,

$$P = I V \quad (3-5)$$

$$P = I (2.5 I + 1.17) \quad (3-6)$$

$$.224 \text{ Watts} = 2.6 I^2 + 1.17 I \quad (3-7)$$

Solving equation (3-7) gives the peak current value, $I = 145 \text{ mA}$. The operating level will however be 100 mA to allow a margin for AGC to elevate current without exceeding the 145 mA maximum. The radiant power, P_o at 100 mA is given by TI as

$$P_o = 5 \text{ mW}$$

The emitting surface of the TIL 33 is assumed to be a Lambertian surface such that P_o is radiated into the hemisphere surrounding the LED. The power radiated per unit area per unit solid angle, i.e. the radiance, is given by

$$N = P_o / A \omega \quad (3-8)$$

where A is the emitting surface area of the TIL33

$$A = 1.45 \times 10^{-3} \text{ cm}^2$$

$$N = \frac{5.0 \times 10^{-3} \text{ W}}{(\pi) \times 1.45 \times 10^{-3} \text{ cm}^2} \quad (3-9)$$

$$N = 1.098 \text{ W/cm}^2/\text{ster (peak to peak)} \quad (3-10)$$

This radiance will be used in the next section to calculate the signal level on the detectors.

3.1.1.2 Detectors

The primary signal detectors are associated with beam splitting cube number 2 (Figure 3.2) in the second major subassembly of the optical head and consist of two silicon planar photodetector elements for each axis with a responsivity matching to better than 5%. The separation of the error detector elements is defined by a detector reticle

which is made opaque by means of evaporated aluminum or nickel except for the active areas; this separation being 0.089 mm, (0.0035 in.) to provide the push-pull effect in the open loop operation described in Section 2. The active areas are 1 mm squares. Each pair of detectors will be encased in a TO-5 case and fitted with an AR coated window. The error detector configuration is shown in Figure 3.3. An SCD defining the device as required for another program is included in Appendix D, with the few modifications required for this system indicated.

The configuration of the AGC detector is the same except for the photodetector element. In the AGC and compensation detectors there will be only one element 1.0 mm x 2.0 mm in size.

3.1.1.2.1 Signal Amplitude

The necessary calculations to determine the signal current amplitudes generated by the acquisition (AGC) detectors and error detectors are described below. There are four amplitudes that must be calculated; the acquisition detector and error detector amplitudes in the YZ channel and the acquisition detector and error detector amplitudes in the X channel. This is made necessary because of the difference in transmittance of the four different optical paths but particularly because the error detectors sense only a small portion of the image while the AGC detectors respond to its entire area. The signal current amplitudes for each path are listed in Table 3.2 with all other parameters used in the calculations. The optical paths are designated (see Figure 3.1A and 3.1B) as follows:

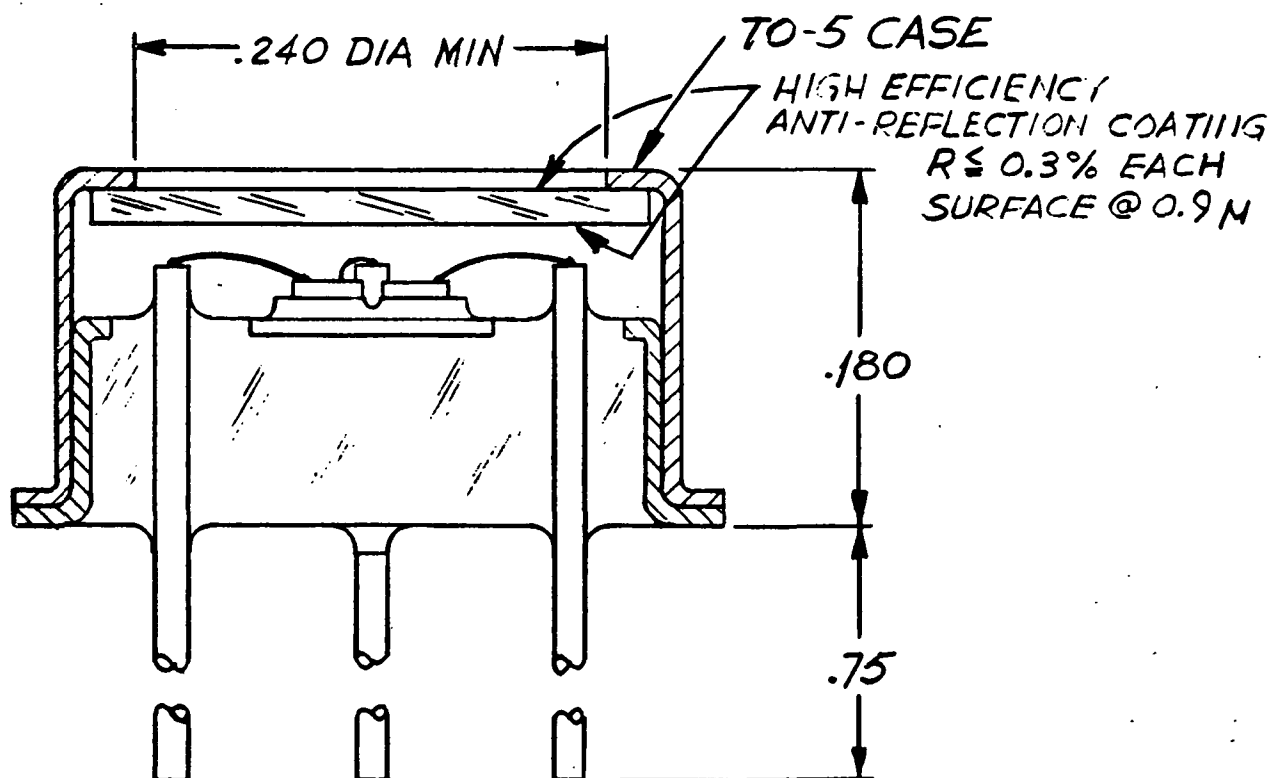
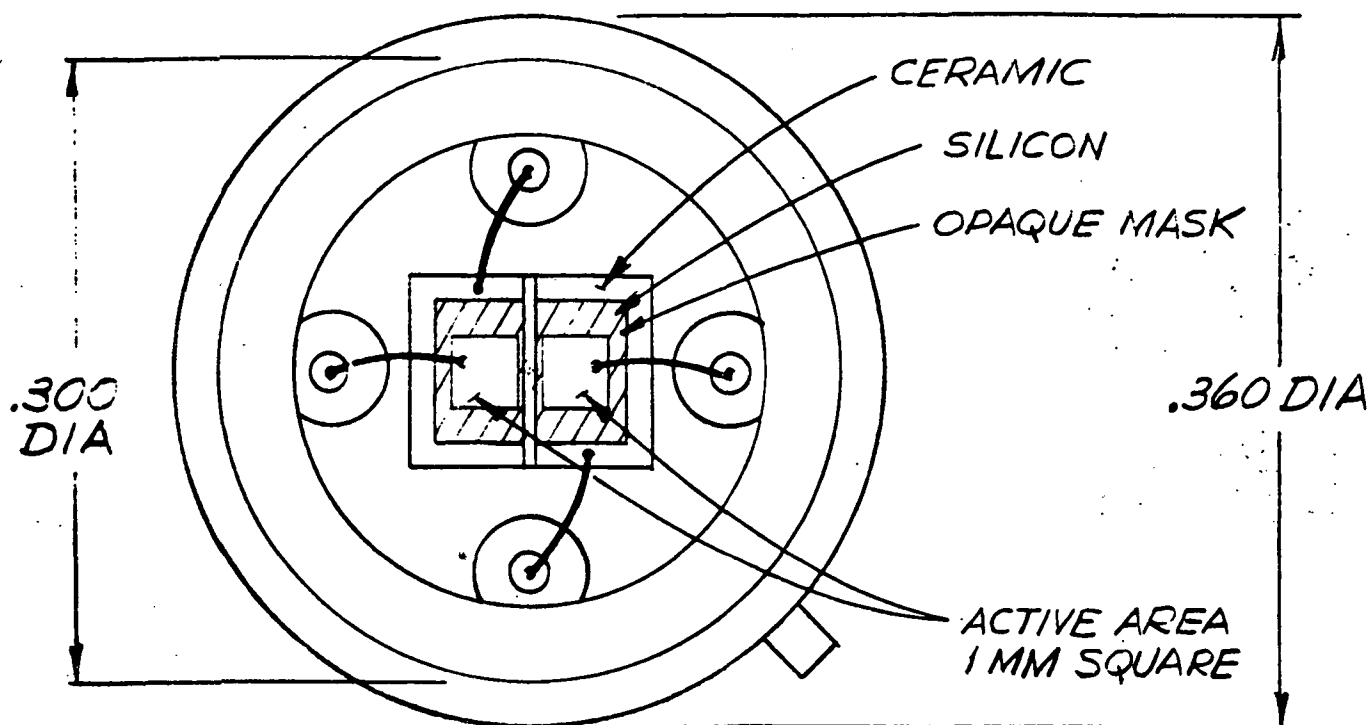


Fig. 3.3 ERROR DETECTOR CONFIGURATION

in the YZ Channel:

1. LED to AGC detector path = AGC_{YZ}
2. LED to Error detector path = $ERROR_{YZ}$

in the X Channel:

3. LED to AGC detector path = AGC_X
4. LED to Error detector path = $ERROR_X$

The parameters associated with all paths are listed in the System column. The signal current amplitude is determined from the irradiance (watts/cm^2) in the image plane, the characteristics (i.e. responsivity) of the detectors, and the image area contributing to signal.

The irradiance at the center of the image is given by

$$H = NT\omega \quad (3-11)$$

where H = irradiance in image plane (watts/cm^2)
 N = radiance of source ($\text{watts/cm}^2/\text{ster}$) as calculated in Section 3.1.1.1.1

T = transmittance of the system for each of the four optical paths

ω = solid angle subtended by the pupil as seen in the image plane, equal to the area of the pupil / (focal length)²

For the $ERROR_{YZ}$ and $ERROR_X$ paths it is important to determine the incremental signal current amplitude generated by an incremental change in equivalent mirror rotation. The mirror rotations are defined as follows:

dx = incremental mirror rotation about X axis (twist)

dy = incremental mirror rotation about Y axis

dz = incremental mirror rotation about Z axis

In discussing ERROR_{YZ} , dy is considered equivalent to dz .

The image area dA_{YZ} transferred onto the detector resulting from an equivalent mirror rotation dy is

$$dA_{YZ} = h \delta \quad (3-12)$$

where δ_{YZ} = incremental width

The incremental width δ_{YZ} may be expressed in terms of incremental angle dy and the focal length, f

$$\delta_{YZ} = 2 f dy \quad (3-13)$$

Substituting for δ , the incremental area dA_{YZ} is written as

$$dA_{YZ} = 2 h f dy \text{ (cm}^2\text{)} \quad (3-14)$$

The value of dA_{YZ} for an equivalent mirror rotation of

$dy = 1 \text{ arc sec } (4.848 \times 10^{-6} \text{ rad})$ is

$$dA_{YZ} = 1.25 \times 10^{-6} \text{ cm}^2$$

In the twist sensing X channel, a twist dx of the Porro reflector will result in an incremental beam deviation dD_X (the angle between the optical axis and return beam) given by

$$dD_X = 4 dx \sin \theta \quad (3-15)$$

where θ is the offset angle = 2.866 degrees

$$\sin \theta = 0.0500$$

The incremental image translation onto the detector, as above, is related to beam deviation by

$$\delta_X = f dD_X \quad (3-16)$$

It should be noted that the factor of 2 is not needed in the above equation since it is already expressed in terms of beam deviation not mirror rotation angle as is the expression for δ_{YZ} .

The incremental area of the image dA_X transferred onto the detector is given as above

$$dA_X = h' \delta_X \quad (3-17)$$

where h' is the width of the image in the X channel autocollimator. The width of the image is not the same as the width of the reticle in the X channel (0.0127 cm x 0.102 cm) due to vignetting. The value of h' is determined from a consideration of the distance from the optical axis ($\frac{h'}{2}$) in the image plane at which the intensity has decreased to zero.

This value is

$$h' = 0.024 \text{ cm} = 0.0095 \text{ inch}$$

The final expression for the incremental area dA_X is thus

$$dA_X = 4 h' f dx \sin \theta \quad (3-18)$$

The value of dA_X for a twist angle $dx = 1 \text{ arc sec} = 4.848 \times 10^{-6} \text{ rad}$

$$dA_X = 2.377 \times 10^{-7} \text{ cm}^2$$

The incremental incident flux, dP is given by (for both Y-Z channel and X channel)

$$dP = H_e V dA \text{ (watts)} \quad (3-19)$$

Where V is a vignetting factor (less than one) introduced to account for decreased intensity of the edge of the image due to vignetting. Vignetting and its effects are discussed

in Section 3.1.1.4. The effective irradiance in the image plane may thus be defined as

$$H_e = HV$$

The incremental signal current generated by the incident flux, dP is given by

$$dI = 2R \, dP \text{ (amps)} \quad (3-20)$$

The factor of 2 appears because the image overlaps the detectors at null (see Section 2).

where R = responsivity of the detectors = 0.4 amps/watt.

The value for the incremental current in $ERROR_{YZ}$ and $ERROR_X$ is listed in Table 3.2.

For the AGC_{YZ} and AGC_X paths the full image area is incident on the detector whenever the remote mirror deviations are within the acquisition range. Thus the full image area is

$$A_{YZ} = 1.613 \times 10^{-4} \text{ cm}^2 \quad \text{image area for YZ channel}$$

$$A_X = 3.073 \times 10^{-4} \text{ cm}^2 \quad \text{image area for X channel}$$

The image dimensions are given in Table 3.2. The radiant power, P , incident on the detector is given by

$$P = H_e A \quad (3-21)$$

The signal current generated by the incident flux (power) is,

$$I = P R \text{ (amps)} \quad (3-22)$$

All values are listed in Table 3.2.

3.1.1.3 Objective Lens

The objective lens is a cemented doublet 3.2 cm in diameter with a clear aperture of 2.9 cm and focal length of 10.16 cm (4 inches). The lens was designed as part of the

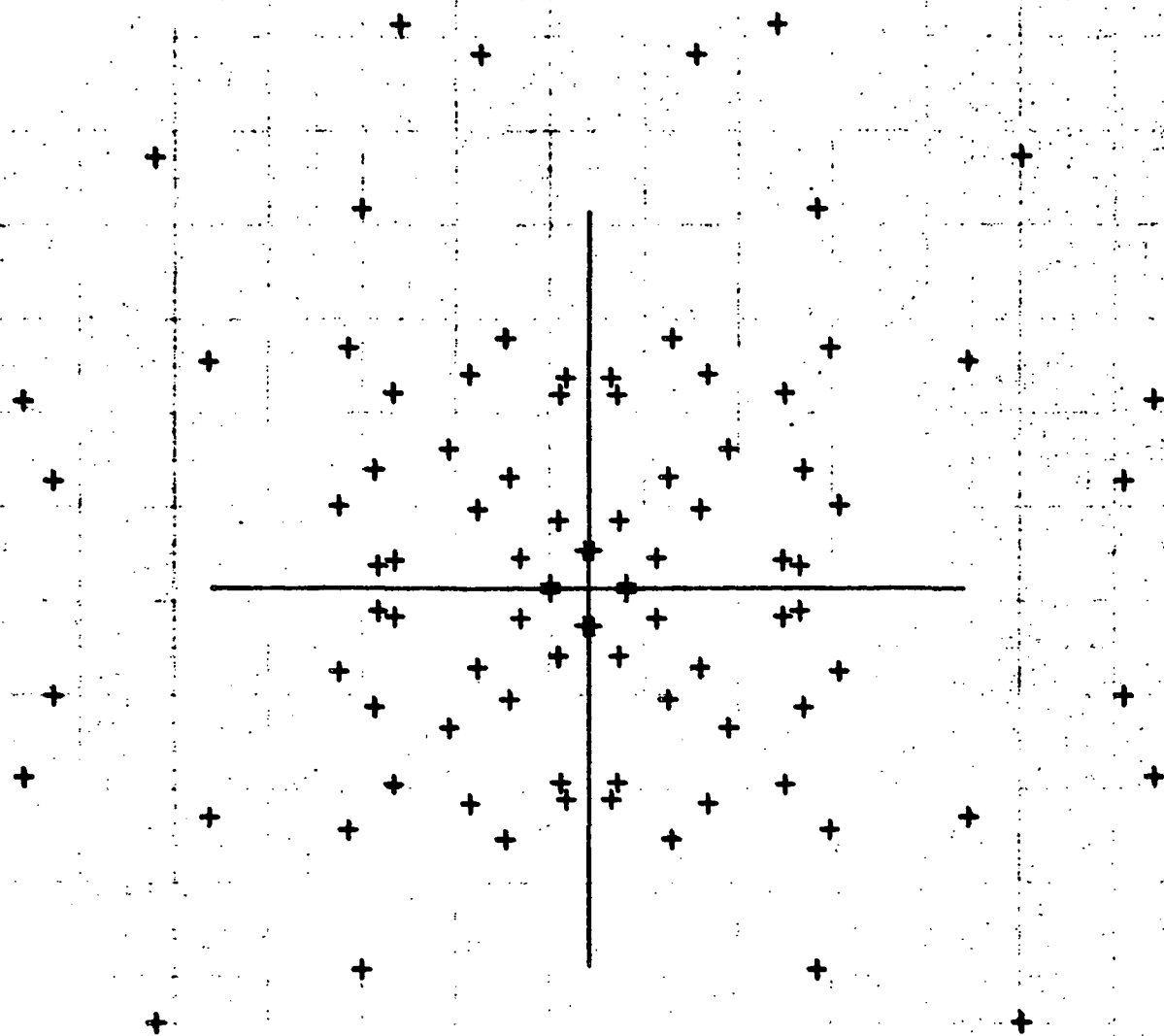
RADIOMETRIC SYSTEM PARAMETERS

Table 3.2

	System	ERROR _{YZ}	AGC _{YZ}	ERROR _X	AGC _X
f, focal length (cm)	10.16	-	-	-	-
d, aperture (cm)	2.9	-	-	-	-
$\omega = \pi d^2 / 4f^2$, solid angle (ster)	0.064	-	-	-	-
T, transmittance	-	0.044	0.009	0.085	0.008
N, source radiance (watts/cm ² /ster)	1.098	-	-	-	-
H = NT ω , irradiance (watts/cm ²)	-	3.091 x 10 ⁻³	6.322 x 10 ⁻⁴	5.973 x 10 ⁻³	5.619 x 10 ⁻⁴
V = Vignetting factor	-	0.65	0.70	0.25	0.40
H _e = effective irradiance (w/cm ²)	-	2.01 x 10 ⁻³	4.43 x 10 ⁻⁴	1.49 x 10 ⁻³	2.25 x 10 ⁻⁴
hr x hr, reticle size (cm)	-	0.0127 x 0.0127	0.0127 x 0.0127	0.0127 x 0.1020	0.0127 x 0.1020
hi x hi image size (cm)	-	0.0127 x 0.0127	0.0127 x 0.0127	0.0127 x 0.0242	0.0127 x 0.0242
g, detector spacing (cm)	0.0089	-	-	-	-
R, detector responsivity (amps/watt)	0.4	-	-	-	-
dA _{yz} = 2h _i fdy incremental area on ₂ ERROR _{yz} detector (cm ²)	-	1.25 x 10 ⁻⁶	-	-	-
dA _x = 4H _i fdxsine incremental area on ERROR _x detector (cm ²)	-	-	-	2.377 x 10 ⁻⁷ cm ²	-
dP = H _e dA incremental flux (watts, p-p)	-	2.51 x 10 ⁻⁹	-	3.54 x 10 ⁻¹⁰	-
dI = 2R dP incremental signal current (amps) for / arc-sec	-	[2.01 x 10 ⁻⁹ (p-p)] [9.04 x 10 ⁻¹⁰ (rms)]	-	[2.83x10 ⁻¹⁰ (p-p)] [1.27x10 ⁻¹⁰ (rms)]	-
A, image area (cm ²)	-	-	1.613 x 10 ⁻⁴	-	3.07 x 10 ⁻⁴
P = H _e A, incident flux on AGC detectors (watts) (p-p)	-	-	7.22 x 10 ⁻⁸	-	6.91 x 10 ⁻⁸
I = RP generated signal current (amps)	-	-	[2.89x10 ⁻⁸ (p-p)] [1.30x10 ⁻⁸ (rms)]	-	[2.76 x 10 ⁻⁸ (p-p)] [1.24 x 10 ⁻⁸ (rms)]

complete system, that is, in use the light passes through the beam splitter, micrometer plate and lens twice. Although the lens is corrected for coma, spherical aberration, astigmatism and color a certain amount of astigmatism is introduced by the tilted parallel plates (micrometer plate and beam splitter) which cannot be corrected. Ray tracing was done for the lens alone and for the entire system (double pass). Spot diagrams were made for the doublepass configuration with all plates perpendicular to the optical axis and with the plates tilted as they will be in actuality. The former indicates the state of correction of the system, and is shown in Figure 3.4, whereas the latter indicates the astigmatism introduced by the tilted plates. The performance of any lens is limited by diffraction. In systems where high resolution is desired diffraction limited performance may be important. For a system, such as the ATA, designed to detect the motion of an image and not to resolve two closely spaced object points, diffraction limited performance is of academic interest. The spot diagrams shown in Figure 3.4 represents a spot size approximately 2.4 times the diffraction limit (for this lens the diffraction limit spot size is 0.008 mm). In Figure 3.5 the spot size has increased to 5.4 times the diffraction limit due to the astigmatism introduced by the tilted plates, but still constitutes a well corrected system.

To determine the best focal plane under the actual astigmatic conditions, energy distributions, i.e. knife-edge plots were made in both the tangential plane (plane of Figure 3.2) and sagittal plane (perpendicular to the plane of Figure 3.2). By shifting the plane in which the "knife" moves, the slope of the knife edge plots shown in



SPOT=0.019MM

CHIEF RAY HEIGHT

0.0000

FOCUS SHIFT

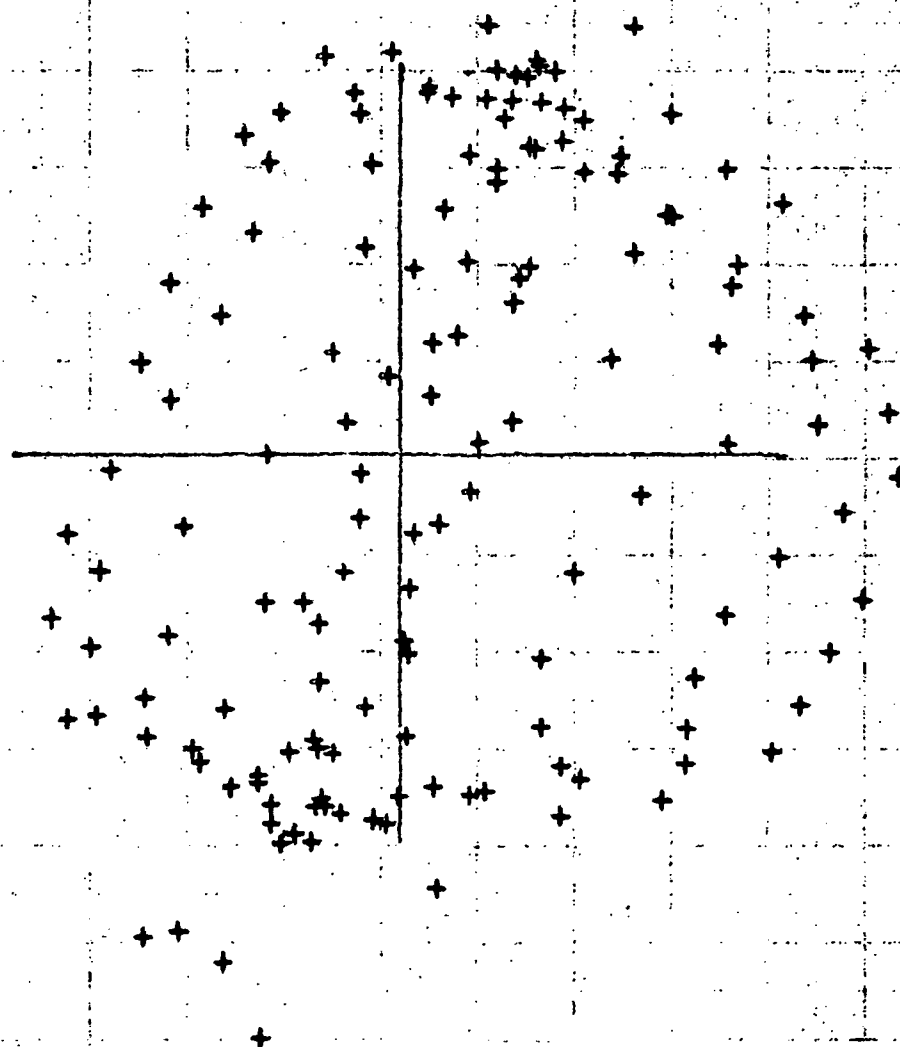
-0.050000

1 INCH = 0.003139

MAGSAT-ATA 2 PASS
WITHOUT TILT

FIGURE 3.4

MAGSAT
SPOT DIAGRAM - 2 PASS
BEST FOCUS



CHIEF RAY HEIGHT

-0.0000

FOCUS SHIFT

-0.220000

1 INCH = 0.010841

SPOT SIZE = 0.043 MM

FIGURE 3.5

Figures 3.6 and 3.7 may be made approximately the same. The plane in which this approximate equality of slope occurs will be the nominal "best focus" plane. The spot diagram shown in Figure 3.5 is in the plane of best focus.

The lens surfaces are coated with a high efficiency anti-reflection coating peaked for 0.94 microns. Specifications for the lens are given in Table 3.1.

3.1.1.3.1 Open Loop Linear Range

In general, the linear range of an autocollimator with a fixed pointing direction and where the reticle size and detector gap have the same nominal dimensions is a function of the source reticle size and focal length and is given by the relationship

$$\alpha = h / 2 f \quad (3-23)$$

h = source reticle size

f = focal length

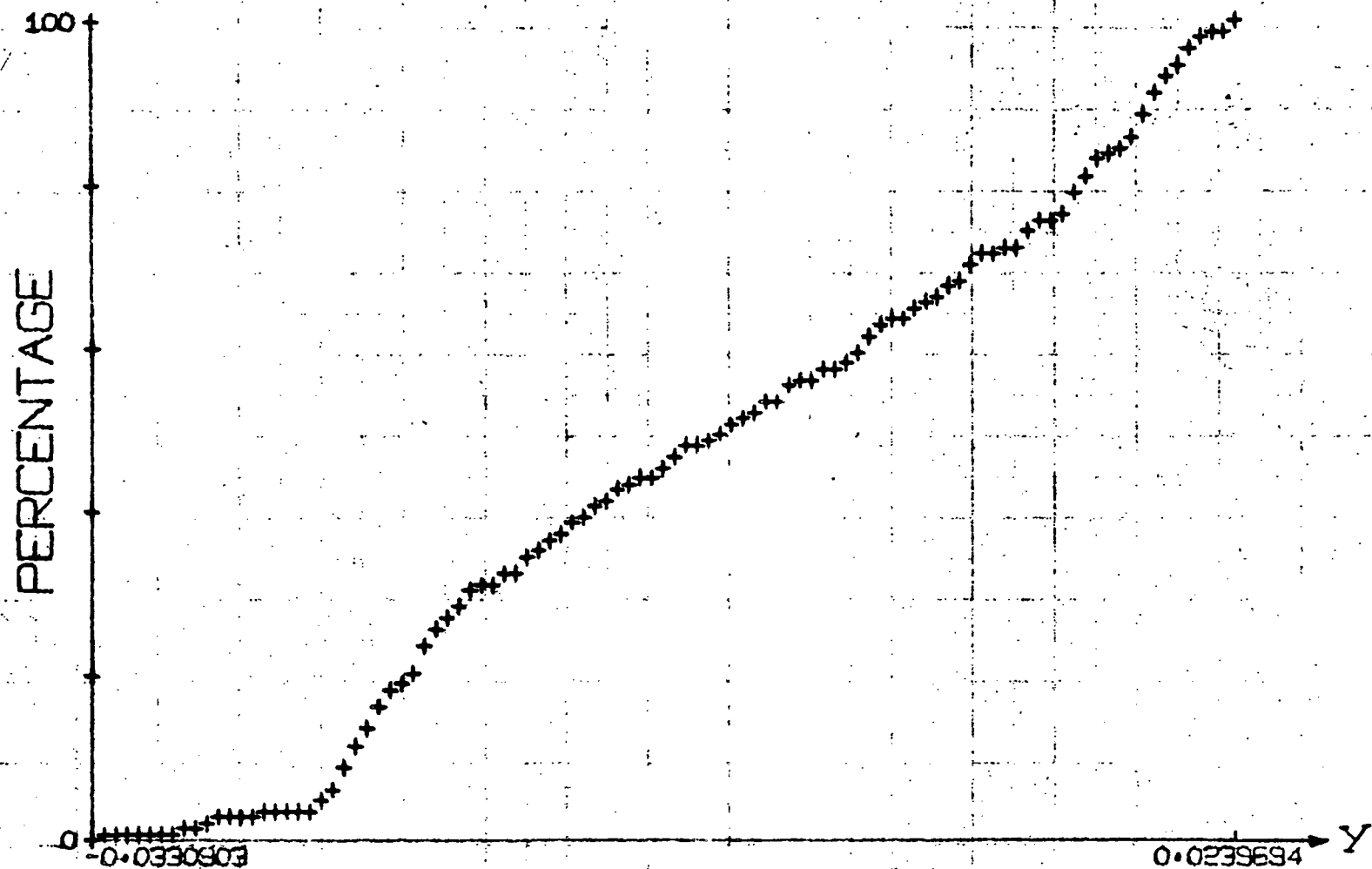
α = mirror rotation

The factor of 2 is due to the angular beam deviation being twice the mirror rotation (Law of Reflection).

In the ATA, the above case is modified due to the difference in size of the detector gap and reticle size. As explained in section 2 the overlap of the image on the detector allows the sensitivity to be doubled in the range of overlap. This is of importance mainly in the twist channel where the intensity of the image is decreased by more severe vignetting than the YZ channel due to the doubled optical path (four times the boom length).

The overlap on each detector, b , (see Figure 2.3A) is given by

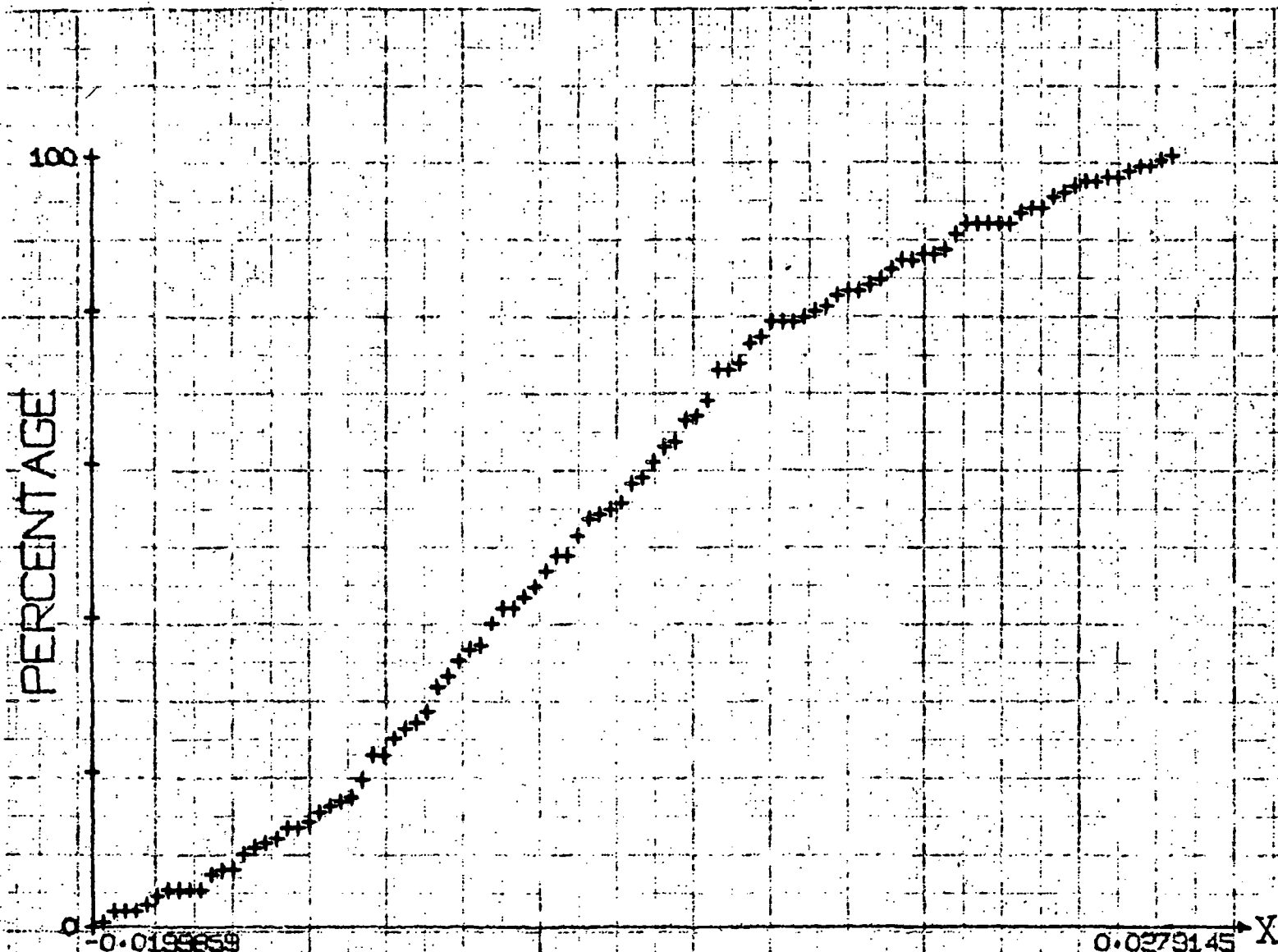
$$b = \frac{h-g}{2} \quad (3-24)$$



KNIFE POSITION- PARALLEL TO X-AXIS

CHIEF RAY HEIGHT	-0.0000
FOCUS SHIFT	-0.220000
ORIENTATION ANGLE	0.0

FIGURE 3.6



KNIFE POSITION-PARALLEL TO Y-AXIS

CHIEF RAY HEIGHT	-0.0000
FOCUS SHIFT	-0.220000
ORIENTATION ANGLE	0.0

FIGURE 3.7

where the magnitude of h is 0.005 in. (0.0127 cm) and g , the detector gap is 0.0035 in. (0.0089 cm).

The open loop linear range may thus be limited to that range in which the transfer function increases at twice the rate as it does in equation (3-23) (see Figure 2.3B) and is given by (for the YZ channel)

$$y_L = b / 2 f = (h-g)/4f \quad (3-25)$$

and substituting the above values ($f = 4$ in. or 10.16 cm) gives a magnitude for the open loop linear range of

$$y_L = 19.34 \text{ arc sec}$$

For practical reasons the open loop linear range has been set at 15 arc sec.

3.1.1.4 Vignetting

"Light" (actually near infrared energy) from each point in the source reticle aperture fills the objective lens aperture or pupil and then is projected in a cylindrical bundle toward the reflector. (The effects of aberration and diffraction will be treated separately.) That bundle which originates at the center of the source reticle emerges parallel to the optical axis; all other bundles are inclined to the axis by an angle given by a/f , where a is the distance of any point in the reticle from the center, and f is the auto-collimator focal length.

The full beam has a divergence, therefore, determined by reticle size and focal length. Immediately in front of the objective lens the beam has a circular cross-section as determined by the objective lens; at greater distances its shape is square with rounded corners, and increases in size with projection distance.

This beam is incident on the remote mirror and reflected back to the aperture of the autocollimator. It continues to increase in size, so that when it re-enters the autocollimator the outer part of the beam is "vignetted" or lost by the trimming effect of the lens aperture. Therefore, the outer portions of the refocused image have lower intensity, since the vignetting effect afflicts the outer edges more severely; the center is not affected. It does no good to increase the size of the remote reflector, beyond that of the lens since the vignetting depends only on the lens aperture size, focal length, source reticle size, and distance to the reflector and back.

By means of similar triangles, it may be shown that the maximum image dimension that may be formed is given by:

$$h_{\max} = d f / D \quad (3-26)$$

where d = pupil diameter or width

D = distance to reflector

f = focal length

Restating the same relationship differently, the maximum distance at which a given point in the source reticle can be reimaged by reflection is given by

$$D_{\max} = 2 d f / a \quad (3-27)$$

The intensity for a given point in the image is proportional to the area of the effective pupil for that point. This is the common area of the actual autocollimator aperture and the displaced circular bundle returning to the autocollimator. The area of overlap is given by the expression:

$$A = 2 \left[r^2 \arcsin \left(\frac{\sqrt{r^2 - s'^2}}{r} \right) - s \sqrt{r^2 - s'^2} \right] \quad (3-28)$$

where r = radius of circular aperture
 s = (displacement of reflected bundle)/2
 $= a D/f$ (when reflected image is not displaced
 by reflector rotation)

This function is normalized and plotted as a function of D/D_{\max} in Figure 3.8. As indicated by equation (3-27) there is a value of D_{\max} associated with every point in the image. By dividing the actual working distance to the reflector by the value of D_{\max} for any point, the relative intensity at that point in the image may be found from Figure 3.8.

The relative intensity for points along the edge of the detector may be calculated by summation or integration, and the amount of energy in an incremental strip calculated. From this, the signal generated by a small angular deviation of the reflector may be calculated.

Following this procedure for the image in the YZ autocollimator, we find that an average factor to represent vignetting of the edges of the image is 0.65. This factor is used to modify the calculation of irradiance H at the center of the image as shown in Table 3.2, and to provide an effective irradiance H_e .

Similar procedure for the X axis error channel yields a vignetting factor of 0.25. The factors for the AGC channels are somewhat larger, since the effective value may be averaged over the entire image.

When the angular deviation is larger, the signal may be calculated by a double integration over the entire image area on one detector vs that on the other detector. Although for a rectangular pupil the resultant expression is not unduly

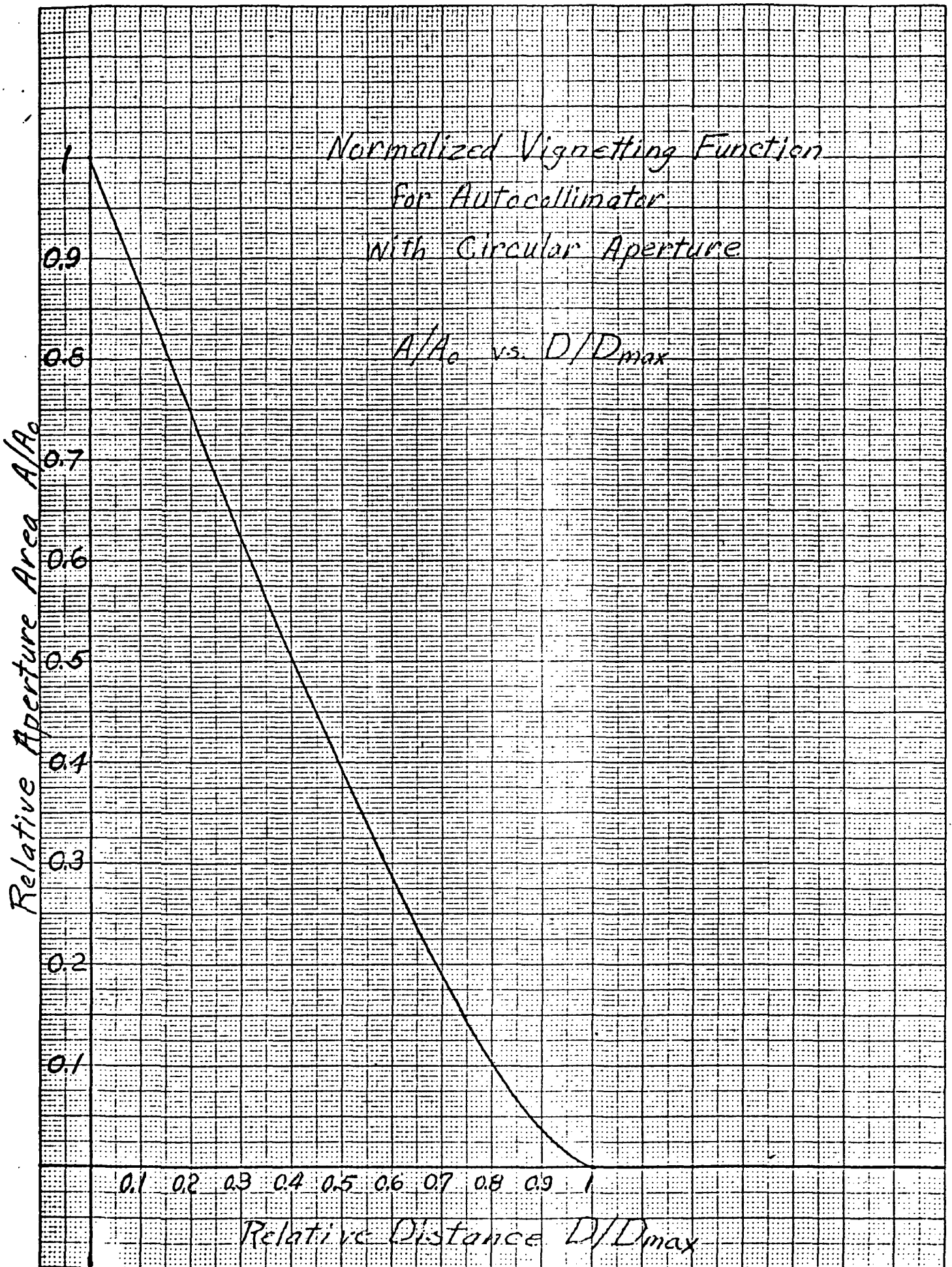


FIGURE 3.8

complicated, it becomes very much so for a circular aperture. The transfer function can be approximated, however, by finite summation. For the limited angular range required by the open loop output of the ATA, this is not difficult.

For larger deviations recognition must be made of the fact that the point of maximum intensity in the image is neither on the optical axis nor at the center of the image, but at a point halfway between, and distance (a) for use in the above equations is taken from this point in calculating intensity in various parts of the image.

Because the large-angle output information will be derived from the wedge-coupled encoders, further analysis of the transfer function is not relevant to the subject of this study.

3.1.1.5 Micrometer Plate

The necessary pre-launch alignment requires precise positioning of the instrument on its base plate with respect to the remote mirror. To expect precise positioning on a one-to-one basis is unrealistic. It is however, possible to make the final precise alignment optically, that is adjusting the angular deviation from the optical axis of the collimated beam so that it is normally incident on the mirror. It may be shown that the beam deviation, α , generated by a tilted plate (the micrometer plate shown in Figure 3.2) is given by the expression

$$\alpha = (t (n-1) / fn) \tan \beta \quad (3-29)$$

where T = micrometer plate thickness = .1 cm
 n = index of refraction = 1.508378 (BK-7 @ 0.94 microns)
 f = focal length = 10.16 cm
 β = tilt of plate

The plate is initially tilted 20° about the Y axis (see Figure 3.2) so that spurious reflections do not enter any detector. The initial beam deviation α_i introduced by the 20° tilt is compensated in alignment by an offset in the optical components such that the outgoing beam is parallel to the optical axis. The angular range β of tilt plate is ± 10 degrees i.e. the range is

$$10^\circ \leq \beta \leq 30^\circ$$

The effective beam deviation α_e is generated by tilting the micrometer plate through its entire range and is obtained from equation (3-29)

$$\alpha_e = \alpha - \alpha_i = (t(n-1) / fn) (\tan \beta - \tan 20^\circ) \quad (3-30)$$

Substituting the various values into equation (3-30) gives the effective beam deviation and therefore the allowable misalignment between the autocollimator and the remote reflector.

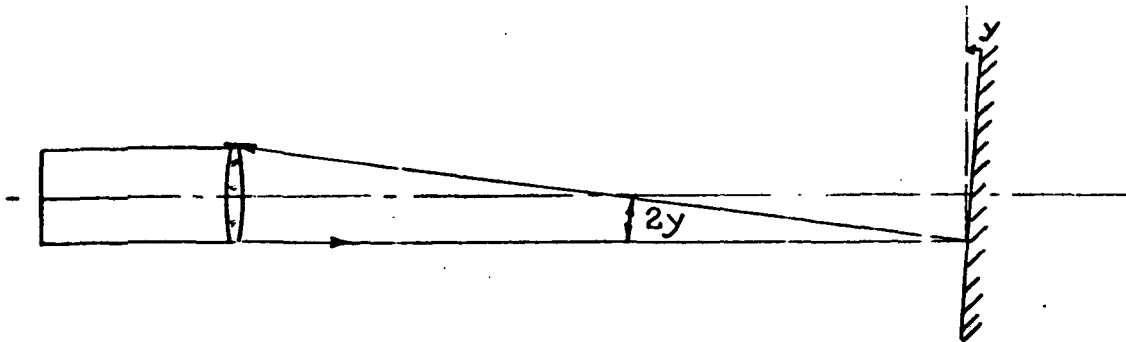
$$-128 \text{ arc sec} \leq \alpha_e \leq 162 \text{ arc sec}$$

From the above discussion, the reduction factor introduced by the tilt plate is 222 to 1, i.e. an adjustment of 222 arc seconds of the tilt plate is required for a 1 arc second deviation of the light beam. It is thus possible to use adjusting components of ordinary precision in the adjusting mechanism. Adjustment of the plate will be accomplished through push-push screws for each axis. Once the adjustments are made, the plate adjusting mechanism is locked in place to assure stability through the launch environment.

3.1.2 Beam Deviation Wedges

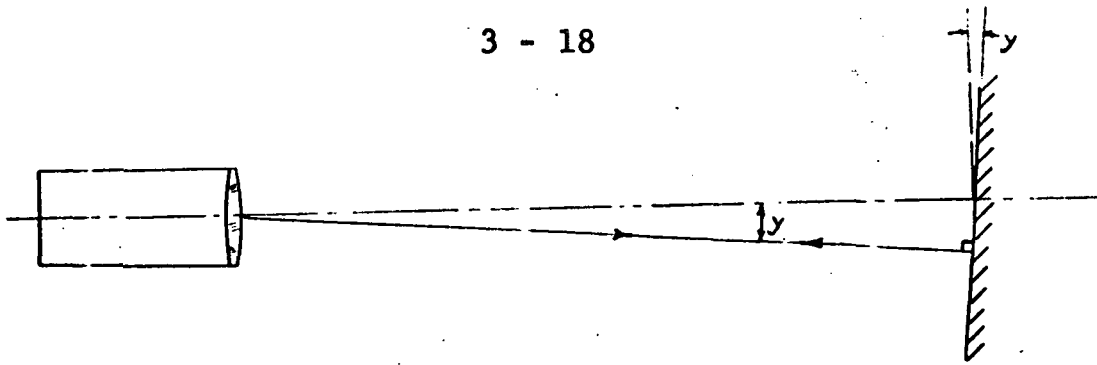
The open loop linear range of the ATA with fixed pointing direction was calculated in section 3.1.1.3.1 to be 19.34 arc-sec. This is much less than the MAGSAT system

requirement of 0.25 degrees (900 arc sec). When mirror rotation exceeds 109.6 arc sec the reticle image will be entirely on one detector as shown in Figure 2.2C. For mirror rotation exceeding 490.6 arc sec, the return beam misses the aperture entirely. This is illustrated schematically below with a single ray.



It is possible to change ATA parameters to meet the linear requirements i.e. enlarge aperture, change focal length and source reticle, but this is not compatible with MAGSAT spacecraft installation, volume and weight constraints. For instance for a static sensor with linear range of 0.25 degrees the aperture would have to be enlarged to 10 or 12 inches.

The approach taken to meet the range requirement for MAGSAT in this study is to deviate from its fixed pointing direction i.e. to track the mirror such that the beam is always normally incident on the mirror. The angular beam deviation is therefore equal to mirror rotation as seen in the illustration below.



In the YZ channel the collimated beam is deflected by means of two optical wedges (thin prisms) for each measuring axis. The two wedges rotate about the optical axis in opposite directions by equal angular amounts, driven by a servo system responding to error detector signals. The wedge function is illustrated in Figure 3.9, the beam deviation of each wedge being represented as a vector. The vector length is the full deviation produced by each wedge, and the direction of the vector is the direction of the deviation.

At the zero position, the two wedges are set so that their deviations cancel; the apex angles are in the plane of the side view of Figure 3.9a.

In response to a signal from the autocollimator error detectors, the wedges rotate equal amounts in opposite directions as in Figure 3.9b. For a given rotation $\phi_1 = \phi_2 = \phi$, the total angular deviation of the transmitted beam is given by

$$D = 2D_1 \sin \phi \quad (3-32)$$

where $D_1 = D_2$, The full deviation of the beam, D , is known when the angle ϕ is determined, since D_1 is a constant and is known. The angular determination is made with an optical encoder.

The rotation angle is limited to $\pm 45^\circ$ because of the more uniform behavior of the sine function in this domain than in the 45° to 90° domain. In addition, by keeping the rotation angle limited to $\pm 45^\circ$, the eccentricity errors of the encoder are minimized.

3.1.2.1 Calculation of Wedge Apex Angle

In order to maintain the rotation angle of $\pm 45^\circ$ in both YZ channels and X channel, thereby allowing the use of similar mechanical and electro mechanical components, the apex angles of the YZ wedges and X wedges must be different. By combining the equation for D and D_1 , the apex angle for the YZ channel may be calculated. From basic optics, the deviation D_1 , of a ray through a thin prism is given by

$$D_1 = A (n - 1) \quad (3-31)$$

where A = apex angle of prism
 n = index of refraction

$$A_{YZ} = D_{YZ} / 2(n-1) \sin \phi \quad (3-33)$$

where $\phi = 45^\circ$
 $D_{YZ} = 0.25^\circ$

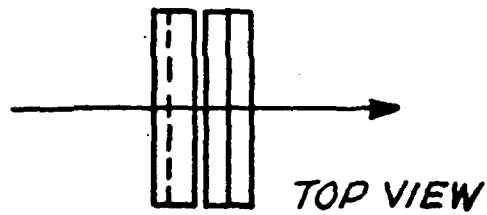
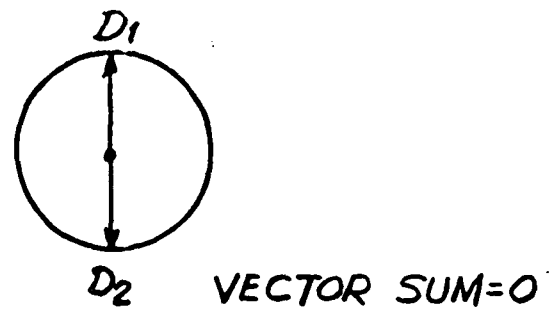
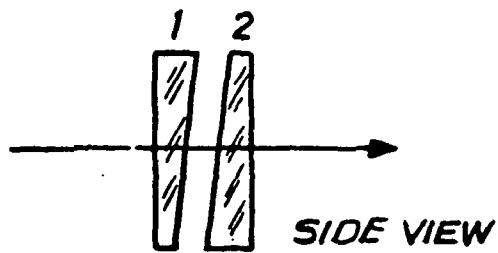
$$n = 1.508378 \text{ (BK-7 @ 0.94 microns)}$$

Then $A_{YZ} = 0.348 \text{ deg} = 1252.80 \text{ arc-sec.}$

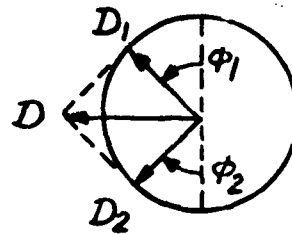
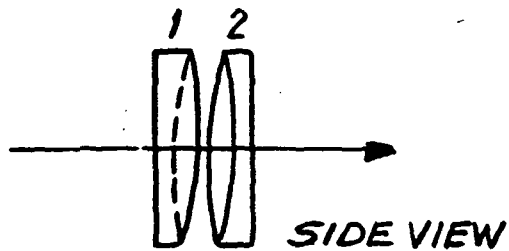
In the X channel only one beam deviation wedge is needed to track the twisting of the boom and therefore the total beam deviation D_X is given by

$$D_X = D_1 \sin \phi_1 = A_X (n-1) \sin \phi_1 \quad (3-34)$$

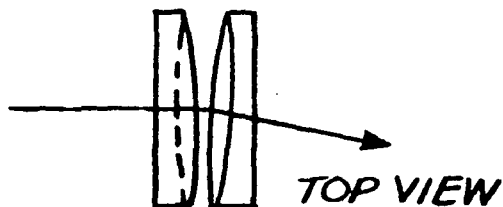
where A_X is the apex angle for the wedge in the X channel. The total beam deviation, D_X , required to null out a twist of amount X is given by



a. "ZERO" POSITION



$$D = D_1 \sin \phi_1 + D_2 \sin \phi_2 = 2 D_1 \sin \phi_1$$



b. ROTATED POSITION

Fig. 3.9 ROTATION AND DEVIATION OF OPTICAL WEDGES IN THE YZ CHANNEL

$$D_X = 2 \times \sin \theta \quad (3-35)$$

where $\theta = 2.866$ degrees, the offset of the X channel autocollimator. The necessary apex angle for the wedge is given by

$$A_X = 2 \times \sin \phi / (n-1) \sin \phi \quad (3-36)$$

$$= 0.023 \text{ degrees} = 83.4 \text{ arc-sec}$$

where $X = 300 \text{ arc sec.}$

In the actual manufacturing process, a large disc is ground and polished to the specified apex angle and surface flatness. The required number of wedges are then cut from this blank, thus assuring that all wedges have the same apex angle. For the ATA these wedges will be sent to NBS for calibration and certification.

3.1.2.2 Optical Wedge Specification

The optical wedges are made of Grade A, fine annealed optical glass, Type BK-7, which has the best combination of characteristics for this application. The wedges will be coated with multilayer antireflection coatings to keep the intensity of reflection at less than 0.3 percent per surface. In addition to this protection, each wedge will be tilted in its cell by 1° so that residual ghost reflections cannot intersect the detectors.

The control of flatness of wedge surfaces and of wedge angle will be achieved by means of proven techniques used in previous programs. The basic approach is to fabricate a wedge blank from which the four required discs can be trepanned. Wedge angle can be controlled more precisely on the large blank, and with the help of flatness specifications, the variation in angle can be kept within acceptable limits.

The close matching of wedges in a given pair is not critical for generation of the required deviation angle, but since cross-coupling error introduced into the orthogonal direction is a function of the difference $(D_1 - D_2) (1 - \cos \phi)$, it is desirable to limit this difference.

Figure 3.10A incorporates the requirements for fabrication of the wedges, with appropriate tolerances and a 2-sheet drawing of the wedge measurement ring 252507-2001.

One half fringe of net curvature as seen on the Twyman-Green interferometer represents a wave deformation of $\frac{1}{2}$ wavelength between the center and the edge of the specified 92 mm measuring aperture. Then a single passage would produce 0.25λ , which at 546.1 nm would equal 1.365×10^{-4} in/in.

Then $t = \text{wavelength retardation} / (n-1)$

$$= 1.365 \times 10^{-4} / 0.50838$$

$$= 2.685 \times 10^{-4} \text{ mm}$$

At radius 28 mm from center, $t = (28/46)^2 \times 2.685 \times 10^{-4} \text{ mm}$

$$= 9.948 \times 10^{-5} \text{ in/in relative to center.}$$

Then slope at 28 mm radius relative to center

$$= 9.948 \times 10^{-5} / 28$$

$$= 3.553 \times 10^{-6} \text{ rad}$$

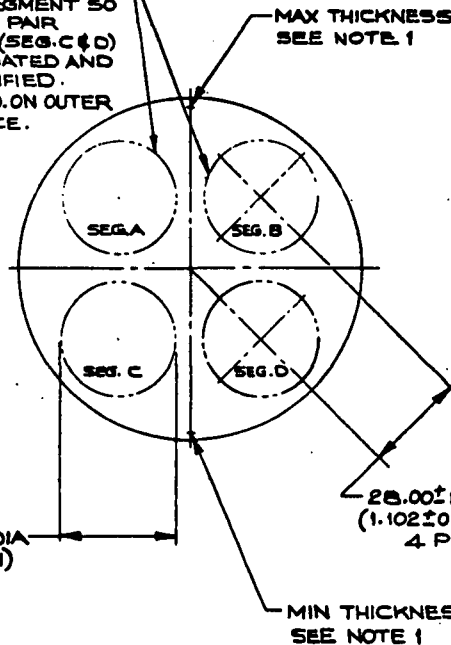
$$= 0.73 \text{ arc-sec}$$

The deviation through the wedge due to this difference in slope is $0.733 (n-1) = 0.373 \text{ arc-sec}$. The maximum cross-coupling error due to this difference would be $2 \times 0.373 \times (1 - \cos 45^\circ) = 0.218 \text{ arc-sec}$, 3σ , which is considered acceptable.

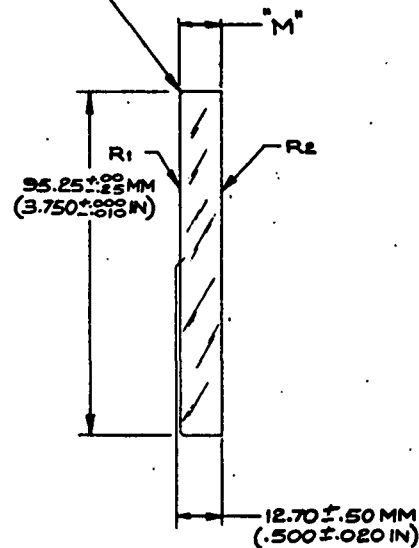
RADII	TOL	CC	CS	SURFACE CODE	SURF TOL OVER CA IN FRAMES	COATINGS			CLEAR APERTURE
						TYPE	THK	λ/4 ±	
R ₁	±.00			80-50	—	HEAR	0.3%	0.94	90.00
R ₂	±.00			80-50	—	HEAR	0.3%	0.94	90.00

REVISIONS				
SYM	ZONE	DESCRIPTION	DATE	APPROVED

THIS BLANK WILL PROVIDE FOUR (4) WEDGE SEGMENTS. MARK EACH SEGMENT SO THAT MATCHED PAIR (SEG. A & B) AND (SEG. C & D) WILL REMAIN MATED AND EASILY IDENTIFIED. MARK SERIAL NO. ON OUTER CIRCUMFERENCE.



$0.50 \pm 0.20 \text{ MM}$
($0.020 \pm 0.008 \text{ IN}$) $\times 45^\circ$



NOTES:

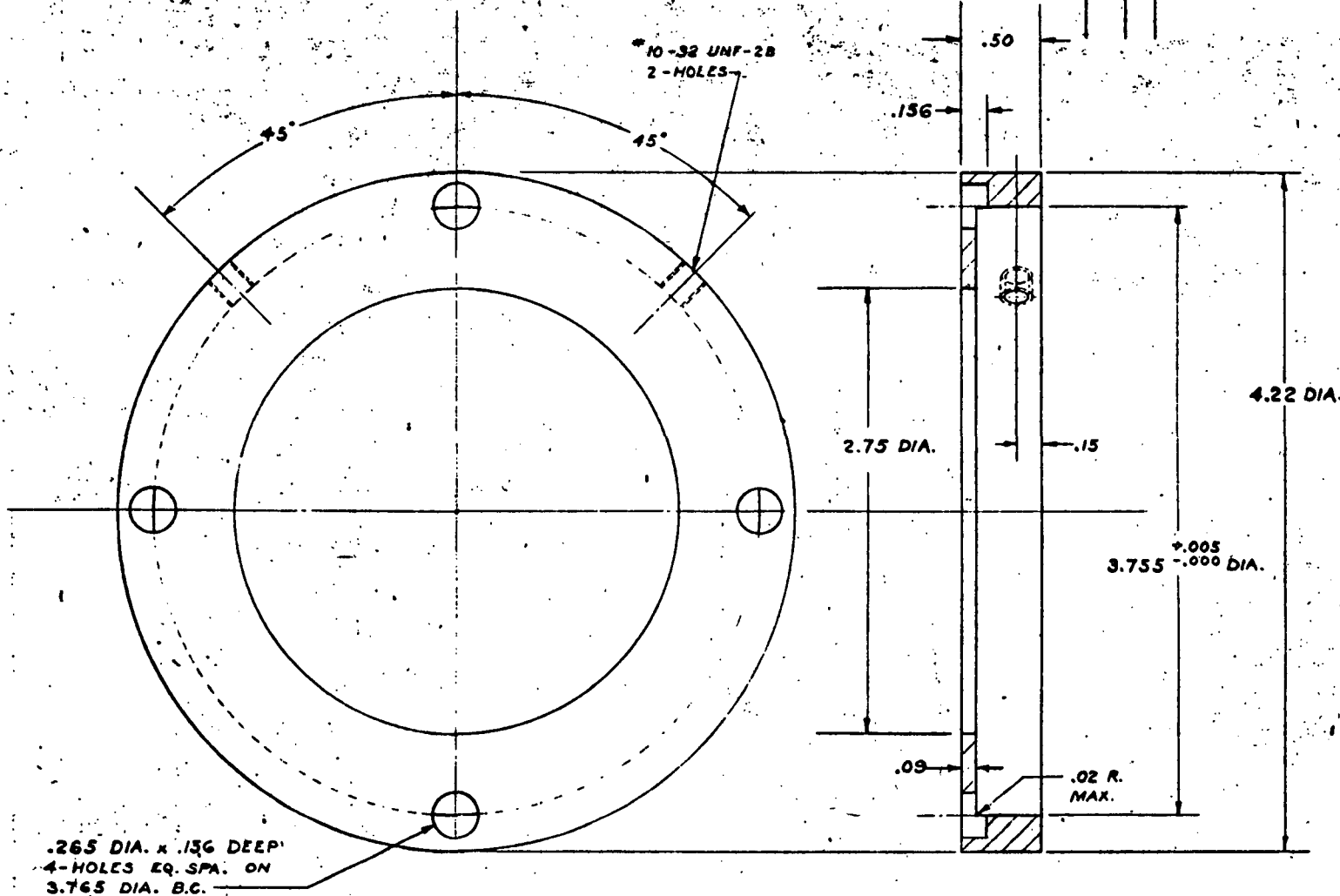
1. THICKNESS DIFFERENCE OVER 92.08 MM DIA = "K". WHEN MEASURED WITH MEASURING RING 252507-2001 AND METRIC MICROMETER (92.08 MM SPAN)
2. NOMINAL DEVIATION THRU WEDGE = "L" SEC @ 0.94 μm (REF).
3. TWYMAN-GREEN INTERFEROMETER TEST SHALL INDICATE NOT MORE THAN "N" FRINGE NET CURVATURE OVER CENTRAL 92 MM DIAMETER AT λ = 546 nm.

DASH NO	CHANNEL	K MM	L	M	N
-1	Y AND Z	0.559 ± 0.010	636.4	0° 20' 52"	0.5
-2	X	0.037 ± 0.002	42.43	0° 01' 23.5"	0.25

UNLESS OTHERWISE SPECIFIED:		SIGNATURE		DATE	
DIMENSIONS ARE IN MILLIMETERS		DRAWN		10/14/76	
WEDGE TOLERANCE		CHECKED			
ELEMENT TO BE IN ACCORDANCE WITH MIL-Q-13630		APPROD			
MIN ± 45° MINIMUM BEVELS ON ALL CORNERS AND EDGES		APPROD			
MATERIAL		ISSUED			
OPTICAL GLASS		SEC APPROVAL			
TYP BK-7		OTHER APPROVAL			
GRADE A		SPEC NO.		FINE ANNELED	

BARNES ENGINEERING COMPANY STAMFORD, CONNECTICUT	
WEDGE, DEVIATION ATA	
CODE IDENT NO. 00430	DWG C
208100-4005	
SCALE 1/1	SHEET

EXCEPT AS MAY BE OTHERWISE PROVIDED BY CONTRACT, THESE DRAWINGS AND SPECIFICATIONS ARE THE PROPERTY OF BARNES ENGINEERING COMPANY, ARE ISSUED IN STRICT CONFIDENCE, AND SHALL NOT BE REPRODUCED, OR COPIED, OR USED AS THE BASIS FOR THE MANUFACTURE OR SALE OF APPARATUS WITHOUT PERMISSION.



MATERIAL			UNLESS OTHERWISE SPECIFIED:			SIGNATURE		DATE		BARNES ENGINEERING COMPANY STAMFORD, CONNECTICUT MEASURING RING WEDGE BLANK ATS
ALUM.			DIMENSIONS ARE IN INCHES AND INCLUDE CHEMICALLY APPLIED OR PLATED FINISHES			DRAWN		12-16-70		
2024-T4						CHECKED		2-19-71		
FINISH			TOLERANCES			APPD.				
NONE			FRACTIONS DECIMALS ANGLES			APPD.				
QTY	NEXT ASSY	USED ON	PLACE 2 PLACE 3 $\pm 1/64$ $\pm .01$ $\pm .005$ $\pm 1/2^\circ$			ISSUED		6-10-71		
APPLICATION			ALL MACHINED SURFACES			BEC APPROVAL		DWG	CODE IDENT NO.	
EXCEPT AS MAY BE OTHERWISE PROVIDED BY CONTRACT, THESE DRAWINGS AND SPECIFICATIONS ARE THE PROPERTY OF BARNES ENGINEERING COMPANY, ARE ISSUED IN STRICT CONFIDENCE, AND SHALL NOT BE REPRODUCED, OR COPIED, OR USED AS THE BASIS FOR THE MANUFACTURE OR SALE OF APPARATUS WITHOUT PERMISSION.			ALL MACHINED DIAMETERS CONCENTRIC WITHIN			OTHER APPROVAL		C	00430	
			BREAK SHARP EDGES .005 MAX RAD					SIZE	252507-2001-1	
								SCALE	2X	
								SHEET		

FIGURE 3.10B

4

3

2

1

D

D

C

C

B

B [252507-2001-2]

A

A

ROTATING MIC
SPINDLE#10-32 UNF-28
2-HOLES

REVISIONS				
ZONE	LTR	DESCRIPTION	DATE	APPROVED

WEDGE BLANK

METRIC MIC ANVIL

4.22 DIA.

9208MM
REF

2.75 DIA.

+0.005
-0.000 DIA..265 DIA. x .156 DEEP
4-HOLES EQ. SPA. ON
3.765 DIA. B.C.

NOTE 1. ROTATE GLASS WEDGE IN RING
UNTIL THICKNESS AT 'B' EQUALS
THAT AT 'D' $\pm .001$ MM
2. MEASURE THICKNESS DIFFERENCE
AT 'A' & 'C'


			MATERIAL		UNLESS OTHERWISE SPECIFIED:		SIGNATURE		DATE		 BARNES ENGINEERING COMPANY STAMFORD, CONNECTICUT					
			ALUM 2024-T4		DIMENSIONS ARE IN INCHES AND INCLUDE CHEMICALLY APPLIED OR PLATED FINISHES		DRAWN		5-6-78							
			FINISH		TOLERANCES		CHECKED		9-8-78		MEASURING METHOD WITH WEDGE BLANK					
			NONE		FRACTIONS DECIMALS ANGLES		APPD		9-8-78							
QTY			NEXT ASSY		USED ON		APPD				DWG CODE IDENT NO. C 00430 252507-2001-2					
APPLICATION							ISSUED									
EXCEPT AS MAY BE OTHERWISE PROVIDED BY CONTRACT, THESE DRAWINGS AND SPECIFICATIONS ARE THE PROPERTY OF BARNES ENGINEERING COMPANY AND ISSUED IN STRICT CONFIDENCE, AND SHALL NOT BE REPRODUCED, OR COPIED, OR USED AS THE BASIS FOR THE MANUFACTURE OR SALE OF APPARATUS WITHOUT PERMISSION.					ALL MACHINED SURFACES <input checked="" type="checkbox"/> RMS					BEC APPROVAL					SCALE 2X	
					ALL MACHINED DIAMETERS CONCENTRIC WITHIN					OTHER APPROVAL					SHEET	

Figure 3.10C

The flatness specification on the X channel wedge is set at 0.25 fringe resulting in a beam deviation of $0.373/2 = 0.187$ arc-sec. Since there is only one wedge in the X channel, however, there is no cross-coupling error due to deviation difference, and the tolerance is selected as a compromise between difficult fabrication and reasonable conformance to nominal values.

3.1.3 Reflectors

3.1.3.1 Remote Reflector Assembly Design

Emphasis in the design of the remote reflector assembly has been centered on three primary requirements. The first is the establishment of the minimum safe dimensions compatible with autocollimator aperture and translation of the end of the boom resulting from the various bending modes. Associated with this is the determination of optimum angles for the Porro reflector in order to return the beam to the same height above the base plate as the autocollimator itself.

A second consideration is the establishment of flatness requirements for the reflectors, especially the Porro. The flatness is determined by the fact that the beam is incident on different parts of the aperture as the end of the boom translates, and deviations from flatness can simulate a true rotation. This is particularly true of the Porro because the foreshortening effect of the Porro inclined faces increases the true curvature by $\sqrt{2}$ in the Z direction, and also because actual beam deviation in the X system are multiplied by 10 in determining their effect on X-rotation output. The pertinent calculations for ascertaining the required flatness of both the plane mirror and the twist sensing Porro are given below.

The flatness requirements on the base line Porro reflectors are not as stringent as the requirements on the remote Porro since it can be seen from Figure 2.4 that the full aperture of this Porro is illuminated at all times.

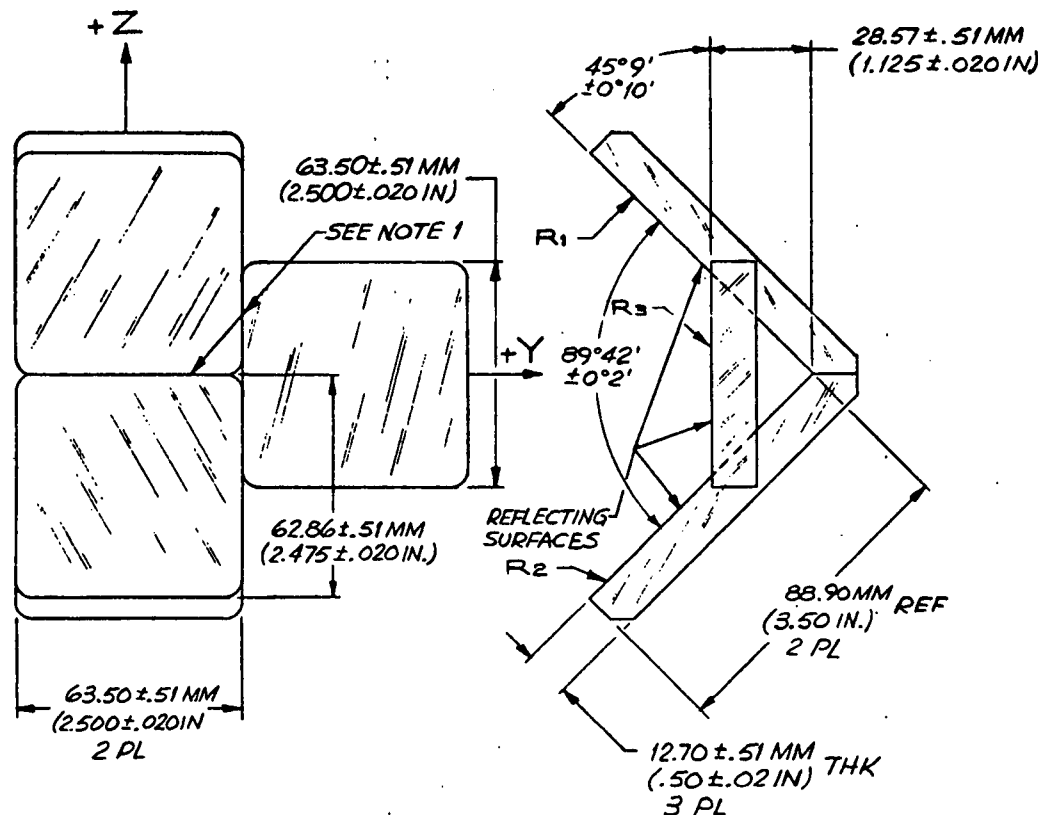
The design effort regarding the Porro reflectors has been directed toward first surface reflectors only. Solid Porro prisms have been excluded from consideration due to the material inhomogeneity problems, the extra contribution to deviation necessitated by refractive index, and the probable need for hand figuring of the prism surfaces. The configuration developed, in conference with Precision Lapping Inc. of Valley Stream, New York for the remote reflector assembly is shown in Figure 3.11A. The material will be the low expansion glass Cervit with an eggcrate structure also of Cervit. The joined surfaces will be bonded with a proprietary process by Precision Lapping Inc. Gussets not shown in Figure 3.11A will be added to the side opposite the flat mirror and elsewhere as determined necessary.

The base-line Porro reflector is of the same open first surface type as the remote reflector assembly shown in Figure 3.11A. Dimensions for this reflector are developed in the next subsection and are shown in Figure 3.11B.

With the center of the remote reflectors at the same height as in Figure 3.11A an upward tilt of magnitude $\tan^{-1} (1.237 / 240) = \tan^{-1} 0.00416 = 0.295^\circ$ is required. This magnitude exceeds the range of the tilt mechanism, and therefore the 0.295° vertical tilt will be provided by a wedged spacer between the X autocollimator and the mounting plane. The vertical distance between the centers of the two Porro surfaces is 2.475 in. If the reflected beam from the lower surface

RADIUS	TOL	CC	CX	SURFACE CODE	HIGHEST TOL OVER CA IN FIGURES	COATING			CLEAR APERTURE
						TYPE	THK	λ IN μ	
R ₁	∞	HH	—	80-50	$\lambda/50$	SEE NOTES	—	—	—
R ₂	∞	HH	—	80-50	$\lambda/50$	"	—	—	—
R ₃	∞	HH	—	80-50	$\lambda/20$	"	—	—	—

REVISIONS				
SYM	ZONE	DESCRIPTION	DATE	APPROVED



NOTES

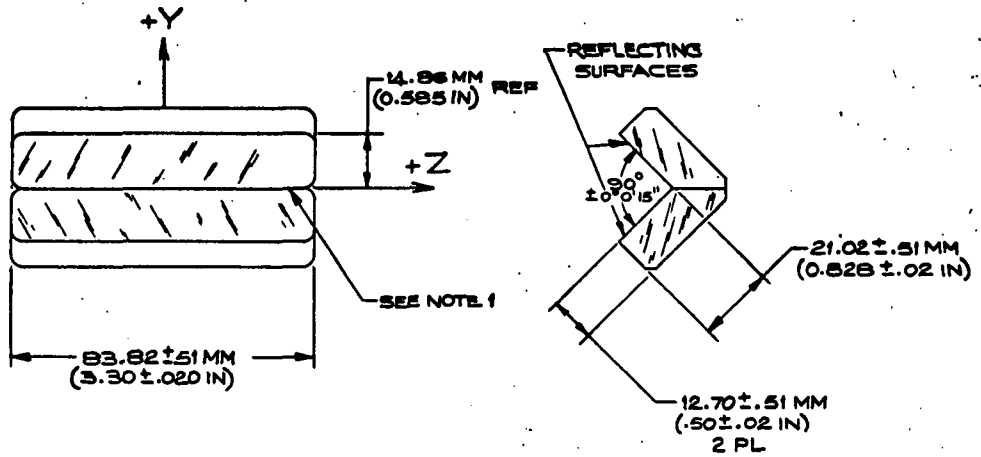
1. LINE-TO-LINE MATCHING NOT REQUIRED. GAP WIDTH MAY BE UP TO 1.02 MM (.040 IN).
2. FLATNESS REQUIREMENTS TO APPLY AFTER ASSEMBLY
3. REFLECTING SURFACES TO BE COATED WITH ENHANCED SILVER SUCH AS DENTON VACUUM FSS-99 OR EQUIVALENT.
4. BEVEL ALL EDGES .38 ± .13 MM (.015 ± .005 IN) AT 45°.
5. WEIGHT OF ASSEMBLY NOT TO EXCEED 7 OZ.
6. ORIGINAL SOURCE OF SUPPLY:
PRECISION LAPPING COMPANY,
VALLEY STREAM L.I., N.Y.
7. MATERIAL: CERUIT, LOW DENSITY EGG CRATE WITH FRONT AND REAR COVER PLATES.

UNLESS OTHERWISE SPECIFIED:			SIGNATURE	DATE
DIMENSIONS ARE IN MILLIMETERS	DRAWN	B/WILLIS	9-17-76	
WEDGE TOLERANCE — TIR	CHECKED			
ELEMENT TO BE IN ACCORDANCE WITH MIL-Q-13830	APPRO			
— MM ± 45° MINIMUM BEVELS ON ALL CORNERS AND EDGES	ISSUED			
MATERIAL	BEC APPROVAL			
SEE NOTE 7	OTHER APPROVAL			
GRADE	SPEC NO.			
OPTICAL				

BARNES ENGINEERING COMPANY STAMFORD, CONNECTICUT			
REFLECTOR ASSY ATA FOR MAGSAT			
CODE IDENT NO.	DWG	SIZE	SHEET
00430	C	208100-4006	
SCALE 1/1			

EXCEPT AS MAY BE OTHERWISE PROVIDED BY CONTRACT, THESE DRAWINGS AND SPECIFICATIONS ARE THE PROPERTY OF BARNES ENGINEERING COMPANY, ARE ISSUED IN STRICT CONFIDENCE, AND SHALL NOT BE REPRODUCED, OR COPIED, OR USED AS THE BASIS FOR THE MANUFACTURE OR SALE OF APPARATUS WITHOUT PERMISSION

4							3				2		1			
RADIUS		TOL	CC	CH	SURFACE CODE	IRRENTY TOL OVER CA IN PERCENTS	COATING			CLEAR APERTURE		REVISIONS				
							TYPE	THK	λ IN μ			SYN	ZONE	DESCRIPTION	DATE	APPROVED
R ₁	∞	±	λ/25	-	80-50	λ/50	SEE NOTES	—	—							
		±														
R ₂	∞	±	λ/25	-	80-50	λ/50	"	—	—							
		±														



NOTES:

1. LINE-TO-LINE MATCHING NOT REQUIRED. GAP WIDTH MAY BE UP TO 0.51MM (.020 IN)
2. ALL REFLECTING SURFACES FLAT TO λ/25 AT 0.5 μM AFTER ASSEMBLY.
3. REFLECTING SURFACES TO BE COATED WITH ENHANCED SILVER SUCH AS DENTON VACUUM FSS-99 OR EQUIVALENT.
4. BEVEL ALL EDGES .38 ± .13 MM (.015 ± .005 IN) AT 45°
5. ORIGINAL SOURCE OF SUPPLY: PRECISION LAPPING COMPANY VALLEY STREAM L.I., N.Y.
6. MATERIAL: CERUIT, LOW DENSITY EGG CRATE WITH FRONT AND REAR COVER PLATES.

UNLESS OTHERWISE SPECIFIED:				SIGNATURE		DATE	
DIMENSIONS ARE IN MILLIMETERS				DRAWN		10/15/76	
WEDGE TOLERANCE				CHECKED			
ELEMENT TO BE IN ACCORDANCE WITH MIL-Q-12830				APPRO			
MM x 45° MINIMUM BEVELS ON ALL CORNERS AND EDGES				APPRO			
MATERIAL				ISSUED			
SEE NOTE 6				BEC APPROVAL			
GRADE				OTHER APPROVAL			
OPTICAL				SPEC NO.			
QTY				NEXT ASSY		USED ON	
APPLICATION							
EXCEPT AS MAY BE OTHERWISE PROVIDED BY CONTRACT, THESE DRAWINGS AND SPECIFICATIONS ARE THE PROPERTY OF BARNES ENGINEERING COMPANY, ARE ISSUED IN STRICT CONFIDENCE, AND SHALL NOT BE REPRODUCED, OR COPIED, OR USED AS THE BASIS FOR THE MANUFACTURE OR SALE OF APPARATUS WITHOUT PERMISSION.							
BARNES ENGINEERING COMPANY STAMFORD, CONNECTICUT				BASE LINE REFLECTOR ASSY ATA FOR MAGSAT			
CODE IDENT NO. 00430				DWS C			
SCALE 1/1				208100-4004			
SHEET							

is parallel to the incident beam, this would be below the mounting surface. In order to return the beam to the same height, the reflected beam should be inclined up by the same angle as the projected beam. Then the convergence angle of the two beams is 0.590° , and the angle bias necessary to achieve this is $0.590^\circ/2 = 0.295^\circ \approx 0.3^\circ$.

Thus the two Porro mirrors should have an included angle of 89.7° . The base line Porro must be tilted downward 0.3° in order to "meet" the beam from the remote Porro normally.

The enclosure design for the remote reflector assembly awaits further definition of attachment availability at the boom end. It is expected that a light weight material such as a space-qualified graphite/epoxy composite will be used for this purpose with the reflectors mounted to the enclosure on isolating resilient pads. Thermal blankets surrounding the reflectors will further enhance the stability of the Cervit glass material.

3.1.3.2 Calculation of Required Reflector Sizes

3.1.3.2.1 Y-Z System (single plane mirror)

If the boom bends at its root, mirror movement is
 $\pm L \sin 0.25^\circ = 240 \times 0.00436$
 $= 1.047 \text{ inches}$

Since the collimated beam deflection produced by the wedges is always in a direction to follow the boom motion, the beam again becomes centered on the mirror, so no extra aperture is required. A minimum diameter of about 1.25 inches would thus be adequate.

If boom bends as a circular arc (approximated by the parabola) the equation for deflection as a function of distance from the vehicle is

$$y = a x^2 \quad (3-37)$$

where y = lateral deflection

a = constant

x = distance

Also $dy/dx = 2 a x$

$$= 2 y/x \quad (3-38)$$

Then for $x = 240$ inches and $dy/dx = 0.00436$ rad.

$$\begin{aligned} y &= 240 \times 0.00436/2 \\ &= 0.523 \text{ inches (1.328 cm)} \end{aligned}$$

Again, the motion of the deviated beam is in a direction to follow the boom motion, and the net displacement between the two is $(1.047 - 0.523) = 0.524$ inches.

Since the boom can deviate in either direction, the extra diameter which needs to be provided is 1.048 inches, and total mirror diameter is then $(1.048 + 1.142) = 2.190$ inches.

Therefore, a diameter of 2.5 inches is appropriate.

3.1.3.2.2 X-System (Porro Reflectors)

3.1.3.2.2.1 Boom End or Twist Sensing Porro Reflector

In order to avoid the threat of a double image due to angle error in the first Porro reflector, it is necessary to keep the first beam incident on the upper reflecting surface at all times.

Z-axis rotation (circular bending) displaces the boom-end laterally by 0.523 inches, as previously indicated. The portion of the reflector which actually reflects the useable portion of the boom to the second Porro and back to the auto-collimator is that portion which is spread by the angle Z from the axis, and is displaced 1.047 inches at the first Porro. Thus the require enlargement is $2 (1.047 - 0.523) = 1.048$ as before, yielding a practical minimum width of 2.5 inches.

The projected height of the upper reflecting surface of the Porro must be large enough to accommodate the Y deflection of the boom, or ± 0.523 inches. Therefore, the minimum possible height without vignetting is 2.190 inches. Because of the cumulative effect of aperture on weight, this will be made 2.475 projected height, or 3.5 inches true dimension

3.1.3.2.2 Base Line Porro Reflector

The base line Porro reflector is oriented with its roof edge in a Z direction that is, in the insensitive direction. It is thus not necessary to consider the double image problem caused by angle error of the remote Porro roof.

The X rotation (twist) produces a beam displacement in the Z direction of $\pm 2 D \sin \theta \sin X$ or ± 0.035 in (± 0.0889 cm). This is added to the aperture of the collimator 1.412 inches (2.90 cm).

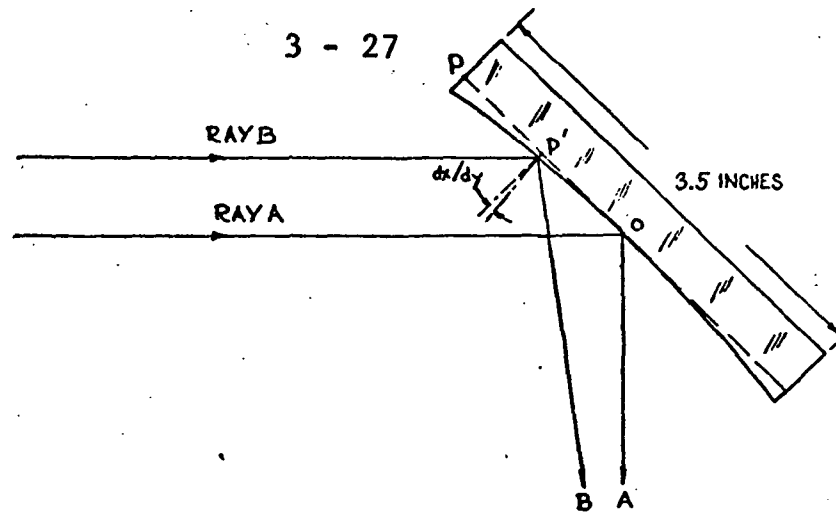
In addition, boom bending in the XZ plane displaces the end of the boom by ± 0.523 in (1.328 cm). After reflection from the remote Porro the beam is displaced by twice the above amount or ± 1.046 inches (2.657 cm). The total necessary dimension in the Z direction of the base line Porro is thus 3.30 inches (8.382 cm).

The hypotenuse dimension of the base line Porro need be only the dimension of the autocollimator aperture, that is 1.142 inches.

3.1.3.3 Required Flatness of Reflector

The flatness requirements of the reflectors are based on the error contributions these surfaces make to the rms system error. To find the contribution of the reflectors to the system error consider the diagram below:

3 - 27



The reflecting surface represents one surface of the Porro reflector (the diagram is also valid in discussing the errors introduced by the plane mirror when the above surface is normal to ray A). Ray A is incident on the center of the reflector at 45° and reflected downward. When maximum Y-axis bending of the boom occurs, the reflector is displaced downward 0.523 in. (1.328 cm). Ray A is now incident on the reflector at a point 1.328 cm x 1.414 = 1.879 cm above point 0 and is represented by Ray B in the diagram. If the surface is concave Ray B is deviated as shown above.

The equation of a circle may be approximated by

$$x = y^2 / 2r_0 \quad (3-39)$$

which is valid for large radius, r_0 . The change in direction of the mirror normal, dx/dy is found by differentiation and substitution

$$dx/dy = 2x/y \quad (3-40)$$

x is the sag at point P' given by the expression

$$x = \lambda (y/y_0)^2 \quad (\text{when } \lambda \text{ equals sag at } P) \quad (3-41)$$

where y is the line segment $OP' = 1.879$ cm

y_0 is the line segment $OP = 4.445$ cm (1.75 inches)

λ is the HeNe linear wavelength in common interferometric usage = 6.3×10^{-5} cm

Substituting (3-41) in (3-40) the expression for the change in direction in mirror normal becomes

$$dx/dy = 2\lambda y/y_0^2 \quad (3-42)$$

After substitution of the values for y, y_0 and r_0 dx/dy becomes

$$dx/dy = 2.47 \text{ arc sec}$$

The convergence between Ray A and Ray B is twice the change in angle dx/dy or 4.94 arc sec for a mirror curvature of one wavelength.

There are two surfaces of the remote Porro reflector to be considered. The convergence after two similar reflections (assuming similar curvature) is $2 \times 4.94 \text{ arc sec} = 9.89 \text{ arc sec}$. To obtain the equivalent twist, the above value is divided by $2 \sin \theta = .1$ resulting in 98.9 arc sec. By specifying a mirror flatness of $\lambda/25$ the above equivalent twist may be divided by 25 to obtain 3.956 arc sec equivalent twist (3σ value).

The calculation for the base line Porro proceeds in the same manner. The maximum displacement of the center of the beam is calculated in section 3.1.3.2.2.2 to be 1.081 inches (2.746 cm). The maximum dimension from the center of the reflector is 1.650 inches (4.191 cm). The change in direction of the reflector is given by equation (3-42).

$$dx/dy = 2\lambda y/y_0^2$$

where λ is as above

$$y = 1.081 \text{ inches (2.746 cm)}$$

$$y_0 = 1.650 \text{ inches (4.191 cm)}$$

resulting in a magnitude of

$$dx/dy = 4.06 \text{ arc sec}$$

The beam convergence for a reflector flatness of one wavelength is twice the change of the normal direction above or 8.12 arc sec. By specifying a flatness of $\lambda/25$ this result becomes 0.324 arc sec. The contribution from the second surface

(with $\lambda/25$ flatness specification) is also 0.324 arc sec thus making the total beam convergence due to the base-line Porro reflector 0.648 arc sec. The equivalent twist is obtained by dividing the above value by $4 \sin \theta = .2$, instead of $2 \sin \theta$ since this reflector is encountered only once by the optical beam. The system error due to the base-line reflector is thus 3.24 arc sec (3σ value).

Employing equation 3-42 again, the error contribution of the flat mirror in the YZ channel may be found.

where y = maximum displacement of the center of the beam =
0.523 in (1.328 cm)

y_0 = maximum dimension from the center of the reflector
is 1.25 in (3.175 cm)

Solving equation (3-42) with the above values gives

$$dx/dy = 3.42 \text{ arc sec}$$

The equivalent mirror rotation is thus 3.42 arc sec. for a one wavelength flatness. By specifying $\lambda/25$ the above result becomes 0.137 arc sec (3σ value).

3.2 MECHANICAL SYSTEM

As explained in the original technical proposal (P-6185, Volume 2), deflection measurements obtained by the ATA are derived from contra-rotating optical wedge pairs placed in the front section of a tracking autocollimator. In this connection, it is important to note that the wedge pairs need not be precisely orthogonal to the autocollimator's optical axis since the rotational positions of the wedges principally determine the direction of optical beam deflections. This characteristic, coupled with autocollimator static bending thermal strain considerations, has led to a revised design concept (compared to the original proposal) wherein the auto-

collimator and optical tracking functions have been structurally as well as conceptually isolated from each other. This concept is shown in Figure 3.12. The complete ATA thus is physically composed of the following physical assemblies:

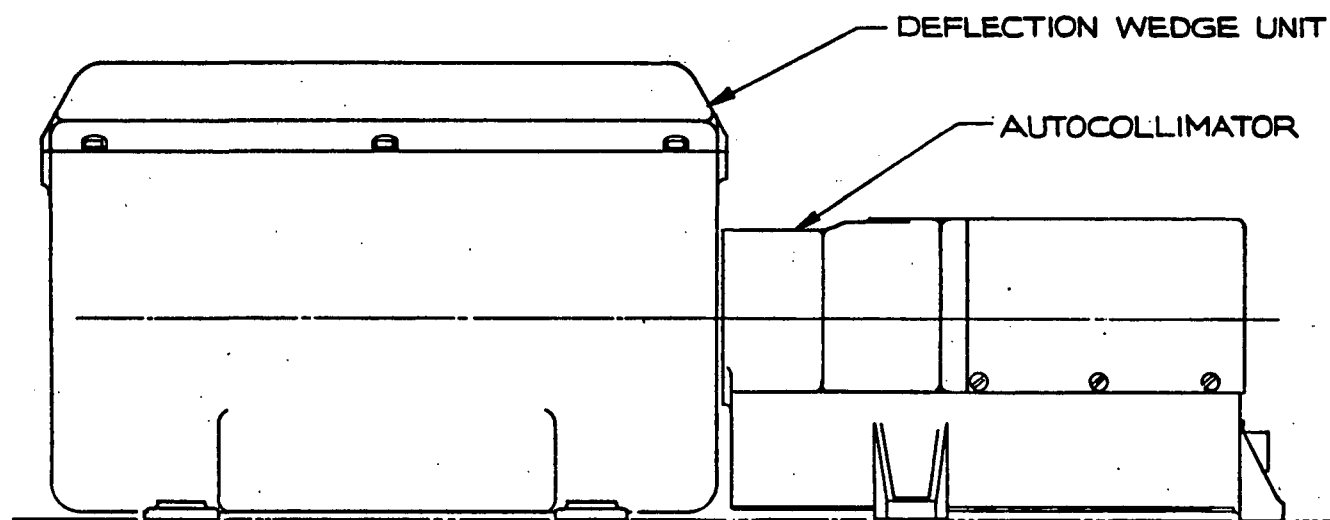
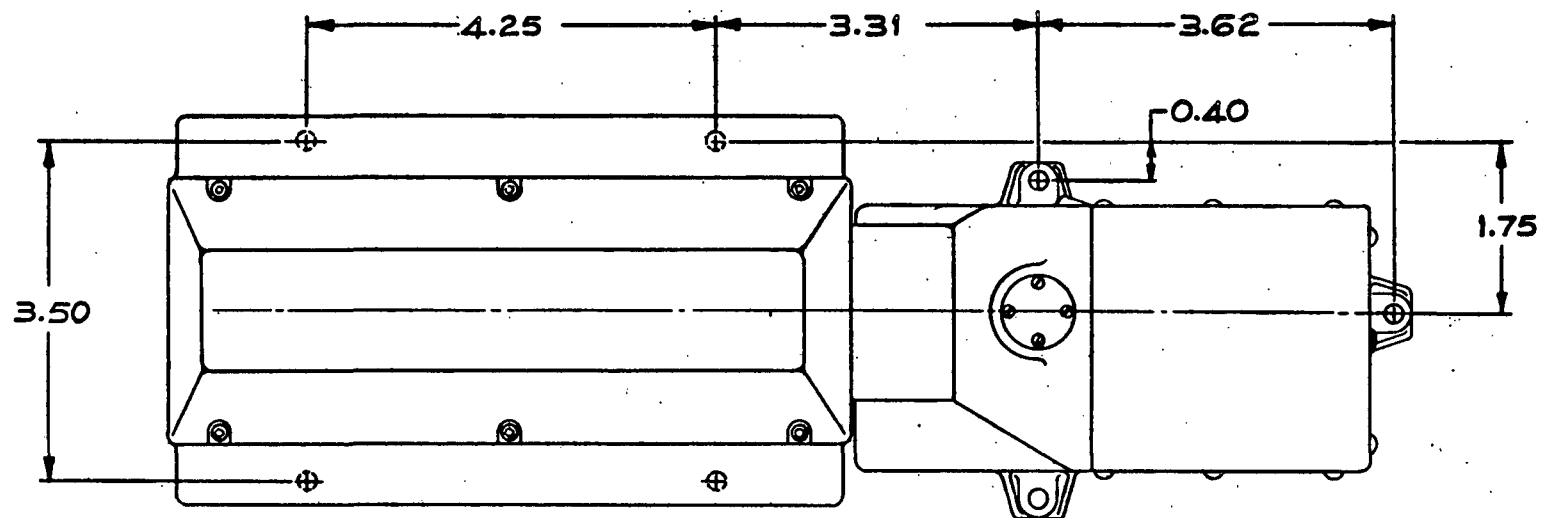
- Z-Y Autocollimator
- Z-Y Beam Deflector
- X (Twist) Autocollimator
- X (Twist) Beam Deflector
- Remote Reflector Assembly
- Base-line Porro Reflector

Except for minor difference in AGC linear range, the Z-Y and Twist Autocollimators of the ATA are essentially identical. Similarly, the beam deflectors associated with the Z-Y twist measurement functions conceptually differ primarily only in their optical scale factors and in elimination of unnecessary components in the X axis instrument. For these reasons the discussion which follows is applicable to both Z-Y and twist subassemblies except where otherwise noted.

3.2.1 Autocollimator Assembly (See Figure 3.13)

3.2.1.1 Materials Selection

An optimum selection of structural materials for the ATA autocollimators must involve recognition of the opto-mechanical requirements involved. At the four inch focal length of the objective, a lateral shift of 4.93×10^{-4} mm at the focal surface (with respect to the objective axis) is equivalent to a one arc-second change in the pointing direction of the autocollimator. The maintenance of an initially established optical geometry (boresight) over the operational life of the instrument obviously presents a formidable challenge not only in instrument design but in the materials selection



SCALE 1 INCH

ATTITUDE TRANSFER ASSEMBLY
AUTOCOLLIMATOR AND DEFLECTION WEDGE UNIT

FIGURE 3.12

process as well. With the stated geometrical requirement in mind, candidate structural materials for the autocollimator must be evaluated from a variety of conflicting viewpoints. These may be summarized approximately as follows:

a) The telescope housing should be fabricated of a low-density material to minimize total weight. From this viewpoint, magnesium, beryllium and aluminum and their alloys would have to receive prime consideration.

b) The housing material must possess adequate intrinsic stiffness to resist elastic, anelastic (time dependent elastic) and plastic strains arising from such diverse causes as normal handling, launch environment loads, operation of zero-g and one-g fields, etc. With respect to this criterion, beryllium is clearly superior to other metal candidates, while magnesium would be least desirable because of its low elastic moduli in both shear and bending.

c) The housing and structural parts attached to it should be reasonably resistant to distortions arising solely from thermal sources. Since direct attachment to a temperature controlled sink is contemplated, differential expansion between unlike materials internal to the telescope is not a source of serious concern by itself. However, internal temperature gradients of both the transient and steady state varieties can lead to systematic variations in the autocollimation axis unrecognizable from real target deflections. The parameter of interest for studying dimension at transient behavior is thermal diffusivity, while steady-state dimensional distortions are relatable to the coefficient of expansion. Thermal conductivity ratio of a candidate material for both types of problems (steady-state and time-varying heat inputs to the autocollimator structure),

beryllium and aluminum can be shown to be clearly superior to almost any other conceivable choice.¹

d) All of the autocollimator parts and especially the main housing must be highly stable and exhibit little evidence of dimensional creep under light loading over relatively long time periods. While the literature provides adequate guidelines for optimizing the stability of any chosen material, the stainless steels, aluminum alloys and pure beryllium apparently are among the materials least susceptible to microcreep² when properly processed in fabrication.

e) To as large an extent as practical, a multiplicity of small mechanical parts and resultant ill-defined thermal and mechanical interfaces is to be avoided. This statement implies that smooth un-jointed contours obtained by casting and similar fabrication techniques are highly desirable for the autocollimator housing. Aluminum (e.g. alloy 356) clearly leads all other candidate materials from the viewpoint of fabrication ease, while beryllium is unquestionably a last choice.

The considerations cited in the preceding paragraphs strongly suggest that only cast aluminum and perhaps beryllium are viable candidates for the design of ATA instrument structures. Since casting techniques permit an optimum placement of material for the minimization of deflections under changing load conditions while largely avoiding thermal joint problems, it clearly emerges as a prime choice.

Over the years a considerable body of experience relative to the proper processing of materials for the enhancement

1. R. Grudee, "Holding Dimensions Thermally Stable", Machine Design Nov. 2, 1972.

2. A Review of Dimensional Instability in Metals, DMIC Batelle Memorial Institute, March 19, 1964.

of intrinsic dimensional stability has been amassed by this company. For all critical parts of the ATA, Company specification PM-33 will be invoked throughout the design/fabrication sequence. This document will be used to control machining depths of cuts, heat treatment sequences, etc. so that optimum stability properties are developed for all component parts of the ATA.

3.2.1.2 Mounting of Optical Elements (see Figure 3.13)

In preparing the design of both the Z-Y and twist ATA autocollimators, successful test experience gained during the design and manufacture of Azimuth Transfer Auto-Collimators (ATAC) for the Trident missile program has been utilized. The various optical and electro-optical elements are conceptually mounted in a manner consistent not only with end-use requirements (maintenance of boresight after various environmental exposures), but also in accordance with specific alignment/test sequence requirements. In general, the following list outlines the mounting philosophy:

(1) The objective lens is to be mounted in a threaded cell for axial focusing with respect to the source aperture. After focusing, radial locking screws are utilized to hold the lens cell position firmly in place. (Boresight shifts caused by eccentric rotation of the objective during focusing are ultimately cancelled out by the plate adjustments).

(2) The source LED is focused with respect to the source aperture by axial sliding within a split-ring clamp. The same clamp permits rotation of the source LED for best alignment with respect to the source aperture mask.

(3) The AGC detector is not independently focusable with respect to the objective lens. Instead, beamsplitter

cube symmetry is utilized in conjunction with objective focusing to provide conjugate but non-critical imaging of the source aperture mask on the AGC detector focal surface.

(4) The AGC detector and background compensation detectors are mounted on a common bracket which can be translated in the Y-Y direction by opposed push-push screws. Movement of these screws has two effects.

(a) Since the beamsplitter cube and source aperture mask are mounted to the same bracket (as the AGC and background), Z axis boresight shifts result. These are compensated for, if necessary, by tilt plate adjustments.

(b) The return image is laterally displaced, and hence can be made to fall on the AGC detector in the horizontal plane.

(5) Mounted on the same bracket as the AGC and compensation detectors, the beamsplitter and source may be vertically (Z-Z) adjusted independently using a push-screw/return spring adjustment. This adjustment permits imaging of the return energy on the AGC detector, since that detector is fixed and does not move with the adjustment.

(6) The Y-axis and Z-axis nulling detectors are positioned for best focus independently by mounting on ground spacers which affect displacements along the optical axis only.

(7) The Y-axis nulling detector is adjustable vertically in the Z-Z direction to permit nulling the nominal "boresight zero" position of the tilt plate. As with the adjustment described in (5), a push-screw/return spring combination is used.

(8) The Z-axis nulling detector may be independently moved horizontally (in the Y-Y direction) to permit nulling in this direction in the same manner as above, except that push-push opposed screws are used because of improved access.

The various adjustments described above have been designed to permit independent focusing and lateral trimming to as large a degree as practicable. Hardened surfaces will be used at all contact points of the various adjustments so that problems associated with movements under Hertzian stress concentrations will be minimized. Further confidence in maintaining adjustments will be achieved by fillet-bonding of all moveable brackets to the main structure after all optical adjustments and testing have been completed.

3.2.1.3 Thermal/Vibration Characteristics

It is expected that both the "Z-Y" and "X" measurement autocollimators will be directly mounted on a temperature-controlled thermal sink which is stable within $\pm 2^{\circ}\text{C}$ over an orbital period. Since both telescopes contain only small steady-state thermal sources (LEDs and preamplifiers), the allowance of a reasonable warm-up time should assure boresight repeatability. Under these conditions, no analysis is deemed necessary.

Because both autocollimators are mechanically passive in operation, boresight shifts resulting from the launch vibration environment can occur only if relative displacements are introduced at bolted interfaces. Events of this type are not readily amenable to analysis; prevention will be assured through the following precautions:

a) The number of clamped interfaces will be held at an irreducible minimum; fasteners will be torqued to specified limits.

b) Fillet-bonding techniques will be employed extensively to hold critical relationships and avoid interfacial creep.

As indicated, these conditions preclude the necessity for multinode vibration response modeling of both ATA autocollimators.

3.2.2 Deflection Wedge (See Figure 3.14)

3.2.2.1 Structural Arrangements

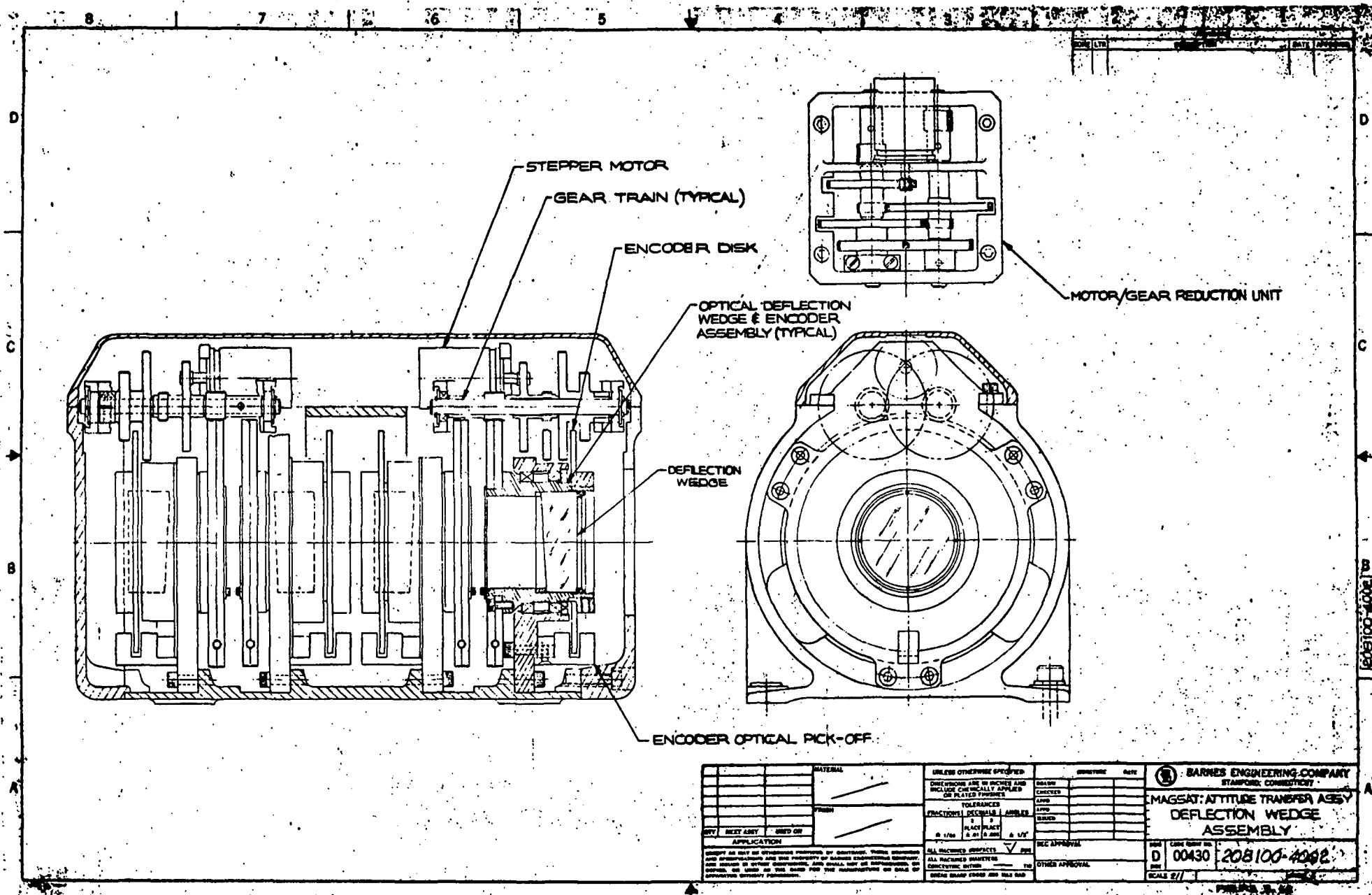
The Z-Y and X-axis beam deflector assemblies of the ATA are essentially identical except for the elimination of three wedges and associated drive components in the X-instrument. To a first order approximation, both assemblies are conceptually incapable of introducing total instrument boresight shifts due to linear or rotational displacements about any axis other than pure rotations about the optical axes. This characteristic permits considerable latitude in design, and materials selection but places definite requirements on the twist stability of the common mounting surface for the respective autocollimator/beam deflector pairs.

3.2.2.2 Mechanical Packaging

The Z-Y beam deflector assembly has been designed as a cast aluminum housing which accommodates four individual and identical deflection units as well as the two motor/gear drive units which rotationally position the contra-rotating wedge pairs. A typical deflection unit is shown in figure 3.15, while a typical motor/gear reduction unit is shown in figure 3.14.

NOTE:

Since the X-axis beam deflector has only a single optical wedge, only a single deflection unit and single motor/gear reduction unit (with contra-rotating gears eliminated) are required. These changes will be carried out through elimination of parts from the basic design in order to maintain commonality as much as possible.



4

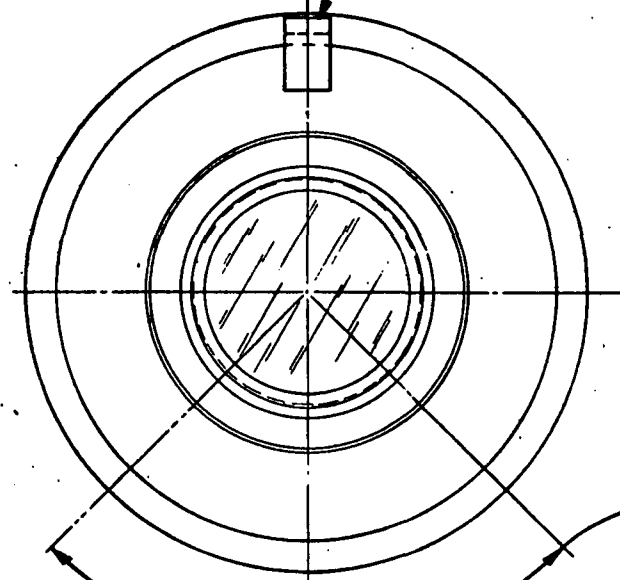
3

2

1

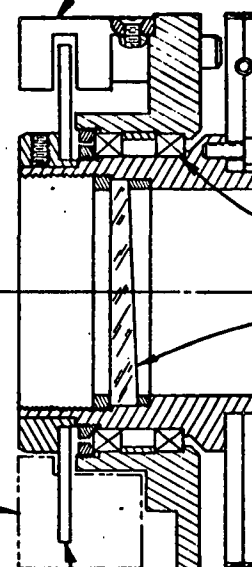
REVISIONS				
ZONE	LTR	DESCRIPTION	DATE	APPROVED

NUMBER AND LOCATION OF CODEWHEEL PICKOFFS TO BE DETERMINED BY ENCODER SUPPLIER



NO PICK-OFFS IN APPROX 90° ZONE

ENCODER PICKOFF (TYPICAL)



ANTI-BACKLASH DRIVE GEAR *

3 TAP 24-28 (SBB) BEARINGS *
OR EQUIV. (ABEC CL 7T)

OPTICAL WEDGE *

ROTOR *

NOTES:

1. ORIGINAL SOURCE OF SUPPLY;
ITEK MEASUREMENT SYSTEM
DIVISION, NEWTON, MA. 02161

FRAME *

2¹³ CYCLE CODE WHEEL
(2 TRACK) AND MOUNTING HUB

* DENOTES BEC. SUPPLIED ITEM

<table border="1"> <tr> <td>QTY</td> <td>NEXT ASSY</td> <td>USED ON</td> </tr> <tr> <td colspan="3">APPLICATION</td> </tr> </table>			QTY	NEXT ASSY	USED ON	APPLICATION			<table border="1"> <tr> <td colspan="3">MATERIAL</td> </tr> <tr> <td colspan="3">FINISH</td> </tr> </table>	MATERIAL			FINISH			UNLESS OTHERWISE SPECIFIED: DIMENSIONS ARE IN INCHES AND INCLUDE CHEMICALLY APPLIED OR PLATED FINISHES			SIGNATURE DATE DRAWN <i>B. D. Hall</i> 10 Aug 76 CHECKED <i>S. H. Hall</i> 10 Aug 76 APPD <i>B. D. Hall</i> 11 Aug 76 APPD ISSUED		BARNES ENGINEERING COMPANY STAMFORD, CONNECTICUT	
			QTY	NEXT ASSY	USED ON																	
APPLICATION																						
MATERIAL																						
FINISH																						
TOLERANCES <table border="1"> <tr> <th>FRACTIONS</th> <th>DECIMALS</th> <th>ANGLES</th> </tr> <tr> <td>± 1/64</td> <td>± .01 ± .005</td> <td>± 1/8°</td> </tr> </table>			FRACTIONS	DECIMALS	ANGLES	± 1/64	± .01 ± .005	± 1/8°	ALL MACHINED SURFACES <input checked="" type="checkbox"/> RMS ALL MACHINED DIAMETERS CONCENTRIC WITHIN <input type="checkbox"/> TIR BREAK SHARP EDGES .005 MAX RAD		WEDGE DRIVE UNIT		DWS C SIZE		CODE IDENT NO. 00430		208100-4003					
FRACTIONS	DECIMALS	ANGLES																				
± 1/64	± .01 ± .005	± 1/8°																				
EXCEPT AS MAY BE OTHERWISE PROVIDED BY CONTRACT, THESE DRAWINGS AND SPECIFICATIONS ARE THE PROPERTY OF BARNES ENGINEERING COMPANY, ARE ISSUED IN STRICT CONFIDENCE, AND SHALL NOT BE REPRODUCED, OR COPIED, OR USED AS THE BASIS FOR THE MANUFACTURE OR SALE OF APPARATUS WITHOUT PERMISSION.						BEC APPROVAL OTHER APPROVAL		SCALE 2/1		SHEET 1 OF 1												

FIGURE 3.15

3.2.2.3 Encoder Mounting

As shown in figure 3.15, each Z-Y deflection drive unit will include its own 2^{13} cycle incremental encoder to directly provide wedge cross-coupling error information in real time as well as to provide redundancy in the two measurement axes. The individual assemblies, less encoders, will be forwarded to the encoder subcontractor (Itek or Baldwin) for mounting and centration of code wheel and optical pickoff components. The same vendor will be responsible for spin testing and electrical alignment of these parts in such a manner as to minimize bearing runout effects by selecting the 90 degree rotational zone of each assembly wherein output response most nearly approaches perfect linearity. Upon return from the vendor individual optical wedges will be rotationally re-oriented so that the optical deviation axis of each wedge approximately coincides with the center of the selected 90-degree use zone of the encoder. Deflection unit pair members will be aligned to each other and encoder reference zero output positions established following the general procedures outlined in para. 3.2.1.2.

3.2.2.4 Servo Drive

3.2.2.4.1 Motor

The drive source for each wedge pair will be a size 8, 45° stepper permanent magnet stepper motor similar to Computer Devices P/N 08M01. The motor will be rewound without change in torque output characteristics to operate from a nominal 16 volt source. The normally-supplied bearings will be removed and replaced with Krytox 143AB lubricated parts of the same size (see paragraph 3.2.2.4.3) in order to assure uniform operation during the mission lifetime in a hard vacuum environment.

The external magnetic signature of the proposed stepping motor is unknown at the present time, because of the rewinding necessitated by the reduced operating voltage level. It is anticipated that external magnetic fields propagated by step-switching will be minimal and tolerable for the following reasons:

(1) Because of its small size and high winding phase resistances, current transient levels will be relatively low.

(2) The motor design utilizes a total enclosed ferromagnetic case with no apertures except through the shaft-end ball bearing.

(3) Adequate space exists to totally enclose the motor, if necessary, in a separate enclosure or shield. Similarly, the entire beam deflector could be shielded if necessary.

(4) As a last resort, the MAGSAT magnetometer's output might be momentarily suppressed during the transient time (less than $\frac{1}{2}$ second) required for periodic updating of the ATA's servos during orbital operation.

3.2.2.4.2 Gear Train (See Figure 3.16)

Two identical gear drive units are required for the Z-Y beam deflector, with a similar unit (contra-rotating component removed) used to rotationally position the single wedge of the X-axis deflector. Each unit will be assembled as a removable module by "breaking" the last gear meshes (anti-backlash gears on deflection drive units) with drive unit removal.

It has been chosen to avoid commercially available gear-head units because of the many unknowns inherent in their construction, e.g., gear tooth materials and hardness, tolerances,

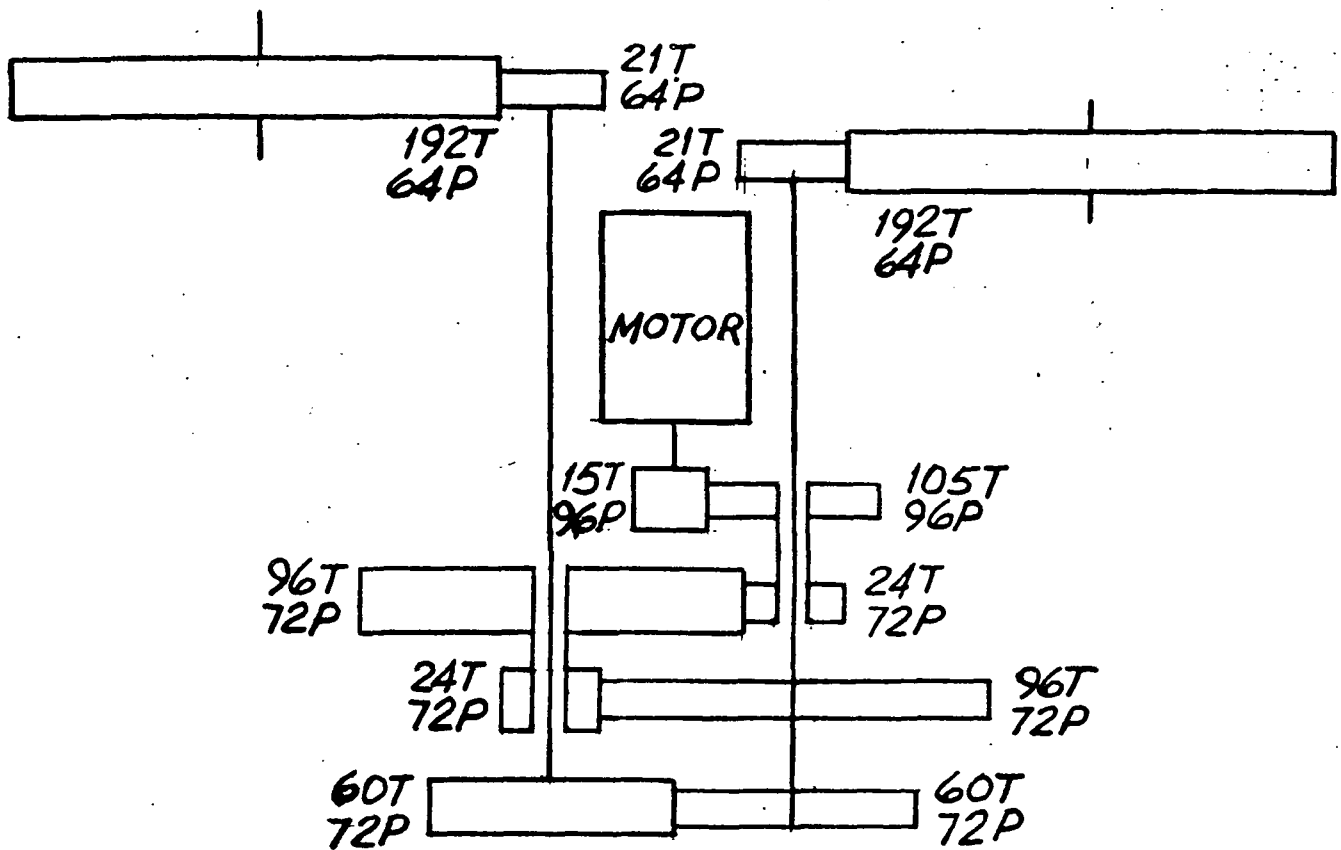


Fig. 3.16 DEVIATION WEDGES GEAR SCHEMATIC

lubrication, etc. Instead, a completely compatible dual output reduction of 1024/1 has been obtained in the manner shown, with the reduction sequence of 7:1, 4:1, 4:1 and 64:7.

The drive gear arrangement shown is technically known as a reverted type and was selected for the following reasons:

(1) Only two shafts separated by a single center distance are required for all the gear meshes except the first and last. This artifice not only saves space and weight but minimizes complexity in the "gear box" structure.

(2) Except for the motor shaft and wedge carrier, only four ball bearings, one at each shaft end, are required for the entire drive train. Differential motion between the intermediate compound gears and output shafting is permitted by carefully fitting the gear bores to the hardened (RC 60) and ground shafting.

(3) Variations in the lubricant used between the compound intermediate gears and shafting permit considerable latitude in optimizing damping performance and minimizing the single-step overshoot characteristics normally associated with stepper motor operation.

No final determination has been made for the material(s) to be used in the various gears, pending possible further calculations as to maximum stress levels, fatigue life, etc. It is expected, however, that AGMA precision 14 fabricated of type 302 stainless steel will provide both the needed accuracy and low wear characteristics desired for extended operational life.

3.2.2.4.3 Bearings and Lubrication

The several servo drives of the ATA complex operate at minimal duty cycles (less than 2.5% "on" time at maximum tracking deviations) consistent with MAGSAT's orbital period. While the accumulated hours of dynamic use will undoubtedly be small compared to the total mission life, due attention must be paid in the bearing selection lubrication design process to provide long-term reliability and operational readiness at all times.

In both ATA beam deflectors, high quality (ABEC 7 and 7T) bearings consistent in size with the intended functions and load constraints will be specified. All bearings can be purchased in an unlubricated condition (or lubricated with the service lubricant for shipment only), with cleaning, lubrication and torque testing as required under the appropriate documentation control. While exact descriptions are inappropriate in this study, mention may be made of the extensive experience in aerospace lubrication control in other NASA/Goddard programs (ITOS/Vertical Temperature Profile Radiometer) as well as Air Force (SAMSO) programs.

Under the nearly invariant and temperature thermal conditions anticipated for the ATA, the perfluoroalkylpolyether lubricants typified by Krytox 143AB appear to be clearly suitable for the various bearings, and their use will be specified at the appropriate detail design level. Compound gears not pinned to the gear box output shafts will be lubricated either with a light film of 240AB grease, or with an appropriate resin-bonded molybdenum disulphide film if contamination or lubricant creep appears to threaten the design's inherent longevity.

3.2.2.5 Servo Performance

3.2.2.5.1 Gearing Reduction Ratio Optimization

The choice of a numerical reduction ratio between the servo (stepper) motor and optical wedges involves several conflicting considerations. Larger ratios generally involve more components and hence increased size, weight, etc. For the ATA, large numerical

ratio drives also must be operated for longer periods during target acquisition and tracking, and hence involve larger "motor-on" duty cycles. Against these considerations, it is necessary to weigh the drawbacks of very low numerical reductions. Lower ratios generally provide less absolute repeatability of position at the output member, and less torque multiplication. More subtly, the lower coulomb friction associated with fewer gear passes generally means poorer damping and hence greater overshoot, etc. in a step servo drive of the type contemplated.

For the ATA beam deflectors, an overall reduction ratio of 1024:1 has been chosen as near-optimum. This numerical value results in a wedge rotation of approximately 2.64 arc minutes (.77 mr) for each motor step and hence leads to optical deviation increments ranging from 0.70 to 0.98 arc seconds at the tracking range extremes and center respectively. The narrowness of the variation in deviation permits a fixed string of step-pulses to be fed to the drive motor so that no closed-loop comparisons are necessary when driving to near the center of any detector's linear range. For instance, a string of 16 pulses will result in an "average" deviation change of approximately 13 arc seconds and will always suffice to restore the system to near its linear center if the out-of-linear range thresholds are set at approximately the same levels.

The chosen 1024:1 ratio in addition to being eminently well suited to a purely binary (16) input pulse string (with resultant reduction in parts count), is also highly compatible with stepper drive damping characteristics. Experience with similar stepper drive systems has shown that end-of-step oscillations in the range of 10-30% of the step amplitude are normal and should be expected. With 2^{13} cycles on the code wheel and 2^{15} count increments per revolution, each motor step theoretically results in exactly 4 encoder output "counts." With reasonable control over damping (less than 25% overshoot and undershoot), up-down count oscillations

are limited to ± 1 increment, considerably reducing the chances of false counting or error accumulation.

3.2.2.5.2 Gear Train Accuracy and Backlash

As described in paragraph 3.2.2.4.2 and in Appendix E, gear profile errors in the ATA beam deflectors introduce cross-coupled optical deviation errors which may approach one arc second in magnitude. Although these are almost entirely systematic and repeatable, the incorporation of a second (redundant) encoder output in each deflection channel provides an opportunity for continuous correction without resorting to calibration data which may no longer be entirely valid after a long time period and launch exposure.

A significant list of assumptions must be made before analysis of gear train backlash can be attempted. The assumptions involve tolerancing of the various fits involved as well as estimating gear profile errors, bearing raceways errors, etc. The various factors involved have been listed in Appendix E of this study; subsequent calculations show that the worst case and RMS "average" backlash values measured between any pair of wedges are 149 and 50 arc seconds respectively. The effect of the above noted relative motion is to introduce a random uncertainty in optical deviation due to the drive ranging from 0.15 to 0.45 arc seconds in the desired deviation direction. These values are entirely consistent with the one-quarter second optical resolution derivable from the least significant bit size of the encoder used, and suggest that the predicted backlash amplitude will not be objectionable so long as sufficient coulomb friction is present to prevent count dithering when the sero is in an "off" condition. The use of large bearings together with anti-backlash gearing in the last mesh virtually guarantees reasonable levels of coulomb friction and assures stable performance.

3.3 ELECTRONICS

3.3.1 Electronics System Description

The electronics of the Attitude Transfer Assembly receives the signals generated by the remote reflector deviations in response to boom deflections and provides the drives for the stepper motors in the proper direction to null the input error signal. The wedge position data is generated from optical encoders presented in digital form. The data output supplemented by the residual open-loop error signal is a measure of the boom end attitude. The Automatic Gain Control loop in both the YZ and X channels keep the radiant energy incident on the acquisition detectors (and therefore on the error detectors) a constant, independent of LED degradation, change in detector responsivity and increased transmission losses.

The system block diagrams are shown in Figures 3.17, 3.18, 3.19, and 3.20. They include analog channels from open loop X, Y and Z information, digital channels for closed loop information from the encoders on the X, Y and Z optical wedges, motor control circuitry to control the movement of the optical wedges and keep the open loop outputs within certain limits, and a power supply.

3.3.1.1 Calculated Power Consumption

<u>±15 VDC Regulated Supply</u>	<u>±15</u>	<u>-15</u>
44 LM108s at 0.6 mA max each	26.4 mA	26.4 mA
10 LM111s at 6 ma max each	60.0 mA	50.0 mA
7 preamplifier current sources @ 1 mA each	7.0 mA	7.0 mA
2 differential transistor pairs 2N2060	6.0 mA	6.0 mA
10 FET switch drivers	6.0 mA	10.0 mA
Misc. discrete components	5.5 mA	2.5 mA
Regulator standby current	<u>2.0 mA</u>	<u>5.0 mA</u>
Total	112.9 mA	106.9 mA

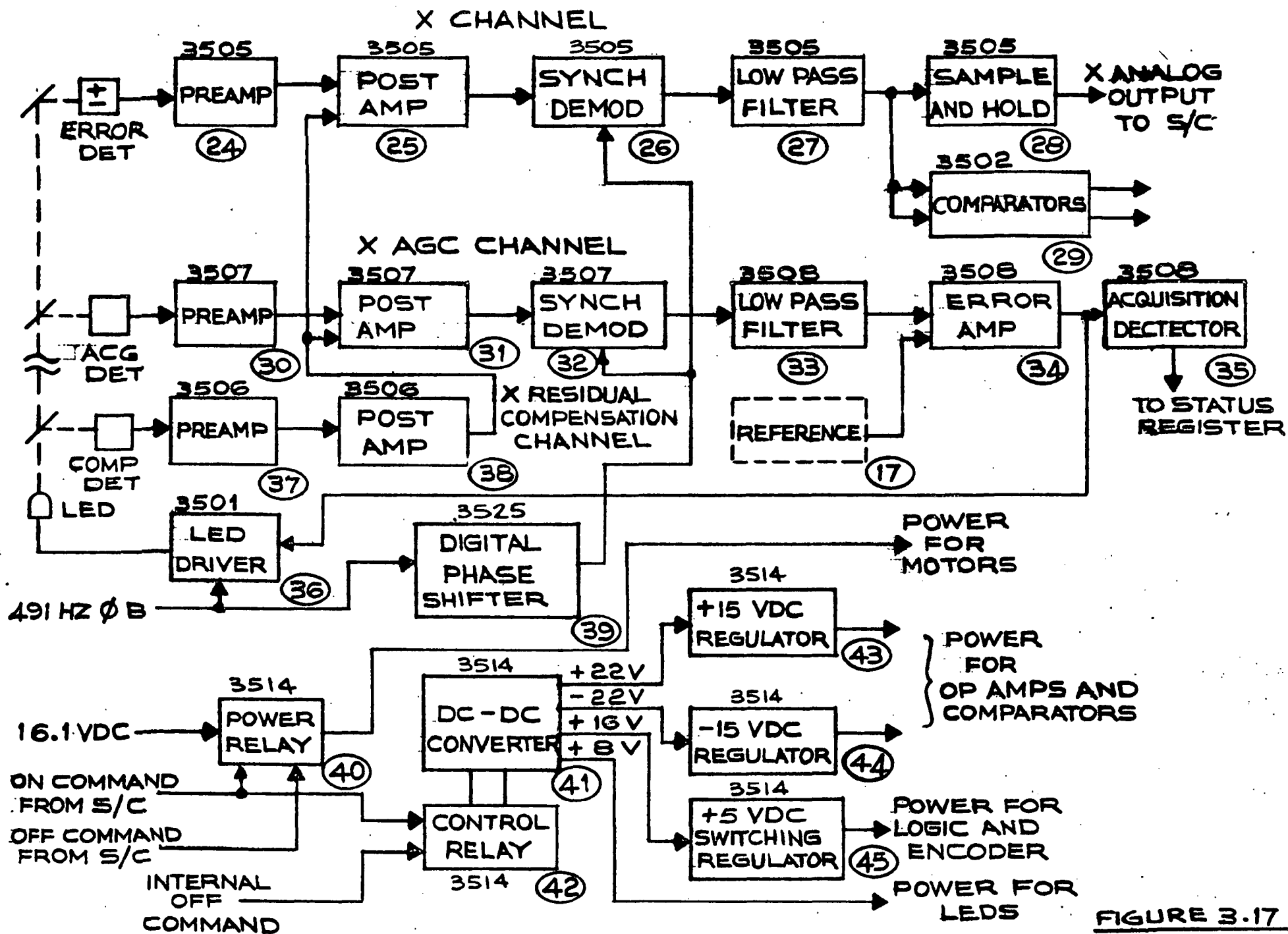


FIGURE 3.17

BLOCK DIAGRAM POWER SUPPLY AND X ANALOG SIGNAL PROCESSING
MAGSAT-ATA

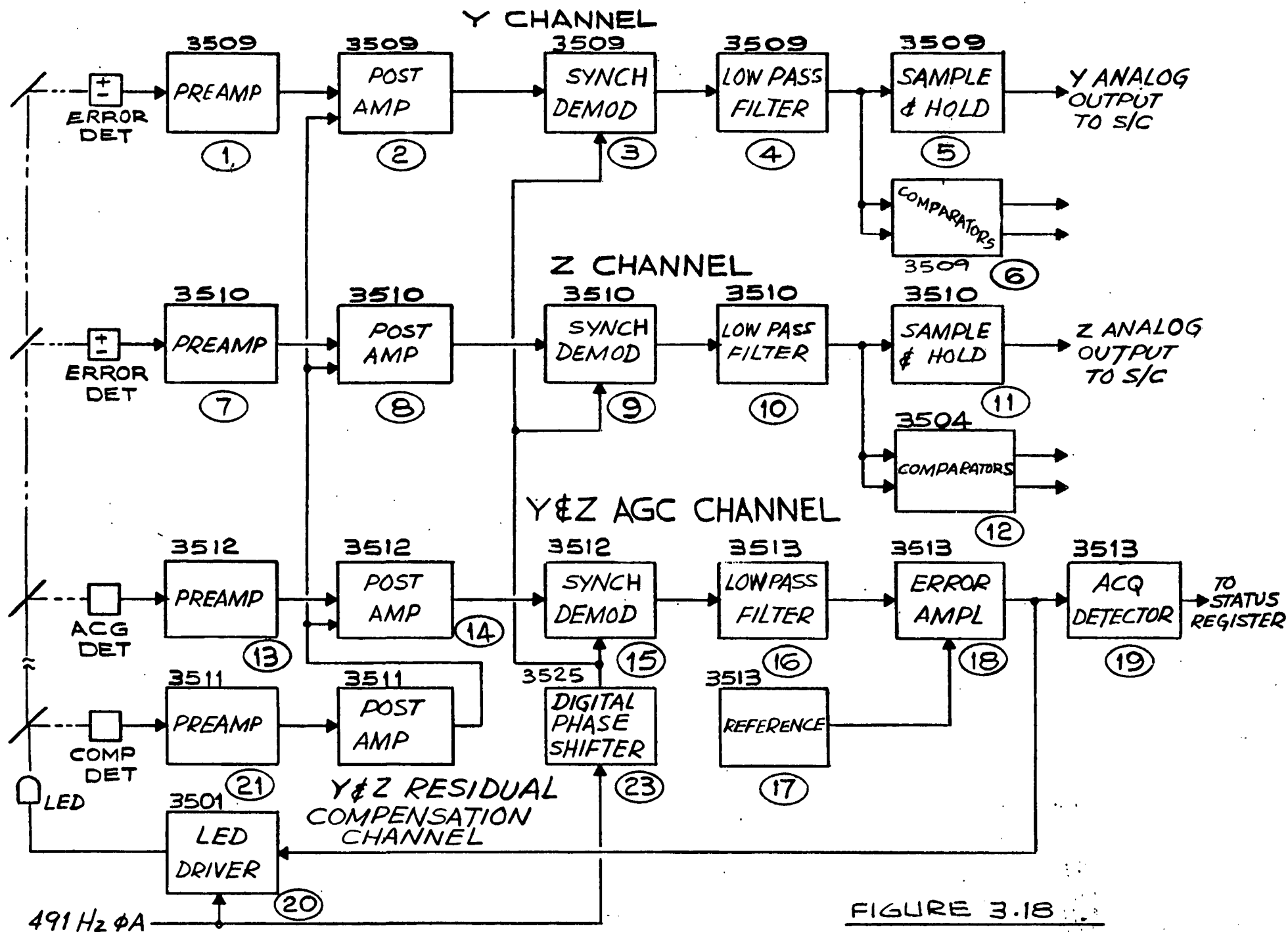


FIGURE 3.18

Y & Z ANALOG SIGNAL PROCESSING BLOCK DIAGRAM MAGSAT-ATA

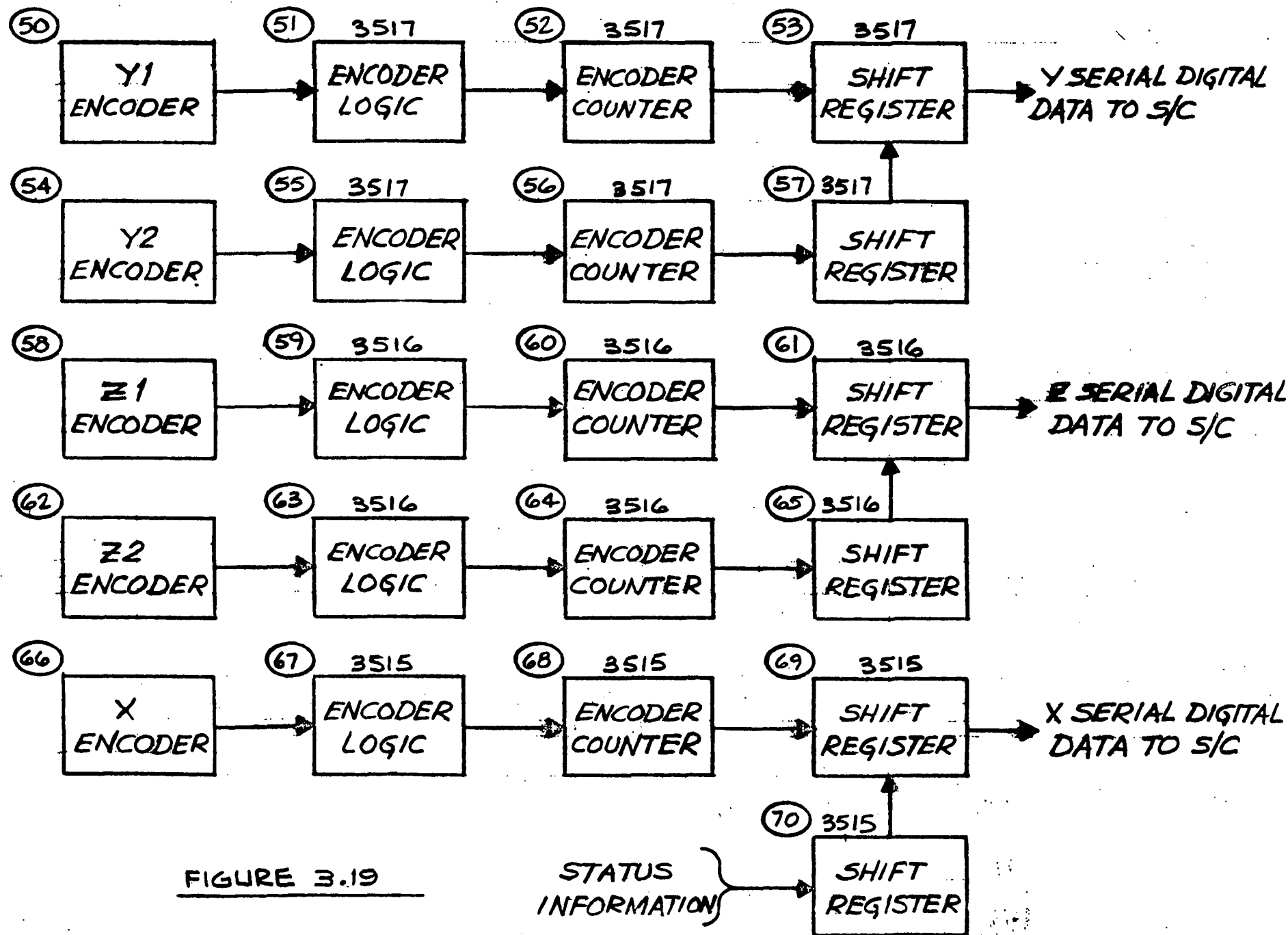


FIGURE 3.19

ENCODER DIGITAL PROCESSING BLOCK DIAGRAM
MAGSAT-ATA

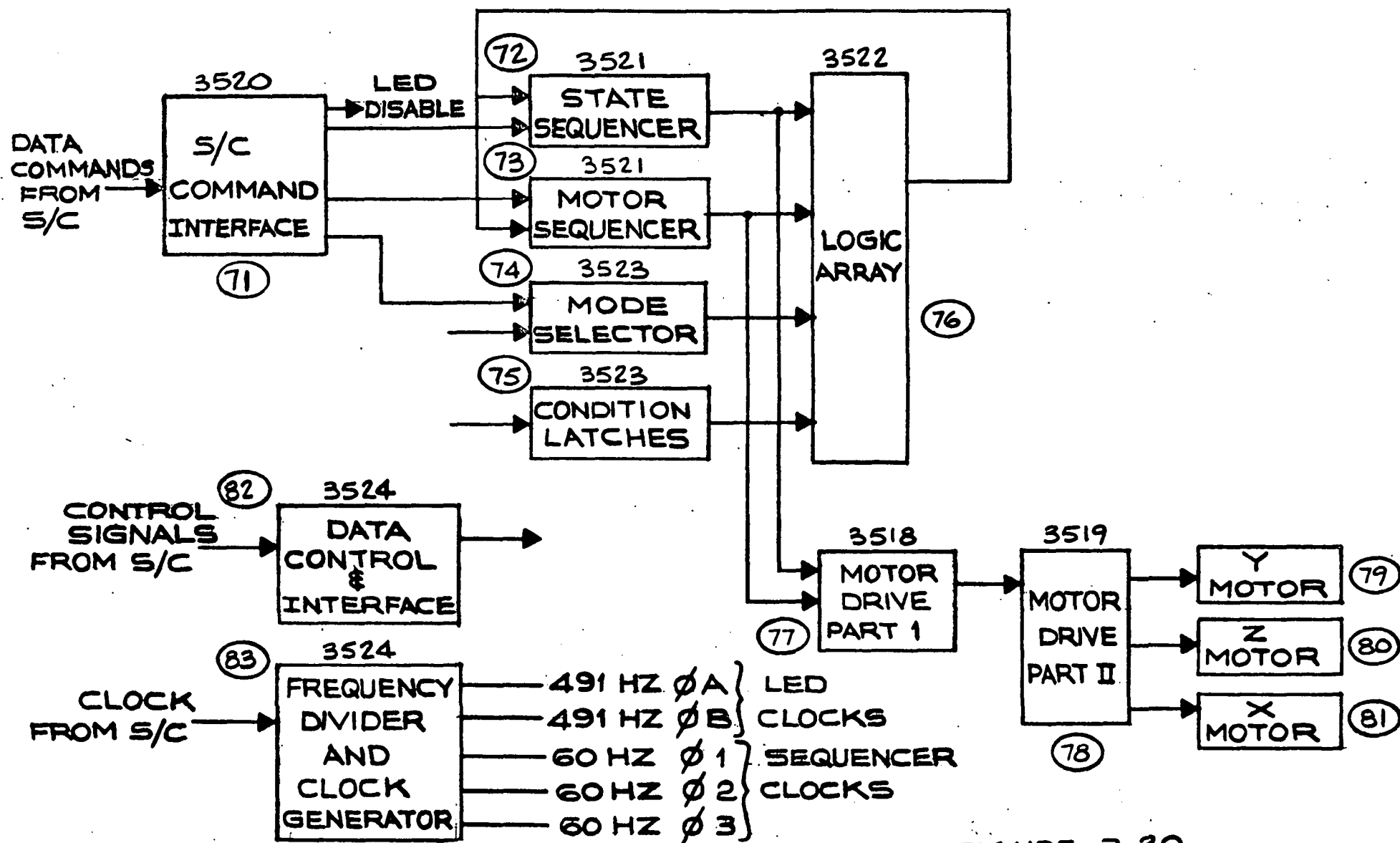


FIGURE 3.20

BLOCK DIAGRAM-MOTOR CONTROL AND DIGITAL SIGNAL PROCESSING
MAGSAT-ATA

The output voltage at the secondary of the DC/DC
cpmverter is ± 22 vdc.

$$\therefore P_{\text{sec}} = (22\text{V} \times 112.9 \text{ mA}) + (22\text{V} \times 106.9 \text{ mA}) = 4.8 \text{ watts}$$

+5 vdc Regulated Supply

5 encoders @ 120 ma each	600 mA
Misc. discrete components	<u>13 mA</u>
Total	613 mA

Assume that the switching regulator is 80% efficient.

$$\therefore P_{\text{sec}} = \frac{5\text{V} \times 613 \text{ mA}}{80\%} = 3.8 \text{ watts}$$

+8 vdc Unregulated Supply

$$2 \times 140 \text{ mA} \times 50\% \text{ duty cycle} = 140 \text{ mA}$$

$$\therefore P_{\text{sec}} = 8\text{V} \times 140 \text{ mA} = 1.1 \text{ watts}$$

$$\therefore \text{Total } P_{\text{sec}} = 4.8 + 3.8 + 1.1 = 9.7 \text{ watts}$$

Assume DC/DC converter is 80% efficient.

$$\therefore P_{\text{pri}} = \frac{9.7}{80\%} = 12.1 \text{ watts}$$

Total standby power required = 12.1 watts

Additional power required to rotate optical wedges

5 optical isolators @ 10 ma each

$$\frac{10 \text{ ma} \times 8\text{V}}{80\%} = 0.1 \text{ watts}$$

Switching transistor base drive

$$10 \text{ ma} \times 16.1\text{V} = 0.16 \text{ watts}$$

Stepping motor 10 watts

Switching Transistors

$$P_{\text{motor}} \times 10\% = \underline{1 \text{ watt}}$$

Total 11.3 watts

Assume stepping motor will be operating 2% of the time

$$\therefore \text{average system power} = 12.1 + (.02 \times 11.3) = \underline{\underline{12.3 \text{ watts}}}$$

$$\text{Peak system power} = 12.1 + 11.3 = \underline{\underline{23.4 \text{ watts}}}$$

3.3.1.2 Signal to Noise Calculations

3.3.1.2.1 Signal

The calculated signal levels are shown in Figure 3.21.

Amplifier gains are selected to provide the required scale factors.

3.3.1.2.2 Noise

The output noise of the preamplifier is expressed as

$$e_{NO} = \left[e_F^2 + e_{(i_n)}^2 + e_N^2 + e_D^2 \right]^{1/2}$$

where:

e_{NO} = Preamplifier Output Noise

e_F = Feedback Resistor Noise

$e_{(i_n)}$ = FET current noise

e_N = FET Short Circuit Noise

e_D = Detector Noise

All noise voltages are referred to the preamplifier output.

1. e_F is the Johnson Noise of the feedback resistor

$$e_F / \sqrt{\text{Hz}} = \left[4K T R_F \right]^{1/2}, \text{ where } (R_F = 10 \text{ Meg})$$

$$e_F / \sqrt{\text{Hz}} = 4 \times 10^{-7} \text{ V} / \sqrt{\text{Hz}} = .4 \mu \text{ V} / \sqrt{\text{Hz}}$$

2. 2N5522 FET noise current is due to the gate leakage I_{gss}

which is 500 Pa at 35°C.

	Units	Y-Z Error Channel	Y-Z AGC Channel	X Error Channel	X AGC Channel
Preamp Input Signal (p-p) {	A A/arc-sec	2.01×10^{-9}	2.89×10^{-8}	2.83×10^{-10}	2.76×10^{-8}
Preamp Output Signal (p-p) {	V mV/arc-sec	20.1	.289	2.83	.276
Gain, Postamp 1		1.0	4.0	8.0	4.0
Gain, Postamp 2 (nominal)		4.98	5.54	8.83	5.80
Gain, Synchronous Demodulator		0.5	0.5	0.5	0.5
Gain, Low Pass Filter		2	2	2	2
Gain, Sample & Hold		1		1	
System Gain		4.98	22.15	70.67	23.19
Output	V mV/arc-sec	100	6.4	200	6.4

Note: This table represents final calculations of signal levels and required gains, and calculations in this section are consistent with it. The component values of the schematic diagrams are not fully compliant, however, with these final gain values.

Figure 3.21

Therefore:

$$i_n = \left[2 q I_{gss} \right]^{1/2} = \left[2 (1.6 \times 10^{-19}) 500 \times 10^{-12} \right]^{1/2}$$

$$i_n = 1.3 \times 10^{-14} \text{ A}/\sqrt{\text{Hz}}$$

Referring this to the preamplifier output:

$$e(i_n) = i_n \times R_F = 1.3 \times 10^{-7} \text{ V}/\sqrt{\text{Hz}} = .13 \mu\text{V}/\sqrt{\text{Hz}}$$

3. The 2N5522 short circuit noise e_N is $10 \text{ NV}\sqrt{\text{Hz}}$.

The detectors have a shunt capacitance of 200 PF max. The feedback resistor breaks with this capacitance and causes e_N to be boosted at 6 dB per octave. This break will occur at 80 Hz. Therefore at 400 Hz

$$e_N = \frac{400}{80} \times 10 = 50 \text{ nV}/\sqrt{\text{Hz}} = .05 \mu\text{V}/\sqrt{\text{Hz}}$$

4. Since the detector is operated at zero bias, the predominant noise source is the detector resistance R_D .

$$e_D/\sqrt{\text{Hz}} = \sqrt{4 K T R_D}^{1/2}, R_D = 50 \text{ M}$$

$$e_D/\sqrt{\text{Hz}} = .89 \mu\text{V}/\sqrt{\text{Hz}}$$

Referred to the preamplifier output

$$e_D/\sqrt{\text{Hz}} = .89 \mu\text{V}\sqrt{\text{Hz}} \times 10/50 = .18 \mu\text{V}/\sqrt{\text{Hz}}$$

$$\therefore e_{NO} = \sqrt{.4^2 + .13^2 + .05^2 + .18^2}$$

$$= .46 \mu\text{V}/\sqrt{\text{Hz}}$$

The noise at the output of the system is calculated from

$$V_N = e_{NO} \times G \times 1.414 \times \sqrt{\frac{\pi}{2} B}$$

where e_{NO} = noise at preamp output

G = system gain

1.414 = increase in noise at output of synchronous demod.

$\frac{\pi}{2} B$ = effective BW of 1 pole filter

B = Bandwidth of low pass filter

V_N at the Y or Z output is

$$.46 \times 4.98 \times 1.414 \times \frac{\pi}{2} \times 10 = 12.8 \mu V \text{ (rms)}$$

V_N at the X output is

$$.46 \times 70.7 \times 1.414 \times \frac{\pi}{2} \times 10 = 181.9 \mu V \text{ (rms)}$$

3.3.1.2.3 Signal to Noise

Based on the calculated noise of the system, the noise equivalent angle (NEA) or resolution is calculated from:

$$\begin{aligned} \text{NEA} &= \frac{V_{NO} \text{ (rms)}}{\text{Scale Factor}} = \frac{.0128}{100 \text{ mv/as}} = 1.3 \times 10^{-4} \text{ arc sec (Y,Z channels)} \\ &= \frac{.1819 \text{ mv}}{200 \text{ mv/as}} = 9 \times 10^{-4} \text{ arc sec (X channel)} \end{aligned}$$

The calculated noise of the system is not the limiting noise because there are other noise sources in the detector which were not considered in the above calculations. NEA may also be calculated based on a minimum detector D^* of 5×10^{11} .

$$\text{NEP} = \sqrt{\frac{A_D \times \Delta f}{D^*}} = \sqrt{\frac{.032 \times \frac{\pi}{2} \times 10}{5 \times 10^{11}}} = 1.42 \times 10^{-12} \text{ W}$$

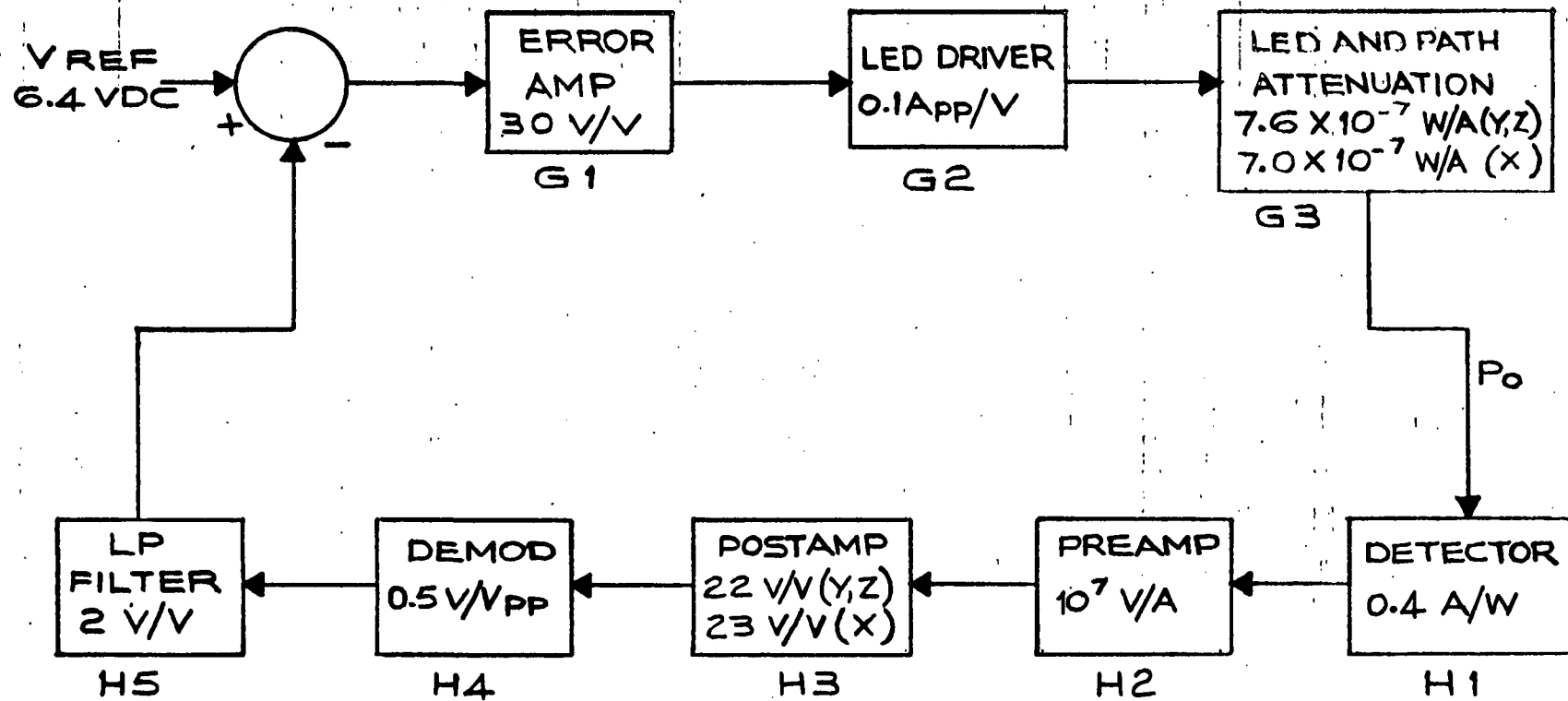
$$\text{NEA} = \frac{\text{NEP}}{dp} = \frac{1.42 \times 10^{-12}}{2.01 \times 10^{-9}} = 7 \times 10^{-4} \text{ arc sec (Y, Z channel)}$$

$$= \frac{1.42 \times 10^{-12}}{2.83 \times 10^{-10}} = 5 \times 10^{-3} \text{ arc sec (X channel)}$$

These calculations show that the performance of the system is detector noise limited and is substantially better than the required 0.1 arc sec in the Y and Z channels and 0.5 arc sec in the X channel.

3.3.1.3 AGC Loop Accuracy

Figure 3.22 shows the block diagram of the AGC loop with simplified transfer functions. The following calculations show that



AGC LOOP

FIGURE 3.22

for a 50% reduction in loop gain over life (including degradation of the LED, variations in distance between autocollimator and experiment, contamination of optical surfaces, etc.) the change in energy on the track detector, and therefore the scale error is less than 0.5%. This may be made even smaller if desired by increasing the gain and reducing the bandwidth of the loop.

$$P_o = \frac{V_{REF}}{H} \times \frac{1}{\frac{1}{GH} + 1} \approx \frac{V_{REF}}{H}$$

$$H = H1 \times H2 \times H3 \times H4 \times H5$$

$$H_{yz} = 0.4 \times 10^7 \times 22 \times 0.5 \times 2 = 8.8 \times 10^{-7} \text{ VW}$$

$$H_X = 0.4 \times 10^7 \times 23 \times 0.5 \times 2 = 9.2 \times 10^{-7} \text{ VW}$$

$$G = G1 \times G2 \times G3$$

$$G_{yz} = 32 \times 0.1 \times 7.6 \times 10^{-7} = 2.4 \times 10^{-6} \text{ W/V}$$

$$G_X = 32 \times 0.1 \times 7.0 \times 10^{-7} = 2.2 \times 10^{-6} \text{ W/V}$$

$$G_{yz} H_{yz} = 2.4 \times 10^{-6} \times 8.8 \times 10^{-7} = 211$$

$$G_X H_X = 2.2 \times 10^{-6} \times 9.2 \times 10^{-7} = 202$$

For a 50% reduction in loop gain over life

$$\Delta P_o = \frac{1}{1/2 GH} - \frac{1}{GH} - \frac{1}{100} - \frac{1}{200} = 0.5\%$$

For a 100% increase in loop gain

$$\Delta P_o = \frac{1}{GH} - \frac{1}{2GH} \approx \frac{1}{200} - \frac{1}{400} = 0.25\%$$

3.3.2 Inputs and Outputs

The instrument has one relay input to turn it off and on, one digital input for data commands, three digital data outputs, and three analog outputs.

3.3.2.1 Digital Outputs

When the spacecraft takes data, it should follow this order:

1. Y digital data (24 bits)
2. Z digital data (24 bits)
3. X analog data
4. Y analog data
5. Z analog data
6. X digital data (16 bits + 8 status bits)

Since the data is not updated while the wedges are moving, it is possible that the data in the shift registers has been shifted out to the spacecraft earlier and not updated. If that has happened, the data valid bit (bit 15) in the Y data will be zero instead of one. The data is shifted out most significant bit (bit 23) first.

The data is formatted as shown below:

	<u>System Output</u>	<u>Meaning</u>
Y Data:	Bit 23	Data Valid Bit
	Bit 22	Bit 14
	.	.
	.	.
	Bit 8	Bit 0
	Bit 7	Bit 7
	.	.
	.	.
	.	.
	Bit 0	Bit 0
Z Data	Bit 23	Not used
	Bit 22	Bit 14
	.	.
	.	.
	Bit 8	Bit 0
	Bit 7	Bit 7
	.	.
	.	.
	.	.
	Bit 0	Bit 0
X Data:	Bit 23	Not used
	Bit 22	Bit 14
	.	.
	.	.
	.	.
	Bit 8	Bit 0
	Bit 7	Y-Z channel signal acquired
	Bit 6	X channel signal acquired
	<u>Bits 5 4</u>	
	0 0	Mode 0
	0 1	Mode 1
	1 0	Mode 2
	1 1	Mode 3
	<u>Bits 3 2</u>	
	0 0	Y motor selected
	0 1	Z motor selected
	1 0	Not used
	1 1	X motor selected

the 1990s, the number of people in the world who are illiterate has increased from 400 million to 600 million. The number of illiterate people in the world is expected to reach 700 million by the year 2000. The number of illiterate people in the world is expected to reach 800 million by the year 2010. The number of illiterate people in the world is expected to reach 900 million by the year 2020. The number of illiterate people in the world is expected to reach 1 billion by the year 2030. The number of illiterate people in the world is expected to reach 1.1 billion by the year 2040. The number of illiterate people in the world is expected to reach 1.2 billion by the year 2050. The number of illiterate people in the world is expected to reach 1.3 billion by the year 2060. The number of illiterate people in the world is expected to reach 1.4 billion by the year 2070. The number of illiterate people in the world is expected to reach 1.5 billion by the year 2080. The number of illiterate people in the world is expected to reach 1.6 billion by the year 2090. The number of illiterate people in the world is expected to reach 1.7 billion by the year 2100.

Data commands provide the capability of testing and controlling the instrument from the ground. A 24 bit data command is accepted from the spacecraft, most significant bit first, and used as follows:

<u>Command</u> <u>Input</u>	<u>Function</u>
Bit 23	Not used
.	
.	
Bit 8	

<u>Bits</u>	<u>7</u>	<u>6</u>	<u>Motor Select</u>
	0	0	Y
	0	1	Z
	1	0	Not used
	1	1	X

<u>Bits</u>	<u>5</u>	<u>4</u>	<u>3</u>	<u>Motor Step Count</u>
0	0	0	0	1
0	0	1		2
0	1	0		4
0	1	1		8
1	0	0		16
1	0	1		64
1	1	0		256
1	1	1		1024

<u>Command Input</u>			<u>Mode</u>	<u>Function</u>	
<u>Bits</u>	<u>2</u>	<u>1</u>			<u>0</u>
	0	0	0	Automatic	Normal Operation
	0	0	1	Automatic	Stow wedges & turn off system
	0	1	0	Automatic	
	0	1	1	Automatic	
	1	0	0	Manual	LED Off
	1	0	1	Manual	
	1	1	0	Manual	Motor Forward (+)
	1	1	1	Manual	Motor Reverse (-)

For example, a command ending in 00000100 would turn off the LED so system offsets could be measured. A command ending in 01011110 would move the Z optical wedge 8 steps in the positive direction for calibration purposes.

3.3.2.3 Analog Outputs

The three analog outputs have scale factors as follows:

X	200 mv/arc second
Y	100 mv/arc second
Z	100 mv/arc second

3.3.3 Circuit Description

In the circuit descriptions that follow, the block numbers refer to the block diagrams in Figures 3.17, 3.18, 3.19, and 3.20. Near each block are the last four digits of the drawing number of the applicable schematic diagram which is located in Appendix F. In the lower left hand corner of each schematic diagram is a list of the blocks contained in that schematic.

Since the three channels are nearly identical, the description will refer to the X channel unless otherwise stated.

3.3.3.1 Preamplifier (Blocks 1, 7, 13, 21, 24, 30 and 37)

The seven current preamplifiers used in this system are identical to each other. They consist of an LM108A operational amplifier buffered at the input by a 2N5522 very low noise differential FET pair. The preamplifier converts the signal current from the silicon detectors into a voltage amplitude $V_o = I_s R_f$. R_f is R_8 on the schematic and is a 10 Megohm precision resistor. R_7 , C_2 and R_9 , C_4 are compensation network to assure stability of the preamplifier. The transistor circuits containing Q_1 and Q_3 are emitter follower regulators whose purpose is to prevent any noise on the +15 vdc and -15 vdc lines from coupling into the preamplifier. This preamplifier design is used on other Barnes autocollimating systems.

3.3.3.2 Post Amplifiers (Blocks 2, 8, 14, 22, 25, 31 and 38)

All post amplifiers use precision resistive components to avoid changes in gain over life and temperature. The forward gain of any post amplifier was kept at 10 or below so that the loop gain of the amplifiers at 400 Hz would be at least 1000. Therefore for a 100% change in open loop gain of the operational amplifier over life the forward gain change would be less than 0.1%.

3.3.3.3 Synchronous Demodulator (Blocks 3, 9, 15, 26 and 32)

The synchronous demodulator consists of an LM108A, two 2N4848A JFET's and 2 precision resistors. The two 20K resistors along with the operational amplifiers form a unity gain amplifier, which depending on how the FETs are energized, is either inverting or non inverting.

When Q_4 is open and Q_5 closed, the gain is unity $\frac{R_{23}}{R_{26}}$ and inverting. When Q_4 is closed and Q_5 open the operational amplifier acts as a voltage follower. It can be seen that the

"ON" resistance of the FETs does not affect the voltage gain for either the inverting or non-inverting modes. R27 and R30 are included to minimize voltage offsets due to the bias current of the operational amplifier.

3.3.3.4 Low Pass Filter

The low pass filter design for the error channels (Blocks 4, 10 and 27) comprises a single pole break at 10 Hz to give a -6db/octave slope with a -3 db point at 10 Hz. The break consists of R33 and C21. The low pass filter design for the acquisition channels (Blocks 16, 33) is slightly different that used for the error channel, because it is the predominant break in the loop and therefore determines the stability of the loop. The first break is provided by R1 and C1. Components R6, R7 and C8 provide lead-lag compensation to ensure that when the loop gain is unity the roll off rate is only 6 db/octave, thus guaranteeing the loop stability.

3.3.3.5 Sample and Hold (Blocks 4, 11, 28)

Since the analog and digital error signals are not sent to the spacecraft simultaneously, and the analog channels have a finite response time, erroneous outputs could occur if an optical wedge was moving while data was being taken. To prevent this, all signals are sampled and held before any optical wedge is moved. In the analog channels this function is provided by an inverting sample and hold circuit. When Q8 is on, U6 is used as an inverting amplifier with a gain of 1. When Q8 turns off, C27 holds the previous output voltage. R38 is provided to properly interface with the spacecraft analog input.

3.3.3.6 Comparators (Blocks 6, 12, and 29)

The maximum allowable analog signal is sensed by the comparators. If the X output exceeds 5 arc seconds or if the Y or Z output exceeds 15 arc seconds, the comparator output tells the motor

sequence to move the proper wedge to reduce the error to near zero.

3.3.3.7 Voltage Reference (Block 17)

The voltage reference circuit for the acquisition loops consists of an LM108A operational amplifier and a 1N4573A voltage reference zener. Total temperature and end of life variations are expected to be less than 0.1% of the -6.4 vdc output voltage

3.3.3.8 Error Amplifier (Blocks 18, 34)

The error amplifier is simply a summing amplifier. It compares the reference voltage with the output voltage of the low pass filter. If the output of the L.P. filter is low then the output of the error amplifier increases, which increases the LED current, or more importantly the radiant energy of the LED. This, in turn, increases the voltage at the output of the L.P. filter until equilibrium is attained. Thus the closed loop control system for the acquisition channel is achieved.

3.3.3.9 Acquisition Detector (Block 19 and 35)

This circuit determines the status of the acquisition or track channel by monitoring the output voltage of the acquisition error amplifier. When the AGC loop is in control this voltage is within a certain range. A window comparator consisting of two LM111A voltage comparators is used to compare this voltage with a reference voltage. The thresholds of the comparators are adjusted such that if the input voltage is within the window the outputs of the LM111A's are high (+5 vdc). Therefore, the output signal is a logic one. If the input voltage traverses the low or high level of the window the output of one of the LM111A's will go to ground and the output logic level then goes to logic 0.

3.3.3.10 LED Driver (Blocks 20 and 36)

Since both LED drivers are identical, only the X LED driver will be discussed. U2, Q10, Q11, R26, R34 and R38 form a

current source. The controlled current flows through Q11, R38 and the LED. If Q9 is off, the magnitude of the current is $I = -V_i \cdot \frac{R_{34}}{R_{26}} \cdot \frac{1}{R_{38}}$. Typically $V_i = -1V$, $R_{38} = 10\Omega$, and $R_{34} = R_{26}$ so the current through the LED is 100 mA. If Q9 is on, the voltage at the base of Q10 is $V_o = V_i \cdot \frac{R_{on}}{R_{26}} = 15 \cdot \frac{25}{10000} = 38 \text{ mv max}$, so Q10, Q11 and the LED are off. Q7 and Q8 provide level translation from the (0V or 5V) logic levels to the gate of Q9 (0V or -15V). The LED is modulated by turning Q9 off and on at a 491 Hz rate.

Q12 and its associated circuitry form an LED current limit circuit. If the signal on the AGC detector is not present, V_i will increase to nearly -15V. In order to protect the LED, the base of the right hand side of differential transistor Q12 is set to +1.4 vdc by the divider network R40 and R41. If the base of the left hand transistor exceeds 1.4 vdc the collector of the same transistor starts to draw base current away from Q10 and Q11 and so limits the collector current of Q11. Thus for 1.4 vdc at R38, I current limit = $\frac{1.4}{10} = 140 \text{ mA}$.

If the -15V power supply fails, U2 and Q12 may not work properly and excessive LED current could result. However, if the gate of Q9 is more positive than -4V, Q9 turns on and the voltage at the base of Q10 is limited to slightly more than 0.6V, and Q10 and Q11 will be off.

3.3.3.11 Digital Phase Shifter (Blocks 23 and 39)

The digital phase shifter provides a fixed selectable phase shift for the drive signal to the synchronous demodulator.

The phase shifting is required to compensate for the phase shifts through the pre-and post-amplifiers so that when the signal appears at the synchronous demodulator input the clocks are in phase with the signal. If this was not done there would be an

attenuation of the output signal due to the phase difference.

The phase shift is provided by passing the 491 Hz clock through a shift register of N stages being clocked by the 251KHz clock. This provides a phase shift of $N \cdot \frac{1}{251 \times 10^3} \cdot 360 \cdot 491$ degrees, or 0.7°/stage.

3.3.3.12 Clock Generator (Block 83)

The clock generator uses the 251 KHz spacecraft clock to generate all other clocks. The clock is divided down to 1960 Hz by counter U3 and further divided by U12 to generate two 491 Hz clocks which are 90° out of phase with each other. One of these clocks is used for each channel to provide maximum rejection of any unwanted signal from the other channel. CR2, C2 and R12 with one section of gate U13 cause the Y-Z LED to turn off in case of clock failure. Normally C1 is charged to +4.4V through CR2 and R11, enabling the gate. If the clock stops, C2 discharges through R11 and R12 and disables the gate within 30 ms and before the LED can overheat. Components CR3, C3, R12 and another section of gate U13 provide the same function for the X channel.

The Motor Controller requires a three phase 60 Hz clock which is generated by counter U4. When the 60 Hz clock from U3 is high, counter U4 is held at zero and Ø1, Ø2 and Ø3 are low. When the 60 Hz clock goes low, U4 begins counting. Clock Ø1, Ø2 and Ø3 go high with the counts of 2, 4 and 6 respectively. When the counter reaches nine, further counting is inhibited until the cycle repeats.

3.3.3.13 Encoders (Blocks 50, 54, 58, 62 and 66)

Each of the five encoders operates on +5vdc and provides a two phase output and a once around output, all at standard logic levels.

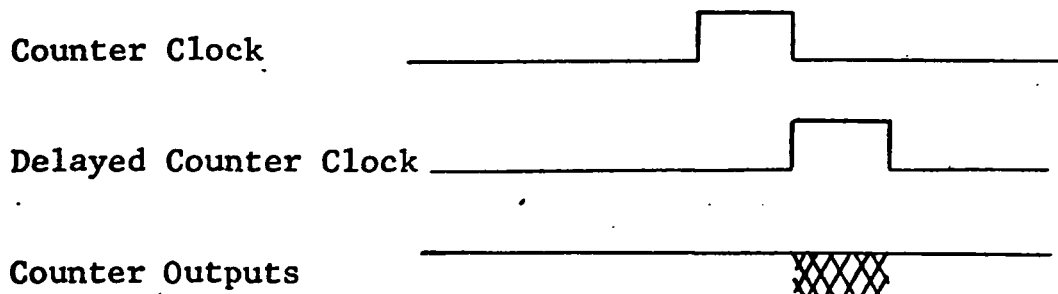
3.3.3.14 Encoder Logic

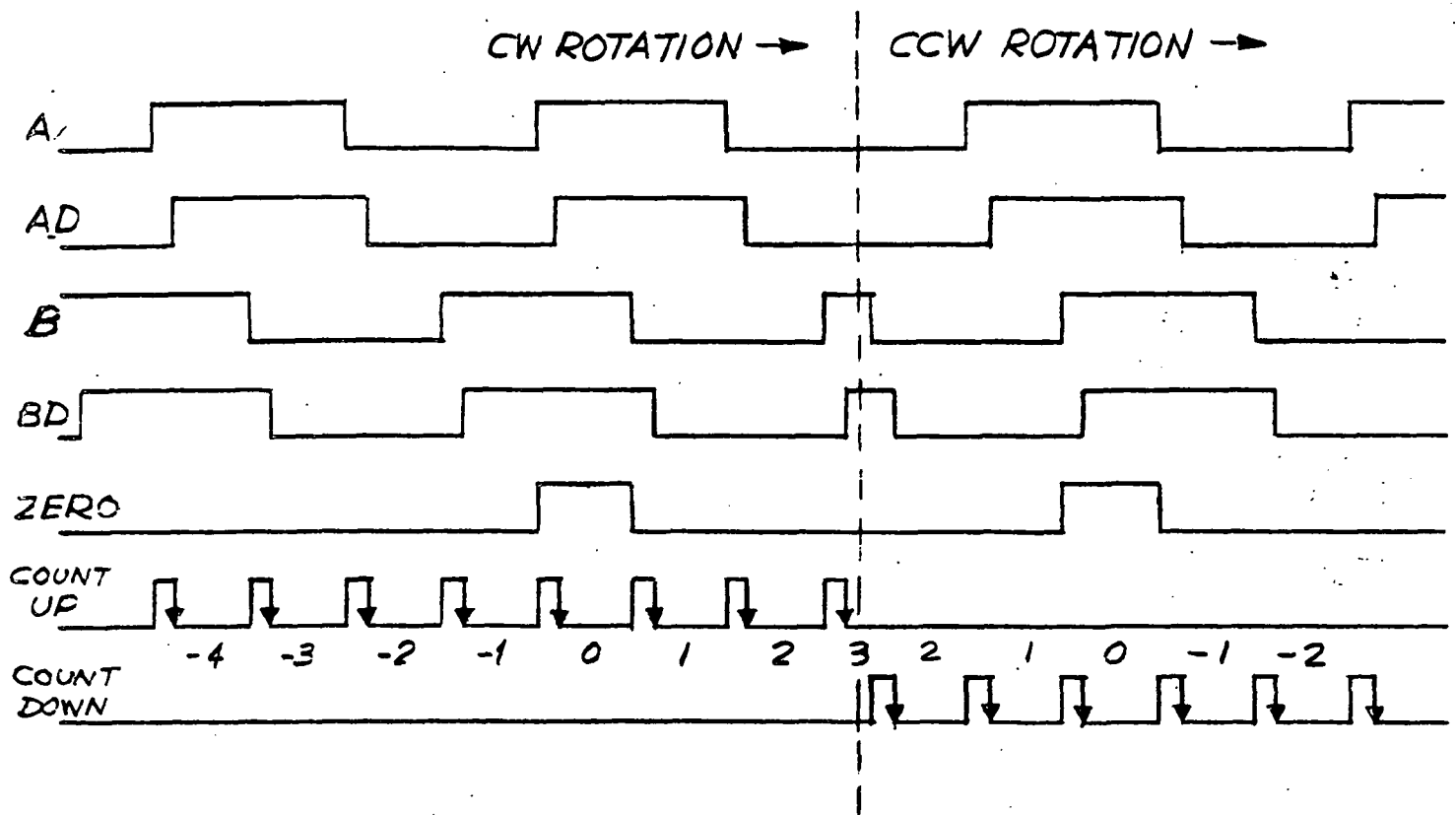
The two phase encoder outputs must be processed to provide count up, count down and clear signals to the counter which keeps track of the absolute encoder position. Since all channels are identical, only the X channel will be discussed. Shift register U1 is used to synchronize the A and B encoder outputs to the 251 KHz clock and also provide delayed outputs, AD and BD. Figure 3.23 shows the outputs from U1 as the encoder rotates through zero and back again. Also shown are the desired input signals to the up-down counter. An examination of the six logic signals will verify that $\text{COUNT UP} = (\overline{A \oplus BD}) \cdot (\overline{B \oplus AD})$ and $\text{COUNT DOWN} = (A \oplus BD) \cdot (B \oplus AD)$

Since the u-down counter is the type with a mode control and a single clock, an R-S flip flop and an OR gate is used to provide the correct signals to the counter.

The zero reset output from the encoder is actually slightly wider than one count so after being synchronized to the 251 KHz clock by U2 section 1 it is ANDed with the A and B outputs to provide a true reset pulse to the counters.

The outputs from the encoder counter are parallel loaded into shift registers U13 and U14 when DIGSAMPO GO is low. When DIGSAMPO GO goes high the data is held in the shift registers if it is valid. Immediately after the counter is clocked, the counter outputs are changing states and cannot be considered valid. U2 section 2 provides a delayed counter clock which indicates invalid data as shown below.





	A	AD	B	BD	$A \oplus AD$	$B \oplus BD$		A	AD	B	BD	$A \oplus AD$	$B \oplus BD$
UP =	1	0	1	1	0	1	DN =	1	0	0	0	1	0
OR	1	1	0	1	0	1	OR	1	1	1	0	1	0
OR	0	1	0	0	0	1	OR	0	1	1	1	1	0
OR	0	0	1	0	0	1	OR	0	0	0	1	1	0

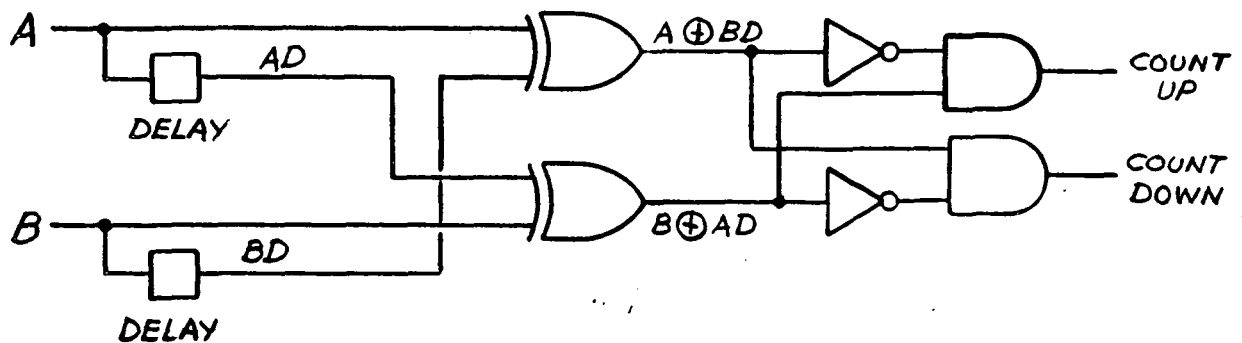


FIGURE 3.23

INCREMENTAL ENCODER LOGIC

If DIGSAMPO GO goes high while the delayed counter clock is high two sections of gate U8 act as an R-S flip flop and prevent the data from being held until the delayed counter clock goes low indicating data is valid. This delay is a maximum of 4 microseconds long and will not interfere with shifting the data out serially.

3.3.3.15 Encoder Counters (Blocs 52, 56, 60, 64 and 68)

The UP/DOWN counters used with the encoders are type CD4029. They provide synchronous operation even when cascaded. To clear the counters, they are preset to zero. Sixteen bit counters are used with the X, Y1 and Z1 encoders, but only the least significant 8 bits are used with the Y2 and Z2 encoders since the approximate encoder position is already known.

3.3.3.16 Data Shift Registers (Blocks 53, 57, 51, 65, 69 and 70)

The shift registers used are type CD4021. When the parallel/serial input is high, data is loaded in parallel asynchronously. When the P/S input is low, the data is held until it is shifted out serially by the clock. An additional 8 bit shift register is provided for status information.

3.3.3.17 Spacecraft Data Interface (Block 82)

All digital signals from the spacecraft are buffered with CD4093 schmitt triggers for maximum noise immunity. Digital data is sent to the spacecraft serially when the readout gate is received. When the Y Readout Gate is received an R-S flip flop is set to indicate that the interface is busy. Data is considered valid during Mode 0, Mode 1, Mode 2 State 0, Mode 3 and Manual operation. If data is valid and the interface is not busy both analog and digital data is sampled. Flip flop U11 is clocked by the 8 kHz clock to provide the digital sample signal. The flip flop insures that the sample command will remain long enough for the sampling to occur, but not long enough to cause interference with shifting out the data. The R-S flip flop made with sections of

gate U10 allows the analog sample signal to remain as long as data is valid. This insures that the sample and hold circuit will have reached its final value when the spacecraft takes the analog data. After the analog data is taken, the X digital data is taken, which also resets the interface busy flip flop.

3.3.3.18 Motor Control Operation (Blocks 72 - 81)

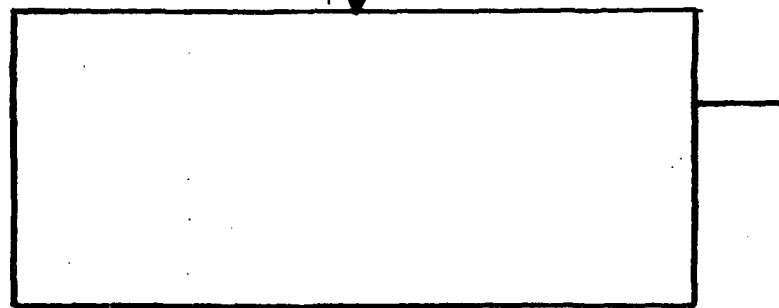
Each channel of the system has optical wedges for nulling error and a stepping motor to rotate the wedges. In order to minimize the peak power requirements, only one motor is operated at a time. The motor control operates in one of four modes. When power is applied it is in Mode 0 and each motor in turn is operated to reset the encoder counters. When all the encoder counters have been reset, the absolute encoder positions are known and the system changes to Mode 1. In Mode 1, the reflected image is searched for by a square search pattern in the Y and Z directions. When a signal is acquired, the system enters its normal operating mode, Mode 2, and motors are only operated when required to keep the error signal within preset limits. The system may be turned off by a Data Command which forces it into Mode 3. In this mode each motor is operated until its encoder is on the negative side of zero. When all encoder outputs are negative, the system turns itself off. This operation, while neither necessary nor mandatory can result in an average savings of 1000 steps for each motor when both turn off and turn on are considered.

Figure 2.24 shows the possible transitions for control of each of the three motors in each of the four modes. Each box represents States 0, 1, 2 and 3 in Figures 3.25, 3.26, 3.27 or 3.28.

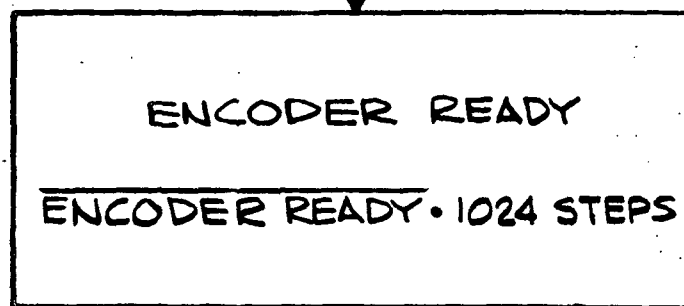
In order to prevent possible logic races all conditions which decide changes in modes or states are latched by the 60 Hz

FIGURE 3.24

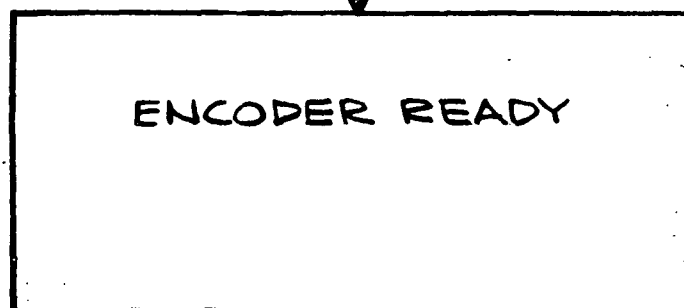
STATE 0
DECISION



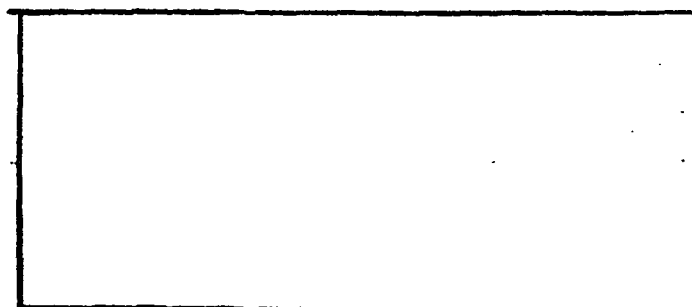
STATE 1
MOVE IN
+ DIRECTION



STATE 2
MOVE IN
- DIRECTION



STATE 3
WAIT



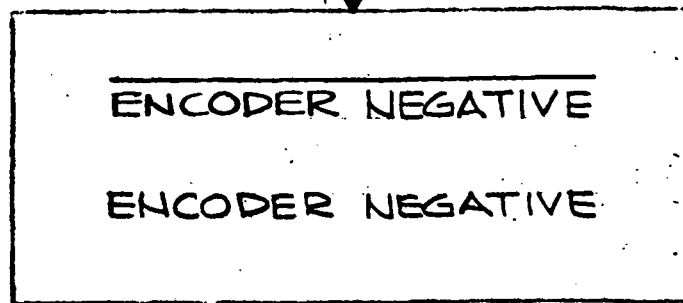
TO FIGURE 3.24

FIGURE 3.25

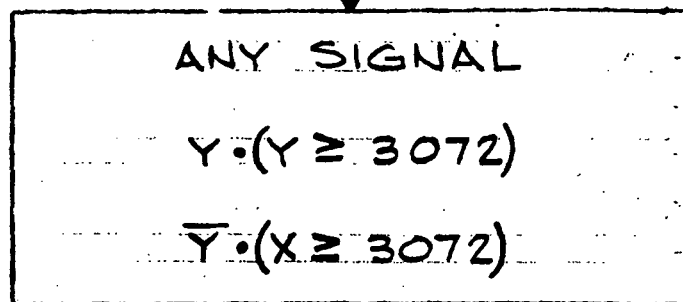
STATE DIAGRAM - MODE 0

FROM
FIGURE 3.24

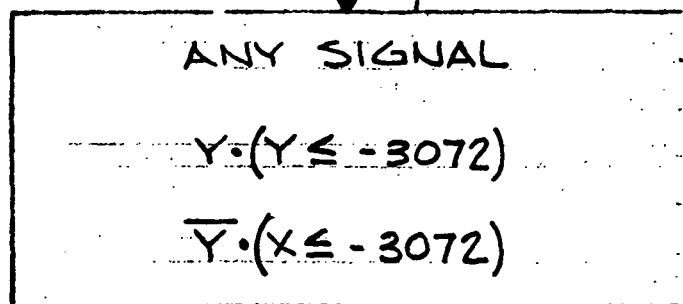
STATE 0
DECISION



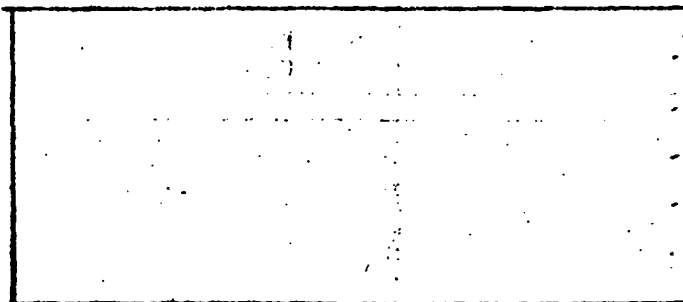
STATE 1
MOVE IN
+ DIRECTION



STATE 2
MOVE IN
- DIRECTION



STATE 3
WAIT

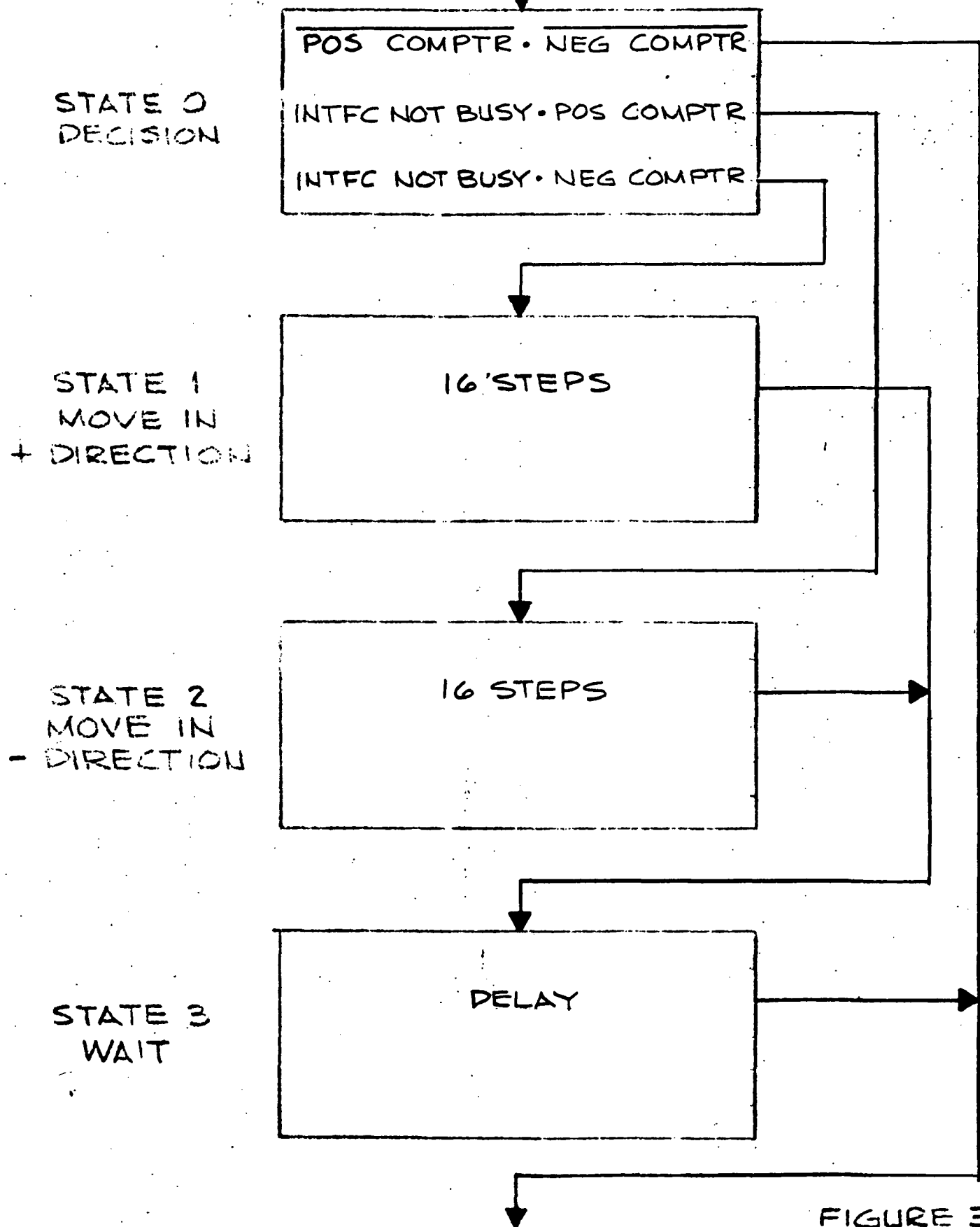


TO FIGURE 3.24

FIGURE 3.26

STATE DIAGRAM - MODE 1

FROM
FIGURE 3.24



TO FIGURE 3.24

FIGURE 3.27

STATE DIAGRAM - MODE 2

clock phase 1; the states, modes, and motor selections are changed by clock phase 2; and the motor is stepped by clock phase 3.

3.3.3.19 State and Motor Sequencer (Blocks 72 and 73)

The state and motor sequencer consists of a CD4008 four bit adder and a CD4035 used as a four bit latch. If the B inputs and carry input to the adder are low, the CD4035 will retain the same state each time it is clocked. If there is an output from the logic array, the state advances 1, 2, 3 or 4 on the next clock pulse. The two least significant bits are used as the state sequencer, and the two most significant bits are used as the motor sequencer. This causes the motor sequencer to advance by one each time the state sequencer advances to state 0. Gate U3 inhibits the most significant bit while in Mode 1 since only the Y and Z motors are used for searching.

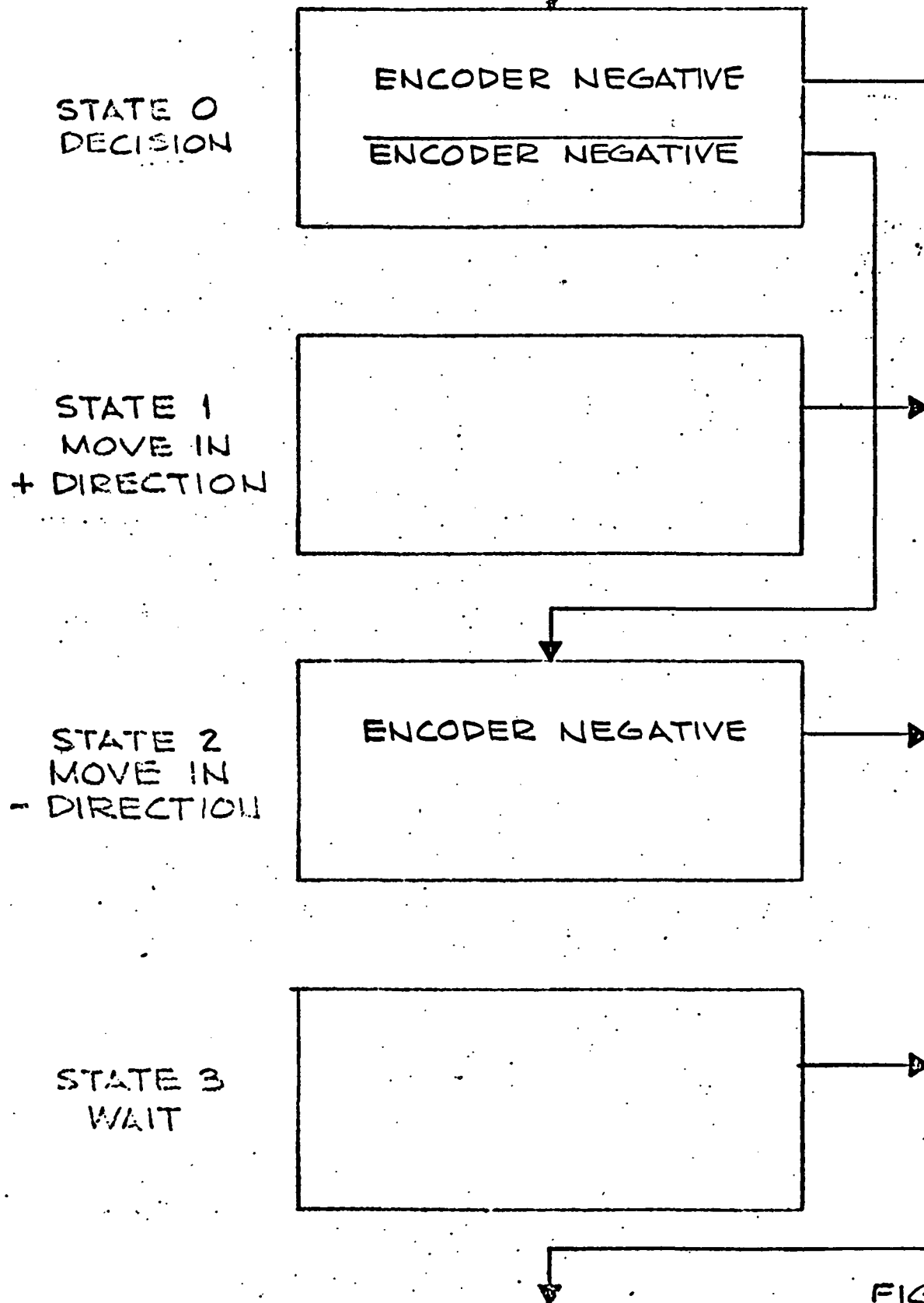
When manual operation is desired, data selector U4 is used to disable the normal state sequencing and enable inputs from the spacecraft.

The state diagrams for operation in Modes 0, 1, 2 and 3 are shown in Figures 3.25, 3.26, 3.27 and 3.28 respectively and described in section 3.3.3.18. State 0 is used as a transition state where decisions were made. States 1 and 2 are used to move the motor in the positive and negative direction respectively. During states one and two the motor is energized but it is not stepped until the second phase three clock after the motor is energized. State 3 is used to provide a delay during Mode 2 to allow the analog error signals to stabilize after moving an optical wedge.

3.3.3.20 Mode Selector (Block 74)

The mode selector specifies what mode of operation will be followed. The modes of operation are defined as follows:

FROM
FIGURE 3.24



TO FIGURE 3.24

FIGURE 3.28

STATE DIAGRAM - MODE 3

Mode 0 = Encoders Reset

Mode 1 = Encoders Reset · Mode 3 · Signal

Mode 2 = Encoders Reset · Mode 3 · Signal

Mode 3 = Encoders Reset · Stow Command

Automatic Off = Stow Command · (Encoders Reset +
Encoders Negative)

3.3.3.21 Condition Latches (Block 75)

Any condition which could result in a possible race and improper operation is latched by latches U12 and U13. Two CD4051 data selectors, U5 and U7, are also used to select the proper signal from the proper channel.

3.3.3.22 Logic Array (Block 76)

The logic array specifies how far the state sequencer should advance according to the conditions presented to it. The two CD4028 decoders provide enabling outputs corresponding to each of the 16 combinations of the four states and four modes. The ADD1, ADD2, and ADD4 outputs go directly to the adder in the state sequencer, while the ADD3 output goes to the carry input and the two input of the adder.

3.3.3.23 Motor Drive (Block 77 and 78)

The motor drive contains a two bit up-down counter for each motor. The outputs from the correct counter are selected by two CD4051 data selectors U8 and U9. The two counter output signals, the two binary motor select signals, and a motor enable signal are coupled to Part II of the drive circuitry through optical isolators to eliminate noise problems. The recovered signals are decoded to energize one winding on the proper motor.

3.3.3.24 Motors (Blocks 79, 80 and 81)

The three stepping motors are the four phase permanent magnet type. Only one winding is energized at a time both to save

power and because in this mode the natural detent and the energized detent occur at the same position.

3.3.3.25 Spacecraft Command Interface (Block 71)

Data commands from the spacecraft can control the instrument as described in section 3.3.2. Signals from the spacecraft are buffered by CD4093 schmitt triggers and selected according to which of the two redundant systems is supplying the commands. The serial command is clocked into shift register U5 and decoded by U9. The command execute signal, indicating a valid command sets flip flop U6, which is cleared on the next phase 1 clock causing the command to be loaded into registers U7 and U8. A command for manual control disables the state and motor sequencer and selects the desired manual operation. The second section of flip flop U6 resets the state and motor sequencer whenever commands are changed. This insures an orderly transition from automatic to manual operation and back again.

3.3.3.26 Power Supply (Blocks 40-45)

Power to the instrument is turned off and on by control from the spacecraft with latching relay K1. The automatic turn off is accomplished by disabling the power supply with latching relay K2.

The DC-DC converter uses a small saturating inverter to drive the main inverter. The main inverter uses a linear core to obtain optimum efficiency.

The DC-DC converter provides +22V and -22V outputs which are regulated to provide +15V and -15V for the instrument. A separate +16V output is provided which is regulated to +5V by a switching regulator to achieve maximum efficiency. A separate unregulated +8V output is provided to power the LED's. Regulation of the +8V supply is not needed because the LED's are driven by current sources.

3.4

WEIGHT AND POWER SUMMARY

The weight of the ATA system has been broken down into the major subassemblies and are listed below:

	<u>Total Weight</u>
Autocollimator each 3.8 lb.	7.6 lb.
YZ Wedge Deviation Assembly	4.2 lb.
X Wedge Deviation Assembly	2.1 lb.
Remote Reflector Assembly (7 oz)	0.438 lb.
Remote Reflector Support Structure (9 oz)	0.563 lb.
Base-line Porro Reflector (5 oz)	0.313 lb.
Base-line Reflector Support Structure (9 oz)	0.563 lb.
Electronics Package including Enclosure	6.00 lb.

The total weight therefore, excluding connecting cables and connectors will be 21.78 lb. The volume of the electronics package is calculated to be 400 cubic inches.

System power consumption has been calculated to be:

Average system power = 12.3 watts

Peak system power = 23.4 watts

4.0 TRADEOFF STUDIES

This section will discuss certain tradeoff considerations that have been studied. Although the system as defined in this report largely represents the results of decisions already made, certain options are still open and the implications will be discussed. The first of these subjects is a major one submitted by GSFC and pertains to the possibility of a gimballed boom.

4.1 Gimballed Boom Mount

A gimballed boom would provide a distinct simplification of the ATA since the wedge deviation unit, with its supporting electronics, would be eliminated from the Y-Z system. The error signals from the autocollimator would provide the inputs to the gimbal drives. Motors and readout encoders (if required) would be part of the gimbal system.

Disadvantages would include the greater power required to move the boom and possible instability associated with inertial lag between the outboard end of the boom and angular deflections imposed at the gimballed end.

As in the system described in this report, a moderate deadband may be provided in the gimbal servo drive, within which the open loop output from the autocollimator becomes an available correction factor to be applied to the spacecraft navigational data to indicate the true magnetometer orientation.

Alternatively, a tight servo response may be employed so that, theoretically, at least, the magnetometer orientation is considered to be the same as that of the spacecraft. A servo analysis would have to be made which would include not only the autocollimator error signal and servo drive characteristics, but also the flexure dynamics of the boom itself. Obviously, this investigation is beyond the scope of this study.

Beyond considerations of servo dynamics is the question of maintaining the signal-generating capability of the

autocollimator. In order to preserve this, it is essential that the collimated beam impinge on the remote reflector and that the reflected beam be recaptured by the autocollimator aperture.

As described elsewhere in this report, two modes of boom deflection must be considered. First is the case of a "stiff" boom which extends from the spacecraft at an angle other than the nominal 90° . This orientation error, which may be caused by non-repeatability of the erection process, is perfectly rectified by a gimballed boom which is driven in the required direction.

If the erection error exceed 0.12° , however, a search pattern will have to be executed by the boom itself--similar to that described in Section 2.3. Figure 4.1 illustrates the case of circular bending. In (a), the bending is shown without any tracking function and the reflected beam misses the aperture. If tracking is accomplished by rotating the gimballed boom as in (b), the correct orientation is achieved. Although the beam is not on the center of the mirror, this is of no consequence provided flatness specifications for the mirror have been adhered to.

Since the boom would not be gimballed in the X axis, the tracking capabilities of the ATA, as described in this report, would be required, if the full accuracy as summarized in the Error Analysis is to be attained.

Since elimination of the wedges in the X-channel would save materially in detailed design and fabrication effort, as well as saving power and weight, it is valuable to explore the effects on accuracy of this option. (The saving in volume and weight is not as great as might first appear. The present deflection wedge assembly is configured for the 4-wedge complement required for the Y-Z assembly, and it is proposed to use the same housing for X to save extra documentation. If the boom is gimballed, eliminating the need for the Y-Z wedge assembly, the package size required for the one X wedge would be substantially smaller.)

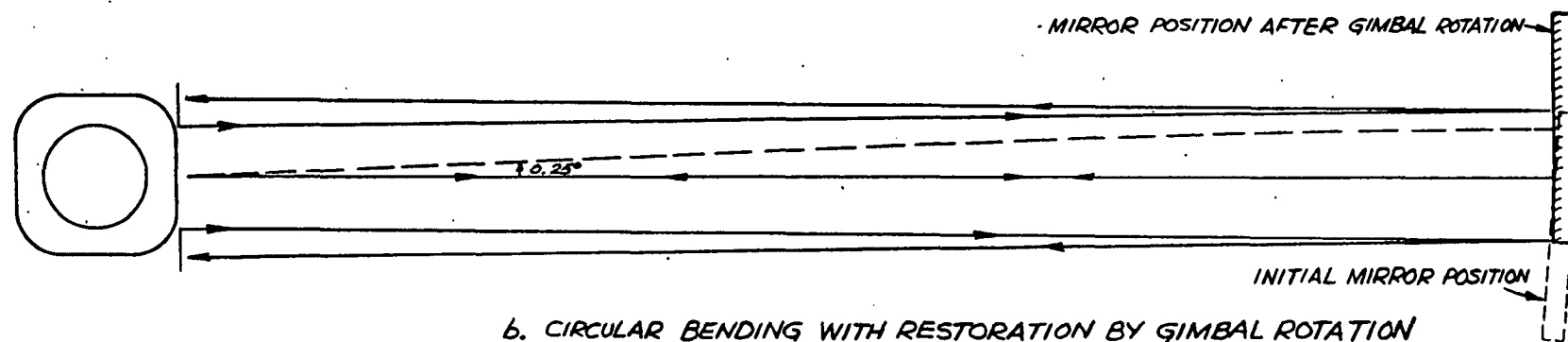
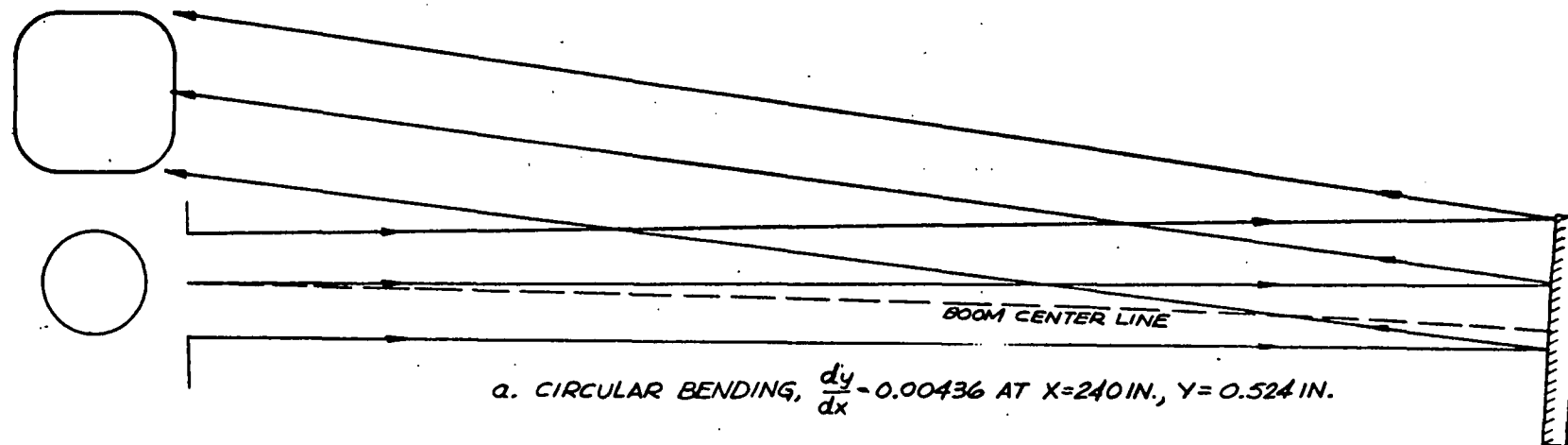
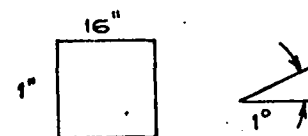


Fig. 4.1



It is pointed out in an earlier section that a calibration must be applied to the X channel data as a function of Z rotation because of small irregularities along the detector edges in the X instrument. This calibration would consist of a correction to be added to the X output independent of the value of X. Other than this, the X data will be highly linear and repeatable since it is derived chiefly from the wedge-encoder.

If the entire range of X channel data is derived from the detectors in open-loop fashion, the output will be substantially non-linear. This is because of the reduction in intensity in the outer portions of the image due to vignetting.

Calculation of the shape of the transfer function is beyond the scope of this study, but it is estimated that the slope or scale factor might decrease by 50 percent for values of X approaching the 300 arc-second limit. This transfer function is subject to calibration, however, and probably can be described by a polynomial of a small number of terms. On the other hand, the need for null offset calibration will probably be eliminated with a gimballed boom since the image position along the detector edges will be much less subject to variation in Z.

The AGC circuit is presently designed to maintain fidelity of calibration to 0.5 percent. Thus, a possible error proportional to the X output must be anticipated due to this cause with a maximum of 1.5 arc-seconds.

The search function required to acquire the image for the YZ autocollimator will simultaneously acquire it in the X channel.

Therefore, it is concluded that a viable measuring system can result from the same complement of autocollimators and reflectors if a gimballed boom is used, but without the necessity for the wedge deflection units. The boom must be driven in Y and Z axes in both a search mode and in a control mode, keeping the reflectors aligned in Y and Z to within a ± 15 arc-second band in response to output signals from the autocollimators.

4.2 Single Encoders in Y and Z Axes

The present configuration of the wedge deflection unit for the YZ subsystem includes a separate encoder with each wedge. The purpose is to avoid the effect of gear errors between the two wedges of each measuring pair.

With respect to the "first" wedge of each axis, it should be noted that mounting the encoder directly to the wedge cell eliminates concern for gear errors between motor and wedge. (Concentricity of the encoder is still important, as is a knowledge of the rotational offset between the encoder zero and the wedge "zero.")

The second wedge, however, cannot be expected to turn through the same precise angle as the first, and, hence, an error may be introduced into the output of both channels because of this. Eccentricity of the last gear mesh and random tooth errors are the principal contributors to output error.

By summing the indicated angles from the two wedges, the effect is eliminated from the primary channel; the difference is used as a correction for the orthogonal channel, as described earlier.

A further benefit is achieved in that the second encoders of each pair provide a redundancy in this part of the system.

Three σ values of error which may be introduced due to last-mesh gear errors, if the second encoders are eliminated, are 0.00009 arc-seconds in each primary channel and 0.535 arc-seconds in each channel due to cross-coupling. Other gear errors do not lend themselves to ready computation, but the effect of the other gear errors on cross-coupling is estimated to be another 1.0 arc-second, 3σ .

The weight saving would be inconsequential but power could be reduced by either eliminating the second encoder in each

pair of wedges or energizing only one encoder, with the second available for redundancy to use only in the event of failure.

5.0 RELIABILITY CONSIDERATIONS

The reliability prediction by part type and count for the ATA is included in Appendix G as a self-contained document. The results stated there indicate a failure rate for the system of

$$\lambda_{\text{total}} = 9718.18 \times 10^{-9} \text{ failures/hour}$$

This gives a MTBF of

$$\text{MTBF} = \frac{1}{\lambda_{\text{total}}} = 102,889.34 \text{ hrs (11.75 years)}$$

The probability of success for a mission life of 8 months (8760 hours) has been calculated to be 94.56%.

6.0

SYSTEM ERROR ANALYSIS

The Attitude Transfer Assembly functions as a tracking or null seeking autocollimator; that is, the collimated beam is deviated by the contra-rotating wedges until it is normally incident on the remote reflectors. It is necessary to determine the processes that could cause the null position to shift and the magnitude of this possible shift.

The mode of operation of the instrument combines the advantages of an edge tracker with the push-pull effect of a centroid tracking instrument as discussed in Section 2.2.1.

In the centroid tracker, half the energy falls on one detector and the other half on the second detector. The two detectors are placed adjacent to each other. This mode of operation requires that the two detectors be matched in responsivity in order to obtain signal balance. If the responsivities of the two detectors are not matched, signal balance is attained with the image translated toward the detector of lower responsivity. Should the detectors, in addition, have different temperature coefficients of responsivity, a temperature change will result in a different signal balance point, thereby changing the null position.

For an edge-tracking instrument, the null position occurs when the image falls in the space between the detectors. Only the edges of the image, which are always spread beyond the geometrical size due to diffraction and residual aberrations, fall onto the detectors. This does not affect the transfer function even around the null position and also assures that there will be no dead zone. Incremental image motion from null adds energy to one detector and removes an equal amount from the other. This addition and subtraction effect produces a signal of the same magnitude as would be achieved with an infinitely sharp image (with no overlap), thereby preserving the basic edge-tracking mode of operation.

The design of the ATA combines the above characteristics by making the gap between detectors less than the nominal image width. To evaluate the null shift caused by a difference in responsivity in the presence of image overlap, consider Figure 2.3A. For the purposes of this calculation, let the image overlap b on detector A be given by b_A and the image overlap on detector B be given by b_B . The detectors, as mentioned previously, can be matched within 5 percent, thus $R_B = 1.05 R_A$. The radiant power incident on each detector is proportional to the image area on the detector, thus

$$P_A = H h b_A \quad (6-1)$$

and

$$P_B = H h b_B \quad (6-2)$$

where H = irradiance in watts/cm² and h = height of image in cm.

The signal current generated in the detectors A and B is given by

$$I_A = P_A R_A \quad (6-3)$$

$$I_B = P_B R_B \quad (6-4)$$

At null the signal currents are equal and equating I_A and I_B , the result is

$$H h b_A R_A = H h b_B (1.05) R_A \quad (6-5)$$

$$b_A = 1.05 b_B$$

In order to find the magnitude of this shift, using Figure 2.3A, b_B can be related to b_A by the known parameters of the system h and g .

$$b_B = h - g - b_A \quad (6-6)$$

Substituting this expression b_B in the above expression and solving for b_A , the result is

$$b_A = 1.05/2.05 (h - g)$$

where

$$h = 0.005 \text{ in} = 0.0127 \text{ cm}$$

$$g = 0.0035 \text{ in} = 0.00889 \text{ cm}$$

Then

$$b_A = 0.001951 \text{ cm}$$

and

$$b_B = 0.001951/1.05 = 0.001859 \text{ cm}$$

The linear shift of the null balance is thus

$$s = (b_A - b_B)/2 = .000046 \text{ cm}$$

This may be expressed in terms of equivalent mirror rotation by equation

$$y = s/2f$$

where y is the mirror rotation about y

f is the focal length = 10.16 cm

$$y = 2.26 \times 10^{-6} \text{ rad.} = 0.46 \text{ arc sec.}$$

(Note in the X or twist axis, this offset is 10×0.46 or 4.6 arc sec.)

This shift, however, is an initial bias in the instrument which will not be seen nor will it have any effect on accuracy. It is included only to illustrate the effect of image spread and becomes significant only as it varies. Possible reasons for variation will next be discussed.

The defocusing effect due to temperature change of 2°C has been calculated as 0.00032 cm shift in focus, with a resulting image spread of $0.00032/3.5 = 9.14 \times 10^{-5} \text{ cm}$. The effect is doubled since it affects both the projected and return beam, or a total spread of $1.83 \times 10^{-4} \text{ cm}$.

The conversion factor from image spread to arc-seconds null shift has been calculated in the beginning of this section as 0.46 arc-sec shift per 0.0038 cm. spread, or 121 arc-sec per cm spread in Y and Z axes. Then, the above spread of $1.83 \times 10^{-4} \text{ cm}$ will produce 0.022 arc-sec shift in Y and Z and 0.22 arc-sec in X.

The change from air to vacuum causes a focal length shortening of 0.0091 cm with a resultant image spread for double passage of $2 \times 0.0091/3.5 = 0.0052 \text{ cm}$. Calculating the equivalent mirror rotation, as done above, results in 0.63 arc sec error (3 σ value) for the YZ channel. In the X channel, the result must be multiplied by 10, giving 6.3 arc-sec (3 σ value).

Since this is a one-time possible null shift, it is desirable to remove its effect by pre-flight calibration. This can be done, of course, by mounting each instrument in a vacuum chamber with a fixed reflector and observing the null shift when a vacuum is applied. For completeness, however, this error contribution is included in the tabulation where it becomes the largest item.

An additional null shift occurs when the instrument is exposed to a 2°C temperature excursion and is due to the relative change in responsivities of the two detectors. This shift in null balance may be shown to be given by the following expression:

$$s = \frac{R_A R_B \gamma r (h-g)}{(R_A + R_B)^2 (1 + r)} \quad (6-7)$$

where s = shift of image position

R_A = responsivity of detector A = 0.4 amps/watt

R_B = responsivity of detector B

r = fractional change in responsivity of detector A

$r(1 + \gamma)$ = fractional change in responsivity of detector B

h = nominal image width = 0.0127 cm

g = detector gap = 0.0089 cm

$R_B = (1.05) R_A$

r , taken from detector SCD (Appendix D)

is to be 0.2%/°C or 0.004 for 2°C excursion.

γ may be expected not to exceed 0.25

$$\text{Then } s = \frac{1.05 R_A^2 \times 0.25 \times 0.004 \times 0.0038}{(2.05)^2 R_A^2 \times 1.004}$$

$$= 9.46 \times 10^{-7} \text{ cm}$$

$$= 9.6 \times 10^{-3} \text{ arc sec.}$$

As before, the effect in the X axis is 10 times as great or 0.096 arc-sec.

In section 3.2.1.1, a measure of sensitivity of the instrument to mechanical distortion is given in terms of lateral

shift of the focal plane with respect to the optical axis; i.e., a lateral shift of 4.93×10^{-4} mm in the focal plane is equivalent to a 1 arc-sec change in pointing direction or 0.5 arc-sec mirror rotation. It is, however, expected from the previously mentioned mechanical design considerations; such as, material compatability, one-piece housing casting, and attachment of the autocollimator to a spacecraft heat sink, that the initially established pointing direction or bore sight will be held within 0.2 arc-sec/°C. The actual change in pointing direction with temperature, however, will be documented by test, as part of the final test of each flight system. It may thus be applied as a correction factor if the temperature of the base plate is known. Distortions due to bending of the plate are considered to be negligible.

The encoder eccentricity error, E, due to bearing runout may be shown to be given by the expression

$$E \text{ (peak to peak)} = \frac{\text{Bearing Runout}}{\text{Code Cycle Length}} \quad (\text{arc seconds/cycle}) \quad (6-8)$$

with the following system parameters;

$$\text{Track Diameter} = 2.7 \text{ inches}$$

$$\text{Track Circumference} = \pi D = 8.48 \text{ inches}$$

$$\text{Cycles} = 2^{13} = 8192$$

$$\text{Number of counts} = 2^{15}$$

$$\text{Cycle Length} = 8.48/8192 = 1.03 \times 10^{-3} \text{ inch}$$

$$\text{Bearing Runout} = 100 \times 10^{-6} \text{ inch}$$

$$\text{Radians Per Cycle} = 7.63 \times 10^{-4} \text{ radians}$$

$$\text{Arc-Seconds Per Cycle} = 147.37 \text{ arc-sec}$$

Least Significant Bit Size

$$\text{Arc-Seconds Per Count} = 360^\circ/2^{15} = 39.55 \text{ arc-sec}$$

$$\begin{aligned} \text{Jitter} &= 25\% \text{ of Least Significant Bit Size} \\ &= 9.89 \text{ arc-sec} \end{aligned}$$

Substituting the above values in the error equation,

$$E = \frac{10^{-4}}{1.03 \times 10^{-3} \text{ inch}} (157.37 \text{ arc-sec}) = 15.28 \text{ arc-sec}$$

Since the ATA Deviation Wedge assembly operates over only 90 degrees; i.e., ± 45 degrees and since E is sinusoidal in nature, it is possible to choose that portion of the cycle for which the error goes through zero. Thus, the effective error due to eccentricity of encoder bearings is,

$$E_{\text{eff}} = .707 E = 10.80 \text{ arc-sec}$$

The error of the encoder is,

$$\text{Error of Encoder} = E_{\text{eff}} + \text{Jitter} = 20.69 \text{ arc-sec}$$

In terms of Beam deviation, D_{YZ} , for the YZ channel, the encoder error will produce an error given by $E_{YZ} = 2D_{YZ} (\sin 20.69 \text{ arc-sec})$

where $D_{YZ} = \text{YZ wedge constant} = 634.4 \text{ arc-sec}$

$$\begin{aligned} D_{YZ} &= 2(636.4) (\sin 20.69 \text{ arc-sec}) \\ &= 0.127 \text{ arc-sec} (3\sigma \text{ value}) \end{aligned}$$

For the X axis, there is one wedge (with wedge constant $D_X = 42.43 \text{ arc-sec}$). The beam deviation error E_X produced by the encoder error is

$$\begin{aligned} E_X &= D_X \sin (20.69 \text{ arc-sec}) \\ &= .0042 \text{ arc-sec} \end{aligned}$$

To find the equivalent twist angle, X, the above value is divided by $2 \sin \theta = 0.1$

$$X = 0.042 \text{ arc-sec} (3\sigma \text{ value})$$

The decoder zero offset from wedge zero is expected to be less than 3 arc-min. This offset would result in an error of 0.28 arc-sec equivalent mirror rotation in the YZ channel and 0.4 arc-sec equivalent twist in the X channel, if not measured. The offset will be calibrated during testing and will be supplied along with other calibration data.

To obtain wedge scan orthogonality, provision has been made in the deviation wedge assembly of the YZ channel to hold one set of wedges stationary while exercising the other set. During assembly and with the autocollimator operative and the beam directed at a plane mirror, one pair of wedges will be driven through its entire range, while the output from the orthogonal channel is monitored. The second pair will be adjusted until the cross-coupling error is less than 0.5 arc-seconds.

The error contributions of the remote reflectors and the base line Porro reflector have been calculated in section 3.1.33. With a reflector flatness of $\lambda/25$, the respective errors are

- 1) The error contribution of the flat mirror in the YZ channel is 0.137 arc-sec (3σ -value)
- 2) The error contribution of the remote Porro Reflector is 3.956 arc-sec (3σ -value)
- 3) The error contribution of the base line Porro reflector is 3.24 arc-sec (3σ -value)

The cross-coupling error contribution in the Z channel due to the residual wedge curvature of the wedge pair in the Y channel is calculated in section 3.1.2.2 to be an equivalent mirror rotation of 0.218 arc-sec (3σ).

Wedge curvature in the X channel does not produce any cross-coupling error and is therefore not part of the error budget of the ATA.

Cross-coupling is fully discussed in section 7. There it is shown that the maximum cross-coupling error in the YZ channel occurred for rotation about the Y axis with a calculated sum of 0.056 arc-seconds.

In the twist measuring axis, a rotation about the Z axis will produce a twist error of 0.009 arc-sec.

As stated in section 3.3.1.3, the AGC loop error is less than 0.5%. At full scale open loop, the magnitude of this error will be 0.075 arc-sec for all three channels. The accuracy of the spacecraft's A to D converter is stated in NASA publication NASA TN D-7725, "The Standardized Functional Support Section for the Small Astronomy Satellite (SAS), p. 14 to be 0.2%. The error introduced at full scale open loop is 0.03 arc-sec in all channels.

6.1 Calibrated Accuracy

The calibrated accuracy which is the RSS value of those errors not eliminated by calibration, is calculated on the basis of the 1σ error values listed in Table 6.1. The errors discussed in section 6.0 and constituting Table 6.1 are considered to be maximum values and are therefore listed in the 3σ column. It is seen that the performance goals of section 2.5, Appendix A, are fulfilled.

6.2 Resolution (Noise Equivalent Angle)

The noise equivalent angle has been calculated in the Electronics section 3.3.1.3 on the basis of D^* , the detectivity of the error detectors, and results in an NEA of:

- 1) for the YZ channel: 7×10^{-4} arc-sec
- 2) for the X channel: 5×10^{-3} arc-sec

It is thus seen that the performance requirements (Section 2.5, Appendix A) are exceeded by 140 to 1 in the YZ channel and 100 to 1 in the twist channel. The system, as stated in section 3.3.1.2.3, is detector noise limited.

6.3 Stability Over 5 Minutes (Time)

The anticipated sources of instability are associated with temperature excursions from ambient. Therefore, considering items 1, 3 and 4 for a 2°C temperature excursion results in an rms instability of 0.067 arc-sec for the YZ channel and 0.67 arc-sec for the X channel. It is, however, anticipated that the thermal time constant will be much greater than 5 minutes so that the above

TABLE 6.1

ERROR BUDGET FOR THE ATTITUDE TRANSFER ASSEMBLY

<u>Item</u>	<u>YZ Channel</u>		<u>X Channel</u>	
	<u>Max(3σ)Value</u> <u>arc-sec</u>	<u>rms(1σ)Value</u> <u>arc-sec</u>	<u>Max(3σ)Value</u> <u>arc-sec</u>	<u>rms(1σ)Value</u> <u>arc-sec</u>
1. Null Shift, Temperature Change of 2°C	0.022	0.007	0.220	0.070
2. Null Shift, Air to Vacuum*	0.630	0.210	6.300	2.100
3. Null Shift Change in Detector Responsivity	0.010	0.003	0.096	0.032
4. Null Shift, Mechanical Distortion	0.200	0.067	2.000	0.667
5. Encoder Resolution	0.122	0.041	0.081	0.027
6. Encoder Eccentricity and Jitter	0.127	0.042	0.042	0.014
7. Wedge Scan Orthogonality	0.500	0.167	-	-
8. Curvature in Remote Porro Reflector	-	-	3.956	1.319
9. Curvature in Base Line Porro Reflector	-	-	3.240	1.080
10. Curvature in Flat Mirror	0.137	0.046	-	-
11. Wedge Curvature	0.218	0.073	-	-
12. Residual Cross Coupling	0.056	0.019	0.007	0.003
13. AGC Loop at Full Scale	0.075	0.025	0.075	0.025
14. Spacecraft A to D Converter	0.030	0.010	0.030	0.010
Total RSS Value (arc-sec)		0.298		2.787
Goal: 1 Value(arc-sec)		1.000		3.000

*Null shift due to change from air to vacuum environment can be precalibrated, materially reducing the above totals.

instabilities will not be seen. The above values exceed the performance requirements by a margin of 7 to 1 in the YZ channel and by 3 to 1 in the X channel.

6.4 Stability Through Environment

The major sources of environmental instability are the thermal changes, vibrations and shock which will contribute to a change in pointing direction of the instrument through the launch phase.

Distortions due to thermal changes have been discussed above and are not anticipated to cause problems. Distortions due to shock and vibration of the launch and mentioned in section 3.2.1.3 are prevented by keeping the number of clamped interfaces to a minimum with fasteners torqued to the specified limits. Critical relationships between components will be secured by fillet bonding techniques.

All sources of instability through the launch environment will be documented as part of the acceptance test applied to each piece of flight hardware.

7.0 CROSS-COUPLING7.1 Mathematical Analysis

The presence or absence of cross-coupling terms in the angular deviation of the reflected beam will first be documented by use of matrix algebra.

A unit vector aligned with the projected beam from the autocollimator will be analyzed as it is projected onto the reflector at the end of the boom, assuming that the reflector has rotated about X, Y, and Z axes by a small angle. The reaction of the beam to the rotated reflector will be derived indicating the resulting deviations imparted to the reflected beam.

7.1.1 Y-Z system

The projected unit vector will have components parallel to X, Y, and Z axes represented by the three magnitudes arranged from top to bottom respectively, in a bracket. Thus if the projected beam is parallel to -X, the unit vector B is represented by:

$$\begin{bmatrix} B \end{bmatrix} = \begin{bmatrix} -1 \\ 0 \\ 0 \end{bmatrix}$$

The reflector may be thought to have in its initial undeviated attitude, a set of coordinate axes X, Y, Z which are parallel to the system axes of the same designations. Rotations will be assumed to take place successively around the X axis, then around the rotated Y axis, which we will call Y', and finally the doubly rotated Z'' axis. These are illustrated in Figure 7-1, in which all rotations are positive in a right-hand coordinate system. This produces a rotated set of axes X''', Y''', Z''', and the projections of the original vector on this rotated set of axes is derived by multiplying the vector components by the matrix operator.

$$\begin{bmatrix} B' \end{bmatrix} = \begin{bmatrix} M_{Z''Y'X} \end{bmatrix} \begin{bmatrix} B \end{bmatrix}$$

It will be shown that although there are terms in the final result which depend on the order of rotation most of these are higher-order terms which with the rotation magnitudes considered here become insignificant. The use of this procedure of successive rotations greatly simplifies the procedure.

The matrix $M_{Z''Y'X}$ has the following components.

$$M_{Z''Y'X} = \begin{bmatrix} \cos y \cos z & \sin x \sin y \cos z + \cos x \sin z & -\cos x \sin y \cos z + \sin x \sin z \\ -\cos y \sin z & -\sin x \sin y \sin z + \cos x \cos z & \cos x \sin y \sin z + \sin x \cos z \\ \sin y & -\sin x \cos y & \cos x \cos y \end{bmatrix}$$

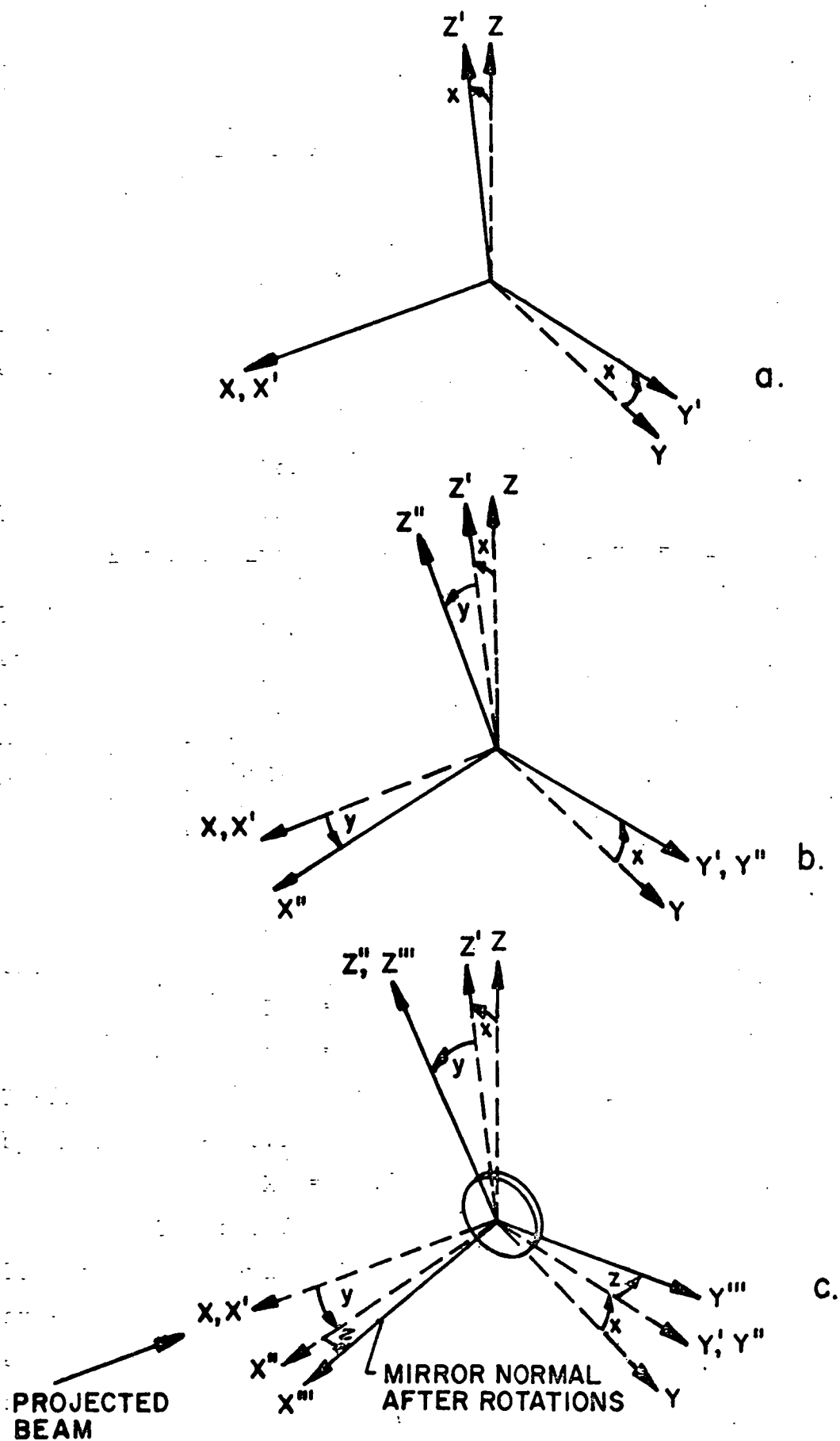
The expression has been simplified thus far by dropping the primes, but it should be remembered that y represents an angular rotation about the Y' axis, and z a rotation about Z''. In proceeding we will further simplify by writing cx, cy, cz for cos x, cos y, and cos z, and sx, sy, sz for the respective sines. Then the components of the unit vector projected onto the rotated axes are:

$$B_p = \begin{bmatrix} cy \, cz & sx \, sy \, cz + cx \, sz & -cx \, sy \, cz + sx \, sz & -1 \\ -cy \, sz & -sx \, sy \, sz + cx \, cz & cx \, sy \, sz + sx \, cz & 0 \\ sy & -sx \, cy & cx \, cy & 0 \end{bmatrix}$$

The resultant components of B' are found by multiplying the column B by the rows of M, with the following result;

$$B_p = B_{Z''Y'X} = \begin{bmatrix} B_{X''} & -cy \, cz \\ B_{Y''} & cy \, sz \\ B_{Z''} & -sy \end{bmatrix}$$

The reflection of this unit vector by the plane mirror whose normal is parallel to +X is represented by changing the sign of $B_{X''}$ only, since the "vertical" and "lateral" components $B_{Y''}$ and $B_{Z''}$ are unchanged.



A 22959 A

Figure 7-1 ROTATION ABOUT X , Y' AND Z''

$$\begin{bmatrix} B_{p'} \end{bmatrix} = \begin{bmatrix} -B_{X'''} \\ B_{Y'''} \\ B_{Z'''} \end{bmatrix} = \begin{bmatrix} cy \ cz \\ cy \ sz \\ -sy \end{bmatrix}$$

To resolve these components of the rotated and reflected unit vector onto the original X, Y, Z axes, we multiply $B_{p'}$ by the inverse matrix $M_{Z''Y'X}^{-1}$. Then

$$\begin{aligned} \begin{bmatrix} B' \end{bmatrix} &= \begin{bmatrix} M_{Z''Y'X} \end{bmatrix}^{-1} \begin{bmatrix} B_{p'} \end{bmatrix} \\ &= \begin{bmatrix} cy \ cz & -cy \ sz & sy & cy \ cz \\ sx \ sy \ cz + cx \ sz & -sx \ sy \ sz + cx \ cz & -sx \ cy & cy \ sz \\ -cx \ sy \ cz + sx \ sz & cx \ sy \ sz + sx \ cz & cx \ cy & -sy \end{bmatrix} \\ \begin{bmatrix} B'_X \\ B'_Y \\ B'_Z \end{bmatrix} &= \begin{bmatrix} cy^2 \ cz^2 - cy^2 \ sz^2 - sy^2 \\ cy \ sx \ sy \ cz^2 + cx \ cy \ cz \ sz - cy \ sx \ sy \ sz^2 \\ \quad + cx \ cy \ cz \ sz + cy \ sx \ sy \\ -sy \ cx \ cy \ cz^2 + cy \ cz \ sx \ sz + cx \ cy \ sy \ sz^2 \\ \quad + cy \ cz \ sx \ sz - cx \ cy \ sy \end{bmatrix} \end{aligned}$$

where $cy^2 = \cos^2 y$, $sx^2 = \sin^2 x$, etc.

In the absence of y and z rotation, the reflected beam would obviously be parallel to +X. This is borne out by the components of B' , which become

$$\begin{bmatrix} 1 \\ 0 \\ 0 \end{bmatrix} \quad \text{when } y = z = 0$$

If y and/or z $\neq 0$, the angles θ'_y and θ'_z may be defined as shown in Figure 7-2. Then $\tan \theta'_y = B'_Z/B'_X$ and $\tan \theta'_z = B'_Y/B'_X$.

Before evaluating these component angles we will simplify and combine terms in the column vector B' , resulting in the following:

$$\begin{bmatrix} B'_x \\ B'_y \\ B'_z \end{bmatrix} = \begin{bmatrix} cy^2 cz^2 - cy^2 sz^2 - sy^2 \\ 2 cx cy cz sz + cy sx sy (1 + cz^2 - sz^2) \\ -cx cy sy (1 + cz^2 - sz^2) + 2 cy cz sx sz \end{bmatrix}$$

$$= \begin{bmatrix} cy^2 cz^2 - cy^2 sz^2 - sy^2 \\ 2 cx cy cz sz + 2 cy cz^2 sx sy \\ -2 cx cy cz^2 sy + 2 cy cz sx sz \end{bmatrix}$$

For maximum values of $x = 0.05^\circ$, $y = z = 0.25^\circ$, exact values for these three components of the reflected unit vector are:

$$B' = \begin{bmatrix} 0.999923847 \\ 0.008739135 \\ -0.008713668 \end{bmatrix}$$

Because the value of B'_x is so close to 1, the angle θ'_y and θ'_z can be taken directly from the values of B'_z and B'_y stated in radians. Considering the fact that all cosines are at least 0.99999, the vector components can be simplified to

$$\begin{bmatrix} 1 \\ 2z + 2xy \\ -2y + 2xz \end{bmatrix}$$

The $2z$ term confirms the familiar fact that the reflected beam is deviated through twice the angle of rotation, and that a positive rotation around the Z axis produces a deviation component parallel to $+Y$. Similarly, a positive rotation around Y produces a deviation in the $-Z$ direction equal to twice the Y rotation.

The second terms are true and valid coupling terms representing the fact that the initial rotation around X rotates the other axes and that subsequent rotation about these other axes is actually around Y' and Z". This can be emphasized if we restore the primes which were dropped earlier:

$$\begin{bmatrix} B' \end{bmatrix} = \begin{bmatrix} 1 \\ 2z'' + 2xy' \\ -2y' + 2xz'' \end{bmatrix}$$

If we evaluate the terms with the cosines still present and each term shown separately we have, for maximum values of x, y' and z'',

$$\begin{bmatrix} B' \end{bmatrix} = \begin{bmatrix} 0.999923847 \\ 0.008726443 + 0.000012692 \\ -0.008726360 + 0.000012692 \end{bmatrix}$$

Interpreting the components B'_Y and B'_Z as radian measure and converting to arc-sec, $B'_Y/2 = 900.00443 + 1.30899$ arc-sec
 $B'_Z/2 = -899.99587 + 1.30899$ arc-sec

The closeness of the first term in each component to the 900 arc-seconds validates the simplifying approximations.

The analysis so far has demonstrated the deviation of the reflected beam, without consideration of the tracking wedges. It is relevant to generation of the open-loop error signal, but must be augmented by introducing the effect of the wedges.

Assume that initially the wedge rotation position is at 0° and that the net deviation through each pair is zero in both Y and Z directions. If the first pair of wedges deviates the beam in the Y direction, it falls on the second pair obliquely, and the deviation imparted by the second pair is slightly less than if the beam were parallel to the X axis. The effect has been calculated, however, for maximum values of Y and Z, and found to be 0.031 arc-seconds. It will be included in the final error summary, but will be omitted in the following development.

Let the beam incident on the mirror be represented by a unit vector having components as follows:

$$\begin{bmatrix} B \\ \end{bmatrix} = \begin{bmatrix} -\sqrt{1 - B_y^2 - B_z^2} & = -cy \, cz \\ -cx \, cy \, cz \, sz - cy \, cz^2 \, sx \, sy \\ cx \, cy \, cz^2 \, sy - cy \, cz \, sx \, sz \end{bmatrix}$$

The value of B_x is derived from the fact that $(B_x^2 + B_y^2 + B_z^2)$ always equal 1.

$$\begin{bmatrix} B_p \\ \end{bmatrix} = \begin{bmatrix} cy \, cz & sx \, sy \, cz + cx \, sz & -cx \, sy \, cz + sx \, sz & B_x \\ -cy \, sz & -sx \, sy \, sz + cx \, cz & cx \, sy \, sz + sx \, cz & B_y \\ sy & -sx \, cy & cx \, cy & B_z \end{bmatrix}$$

$$\begin{aligned} & \begin{bmatrix} -cy^2 \, cz^2 - cx \, cy \, cz^2 \, sx \, sy \, sz - cx^2 \, cy \, cz \, sz^2 - cy \, cz^3 \, sx^2 \, sy^2 \\ -cx \, cy \, cz^2 \, sx \, sy \, sz - cx^2 \, cy \, cz^3 \, sy^2 + cx \, cy \, cz^2 \, sx \, sy \, sz \\ + cx \, cy \, cz^2 \, sx \, sy \, sz - cy \, sz \, sx^2 \, sz^2 \\ cy^2 \, cz \, sz + cx \, cy \, cz \, sx \, sy \, sz^2 - cx^2 \, cy \, cz^2 \, sz + cy \, cz^2 \, sx^2 \, sy^2 \, sz \\ -cx \, cy \, cz^3 \, sx \, sy + cx^2 \, cy \, cz^2 \, sy^2 \, sz + cx \, cy \, cz^3 \, sx \, sy \\ -cx \, cy \, cz \, sx \, sy \, sz^2 - cy \, cz^2 \, sx^2 \, sz \\ -cy \, cz \, sy + cx \, cy^2 \, cz \, sx \, sz + cy^2 \, cz^2 \, sx^2 \, sy + cx^2 \, cy^2 \, cz^2 \, sy \\ -cx \, cy^2 \, cz \, sx \, sz \end{bmatrix} \end{aligned}$$

This may be simplified by cancelling and combining terms and using the identity: $\sin^2 a + \cos^2 a = 1$.

$$\begin{bmatrix} B_p \end{bmatrix} = \begin{bmatrix} -cy^2 cz^2 - cy cz sz^2 - cy cz^3 sy^2 \\ cy^2 cz sz - cy^3 cz^2 sz \\ -cy cz sy + cy^2 cz^2 sy \end{bmatrix}$$

After reflection,

$$\begin{bmatrix} B'_p \end{bmatrix} = \begin{bmatrix} cy^2 cz^2 + cy cz sz^2 + cy cz^3 sy^2 \\ cy^2 cz sz - cy^3 cz^2 sz \\ -cy cz sy + cy^2 cz^2 sy \end{bmatrix}$$

And resolved on the original axes

$$\begin{bmatrix} B' \end{bmatrix} = \begin{bmatrix} cy cz & -cy sz & sy \\ sx sy cz + cx sz & -sx sy sz + cx cz & -sx cy \\ -cx sy cz + sx sz & cx sy sz + sx cz & cx cy \end{bmatrix} \begin{bmatrix} B'_p \end{bmatrix}$$

$$= \begin{bmatrix} cy^3 cz^3 + cy^2 cz^2 sz^2 + cy^2 cz^4 sy^2 - cy^2 sz^2 + cy^4 cz^2 sz^2 - sy^2 + cy^2 cz^2 sy^2 \\ cy^2 cz^3 sx sy + cx cy^2 cz^2 sz + cy cz^2 sx sy sz^2 + cx cy cz cz^3 \\ +cy cz^4 sx sy^3 + cx cy cz^3 sy^2 sz - cy sx sy sz^2 + cx cy cz sz \\ +cy^3 cz^2 sx sy sz^2 - cx cy^3 cz^3 sz + cy sx sy - cy^3 cz^2 sx sy \\ -cx cy^2 cz^3 sy + cy^2 cz^2 sx sz - cx cy cz^2 sy sz^2 + cy cz sx sz^3 \\ -cx cy cz^4 sy^3 + cy cz^3 sx sy^2 sz + cx cy sy sz^2 + cy cz sx sz \\ -cx cy^3 cz^2 sy sz^2 - cy^3 cz^3 sx sz - cx cy sy + cx cy^3 cz^2 sy \end{bmatrix}$$

If the terms of B' were identical to those of B (except for sign) perfect measurement of the y , z , xy and xz rotations by the wedges would be demonstrated. The large number of terms makes it difficult to perceive the near-perfect identity but combination and cancellation of terms makes it possible to simplify B'_y and B'_z as follows:

$$B'_Y = cx \, cy \, cz \, sz \, (1 + sy^2 + sz^2) + cy \, cz^2 \, sx \, sy \, (1 + sy^2 + 2 \, sz^2)$$

$$B'_Z = -cx \, cy \, cz^2 \, sy \, (1 + sy^2 + 2 \, sz^2) + cy \, cz \, sx \, sz \, (1 + sy^2 + sz^2)$$

If the sy^2 and sz^2 terms in the parentheses are dropped, the identity is established. Evaluating these terms for maximum values of y and z rotation reveals a maximum error of 0.017 arc-seconds in z measurement and 0.025 arc-seconds in y. The validity of the wedge-measuring procedure is therefore confirmed.

7.1.2 X-measuring System

Remembering the fact that the projected beam from the X auto-collimator is spread in the XY plane by slightly more than z_{\max} , and that the center of the vignetted image is displaced from the axis of the instrument by fz , the effective beam contributing to the image is inclined to the X axis, not by the offset angle θ alone, but by $(\theta - z)$. The unit vector for this instrument, therefore, is

$$[B] = \begin{bmatrix} -\cos(\theta - z) & -c\theta \, cz - s\theta \, sz \\ \sin(\theta - z) & s\theta \, cz - c\theta \, sz \\ 0 & 0 \end{bmatrix}$$

Multiplying as before by the matrix representing successive rotations about X, Y', and Z'', the components of the unit vector as projected onto the rotated Porro reflector axis are;

$$[B_p] = \begin{bmatrix} -c\theta \, cy \, sz^2 - s\theta \, cy \, cz \, sz + s\theta \, cz^2 \, sx \, sy + s\theta \, cx \, cz \, sz \\ -c\theta \, cz \, sx \, sy \, sz - c\theta \, cx \, sz^2 \\ c\theta \, cy \, cz \, sz + s\theta \, cy \, sz^2 - s\theta \, cz \, sx \, sy \, sz + s\theta \, cx \, cz^2 \\ + c\theta \, sx \, sy \, sz^2 - c\theta \, cx \, cz \, sz \\ -c\theta \, cz \, sy - s\theta \, sy \, sz - s\theta \, cy \, cz \, sx + c\theta \, cy \, sx \, sz \end{bmatrix}$$

Upon reflection from the Porro, signs of X and Z components of B_p change. Resolved onto the original axes, therefore, the vector B_p is multiplied by the inverse matrix $M_{Z''Y'X}^{-1}$ as follows:

$$[B'] = \begin{bmatrix} cy\ cz & -cy\ sz & sy \\ cz\ sx\ sy + cx\ sz & -sx\ sy\ sz + cx\ cz & -cy\ sx \\ -cx\ cz\ sy + sx\ sz & cx\ sy\ sz + cz\ sx & cx\ cy \\ \\ c\theta\ cy\ cz^2 + s\theta\ cy\ cz\ sz - s\theta\ cz^2\ sx\ sy - s\theta\ cx\ cz\ sz \\ + c\theta\ cz\ sx\ sy\ sz + c\theta\ cx\ sz^2 \\ c\theta\ cy\ cz\ sz + s\theta\ cy\ sz^2 - s\theta\ cz\ sx\ sy\ sz + s\theta\ cx\ cz^2 \\ + c\theta\ sx\ sy\ sz^2 - c\theta\ cx\ cz\ sz \\ c\theta\ cz\ sy + s\theta\ sy\ sz + s\theta\ cy\ cz\ sx - c\theta\ cy\ sx\ sz \end{bmatrix}$$

Only the Z component is of interest, however, since it is this component which carries the information on twist. After cancelling like terms and all terms having four or more sines the result is as follows:

$$\begin{aligned} [B']_z &= \sin \theta \cos x \cos z \sin x (\cos^2 y + \cos^2 z) \\ &+ \sin \theta \cos x \sin y \sin z (\cos x \cos^2 z + \cos y) \end{aligned}$$

The first term is of course the principal one, and the second is a valid coupling term, since rotation about Y' and then about Z'' produces a twist around the X axis. The cosine terms are of no consequence, and the approximation

$$[B']_z = 2 \sin \theta \sin x + 2 \sin \theta \sin y \sin z$$

has an error of 0.0089 arc-seconds in the first term, at maximum values of x, y, and z, and 0.000062 arc-seconds in the second term. The difference between x and sin x has a maximum of 0.0001 arc-sec.

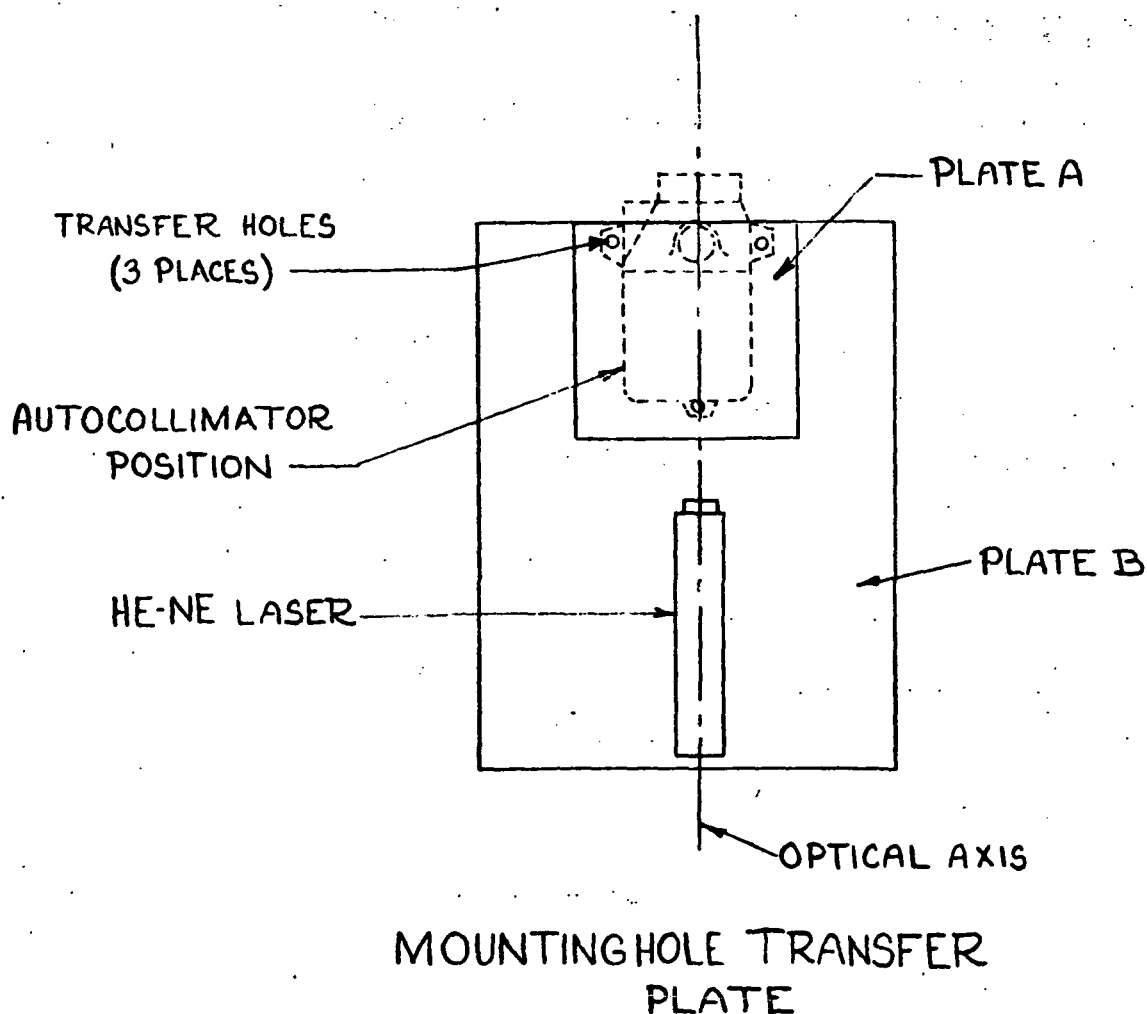
The deviation produced by the second passage doubles the Z component.

The above development demonstrates the ability of the proposed system to measure X, Y, and Z rotations independently and in the presence of maximum rotations about other axes with negligible coupling (except those due to instrument errors).

8.0 SYSTEM ALIGNMENT

The mounting and alignment of the ATA to the MAGSAT spacecraft anticipates that the mounting holes on the spacecraft mounting plane will have been located. A definite procedure is not possible presently since further spacecraft system definitions are needed. The following is a tentative procedure (Figure 2.1 may be used for illustration.)

1) A low power He-Ne laser is mounted at the ATA optical axis on a mounting hole transfer plate. The mounting hole transfer plate is shown below and consists of plate A and U-shaped plate B and is used to align the laser to the autocollimator mounting holes.



After aligning the laser in this manner and fastening plate B (temporarily), plate A may be removed.

2) The remote reflector assembly is now mounted to the boom end and adjusted until the laser beam returns on itself.

3) The YZ channel autocollimator is mounted in the mounting holes forward of the laser and adjusted until the laser beam, reflected from the alignment cube shown in Figure 3.12 and 3.13, returns on itself.

4) The mounting hole transfer plate is next positioned on the X-channel autocollimator mounting holes and plate B fastened. It is necessary in the X-channel alignment to deviate the beam upward 0.295° so as to be incident at the center of the upper reflecting surface of the remote Porro reflector. This is accomplished with a laser beam steerer.

5) The base line Porro reflector is mounted in the position shown in Figure 2.1 and adjusted until the laser's beam returns on itself.

6) With the base line Porro reflector in place, the X-channel autocollimator is positioned in front of the laser and adjusted until the laser beam reflected from the alignment cube returns on itself.

With the preliminary alignment above complete, the Deflection Wedge Assemblies are positioned in front of their respective autocollimator units. All further adjustments are made in the electronic mode (operating at 0.94 microns).

With the wedge pairs in the YZ channel adjusted to their zero position, as determined from encoder output, a null output from the YZ channel autocollimator is achieved by fine adjustment of the micrometer plate. Having achieved this null, the micrometer plate is clamped and secured. Alignment for the YZ channel is now complete.

The X-channel deflection wedge assembly is adjusted to its zero deviation position as determined by the encoder output.

The null output from the X-channel autocollimator is achieved as above--by adjusting the micrometer plate until the output indicates null. The micrometer plate is secured and the alignment is complete.

9.0

CONCLUSIONS

The results of design activity carried out as a result of this study confirm the achievement of all but one performance requirement--many by a substantial margin. The exception is the calculated power level of 12.3 watts (average) versus a specified 10 watt maximum. The specified and achieved values are shown in Table 9-1.

The described system is a valid and viable method, therefore, for measuring the boom deflections. Although requiring careful attention in detailed design of the opto-mechanical package, it does not require any technology which is beyond the present state of the art.

TABLE 9.1

Parameter	Units	Y and Z Axes		X Axis	
		Specified	Calculated	Specified	Calculated
Linear Range	arc-min.	±15 (min.)	±21	±5 (min.)	±7
Linearity	percent	±10 (max.)	< 1	±20 (max.)	< 1
Average Slope	mv/arc-sec.	100 ±10	100 ±0.5	200 ±20	200 ±1.0
Local Slope Variation	percent	±10 (max.)	±1	±10 (max.)	±1
Resolution (NEA).	arc-sec.	0.1 (max.)	0.00071	0.5 (max.)	0.005
Stability Over 5 Minutes	arc-sec.	0.5 (max.)	0.022	2.0 (max.)	0.22
Stability Through Environment	arc-sec.	2.0 (max.)	2.0 (est.)	5.0 (max.)	5.0 (est.)
Calibrated Accuracy	arc-sec.	1.0 (max.)	0.30	3.0 (max.)	2.79

APPENDIX A
PERFORMANCE REQUIREMENTS

EXHIBIT A

ATTITUDE TRANSFER ASSEMBLY FOR MAGSAT

1.0 INSTRUMENT DESCRIPTION

The Attitude Transfer Assembly will be used to monitor the attitude of a boom-mounted Magnetometer Experiment Package relative to the main spacecraft body. Attitude will be measured in orthogonal X and Y axis and in a twist axis around the boom center line.

2.0 PERFORMANCE PARAMETERS

2.1 Performance Concept

An Attitude Transfer Assembly is to be developed with the potential for very accurate measurement of the attitude of a boom-mounted Magnetometer Experiment Package relative to the main spacecraft body. Performance parameters are designated in the following paragraphs. Limits are defined as maximum deviations from desired values. All errors are expected r.m.s. values generated as r.s.s. of contributions by various error sources.

2.2 Linear Range

The linear range of the Attitude Transfer Assembly is defined below for orthogonal X and Y axis and for the twist axis. Outputs in each axis is to be independent of the position in the other axis. The field of view is defined as the angular range over which output signals are generated.

X and Y axis	-	15 arc minutes
twist axis	-	5 arc minutes

2.3 Linearity

Linearity is defined by the deviation of the response characteristic from a best fit straight line passing through the origin. This deviation is expressed as a percentage of the instantaneous value.

X and Y axis	-	±10%
twist axis	-	±20%

2.4 Slope

The average slope of the response characteristic is defined as the slope of a best fit straight line passing through

Exhibit A

the origin. The local slope at any single point within the linear range is defined with respect to the average slope.

Average slope

X and Y axis	100 \pm 10 mv per arc second
twist axis	200 \pm 20 mv per arc second

local slope \pm 10%

2.5 Performance in Linear Range

Calibrated accuracy and stability over the linear range are the most important parameter specifications. The requirements listed below include the effects of all cross-axis coupling.

Resolution (Noise Equivalent Angle)

X and Y axis	0.1 arc second
twist axis	0.5 arc second

Stability over five minutes anywhere in linear range

X and Y axis	0.5 arc seconds
twist axis	2 arc seconds

Stability through environment

X and Y axis	2.0 arc seconds
twist axis	5.0 arc seconds

Calibrated accuracy anywhere in linear range

X and Y axis	1.0 arc second
twist axis	3.0 arc seconds

2.6 Boom Length

The Attitude Transfer Assembly shall meet all performance requirements with a boom length of 15 to 25 feet.

3.0 INTERFACES

Interfaces will be determined by the requirements of the MAGSAT Mission. The Technical Officer shall provide specific and updated interface information as soon as interfaces are defined. General requirements are defined below.

Exhibit A

3.1 Weight

The complete Attitude Transfer Assembly shall have a weight of less than 25 pounds.

3.2 Power

The Attitude Transfer Assembly shall be operated from the spacecraft +16 volts power supply. Power consumption shall not exceed 10 watts.

3.3 Thermal

The temperature of the Attitude Transfer Assembly is to be actively and passively controlled by the contractor to insure temperatures compatible with the performance specification of Section 3.

3.4 Vibration

3.4.1 Sinusoidal Vibration

<u>Axis</u>	<u>Frequency Range</u>	<u>Level (0 to Peak)</u>	<u>Sweep Rate (Oct/Min)</u>
All (X, Y, Z)	10 - 18	5.0g*	4.
	18 - 36	0.3 in (D.A.)	
	36 - 150	20.g	
	150 - 2500	5.g	

*Limited to 0.5 in double amplitude (D.A.)

3.4.2 Random Vibration

<u>Axis</u>	<u>Frequency Range (Hz)</u>	<u>PSD Level (g²/Hz)</u>	<u>Acceleration (g-rms)</u>	<u>Duration Minutes</u>
All (X, Y, Z)	20 - 200	0.045	12.9	2/axis
	200 - 400	+3dB/Oct		
	400 - 2000	0.090		

3.5 Acceleration

The performance specifications of Section 3 shall be satisfied after non-operating exposure of acceleration of 22.5G in the thrust axis and 6.0G in the lateral axis. The acceleration shall be simultaneously applied for a duration of three minutes.

3.6 Magnetic Field

All components mounted on the Magnetometer Experiment Package will have a total induced field of less than 0.5 gamma measured at three inches.

APPENDIX B

SYSTEM PARAMETERS

OPTICAL PARAMETERS

Focal length	101.6 mm (4 inches)
Aperture dia.	29.0 mm (1.412 inches)
Reticle size, YZ channel	0.127 mm x 0.127 mm (0.005 in x 0.005 in)
X channel	0.127 mm x 1.02 mm (0.005 in x 0.040)
Error detector size	1 mm x 1 mm (0.040 in x 0.040 in) each
Acquisition detector size	1 mm x 2 mm (0.040 in x 0.080 in)
Error detector gap	0.0899 mm (0.0035 in)
Light Source	Texas Instruments LED TIL 33 selected
Operating Wavelength	0.94 microns
Pointing Adjustment	±2 min
Reflector Size:	
Flat mirror	63.5 mm square (2.5 inches square)
Remote Porro Reflector (each of 2 surfaces)	63.5 mm wide x 88.9 mm (2.5 inches wide x 3.5 inches)
Base Line Porro Reflector (each of 2 surfaces)	83.82 mm high x 21.02 mm (3.3 inches high x 0.828 inch)
Deviation Wedges:	32 mm diameter (1.26 inch)
Wedge Deviation Angle (Nominal)	636.4 arc-sec YZ channels
Wedge Deviation Angle (Nominal)	42.43 arc-sec. X channel

ELECTRONIC PARAMETERS

Average Power	12.3 watts
Peak Power	23.4 watts
Noise Equivalent Angle	7×10^{-4} arc sec, YZ channels 5×10^{-3} arc sec, X channel
Detector Responsivity	0.4 amps/watt
Scale Factor Stability	0.5 percent
Servo Threshold	15 arc-sec

ELECTRONIC PARAMETERS (Continued)

LED pulse frequency	491 pps
Motor pulse frequency	60 pps
Open-loop bandwidth	10 Hz
Open-loop scale factor	100 mv/arc-sec, YZ channels 200 mv/arc-sec, X channel

WEDGE DEVIATION UNIT PARAMETERS

<u>Item</u>	<u>YZ</u>	<u>X</u>
Detector linear range (Normal)	±15 arc-sec	±15
(Max.)	±20 arc-sec	±200
Servo measuring range (Normal)	±900 arc-sec	±300
(Max.)	±1272 arc-sec	±418
Drive motor	Size 8, 45° PM Stepper	
Gear reduction	1024:1	1024:1
Wedge angle per step	158.2 arc-sec	158.2
Wedge/encoder rotation range (Normal)	±45°	±45°
(Max.)	±90°	±90°
Wedge optical deviation (each)	636.4 arc-sec	42.43
Encoder counts per step	4	4
Optical deviation per step (Max.)	0.98 arc-sec	0.325
(Min.)	0.70 arc-sec	0.23
Deviation resolution from encoders	0.122 arc-sec	0.081

Amplifier	12.5 mv
Re	23.5 mv
1000	7.5 mv
500	5.0 mv
250	2.5 mv
125	1.25 mv
62.5	0.625 mv
31.25	0.3125 mv
15.625	0.15625 mv
7.8125	0.078125 mv
3.90625	0.0390625 mv
1.953125	0.01953125 mv
0.9765625	0.009765625 mv
0.48828125	0.0048828125 mv
0.244140625	0.00244140625 mv
0.1220703125	0.001220703125 mv
0.06103515625	0.0006103515625 mv
0.030517578125	0.00030517578125 mv
0.0152587890625	0.000152587890625 mv
0.00762939453125	0.0000762939453125 mv
0.003814697265625	0.00003814697265625 mv
0.0019073486328125	0.000019073486328125 mv
0.00095367431640625	0.0000095367431640625 mv
0.000476837158203125	0.00000476837158203125 mv
0.0002384185791015625	0.000002384185791015625 mv
0.00011920928955078125	0.0000011920928955078125 mv
5.960464477539062e-05	5.960464477539062e-05 mv
2.980232238769531e-05	2.980232238769531e-05 mv
1.490116119384766e-05	1.490116119384766e-05 mv
7.450580596923828e-06	7.450580596923828e-06 mv
3.725290298461914e-06	3.725290298461914e-06 mv
1.862645149230957e-06	1.862645149230957e-06 mv
9.313225746154785e-07	9.313225746154785e-07 mv
4.656612873077392e-07	4.656612873077392e-07 mv
2.328306436538696e-07	2.328306436538696e-07 mv
1.164153218269348e-07	1.164153218269348e-07 mv
5.82076609134674e-08	5.82076609134674e-08 mv
2.91038304567337e-08	2.91038304567337e-08 mv
1.455191522836685e-08	1.455191522836685e-08 mv
7.275957614183425e-09	7.275957614183425e-09 mv
3.637978807091712e-09	3.637978807091712e-09 mv
1.818989403545856e-09	1.818989403545856e-09 mv
9.09494701772928e-10	9.09494701772928e-10 mv
4.54747350886464e-10	4.54747350886464e-10 mv
2.27373675443232e-10	2.27373675443232e-10 mv
1.13686837721616e-10	1.13686837721616e-10 mv
5.6843418860808e-11	5.6843418860808e-11 mv
2.8421709430404e-11	2.8421709430404e-11 mv
1.4210854715202e-11	1.4210854715202e-11 mv
7.105427357601e-12	7.105427357601e-12 mv
3.5527136788005e-12	3.5527136788005e-12 mv
1.7763568394002e-12	1.7763568394002e-12 mv
8.881784197001e-13	8.881784197001e-13 mv
4.4408920985005e-13	4.4408920985005e-13 mv
2.2204460492502e-13	2.2204460492502e-13 mv
1.1102230246251e-13	1.1102230246251e-13 mv
5.5511151231255e-14	5.5511151231255e-14 mv
2.7755575615627e-14	2.7755575615627e-14 mv
1.3877787807813e-14	1.3877787807813e-14 mv
6.9388939039065e-15	6.9388939039065e-15 mv
3.4694469519532e-15	3.4694469519532e-15 mv
1.7347234759766e-15	1.7347234759766e-15 mv
8.673617379883e-16	8.673617379883e-16 mv
4.3368086899415e-16	4.3368086899415e-16 mv
2.1684043449707e-16	2.1684043449707e-16 mv
1.0842021724854e-16	1.0842021724854e-16 mv
5.421010862427e-17	5.421010862427e-17 mv
2.7105054312135e-17	2.7105054312135e-17 mv
1.3552527156067e-17	1.3552527156067e-17 mv
6.7762635780335e-18	6.7762635780335e-18 mv
3.3881317890167e-18	3.3881317890167e-18 mv
1.6940658945084e-18	1.6940658945084e-18 mv
8.470329472542e-19	8.470329472542e-19 mv
4.235164736271e-19	4.235164736271e-19 mv
2.1175823681355e-19	2.1175823681355e-19 mv
1.0587911840677e-19	1.0587911840677e-19 mv
5.2939559203385e-20	5.2939559203385e-20 mv
2.6469779601692e-20	2.6469779601692e-20 mv
1.3234889800846e-20	1.3234889800846e-20 mv
6.617444900423e-21	6.617444900423e-21 mv
3.3087224502115e-21	3.3087224502115e-21 mv
1.6543612251057e-21	1.6543612251057e-21 mv
8.2718061255285e-22	8.2718061255285e-22 mv
4.1359030627642e-22	4.1359030627642e-22 mv
2.0679515313821e-22	2.0679515313821e-22 mv
1.033975765691e-22	1.033975765691e-22 mv
5.169878828455e-23	5.169878828455e-23 mv
2.5849394142275e-23	2.5849394142275e-23 mv
1.2924697071137e-23	1.2924697071137e-23 mv
6.4623485355685e-24	6.4623485355685e-24 mv
3.2311742677842e-24	3.2311742677842e-24 mv
1.6155871338921e-24	1.6155871338921e-24 mv
8.0779356694605e-25	8.0779356694605e-25 mv
4.0389678347302e-25	4.0389678347302e-25 mv
2.0194839173651e-25	2.0194839173651e-25 mv
1.0097419586825e-25	1.0097419586825e-25 mv
5.0487097934125e-26	5.0487097934125e-26 mv
2.5243548967062e-26	2.5243548967062e-26 mv
1.2621774483531e-26	1.2621774483531e-26 mv
6.3108872417655e-27	6.3108872417655e-27 mv
3.1554436208827e-27	3.1554436208827e-27 mv
1.5777218104414e-27	1.5777218104414e-27 mv
7.888609052207e-28	7.888609052207e-28 mv
3.9443045261035e-28	3.9443045261035e-28 mv
1.9721522630517e-28	1.9721522630517e-28 mv
9.8607613152585e-29	9.8607613152585e-29 mv
4.9303806576292e-29	4.9303806576292e-29 mv
2.4651903288146e-29	2.4651903288146e-29 mv
1.2325951644073e-29	1.2325951644073e-29 mv
6.1629758220365e-30	6.1629758220365e-30 mv
3.0814879110182e-30	3.0814879110182e-30 mv
1.5407439555091e-30	1.5407439555091e-30 mv
7.7037197775455e-31	7.7037197775455e-31 mv
3.8518598887727e-31	3.8518598887727e-31 mv
1.9259299443864e-31	1.9259299443864e-31 mv
9.629649721932e-32	9.629649721932e-32 mv
4.814824860966e-32	4.814824860966e-32 mv
2.407412430483e-32	2.407412430483e-32 mv
1.2037062152415e-32	1.2037062152415e-32 mv
6.0185310762075e-33	6.0185310762075e-33 mv
3.0092655381037e-33	3.0092655381037e-33 mv
1.5046327690519e-33	1.5046327690519e-33 mv
7.5231638452595e-34	7.5231638452595e-34 mv
3.7615819226297e-34	3.7615819226297e-34 mv
1.8807909613149e-34	1.8807909613149e-34 mv
9.4039548065745e-35	9.4039548065745e-35 mv
4.7019774032872e-35	4.7019774032872e-35 mv
2.3509887016436e-35	2.3509887016436e-35 mv
1.1754943508218e-35	1.1754943508218e-35 mv
5.877471754109e-36	5.877471754109e-36 mv
2.9387358770545e-36	2.9387358770545e-36 mv
1.4693679385272e-36	1.4693679385272e-36 mv
7.346839692636e-37	7.346839692636e-37 mv
3.673419846318e-37	3.673419846318e-37 mv
1.836709923159e-37	1.836709923159e-37 mv
9.183549615795e-38	9.183549615795e-38 mv
4.5917748078975e-38	4.5917748078975e-38 mv
2.2958874039487e-38	2.2958874039487e-38 mv
1.1479437019744e-38	1.1479437019744e-38 mv
5.739718509872e-39	5.739718509872e-39 mv
2.869859254936e-39	2.869859254936e-39 mv
1.434929627468e-39	1.434929627468e-39 mv
7.17464813734e-40	7.17464813734e-40 mv
3.58732406867e-40	3.58732406867e-40 mv
1.793662034335e-40	1.793662034335e-40 mv
8.968310171675e-41	8.968310171675e-41 mv
4.4841550858375e-41	4.4841550858375e-41 mv
2.2420775429187e-41	2.2420775429187e-41 mv
1.1210387714594e-41	1.1210387714594e-41 mv
5.605193857297e-42	5.605193857297e-42 mv
2.8025969286485e-42	2.8025969286485e-42 mv
1.4012984643242e-42	1.4012984643242e-42 mv
7.006492321621e-43	7.006492321621e-43 mv
3.5032461608105e-43	3.5032461608105e-43 mv
1.7516230804052e-43	1.7516230804052e-43 mv
8.758115402026e-44	8.758115402026e-44 mv
4.379057701013e-44	4.379057701013e-44 mv
2.1895288505065e-44	2.1895288505065e-44 mv
1.0947644252532e-44	1.0947644252532e-44 mv
5.473822126266e-45	5.473822126266e-45 mv
2.736911063133e-45	2.736911063133e-45 mv
1.3684555315665e-45	1.3684555315665e-45 mv
6.8422776578325e-46	6.8422776578325e-46 mv
3.4211388289162e-46	3.4211388289162e-46 mv
1.7105694144581e-46	1.7105694144581e-46 mv
8.5528470722905e-47	8.5528470722905e-47 mv
4.2764235361452e-47	4.2764235361452e-47 mv
2.1382117680726e-47	2.1382117680726e-47 mv
1.0691058840363e-47	1.0691058840363e-47 mv
5.3455294201815e-48	5.3455294201815e-48 mv
2.6727647100907e-48	2.6727647100907e-48 mv
1.3363823550454e-48	1.3363823550454e-48 mv
6.681911775227e-49	6.681911775227e-49 mv
3.3409558876135e-49	3.3409558876135e-49 mv
1.6704779438067e-49	1.6704779438067e-49 mv
8.352389719034e-50	8.352389719034e-50 mv
4.176194859517e-50	4.176194859517e-50 mv
2.0880974297585e-50	2.0880974297585e-50 mv
1.0440487148792e-50	1.0440487148792e-50 mv
5.220243574396e-51	5.220243574396e-51 mv
2.610121787198e-51	2.610121787198e-51 mv
1.305060893599e-51	1.305060893599e-51 mv
6.525304467995e-52	6.525304467995e-52 mv
3.2626522339975e-52	3.2626522339975e-52 mv
1.6313261169987e-52	1.6313261169987e-52 mv
8.1566305849935e-53	8.1566305849935e-53 mv
4.0783152924967e-53	4.0783152924967e-53 mv
2.0391576462484e-53	2.0391576462484e-53 mv
1.0195788231242e-53	1.0195788231242e-53 mv
5.097894115621e-54	5.097894115621e-54 mv
2.5489470578105e-54	2.5489470578105e-54 mv
1.2744735289052e-54	1.2744735289052e-54 mv
6.372367644526e-55	6.372367644526e-55 mv
3.186183822263e-55	3.186183822263e-55 mv
1.5930919111315e-55	1.5930919111315e-55 mv
7.9654595556575e-56	7.9654595556575e-56 mv
3.9827297778287e-56	3.9827297778287e-56 mv
1.9913648889144e-56	1.9913648889144e-56 mv
9.956824444572e-57	9.956824444572e-57 mv
4.978412222286e-57	4.978412222286e-57 mv
2.489206111143e-57	2.489206111143e-57 mv
1.2446030555715e-57	1.2446030555715e-57 mv
6.2230152778575e-58	6.2230152778575e-58 mv
3.1115076389287e-58	3.1115076389287e-58 mv
1.5557538194644e-58	1.5557538194644e-58 mv
7.778769097322e-59	7.778769097322e-59 mv
3.889384548661e-59	3.889384548661e-59 mv
1.9446922743305e-59	1.9446922743305e-59 mv
9.7234613716525e-60	9.7234613716525e-60 mv
4.8617306858262e-60	4.8617306858262e-60 mv
2.4308653429131e-60	2.4308653429131e-60 mv
1.2154326714565e-60	1.2154326714565e-60 mv
6.0771633572825e-61	6.0771633572825e-61 mv
3.0385816786412e-61	3.0385816786412e-61 mv
1.5192908393206e-61	1.5192908393206e-61 mv
7.596454196603e-62	7.596454196603e-62 mv
3.7982270983015e-62	3.7982270983015e-62 mv
1.8991135491507e-62	1.8991135491507e-62 mv
9.4955677457535e-63	9.4955677457535e-63 mv
4.7477838728767e-63	4.7477838728767e-63 mv
2.3738919364384e-63	2.3738919364384e-63 mv
1.1869459682192e-63	1.1869459682192e-63 mv
5.934729841096e-64	5.934729841096e-64 mv
2.967364920548e-64	2.967364920548e-64 mv
1.483682460274e-64	1.483682460274e-64 mv
7.41841230137e-65	7.41841230137e-65 mv
3.709206150685e-65	

APPENDIX C

LED DATA SHEET

LED INFORMATION

The selected LED is the Texas Instruments Type TIL 33 described in the attached data sheet.

Procurement will be via an SCD which will define optical, mechanical and electrical characteristics as well as temperature conditioning and testing.

An important parameter is the mechanical dimensions of the emitting area, which is nominally 0.015 inches square. This will be assigned a tolerance of ± 0.0005 . The cathode connection is via a spot weld near one corner of the chip; its position will also be controlled by the SCD.

Information received from Mr. John Thomas of Texas Instruments, Lubbock, Texas indicates the TIL 33 is now -65 to 150°C, and that the derating rate is 1.6 mA/°C. This information supersedes that shown on the data sheets. TI has also indicated that this LED can be supplied in the HI-REL version described in the data sheets for their TIL 23 and 24. A flat window would be specified, however.

"Page^s missing from available version"

Pages 1-46

TYPES TIL23, TIL24

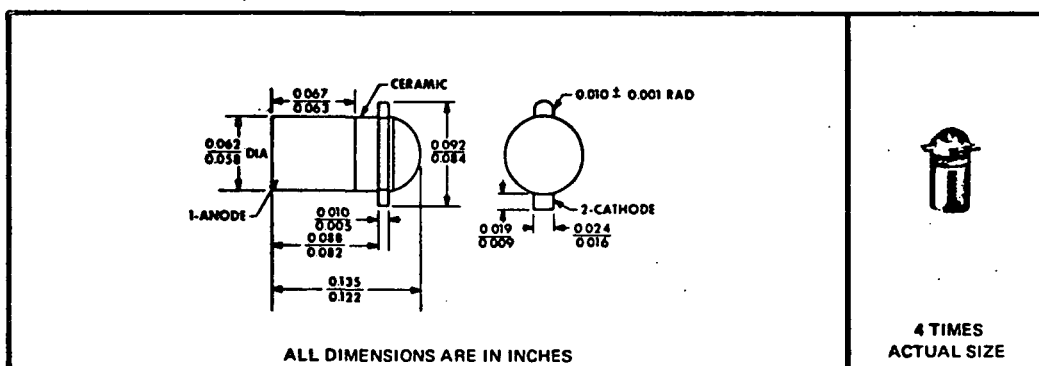
P-N GALLIUM ARSENIDE INFRARED-EMITTING DIODES

BULLETIN NO. DLS 7411312, FEBRUARY 1970—REVISED NOVEMBER 1974

DESIGNED TO EMIT NEAR-INFRARED
RADIATION WHEN FORWARD BIASED

- Output Spectrally Compatible with Silicon Sensors
- High Power Efficiency, Typically 1.5 Percent at 25°C
- High Power Output, Typically 2.0 mW at 25°C
- Small Size Permits Matrix Assembly Directly into Printed Circuit Boards
- High Radiant Intensity, Typically 7 mW/sr for TIL24

mechanical data



absolute maximum ratings

Reverse Voltage at 25°C Case Temperature	2 V
Continuous Forward Current at 25°C Case Temperature (See Note 1)	100 mA
Operating Case Temperature Range	-65°C to 125°C
Storage Temperature Range	-65°C to 150°C
Soldering Temperature (3 Minutes)	240°C

[†] Radiant intensity is calculated from $I_0 = P_O / 2\pi(1 - \cos 0.5\theta_{HI})$. One steradian is the solid angle at the center of a sphere subtended by a portion of the surface area equal to the square of the radius of the sphere. There are 4π steradians in a complete sphere.

NOTE 1: Derate linearly to 125°C case temperature at the rate of 1 mA/°C. For pulsed operation at higher currents, see Figures 8 and 9.

TYPES TIL31, TIL33, TIL34

P-N GALLIUM ARSENIDE INFRARED-EMITTING DIODES

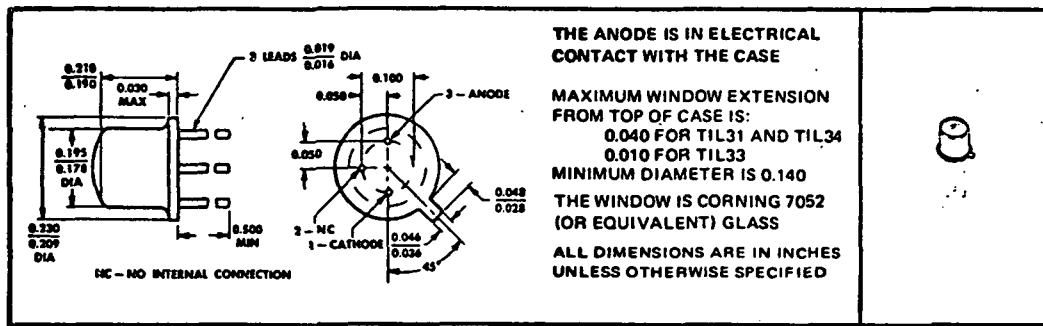
BULLETIN NO. DL-S 7412209, NOVEMBER 1974

DESIGNED TO EMIT NEAR-INFRARED RADIATION WHEN FORWARD BIASED

- Output Spectrally Compatible with Silicon Sensors
- Mechanically Compatible with TIL81
- Typical Applications Include Card Readers, Encoders, Intrusion Alarms, Sector Sensors, Level Indicators, and Beginning-of-Tape/End-of-Tape Indicators

mechanical data

Each device is in a hermetically sealed welded case similar to JEDEC TO-18 with window. The TIL31 and TIL34 have convex lenses while that of the TIL33 is essentially flat. A coin header is used to increase dissipation capability. All TO-18 registration notes also apply to this outline. Approximate weight is 0.35 gram. All metal surfaces are gold plated.



absolute maximum ratings

Reverse Voltage at 25°C Case Temperature	2 V
Continuous Forward Current at 25°C Case Temperature (See Note 1)	200 mA
Operating Case Temperature Range: TIL31, TIL33	-40°C to 80°C
TIL34	-65°C to 150°C
Storage Temperature Range: TIL31, TIL33	-40°C to 100°C
TIL34	-65°C to 150°C
Lead Temperature 1/16 Inch from Case for 10 Seconds	240°C

operating characteristics at 25°C case temperature

PARAMETER	TEST CONDITIONS	TIL31			TIL33			TIL34			UNIT
		MIN	TYP	MAX	MIN	TYP	MAX	MIN	TYP	MAX	
P_O Radiant Power Output	$I_F = 100$ mA	3.3	6		2.5	5		1.6	3		mW
λ_p Wavelength at Peak Emission		915	940	975	915	940	975	915	940	975	nm
$\Delta\lambda$ Spectral Bandwidth			50	75		50	75		50	75	nm
θ_{HI} Half-Intensity Beam Angle			10°			80°			10°		
V_F Static Forward Voltage			1.4	1.75		1.4	1.75		1.4	1.75	V
t_r Radiant Pulse Rise Time†	$I_{FM} = 50$ mA, $t_w = 2$ μ s,		600			600			600		ns
t_f Radiant Pulse Fall Time‡	$I = 45$ kHz		350			350			350		

† Radiant intensity is calculated from $I_\theta = P_O / 2\pi(1 - \cos 0.5\theta_{HI})$. One steradian is the solid angle at the center of a sphere subtended by a portion of the surface area equal to the square of the radius of the sphere. There are 4π steradians in a complete sphere.

‡ Radiant pulse rise time is the time required for a change in radiant intensity from 10% to 90% of its peak value for a step change in current; radiant pulse fall time is the time required for a change in radiant intensity from 90% to 10% of its peak value for a step change in current.

NOTE 1: Derate linearly to 80°C case temperature at the rate of 3.6 mA/°C for the TIL31 and TIL33, and to 150°C case temperature at the rate of 1.6 mA/°C for the TIL34.

TYPES TIL31, TIL33, TIL34 P-N GALLIUM ARSENIDE INFRARED-EMITTING DIODES

TYPICAL CHARACTERISTICS

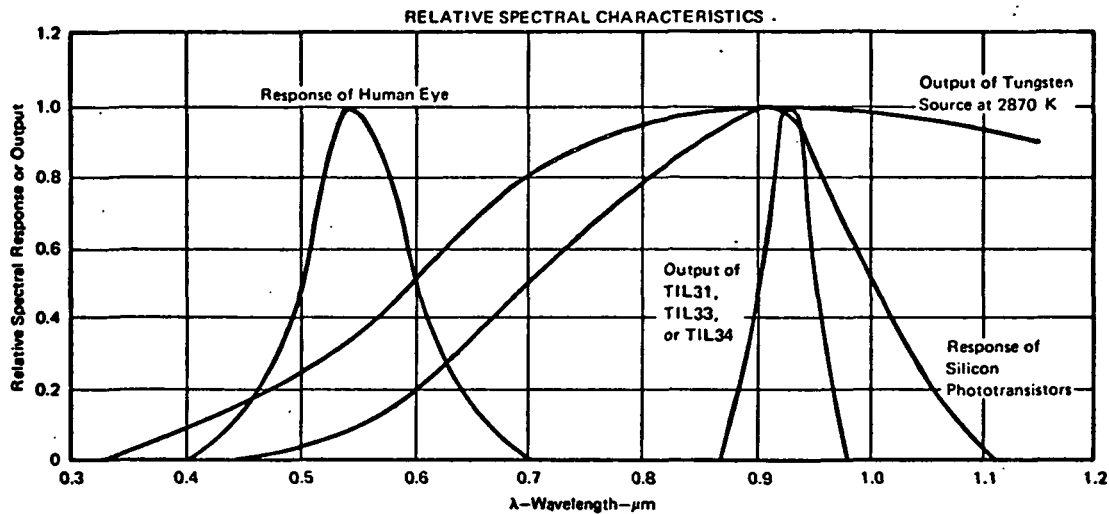


FIGURE 1

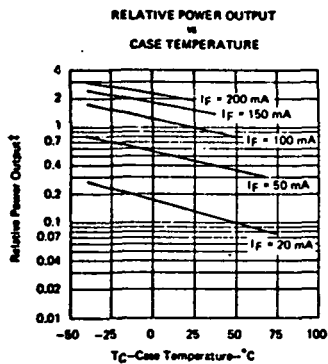


FIGURE 2

TIL31, TIL34

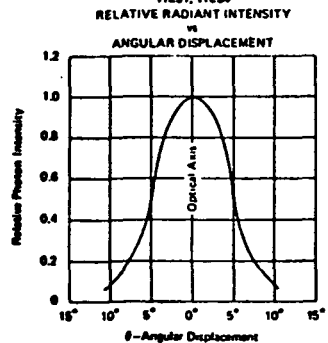


FIGURE 5

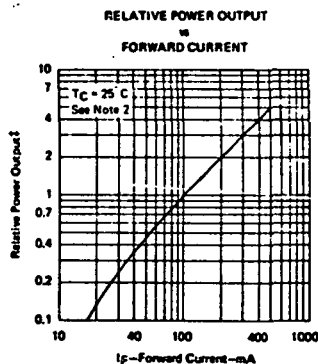


FIGURE 3

TIL33

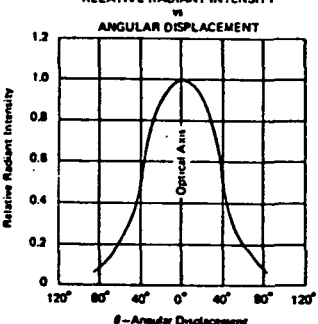


FIGURE 6

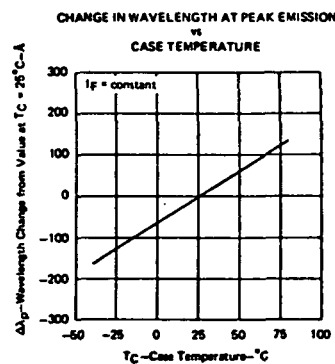


FIGURE 4

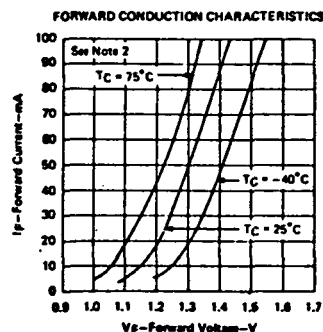


FIGURE 7

NOTE 2: This parameter must be measured using pulse techniques, $t_w = 0.04 \text{ ms}$, duty cycle $\leq 10\%$.

‡Normalized to output at $I_f = 10 \text{ mA}$, $T_C = 25^{\circ}\text{C}$.

PRINTED IN U.S.A.

TIL23, TIL24 RELIABILITY DATA

TIL23, TIL24 RELIABILITY DATA

INTRODUCTION

Texas Instruments has long been noted as a quality producer of semiconductor components. The TIL23 and TIL24 solid-state infrared-emitting diodes (IRED's) are high-quality, reliable additions to its line of optoelectronic products. They have been designed as highly reliable, long-life products capable of meeting demanding military and commercial needs. Quality control of these products begins with incoming inspection of raw materials and is continued throughout the manufacturing process as shown in assembly-test flow diagram (Figure 1). Conscientious quality control practiced by the manufacturing organization and monitored at critical steps by the quality control organization assures that the designed reliability will be achieved in the finished product.

Since this product was announced in 1970, some two million device hours of reliability testing have been accumulated on ungraded, unburned-in samples, and additional data is continuously being accumulated. This report summarizes, in graphical form, data on the operating life of TIL23 and TIL24 at 10, 30, and 50 mA at 25°C and 50 mA at 55°C. Results of various mechanical and temperature stress tests are also presented.

OPERATING LIFE TESTS

Room temperature (25°C) life tests were performed at three different current levels: 10 mA, 30 mA and 50 mA. Readings of power output were made with a solar cell in a short-circuit current mode at 0, 168, 500 and 1,000 hours. Forward voltage was read at these intervals and no significant changes were observed. A total of 175 devices were tested at 10 mA or 30 mA with no device evidencing a change in power output greater than -10%. 96 devices were tested at 50 mA with four devices exceeding -20% reduction of power output (-27% worst case). Extended operating life tests at 25°C (4,000 hours) on 300 units have substantiated the extrapolated degradation rates shown in Figures 2, 3, 4, and 5.

High-temperature (55°C) life tests were performed at $I_f = 50$ mA on units which had 48 hours of pre-conditioning prior to the test. Readings of power output were performed in the same manner as the readings performed at room temperature described in the preceding paragraph. No significant changes of forward voltage were observed. A total of 1384 devices were tested with one catastrophic failure and one device evidenced a change in power output greater than -50%. Data from these tests are illustrated in Figures 6 and 7.

STORAGE LIFE TESTS

High-temperature (85°C) storage tests were performed for 1,000 hours on 1386 units with an insignificant change in power output. Only two devices had changes of power output greater than -5% (-13% worst case). No significant changes of forward voltage were observed.

ENVIRONMENTAL TESTS

The tests listed in Figure 8 were performed on samples of the product with no catastrophic failures observed. It should be noted that the test conditions shown are not the ultimate strength of the product but represent the test requirements imposed by our customers. The ultimate strength of these devices is much higher in most cases. Inquiries concerning response to particular requirements should be addressed to your TI sales representative.

TIL23HR, TIL24HR... HIGH-RELIABILITY INFRARED EMITTERS

Texas Instruments now offers the TIL23HR and TIL24HR as standard product items to customers requiring extra reliability in their applications. Utilizing the same small ceramic pill package design as the LS600 series phototransistor, the TIL23HR and TIL24HR are used to provide dependable and reliable infrared sources in military and aerospace applications. The TIL23HR and TIL24HR infrared emitters and the complementary TIL601HR thru TIL604HR phototransistors are now available as standard product items. For more information, contact your nearest TI sales representative or Optoelectronic Department Product Marketing.

TIL23, TIL24 RELIABILITY DATA

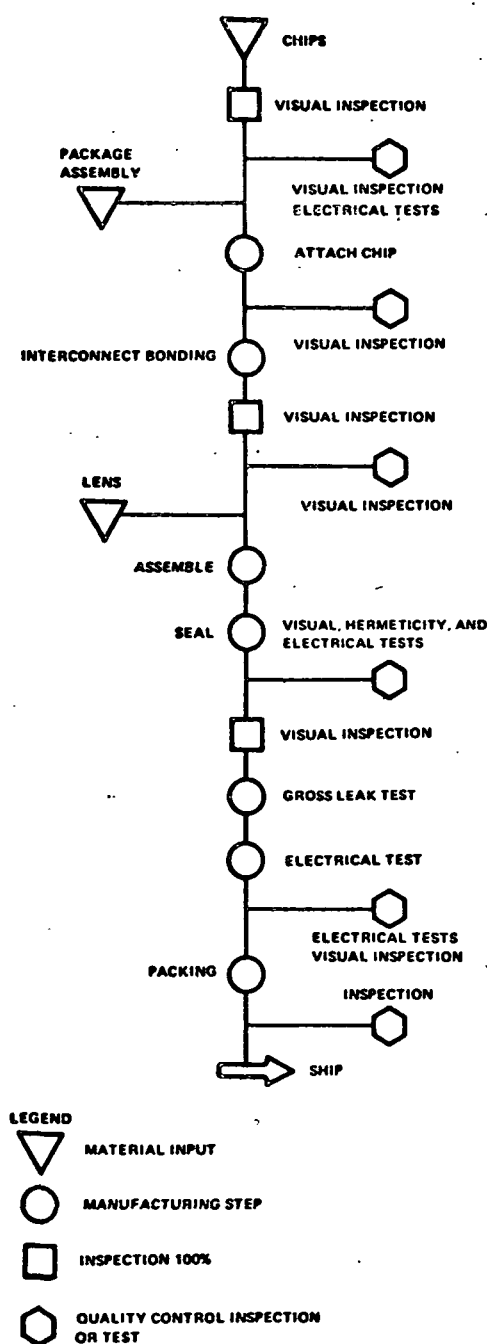


FIGURE 1. TIL23 and TIL24 Infrared-Emitter Flow Diagram

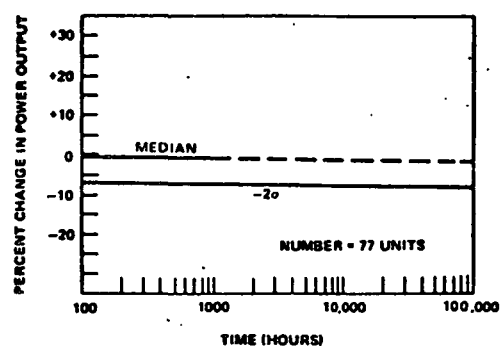


FIGURE 2. Change in Power Output as a Function of Operating Time at $I_F = 10 \text{ mA}$, 25°C

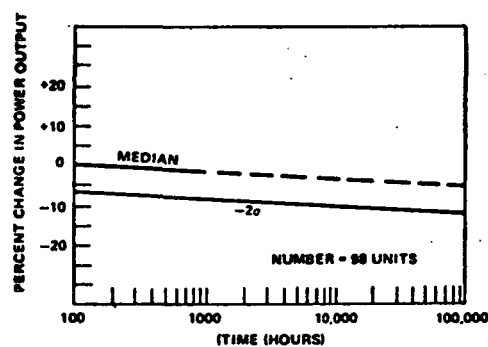


FIGURE 3. Change in Power Output as a Function of Operating Time at $I_F = 30 \text{ mA}$, 25°C

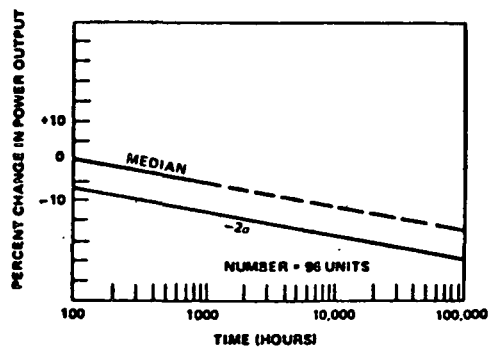


FIGURE 4. Change in Power Output as a Function of Operating Time at $I_F = 50 \text{ mA}$, 25°C

TIL23, TIL24 RELIABILITY DATA

UNITS TESTED	UNIT HOURS	CATASTROPHIC FAILURES	DEGRADATION FAILURES			
			TOTAL	FAILURE RATE IN %/1,000 HOURS		MEAN TIME BETWEEN FAILURES
				60% CONFIDENCE	90% CONFIDENCE	
1384	1,384,000	0	1	0.15	0.28	685,000 HOURS

FIGURE 5. Operating Life at 25°C at 50 mA

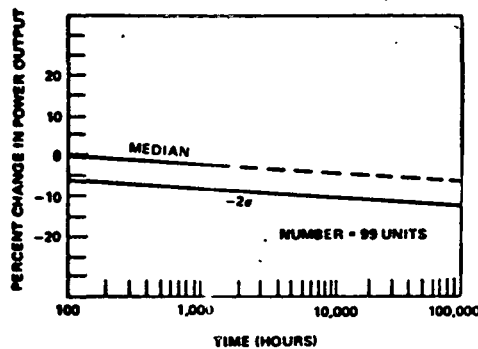


FIGURE 6. Change in Power Output as a Function of Operating Time at $I_F = 50$ mA, 55°C After 48 Hours of Preconditioning

UNITS TESTED	UNIT HOURS	CATASTROPHIC FAILURES	TOTAL	DEGRADATION FAILURES		
				FAILURE RATE IN %/1,000 HOURS		MEAN TIME BETWEEN FAILURES
				60% CONFIDENCE	90% CONFIDENCE	
1384	1,384,000	1	1	0.15	0.28	685,000 HOURS

FIGURE 7. Operating Life at 55°C at $I_F = 50$ mA After 48 Hours of Preconditioning

MIL-STD-750 Test Method	Test	Quantity Tested	Failures (Catastrophic or Degradation)
1051	Temperature Cycle: 5 Cycles, 30 Minutes, -40°C to +100°C	458	0
1051	Temperature Cycle: 5 Cycles, 30 Minutes, -65°C to +150°C	50	0
1056	Thermal Shock: 5 Cycles, Condition A	50	0
1021	Moisture Resistance	50	0
2016	Shock, Impact: 1500 g, Z ₁ Axis, 0.5 milliseconds	830	2
2056	Vibration, Variable Frequency: 20 g	842	1
2006	Constant Acceleration: 20 kg, 1 Min. Z ₁	146	0
1071	Hermetic Seal: Test Condition E	390	1

Figure 8. Environmental Test Results

APPENDIX D

SCD FOR SILICON PLANAR DIFFUSED PHOTO DETECTOR

This appendix presents a typical SCD written for a single-axis instrument operating at 0.670 microns. All references to operating wavelength such as in the specification of anti-reflection coatings and responsivity will be changed to the operating wavelength of the ATA namely 0.940 microns. Responsivity in addition, will be specified to be 0.4 amps/watt and matched to 5%. The error detector gap will also be changed from 0.005 in to 0.0035 in for the ATA.

These changes, discussed with the potential manufacturer, are achievable and will cause no difficulty.

Configurations P_3 and P_4 are designated for the ATA.

NOTE: INTERPRET PER MIL-D-1000, CATEGORY F,
FORM 1 (MIL-STD-100A)

PREPARED BY:
EAPLES ENGINEERING COMPANY
STAMFORD, CONNECTICUT

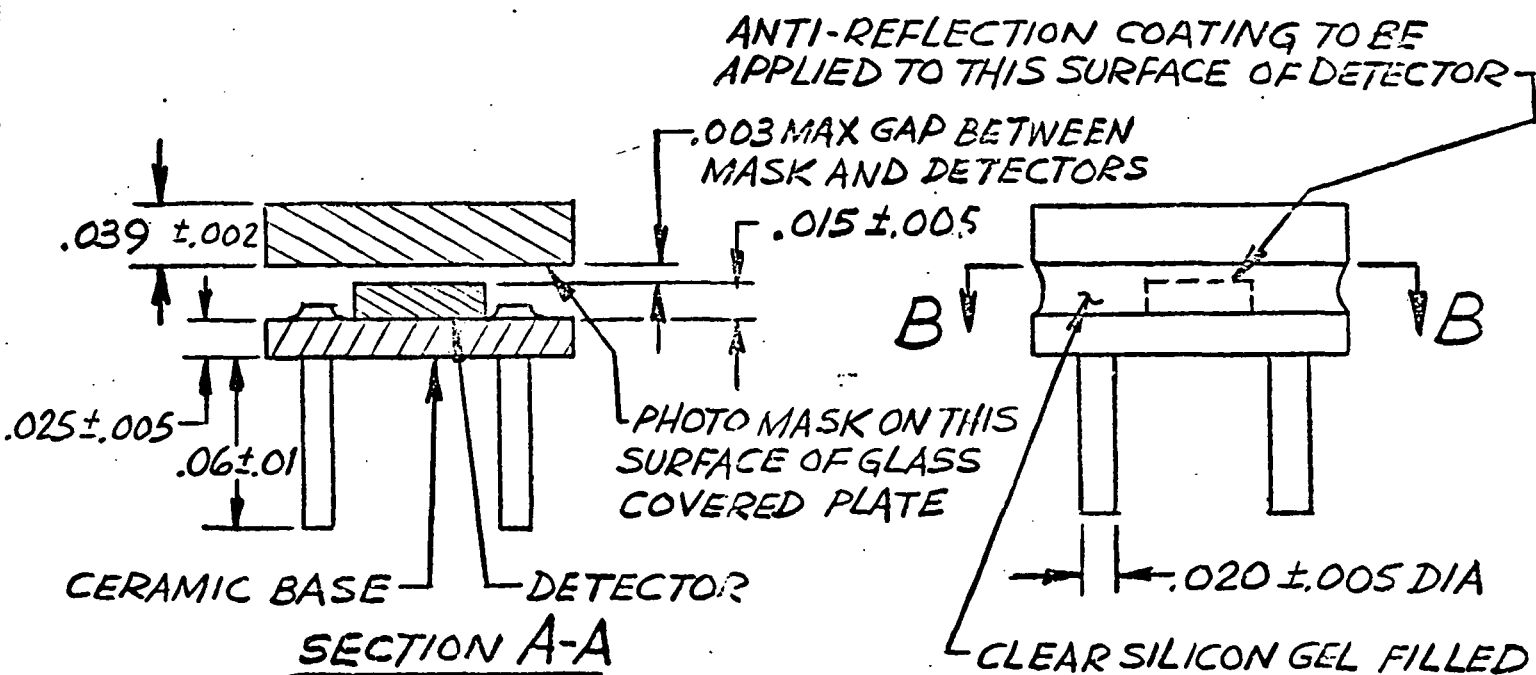
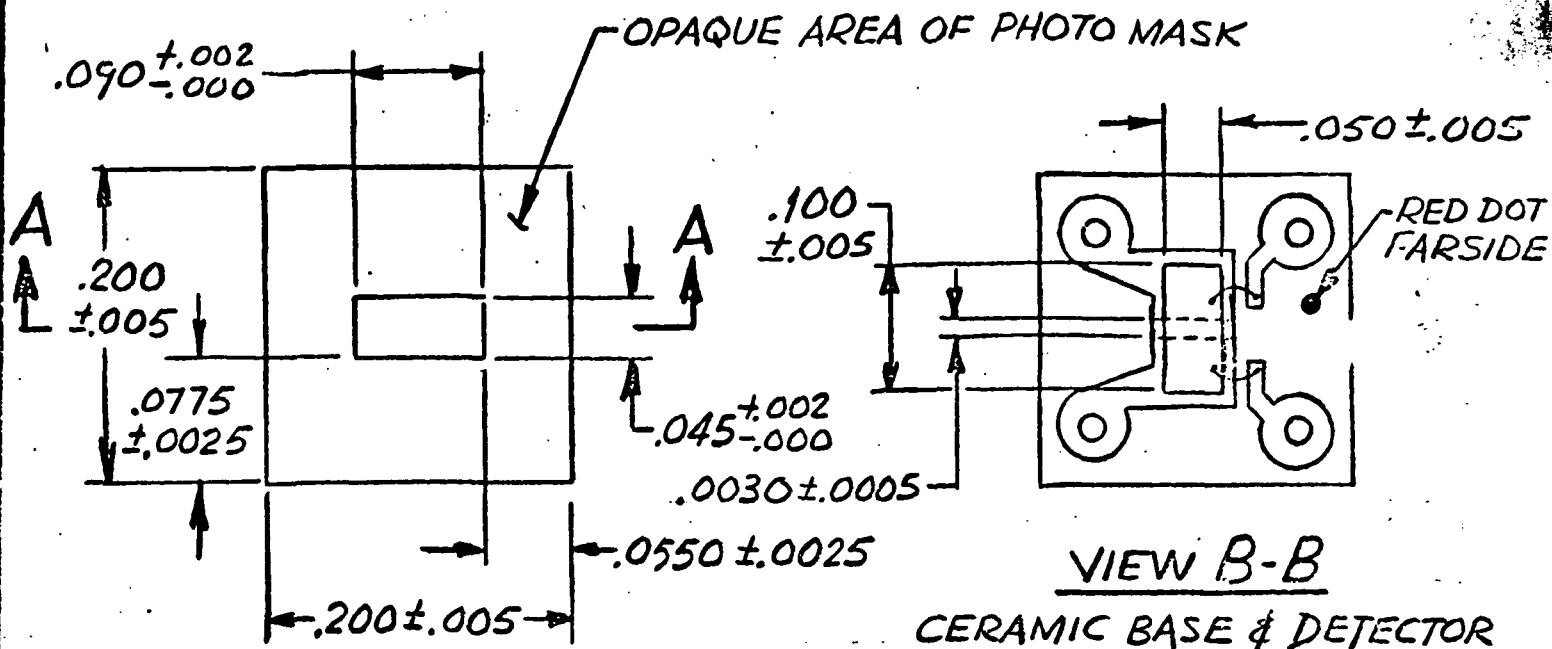
REV									
SHT									
REV	A								
SHT	19								
REV	A	A	A	A	A	A	A	A	A
SHT	10	11	12	13	14	15	16	17	18
REV	A	A	A	A	A	A	A	A	A
SHT	1	2	3	4	5	6	7	8	9

REVISION STATUS OF SHEETS

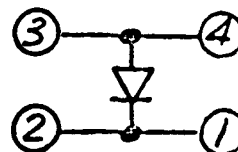
		DO NOT SCALE DWG DIMENSIONS ARE IN INCHES. TOLERANCES ON: DECIMALS ANGLES \pm \pm ALL SURFACES MATL—	GENERAL ELECTRIC 97993		DEPARTMENT OF THE NAVY STRATEGIC SYSTEMS PROJECT OFFICE WASHINGTON, D. C.		
			CONTR 100030740099		SEMICONDUCTOR DEVICE, DIODE SILICON PLAINAR DIFFUSED PHOTO DETECTOR SOURCE CONTROL DRAWING		
			DWN				
			CHK				
			ENG				
				ISS			
		APFD FOR STRATEGIC SYSTEMS PROJECT OFFICE		SIZE A		CODE IDENT NO. 10001	3204120
APPLICATION		BY DIRECTION — DIR SSP		SCALE		SHEET	
ENC-128	DIAG						
ENC-100	IN 3 MOD 0						
NEXT ASSY	USED ON.						

REVISIONS

LTR	DESCRIPTION	DATE	APPROVED
A	ORIGINAL SPG APPROVED ISSUE		



SCHEMATIC DIAG.



REV STATUS

P No. REV

1 A

FIGURE 1

SEMICONDUCTOR DEVICE,
DIODE SILICON PLANNAR DIFFUSED
PHOTO DETECTOR

SIZE

A

CODE IDENT NO.

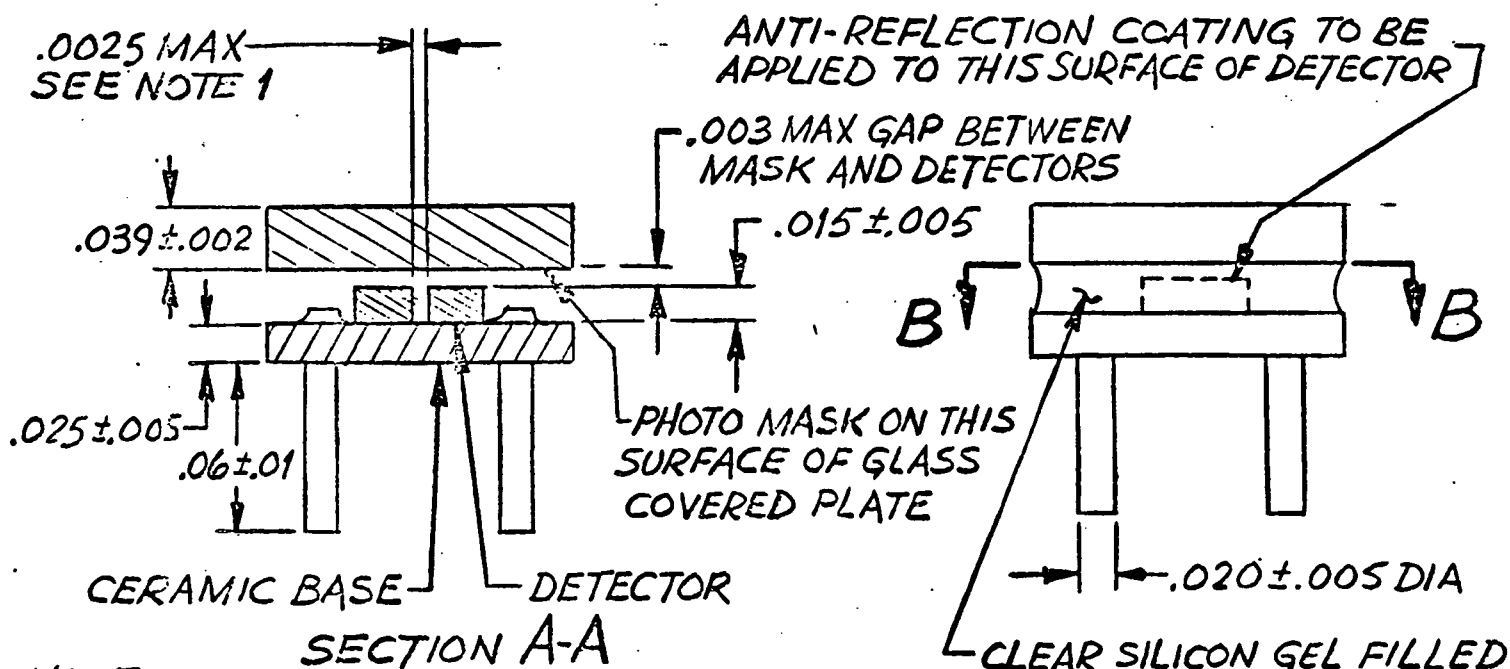
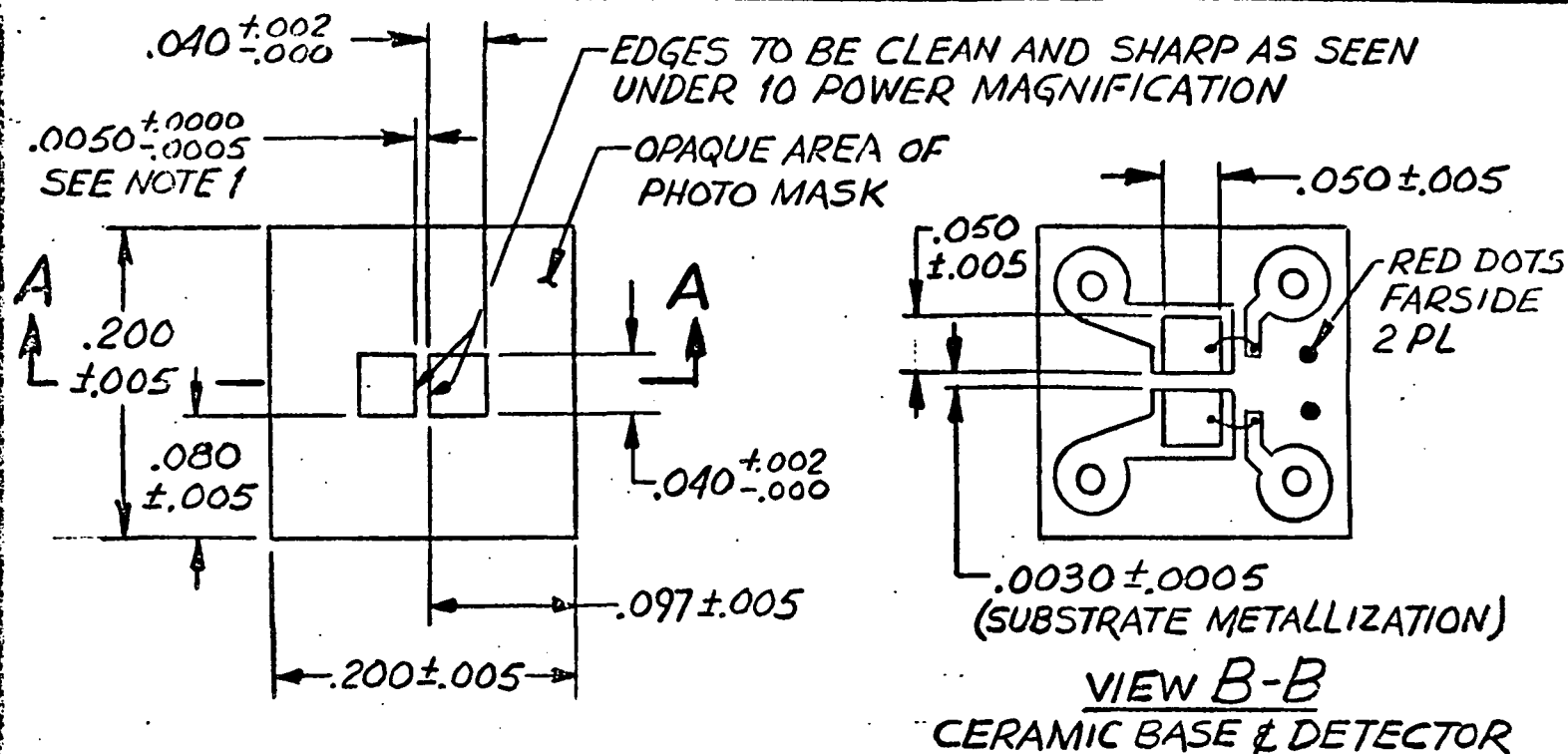
10001

3204120

SCALE NONE

REV A

SHEET 2



NOTE

1. DETECTOR GAP TO BE CENTERED BELOW OPAQUE STRIP OF MASK TO WITHIN .001

SCHEMATIC DIAG.

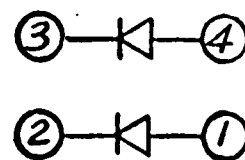


FIGURE 2

REV STATUS

D No. REV

2 A

SEMICONDUCTOR DEVICE,
DIODE SILICON PLANNAR DIFFUSED
PHOTO DETECTOR

SIZE

A

CODE IDENT NO.

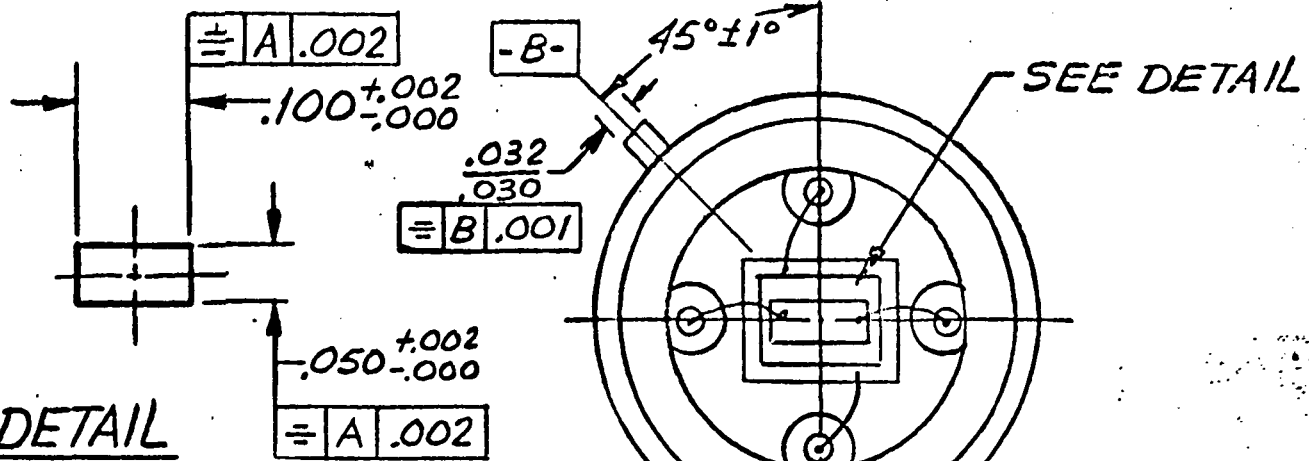
10001

3204120

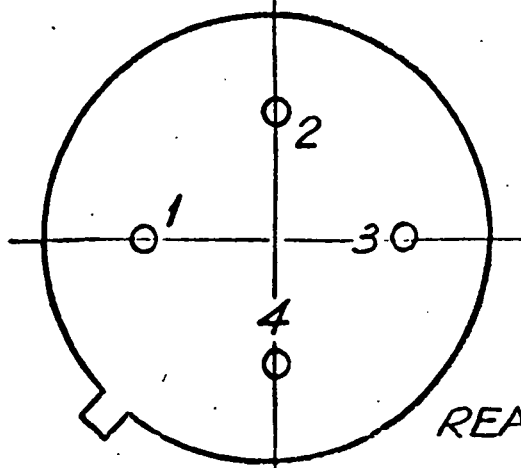
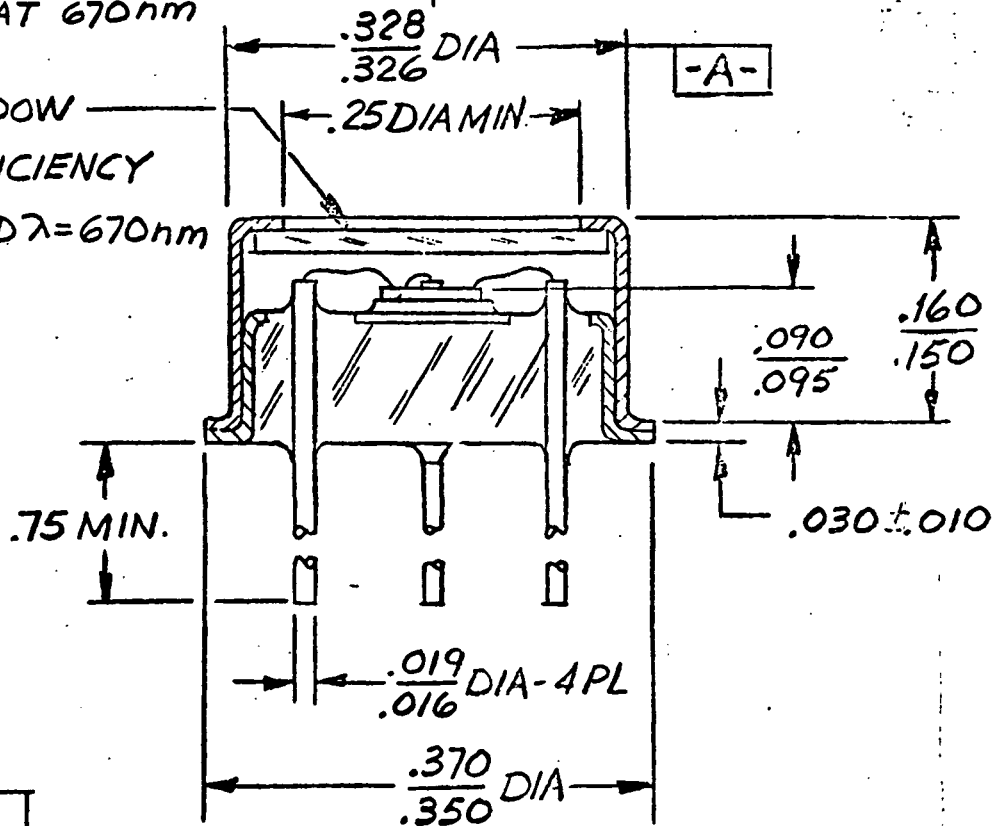
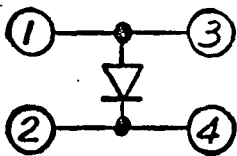
SCALE NONE

REV A

SHEET 3



SCHEMATIC DIAG.

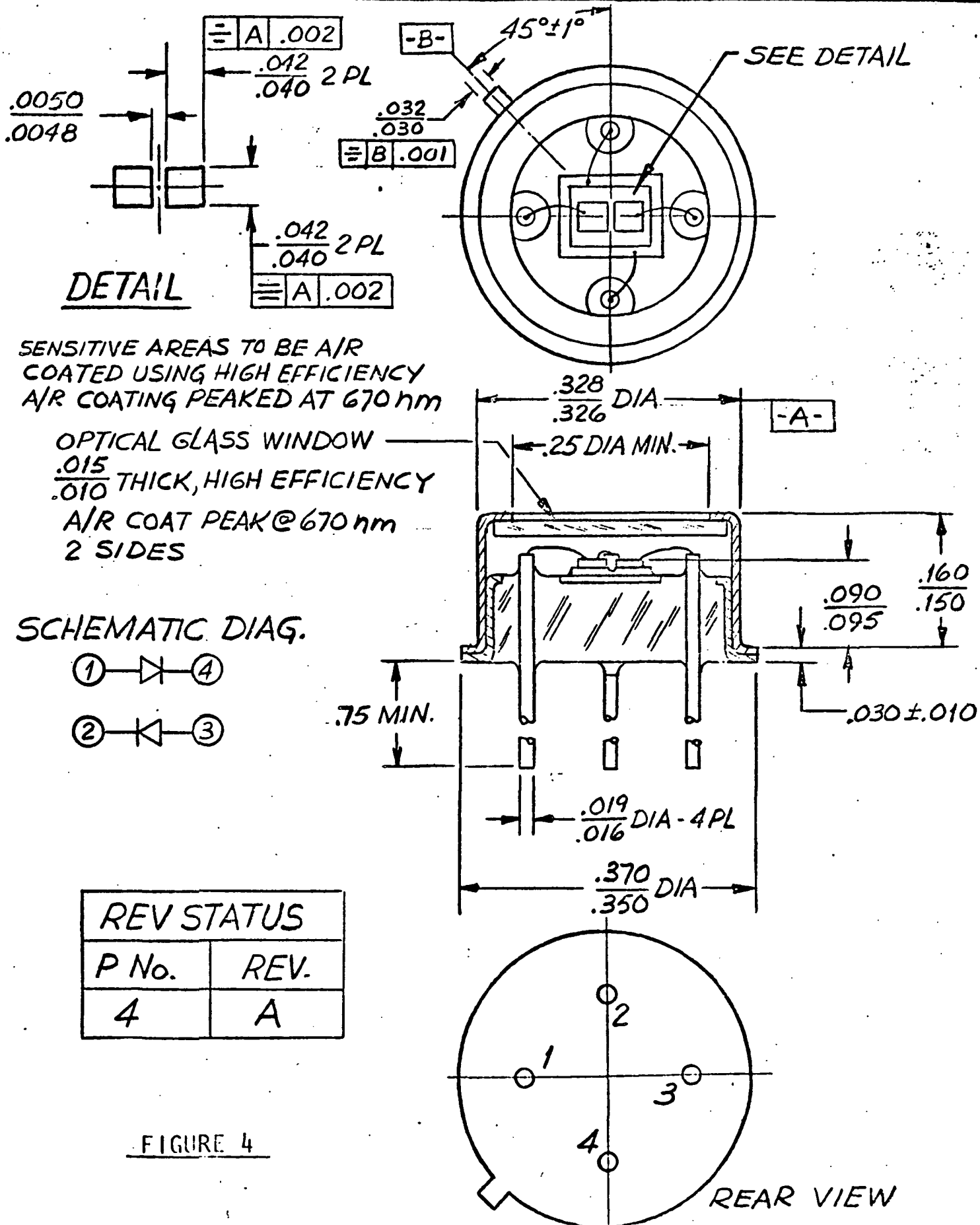


REV STATUS	
P No.	REV.
3	A

FIGURE 3

SEMICONDUCTOR DEVICE,
 DIODE SILICON PLANNAR DIFFUSED
 PHOTO DETECTOR

SIZE	CODE IDENT NO.	
A	10001	3204120
SCALE NONE	REV A	SHEET 4



SEMICONDUCTOR DEVICE,
 DIODE SILICON PLANNAR DIFFUSED
 PHOTO DETECTOR

SIZE CODE IDENT NO.

A

10001

3204120

SCALE NONE

REV A

SHEET 5

TABLE I - ELECTRO OPTICAL PARAMETERS (-P1, -P2, -P3, -P4)

PARAMETER	CONDITIONS	SYM	LIMITS		UNITS
			MIN	MAX	
RESPONSIVITY (NOTE 3)	$\lambda = 670 \text{ nm}$ $T = 25^\circ \pm 5^\circ \text{C}$	R	0.30	---	AMPS/WATT
RESPONSIVITY MATCH (-P2 & -P4 ONLY) (NOTE 4)	$\lambda = 670 \text{ nm}$ $T = 25^\circ \pm 5^\circ \text{C}$	$\frac{R_{\text{MIN}}}{R_{\text{MAX}}}$	0.92	---	
TOTAL JUNCTION CAPACITANCE (NOTE 2)	$T = 25^\circ \pm 5^\circ \text{C}$ $V = 0, E_e = 0,$ $f = 1 \text{ KHZ}$	C_J	---	100	pF
TOTAL ZERO BIAS RESISTANCE (NOTE 1)	$10^\circ \text{C} < T < 25^\circ \text{C}$ $T = 35^\circ \text{C}$ $E_e = 0,$ $V_F = V_R = 0.$	R_D	100	---	MEG-OHM
			50	---	MEG-OHM
OPERATING TEMPERATURE RANGE		---	-10	+35	$^\circ \text{C}$
STORAGE TEMPERA- TURE RANGE		---	-55	+125	$^\circ \text{C}$
THERMAL STABILITY	$10^\circ < T < 35^\circ \text{C}$	$\frac{dR}{R} / dT$	---	0.2	%/ $^\circ \text{C}$
ISOLATION RESISTANCE (-P2 & -P4 ONLY) (NOTE 5)	$T = 25^\circ \text{C} \pm 5^\circ \text{C}$ $V_{\text{IE}} = \pm 100 \text{ mV MAX.}$	IR	200	---	MEG-OHM
NOISE (NOTE 6)	$T = 25^\circ \text{C} \pm 5^\circ \text{C}$	e_n	---	4.7	mVrms/ $\sqrt{\text{Hz}}$
DETECTIVITY (P1 & -P2 ONLY)	$\lambda = 900 \text{ nm}, f = 360 \text{ Hz}$ $\text{BW} = 1 \text{ Hz}$	D^*	5×10^{11}	---	$\text{cm} \sqrt{\text{Hz}}/\text{WATT}$

NOTES: 1. INTERPOLATE R_D AT $V_F = V_R = 0$ FROM E-1 CURVE
WHERE $10 \text{ mV} < V_F = V_R < 100 \text{ MV DC.}$

2. MEASURED ACROSS PINS 1 & 4 WITH PINS 1 & 3
AND 2 & 4 CONNECTED.

SEMICONDUCTOR DEVICE, DIODE
SILICON PLANAR DIFFUSED PHOTO
DETECTOR

SIZE CODE IDENT NO.
A 10001

3204120

SCALE —

REV

SHEET

5

TABLE 1 - (CONTINUED)

NOTES: 3. RESPONSIVITY SHALL BE MEASURED BY MEASURING THE RELATIVE RESPONSIVITY TO A STANDARD DETECTOR WHOSE RESPONSIVITY IN AMPS/WATT IS TRACEABLE TO NBS. A TUNGSTEN SOURCE WILL BE USED FILTERED TO PASS THE SPECTRUM FROM 0.5 μ m TO 0.75 μ m MINIMUM. BOTH THE STANDARD DETECTOR AND THE TEST DETECTOR WILL BE FULLY IRRADIATED. THE RESPONSIVITY WILL BE CALCULATED USING THE EQUATION:

$$R_{\lambda \left\{ \begin{array}{l} \text{TEST} \\ \text{DET.} \\ \text{(TD)} \end{array} \right\}} = R_{\lambda \text{(STD.)}} \times \frac{A \text{(STD)}}{A \text{(TD)}} \times \frac{V_{\text{RMS}} \text{(TD)}}{V_{\text{RMS}} \text{(STD)}}$$

4. RESPONSIVITY MATCH IS THE RATIO OF RMIN/RMAX FOR EACH DETECTOR IN ONE P2 OR P4 DETECTOR ARRAY.
5. IR SHALL BE MEASURED BETWEEN EITHER TERMINALS OF ONE DETECTOR TO EITHER TERMINAL OF THE REMAINING DETECTOR.
6. MEASURED USING INSTRUMENT SA2819615 CALIBRATED FOR e_{no} (OPEN CIRCUIT) NOISE ≤ 3.8 mV RMS/ $\sqrt{\text{HZ}}$ USING A BW OF +10 HZ AT 400 HZ.

SEMICONDUCTOR DEVICE, DIODE
SILICON PLANAR DIFFUSED PHOTO
DETECTOR

SIZE	CODE IDENT NO.	
A	10001	3204120
SCALE	—	REV A
		SHEET 7

1. SCOPE

- 1.1 This document establishes the requirements for the procurement of two configurations of silicon-planar diffused photo detector diodes, packaged using two different techniques. Designs P3 and P4 are hermetically sealed.

2. APPLICABLE DOCUMENTS

- 2.1 In the event of conflict between the requirements specified in the contract or purchase order, this document and other documents referenced herein, the requirements of the contract or purchase order, this document and the referenced documents shall govern in that order.

- 2.2 The following documents form a part of this document to the extent specified herein:

MIL-S-19500..... Semiconductor Devices, General Specification For,

MIL-STD-1285 Marking of Electrical And Electronic Parts

MIL-STD-750..... Test Methods For Semiconductor Devices

MIL-STD-202..... Test Methods For Electronic And Electrical Component Parts

All Military Standards (MIL-STD-), Military Specifications (MIL-), Ordnance Pamphlets (OP-), Federal Standards (FED-STD-), and Federal Specifications shall be ordered from the Naval Publications and Forms Center, 5801 Tabor Avenue, Philadelphia, PA. 19120.

3. REQUIREMENTS

- 3.1 Unless otherwise specified, the silicon diodes shall be in accordance with the general requirements of MIL-S-19500.

3.2 Symbols and Abbreviations.

The symbols and abbreviations used herein are defined in MIL-S-19500.

SEMICONDUCTOR DEVICE, DIODE
SILICON PLANAR DIFFUSED PHOTO
DETECTOR

SIZE
A

CODE IDENT NO.
10001

3204120

SCALE —

REV A

SHEET 8

3.3 Design, Construction and Physical Dimensions.

The design and construction shall be in accordance with MIL-S-19500. Physical dimensions shall be as specified in Figures 1 through 4 for detectors P1 through P4 respectively.

3.3.1 Case Outline.

The case outline shall be in accordance with Figures 1 through 4 as applicable.

3.3.2 Lead Material and Finish.

Lead material shall be Kovar. Finish shall be gold plate.

3.4 Electro-Optical Performance Characteristics.

The electro-optical performance characteristics shall be in accordance with Table I, and apply over the full recommended ambient operating temperature range, unless otherwise specified.

3.5 Electro-Optical Test Requirements.

The electro-optical test requirements shall be as specified in Table II, III, IV and V herein, and shall constitute the minimum electrical test requirements for screening, qualification, and quality conformance.

3.6 Identification.

Do not mark on part. Identify in accordance with MIL-STD-1285, Method 1, using 10001-3204120 P Number, revision letter, manufacturers symbol and date code. For revision letter see Revision Status Table. Any marking that is consistent with the manufacturer's normal, is acceptable providing it does not affect the function of the part.

4. QUALITY ASSURANCE PROVISIONS

SEMICONDUCTOR DEVICE, DIODE
SILICON PLANAR DIFFUSED PHOTO
DETECTOR

SIZE	CODE IDENT NO.		
A	10001	3204120	
SCALE	—	REV	SHEET
		1	1

4.1 The manufacturer shall be responsible for lot conformance to the Group A, and B requirements of Table IV and V, and the requirements of Table II. The manufacturer shall perform as a minimum, the Group A and Table II test, but shall not perform the Group B test unless specified in the contract or purchase order. The Group B Quality Conformance Procedure shall be performed by the procuring agency or their designated representative. Failure to conform to Group A, B or Table II requirements shall be cause for rejection of the procurement.

4.2 Sampling and Inspection.

Unless otherwise specified, sampling and inspection procedures shall be in accordance with MIL-S-19500.

4.3 Preconditioning and Test.

Preconditioning and test shall be in accordance with Table II herein in the order shown, and shall be conducted on all devices prior to quality conformance inspection. The following additions or exceptions shall apply:

4.3.1 Internal Visual Inspection (Precap).

All devices shall be subjected to an internal visual inspection in accordance with MIL-STD-750, Method 2072. All devices which fail to meet the requirements specified therein, shall be removed from the inspection lot.

4.3.2 High Temperature Storage.

All devices shall be stored for at least 48 hours at a minimum temperature (T_A) of 125°C.

4.3.3 Thermal Shock.

All devices shall be subjected to thermal shock in accordance with MIL-STD-202, Method 107, Test Condition A. The high temperature shall be +125°C minimum, the low temperature shall be -55°C minimum, and the number of cycles, 10. This test may be started at any point in the cycle. All devices shall be maintained at each end temperature until thermal equilibrium has been reached, but not less than 15 minutes. The devices shall not be maintained at room ambient temperatures for more than 5 minutes during the transfer period between end temperatures.

SEMICONDUCTOR DEVICE, DIODE
SILICON PLANAR DIFFUSED PHOTO
DETECTOR

SIZE	CODE IDENT NO.	3204120		
A	10001			
SCALE	—	REV	A	SHEET

4.3.4 Acceleration.

All devices shall be subjected to an acceleration test in accordance with MIL-STD-750, Method 2006, with the following exceptions:

The test shall be performed one time in the Y_1 orientation only, at a peak level of 10,000 G, minimum. The one minute hold-time requirement shall not apply. (See Figure 5.)

4.3.5 Stabilizing Bake.

All devices shall be subjected to the stabilizing bake and testing described herein.

4.3.5.1 Measurements Prior to Stabilizing Bake.

The parameters shown in Table II shall be measured and the data recorded for all devices in the inspection lot. The devices shall be identified in a manner that will permit the delta end-points of Table III to be determined at the conclusion of the stabilizing bake.

4.3.5.2 Stabilizing Bake.

All devices shall be baked for a minimum of 168 hours at $125^\circ \pm 5^\circ\text{C}$.

4.3.5.3 Measurements After Stabilizing Bake.

The measurements of Table III shall be performed on all devices and the deltas shall be recorded. Devices whose parameter deltas exceed the limits shall be removed from the lot. The quantity of devices removed shall be recorded on the permanent inspection lot record.

4.4 Quality Conformance Inspection.

Quality conformance inspection shall be in accordance with Table IV, (Group A), and Table V (Group B) when specified in the purchase order.

4.4.1 Group B Inspection.

Group B Inspection shall consist of the test subgroups of Table V herein, and as follows:

A) High Temperature Life (Non Operating).

1) Duration: 1,000 hours, except as otherwise permitted by MIL-S-19500.

2) $T_A = 125^{\circ}\text{C} \begin{matrix} +0^{\circ} \\ -5^{\circ} \end{matrix}$

5. PREPARATION FOR DELIVERY.

5.1 Packaging.

Detectors shall be prepared for delivery in accordance with MIL-S-19500.

6. NOTES.

6.1 The notes specified in MIL-S-19500 are applicable to this document.

6.2 Approved Source of Supply.

Only the item(s) described on this drawing, when procured from the following manufacturer(s), is/are approved by the Strategic Systems Project Office for use in the applications specified herein. A substitute item shall not be used without prior testing and approval by the Strategic Systems Project Office.

Aeroneutronics Ford (P3 and P4 only)
Ford Road
Newport Beach, CA 92663
Code Ident.

United Detector Technology (P1 and P2 only)
1732 21st Street
Santa Monica, California 90404
Code Ident

SEMICONDUCTOR DEVICE, DIODE
SILICON PLANAR DIFFUSED PHOTO
DETECTOR

SIZE CODE IDENT NO.

A

10001

3204120

SCALE

—

REV

A

SHEET

12

TABLE II

100% SCREENING AND CONDITIONING TEST REQUIREMENTS

EXAMINATION OR TEST	MIL - STD - 750		SYM	LIMITS		UNIT
	METHOD	TEST CONDITIONS		MIN	MAX	
INTERNAL VISUAL (PRECAP)	2072	PARA. 4.3.1 HEREIN	---	---	---	---
HIGH TEMPERA- TURE STORAGE (NON-OPERATING)	----	PARA. 4.3.2 HEREIN	---	---	---	---
THERMAL SHOCK (TEMPERATURE CYCLING)	----	PARA. 4.3.3 HEREIN	---	---	---	---
ACCELERATION	2006	PARA. 4.3.4 HEREIN	---	---	---	---
HERMETIC SEAL GROSS LEAK	1071	P3 AND P4 ONLY TEST COND. A, OR C, OR D, OR E, OR F.	---	---	---	---
FINE LEAK		TEST COND II	---	---	---	---
TOTAL ZERO BIAS RESIS- TANCE		$T = 25^{\circ}\text{C} \begin{smallmatrix} +0^{\circ} \\ -5^{\circ} \end{smallmatrix}$ (NOTE 1)	R_D	100	---	MEG-OHM
JUNCTION CAPACITANCE	4001	$V_R = 0,$ $T = 25^{\circ}\text{C} \pm 5^{\circ}$ $E_c = 0,$ $f = 1 \text{ KHZ}$ (NOTE 2)	C_J	---	100	pF
RESPONSIVITY	---	$T = 25^{\circ}\text{C}, \lambda = 670\text{nm}$ (NOTE 3)	R	0.30	---	A/W
RESPONSIVITY MATCH (-P2 & P4 ONLY)		$T = 25^{\circ}\text{C}, \lambda = 670\text{nm}$	$\frac{R_{\min}}{R_{\max}}$	0.92	---	---

SEMICONDUCTOR DEVICE, DIODE
SILICON PLANAR DIFFUSED PHOTO
DETECTOR

SIZE

A

CODE IDENT NO.

10001

3204120

SCALE

—

REV

A

SHEET

13

TABLE II - (CONTINUED)

100% SCREENING AND CONDITIONING TEST REQUIREMENTS

EXAMINATION OR TEST	MIL - STD - 750		SYM	LIMITS		UNIT
	METHOD	TEST CONDITIONS		MIN	MAX	
STABILIZING BAKE	---	PARA. 4.3.5 HEREIN	---	---	---	---
ISOLATION RESISTANCE		$T = 25^{\circ}\text{C} \pm 5^{\circ}$ $V_{IE} = +100\text{mV MAX.}$ (NOTE 5)	IR	200	---	MEG/ORMS
NOISE (NOTE 6) (P3 & P4 ONLY)	---	$T = 25^{\circ}\text{C} \pm 5^{\circ}\text{C}$	e_n	---	4.7	mVrms/ $\sqrt{\text{Hz}}$

NOTES: 1 - 6, SEE TABLE I.

SEMICONDUCTOR DEVICE, DIODE
SILICON PLANAR DIFFUSED PHOTO
DETECTOR

SIZE

A

CODE IDENT NO.

10001

3204120

SCALE —

REV

A

SHEET

14

TABLE III

100% SCREENING AND CONDITIONING TEST REQUIREMENTS

EXAMINATION OR TEST	MIL-STD-750		SYM	LIMITS		UNIT
	METHOD	TEST CONDITIONS		MIN	MAX	
END POINTS (WITHIN 24 HOURS OF BURN-IN)		SAME CONDITIONS AS FOR TABLE II				
Δ TOTAL ZERO BIAS RESIS- TANCE (NOTE 7)			R_D	---	± 25	o/o
Δ JUNCTION CAPACITANCE			C_J	---	± 100 or 20	o/o pF
Δ RESPONSIVITY			R	---	± 5	o/o
Δ RESPONSIVITY MATCH (-P2 & P4 ONLY)			$\left(\begin{matrix} R_{min} \\ R_{max} \end{matrix} \right)$	---	± 5	o/o
NOISE (NOTE 6) (P3 & P4 ONLY)			e_n	---	4.7	nVrms/ \sqrt{Hz}
VISUAL AND MECHANICAL INSPECTION	2071		---	---	---	---

NOTE 7: FOR A POST CONDITIONING TOTAL ZERO BIAS
RESISTANCE IN EXCESS OF 250 MEGOHMS, THE
ALLOWABLE MAX Δ LIMIT WILL BE 100%.

SEMICONDUCTOR DEVICE, DIODE
SILICON PLANAR DIFFUSED PHOTO
DETECTOR

SIZE	CODE IDENT NO.	
A	10001	3204120
SCALE	REV	SHEET
—	A	15

TABLE IV - GROUP A INSPECTION

EXAMINATION OR TEST	TEST CONDITIONS	SYM	LIMITS		UNITS
			MIN	MAX	
<u>SUBGROUP 1</u>					
VISUAL AND MECHANICAL EXAMINATION	MIL-STD-750, METHOD 2071				
<u>SUBGROUP 2</u>					
RESPONSIVITY	$\lambda = 670 \text{ nm},$ $T = 25 \pm 5^{\circ}\text{C}$ (NOTE 3)	R	0.30	--	AMPS/WATT
RESPONSIVITY MATCH (-P2 & -P4 ONLY)	$\lambda = 670 \text{ nm},$ $T = 25 \pm 5^{\circ}\text{C}$ (NOTE 4)	$\frac{R_{\min}}{R_{\max}}$	0.92	--	
TOTAL ZERO BIAS RESISTANCE	$T = 25 \pm 5^{\circ}\text{C}$ $E_c = V_F = V_R = 0$ (NOTE 1)	R_d	100	--	MEG-OHM
TOTAL JUNCTION CAPACITANCE	$V = 0, f = 1\text{KHZ}$ $T = 25 \pm 5^{\circ}\text{C}$ (NOTE 2)	C_{J-}	--	100	pF
NOISE (P3 & P4 ONLY)	$T = 25^{\circ}\text{C} \pm 5^{\circ}\text{C}$ (NOTE 6)	e_n	--	4.7	mV rms/ $\sqrt{\text{HZ}}$
DETECTIVITY (P1 & P2 ONLY)	$T = 25^{\circ}\text{C} \pm 5^{\circ}\text{C}$ $\lambda = 900\text{nm}$ $f = 360 \text{ Hz}$ $\text{BW} = 1 \text{ Hz}$	D^*	5×10^{11}	---	cm $\sqrt{\text{Hz}}$ /WATT
ISOLATION RESISTANCE (P2 & P4 ONLY)	$V_{\text{IE}} = \pm 100\text{mv MAX}$ $T = 25^{\circ}\text{C} \pm 5^{\circ}\text{C}$ (NOTE 5)	IR	200	---	MEG-OHM
NOTES: 1 - 6 SEE TABLE 1.					
SEMICONDUCTOR DEVICE, DIODE SILICON PLANAR DEPLETED PHOTO DETECTOR			SIZE A	CODE IDENT NO. 10001	3204120
			SCALE —	REV A	SHEET 16

TABLE V - GROUP B INSPECTION

EXAMINATION OR TEST	MIL - STD - 750		LTPD	SYM	LIMITS		UNIT
	METHOD	TEST CONDITIONS			MIN	MAX	
<u>SUBGROUP 1</u>			10	---	---	---	---
PHYSICAL DIMENSIONS	2066	SEE OUTLINE DRAWING					
<u>SUBGROUP 2</u>							
SOLDERABILITY	2026	OMIT AGING		---	---	---	---
THERMAL SHOCK (TEMPERATURE CYCLING)	1051	TEST COND.A		---	---	---	---
MOISTURE RESISTANCE	1021			---	---	---	---
END POINTS RESPONSIVITY (NOTE 3)		$\lambda = 670 \text{ nm}$			0.30		AMPS/WATT
RESPONSIVITY MATCH (P2 & P4 ONLY) (NOTE 4)		$\lambda = 670 \text{ nm}$		$\frac{R_{MIN}}{R_{MAX}}$			
<u>SUBGROUP 3</u>			15				
SHOCK	2016	NONOPERATING, 1,500 G, 0.5 MSEC; 5 BLOWS IN EACH ORIENTATION: X ₁ , Y ₁ , Z ₁ AND Z ₁		---	---	---	---

NOTE 3: SEE TABLE I - NOTE 3

NOTE 4: SEE TABLE I - NOTE 4

SEMICONDUCTOR DEVICE, DIODE
SILICON PLANAR DIFFUSED PHOTO
DETECTOR

SIZE CODE IDENT NO.

A

10001

3204120

SCALE

—

REV

A

SHEET

17

TABLE V - GROUP B DETECTOR (CONTINUED)

EXAMINATION OR TEST	MIL - STD - 750		LTPD	SYM	LIMITS		UNIT
	METHOD	TEST CONDITIONS			MIN	MAX	
VIBRATION, VARIABLE FREQUENCY	2055			---	---	---	---
CONSTANT ACCELERATION	2006	10,000 G; IN EACH ORIENTA- TION: X ₁ , Y ₁ , Y ₂ AND Z ₁ SEE FIG.3		---	---	---	---
END POINTS: (SAME AS SUBGROUP 2)							
<u>SUBGROUP 4</u>			=10				
TERMINAL STRENGTH (LEAD FATIGUE)	2036	TEST COND. E		---	---	---	---
<u>SUBGROUP 5</u>			=10				
HIGH TEMPERA- TURE LIFE (NON OPERAT- ING)	1031	T _A = +125°C +0° -5°		---	---	---	---
END POINTS: (SAME AS SUBGROUP 2)							
<u>SUBGROUP 6</u>			=10				
STEADY STATE	1027	2,000 HRS. MIN. T _A = 35°C MIN		---	---	---	---
END POINTS: (SAME AS SUBGROUP 2)							

SEMICONDUCTOR DEVICE, DIODE
SILICON PLANAR DIFFUSED PHOTO
DETECTOR

SIZE

A

CODE IDENT NO.

10001

3204120

SCALE

—

REV

A

SHEET

18

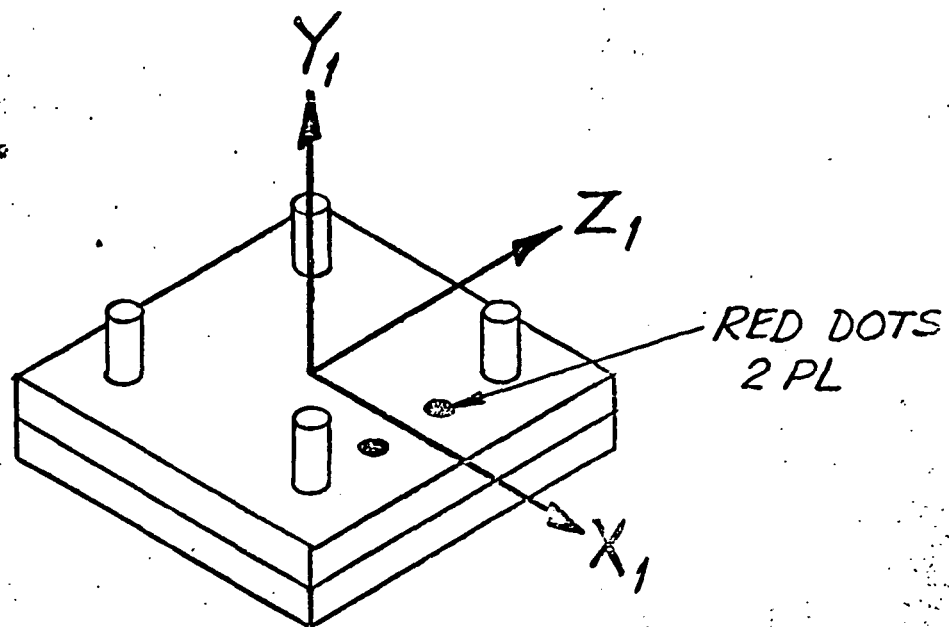


Figure 5A. P_1 & P_2 (ONLY)

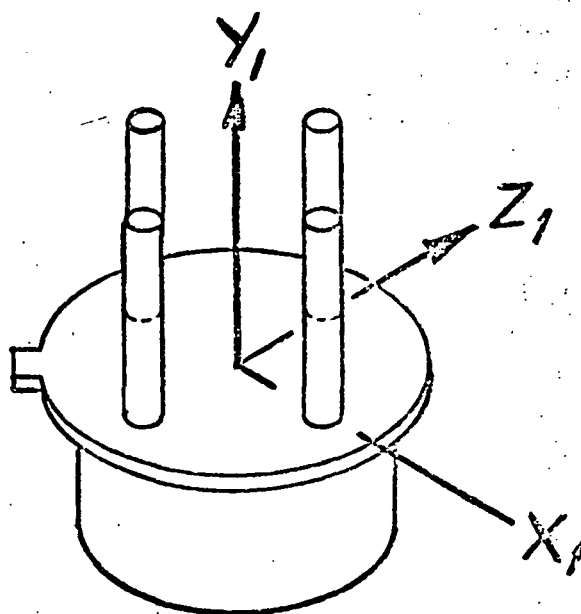


Figure 5B. P_3 & P_4 (ONLY)

SEMICONDUCTOR DEVICE,
DIODE SILICON PLANNAR DIFFUSED
PHOTO DETECTOR

SIZE
A

CODE IDENT NO.
10001

3204/20

SCALE NONE

REV A

SHEET

19

APPENDIX E

PRELIMINARY GEAR TRAIN BACKLASH ANALYSIS

Gear Train Backlash Analysis (Preliminary) (I)

Assume gears are as follows:

- (1) $\frac{105 \text{ t}}{15 \text{ t}}$ } 96 p, 20° pa, Q14C
($\Delta t = .0011$ for "C" gears)
- (2) $\frac{96 \text{ t}}{24 \text{ t}}$ } 72 p, 20° pa, Q14C
- (3) $\frac{96 \text{ t}}{24 \text{ t}}$ } 72 p, 20° pa, Q14C
- (4) $\frac{60 \text{ t}}{60 \text{ t}}$ } 72 p, 20° pa, Q14C
- (5) $\frac{192^* \text{ t}}{21 \text{ t}}$ } 64 p, 20° pa, Q14C
(centers adjustable)

In addition to the above, assume the following:

- (1) Tolerance on centers for reverted gear sets is
+0002
-0000 (bearing hole locations).
- (2) Looseness of reverted gears on shafts is from
.0004 to .0008.
- (3) Bearing bore dia.looseness = .0000 to .0004.
- (4) Bearing looseness on shafts = .0000 to .0003.
- (5) All bearings have .0002 TIR of inner and outer ring
runouts.
- (6) All pinned gears are .0000 to .0003 loose on shafts.
- (7) Nominal CD is decreased by .0010 to compensate for tooth
thinning.
- (8) Max. test radius of gears is .0013; min = .0005
(deviations from perfect CD's).

Under the preceeding list of assumptions, the backlash
distribution is as follows:

Mesh 5 - None, because of the anti-backlash large (driven)
gears.

*Anti-backlash gears

Mesh 4 - Worst case summary of factors leading to increased CD.

- (a) .0008 max allow (.000655 avg) gear test rad.dev. 60 t gear
- (b) .0008 max allow (.000655 avg) gear test rad.other 60 t gear
- (c) .00015 $\frac{1}{2}$ of one (.000075 avg) 60 tooth gear looseness on shaft
- (d) .00020 $\frac{1}{2}$ of other (.000075 avg) 60 tooth gear looseness on shaft
- (e) .00015 $\frac{1}{2}$ of shaft (.000075 avg) looseness in bearings
- (f) .00010 $\frac{1}{2}$ of bearing (.00005 avg) inner race runout
- (g) .00010 $\frac{1}{2}$ of bearing (.00005 avg) outer race runout
- (h) .00020 $\frac{1}{2}$ of bearing (.00010 avg) looseness in bore
- (i) .0002 worst case CD (.00010 avg.) location (tolerance)

.00270 Δ CD max

(RSS of averages = .0009502894)

The above numerical value is related to linear backlash by

$$B = 2 \tan \phi \Delta CD = 2 (\tan 20^\circ) (.00270)$$

$$= .0019654392$$

At the nominal radius of rotation = 30/72 in, the angular

$$\text{rotation} = \alpha = \tan^{-1} \left(\frac{72B}{30} \right)$$

$$= .270 \text{ deg}$$

$$= 16.2 \text{ min}$$

$$= 973 \text{ sec}$$

This is divided down by $\frac{21}{192}$, and gives an uncertainty of wedge

rotation (one wedge with respect to the other) of 106 sec or 1.773 min. or .029 deg.

Since the total wedge rotation is 158 $\widehat{\text{sec}}$ /step, this is acceptable on an absolute worst case basis (on an RSS basis), the equivalent is .0006917541" at the theoretical radius, or 37.4 $\widehat{\text{sec}}$ rotation of one wedge with respect to the other. (At the zero

reference, this means that backlash of one wedge with respect to the other (differential motion) introduces only an 0.1 arc sec RMS error). The conclusion is that Anti backlash gearing of the 60/60 mesh is not necessary.

Mesh 3 - Same as mesh (4), but add .0004 to maximum CD or RSS in an additional .0003

$$\Delta CD = .0031 \text{ max}$$

$$\Delta CD = .0009965189 \text{ RSS of averages}$$

$$\begin{aligned} \alpha_{\text{max}} &= \tan^{-1} \frac{\Delta CD / 72}{48} \\ &= .2664234545^\circ \text{ max} \\ &= .085644428^\circ \text{ RSS} \end{aligned}$$

$$\alpha \times \frac{21}{192} = 104.9 \text{ sec} \quad \text{Max.}$$

$$= 33.7 \text{ sec} \quad \text{RSS}$$

RSS of meshes 3 and 4

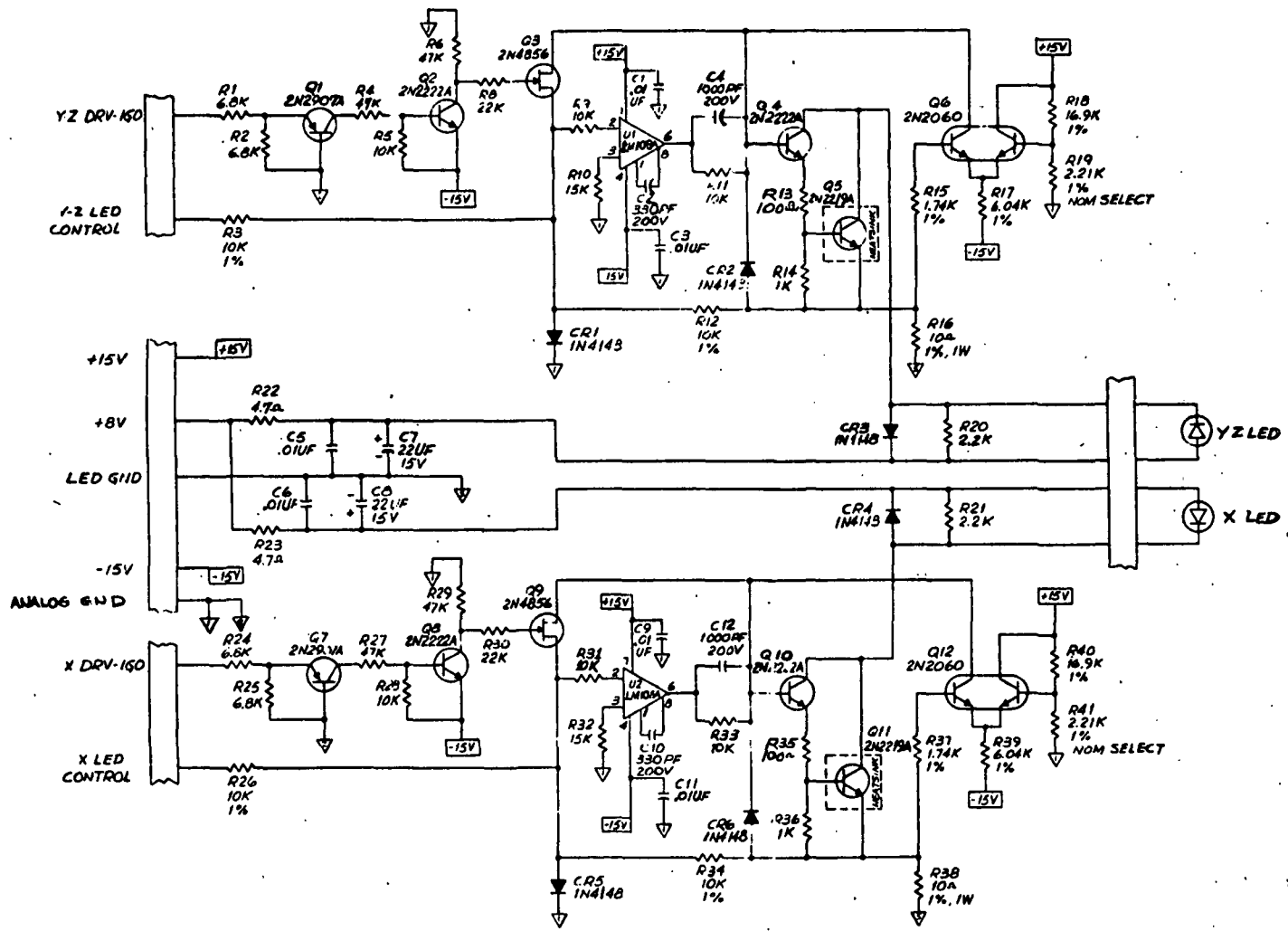
$$= \sqrt{37.4^2 + 33.7^2} = 40.3 \text{ sec}$$

RSS of two worst cases gives 149 sec

APPENDIX F

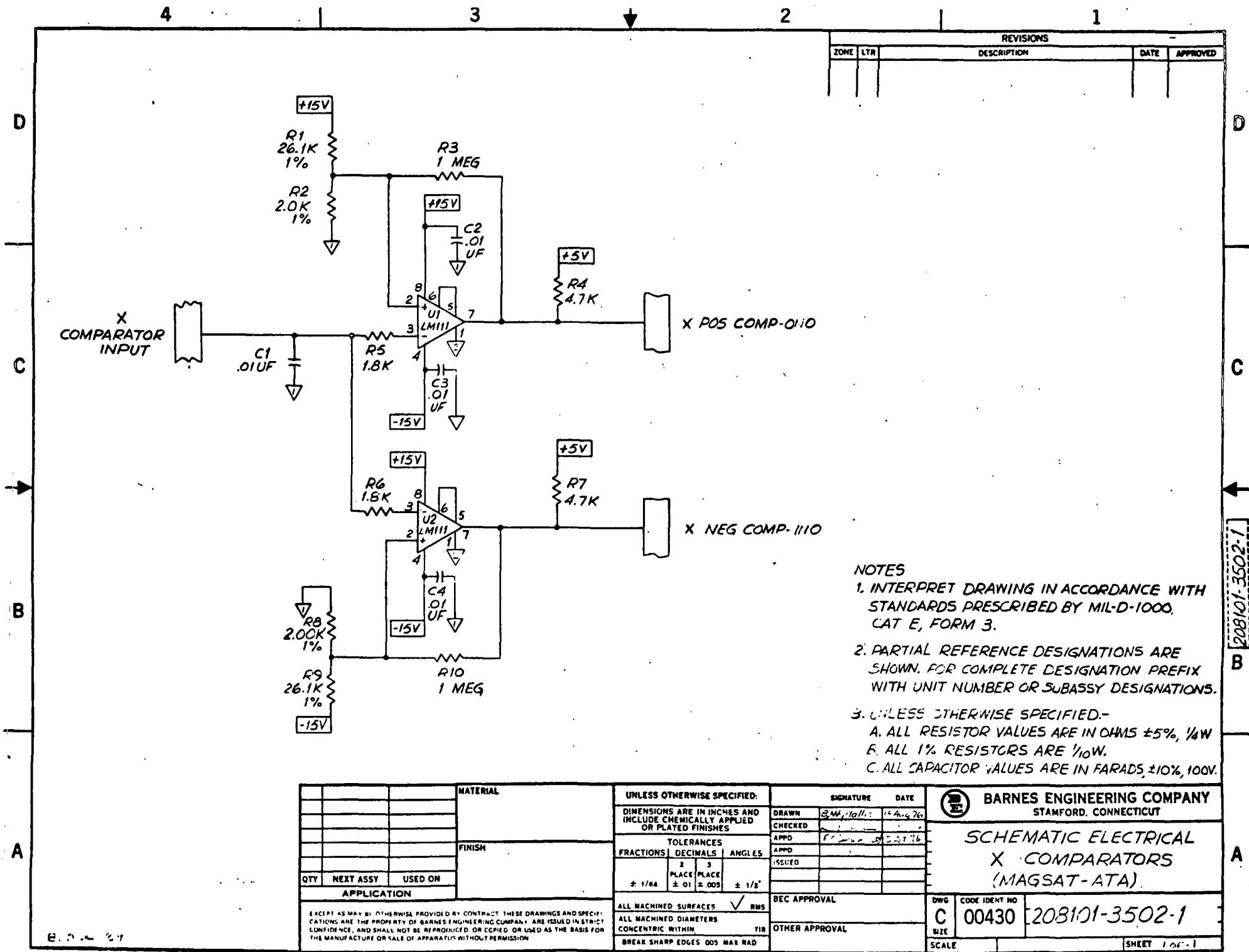
ELECTRONIC SCHEMATICS

REVISE		DATE		APPROVED	
NO.	DESCRIPTION				



- NOTES
1. INTERPRET DRAWING IN ACCORDANCE WITH STANDARDS PRESCRIBED BY MIL-D-1000 CAT E FORM 3.
 2. PARTIAL REFERENCE DESIGNATIONS ARE SHOWN FOR COMPLETE DESIGNATION PREFIX WITH UNIT NUMBER OR SUBASSEMBLY DESIGNATIONS.
 3. UNLESS OTHERWISE SPECIFIED-
 A. ALL RESISTOR VALUES ARE IN OHMS $\pm 5\%$ $\frac{1}{4}$ W.
 B. ALL 1% RESISTORS ARE $\frac{1}{10}$ W.
 C. ALL CAPACITOR VALUES ARE IN FARADS $\pm 10\%$ 100 V.

MATERIAL		UNLESS OTHERWISE SPECIFIED		DRAWN: <u>STANFORD</u> DATE: <u>10-1-76</u>		BARNES ENGINEERING COMPANY STAMFORD, CONNECTICUT SCHEMATIC, ELECTRICAL LED DRIVER (MAGSAT-ATA)
FINISH		DIMENSIONS ARE IN INCHES AND INCLUDE CHEMICALLY APPLIED OR PLATED FINISHES		CHECKED: <u> </u> DATE: <u> </u>		
QTY		TOLERANCES FRACTIONS DECIMALS ANGLES		APPD: <u> </u> DATE: <u> </u>		
RETRY ASSY		ALL DIMENSIONS SURFACES ALL DIMENSIONS SURFACES		ISSUED: <u> </u> DATE: <u> </u>		
USED ON		APPLICATION		BEC APPROVAL		D 00430 208101-3501-1 SCALE: <u> </u> SHEET: <u>1 of 1</u>
				OTHER APPROVAL		

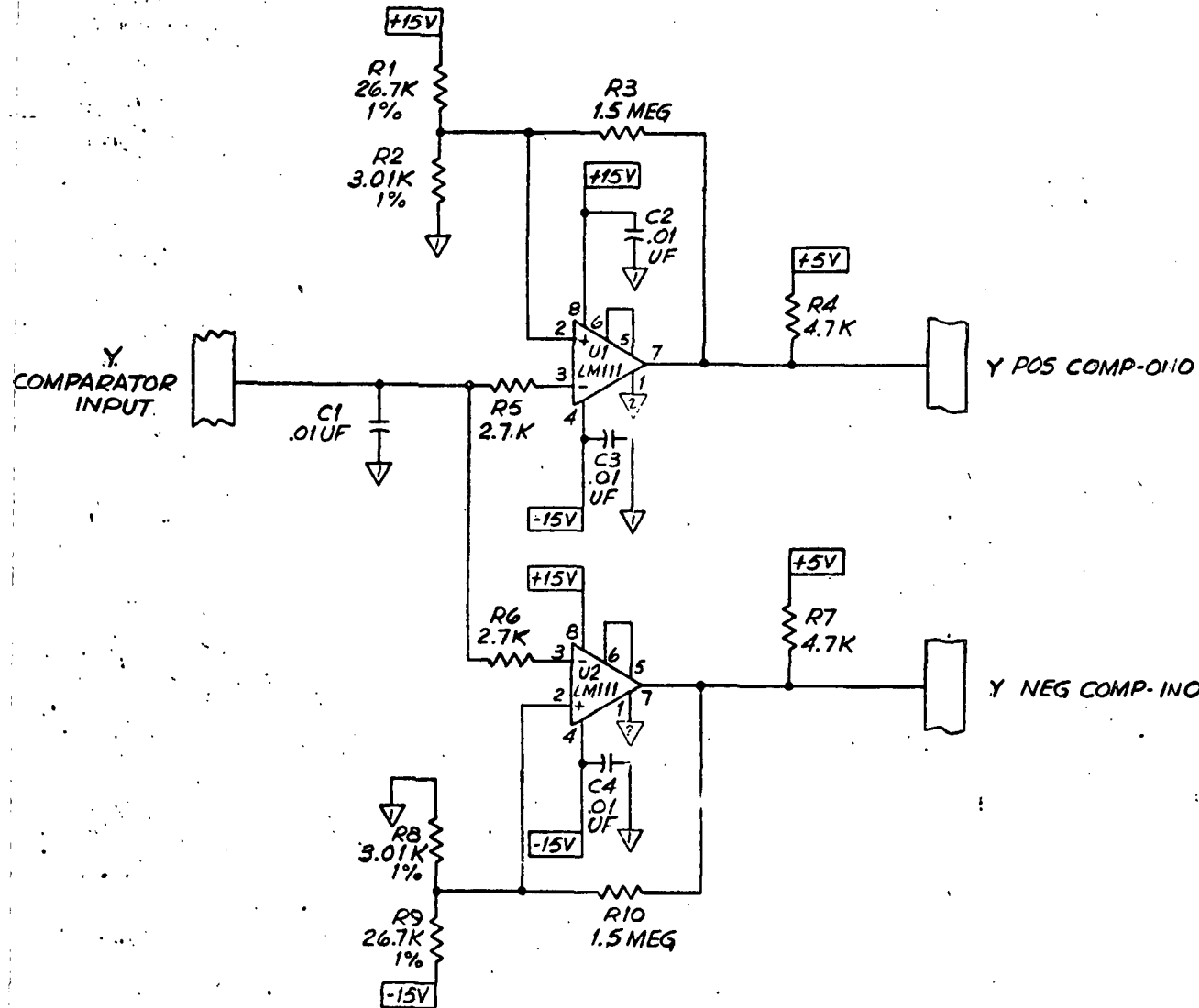


- NOTES
- 1. INTERPRET DRAWING IN ACCORDANCE WITH STANDARDS PRESCRIBED BY MIL-D-1000, CAT E, FORM 3.
 - 2. PARTIAL REFERENCE DESIGNATIONS ARE SHOWN. FOR COMPLETE DESIGNATION PREFIX WITH UNIT NUMBER OR SUBASSY DESIGNATIONS.
 - 3. UNLESS OTHERWISE SPECIFIED:-
 - A. ALL RESISTOR VALUES ARE IN OHMS $\pm 5\%$, $\frac{1}{4}$ W
 - B. ALL 1% RESISTORS ARE $\frac{1}{10}$ W.
 - C. ALL CAPACITOR VALUES ARE IN FARADS, $\pm 10\%$, 100V.

MATERIAL			UNLESS OTHERWISE SPECIFIED:			SIGNATURE		DATE	
			DIMENSIONS ARE IN INCHES AND INCLUDE CHEMICALLY APPLIED OR PLATED FINISHES			DRAWN	BAW/tall	14 Aug 76	
FINISH			TOLERANCES			CHECKED			
			FRACTIONS	DECIMALS	ANGLES	APPRO	14 Aug 76		
QTY			± 1/64			APPRO			
			± .01 ± .005 ± 1/2°			ISSUED			
NEXT ASSY			ALL MACHINED SURFACES			BEC APPROVAL		DWG	
			CONCENTRIC WITHIN			OTHER APPROVAL		C	
USED ON			BREAK SHARP EDGES .005 MAX RAD					CODE IDENT NO	
								00430	
APPLICATION								208101-3502-1	
EXCEPT AS MAY BE OTHERWISE PROVIDED BY CONTRACT THESE DRAWINGS AND SPECIFICATIONS ARE THE PROPERTY OF BARNES ENGINEERING COMPANY. ARE ISSUED IN STRICT CONFIDENCE, AND SHALL NOT BE REPRODUCED OR COPIED OR USED AS THE BASIS FOR THE MANUFACTURE OR SALE OF APPARATUS WITHOUT PERMISSION								SHEET 1 of 1	

E. 2. 2. 2. 2.

REVISIONS			
ZONE	LTR	DESCRIPTION	DATE

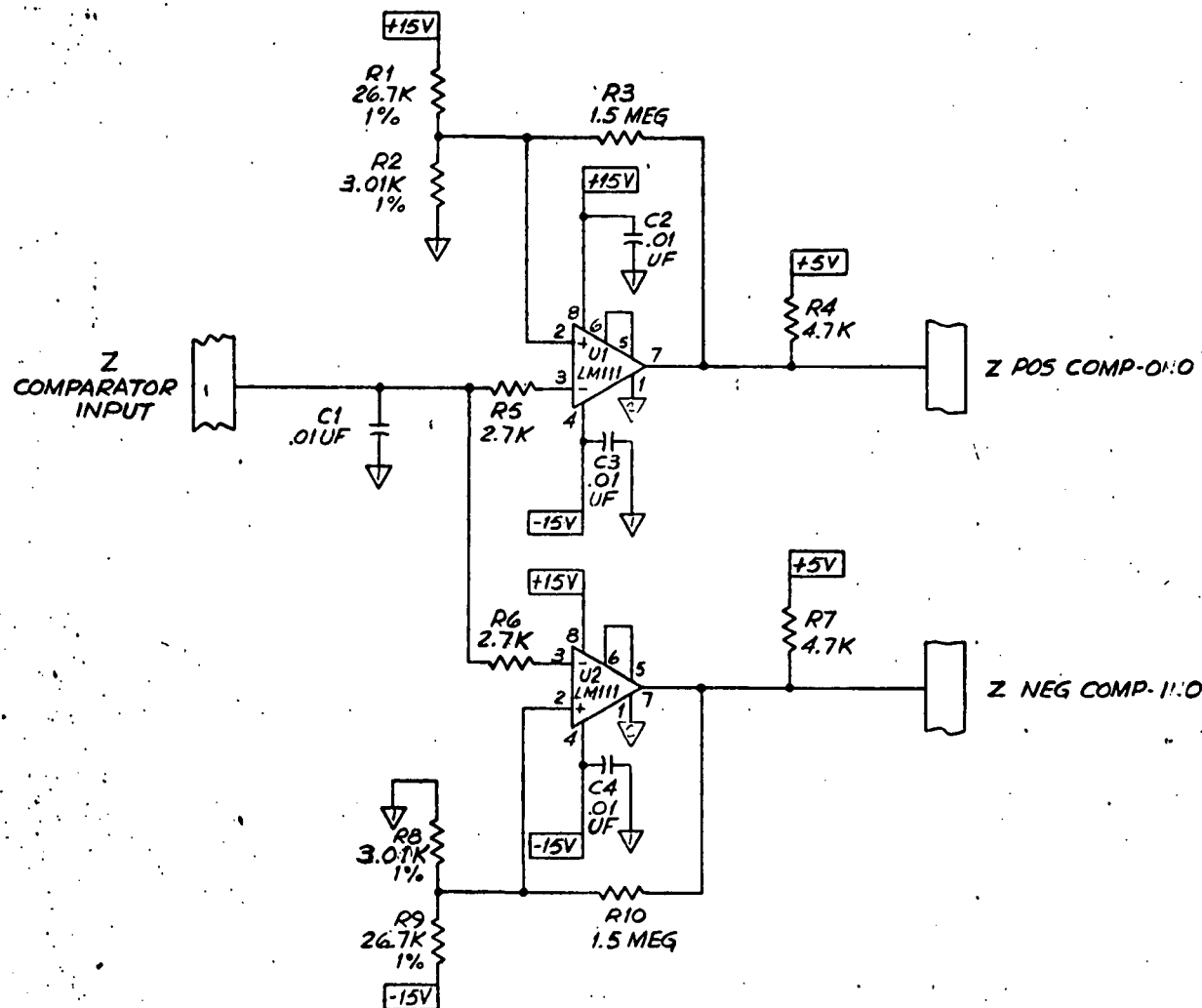


NOTES

- INTERPRET DRAWING IN ACCORDANCE WITH STANDARDS PRESCRIBED BY MIL-D-1000, CAT E, FORM 3.
- PARTIAL REFERENCE DESIGNATIONS ARE SHOWN. FOR COMPLETE DESIGNATION PREFIX WITH UNIT NUMBER OR SUBASSY DESIGNATIONS.
- UNLESS OTHERWISE SPECIFIED:-
 - ALL RESISTOR VALUES ARE IN OHMS $\pm 5\%$, $\frac{1}{4}$ W
 - ALL 1% RESISTORS ARE $\frac{1}{10}$ W.
 - ALL CAPACITOR VALUES ARE IN FARADS, $\pm 10\%$, 100V.

MATERIAL			UNLESS OTHERWISE SPECIFIED:			SIGNATURE		DATE		BARNES ENGINEERING COMPANY STAMFORD, CONNECTICUT
FINISH			DIMENSIONS ARE IN INCHES AND INCLUDE CHEMICALLY APPLIED OR PLATED FINISHES			DRAWN	18 Aug 76			
QTY			TOLERANCES			CHECKED	10-5-76			
NEXT ASSY			FRACTIONS DECIMALS ANGLES			APPRO	5 Oct 76			
USED ON			2 PLACE PLACE $\pm 1/64$ $\pm .01$ $\pm .005$ $\pm 1/2^\circ$			ISSUED			SCHEMATIC, ELECTRICAL Y COMPARATORS (MAGSAT-ATA)	
APPLICATION			ALL MACHINED SURFACES <input checked="" type="checkbox"/> RMS			BEC APPROVAL		DWG		
EXCEPT AS MAY BE OTHERWISE PROVIDED BY CONTRACT, THESE DRAWINGS AND SPECIFICATIONS ARE THE PROPERTY OF BARNES ENGINEERING COMPANY, ARE ISSUED IN STRICT CONFIDENCE, AND SHALL NOT BE REPRODUCED, OR COPIED, OR USED AS THE BASIS FOR THE MANUFACTURE OR SALE OF APPARATUS WITHOUT PERMISSION.			ALL MACHINED DIAMETERS CONCENTRIC WITHIN			OTHER APPROVAL		SIZE		
			BREAK SHARP EDGES .005 MAX RAD					SCALE		
								CODE IDENT NO.	208101-3503-1	
								SHEET	1 of 1	

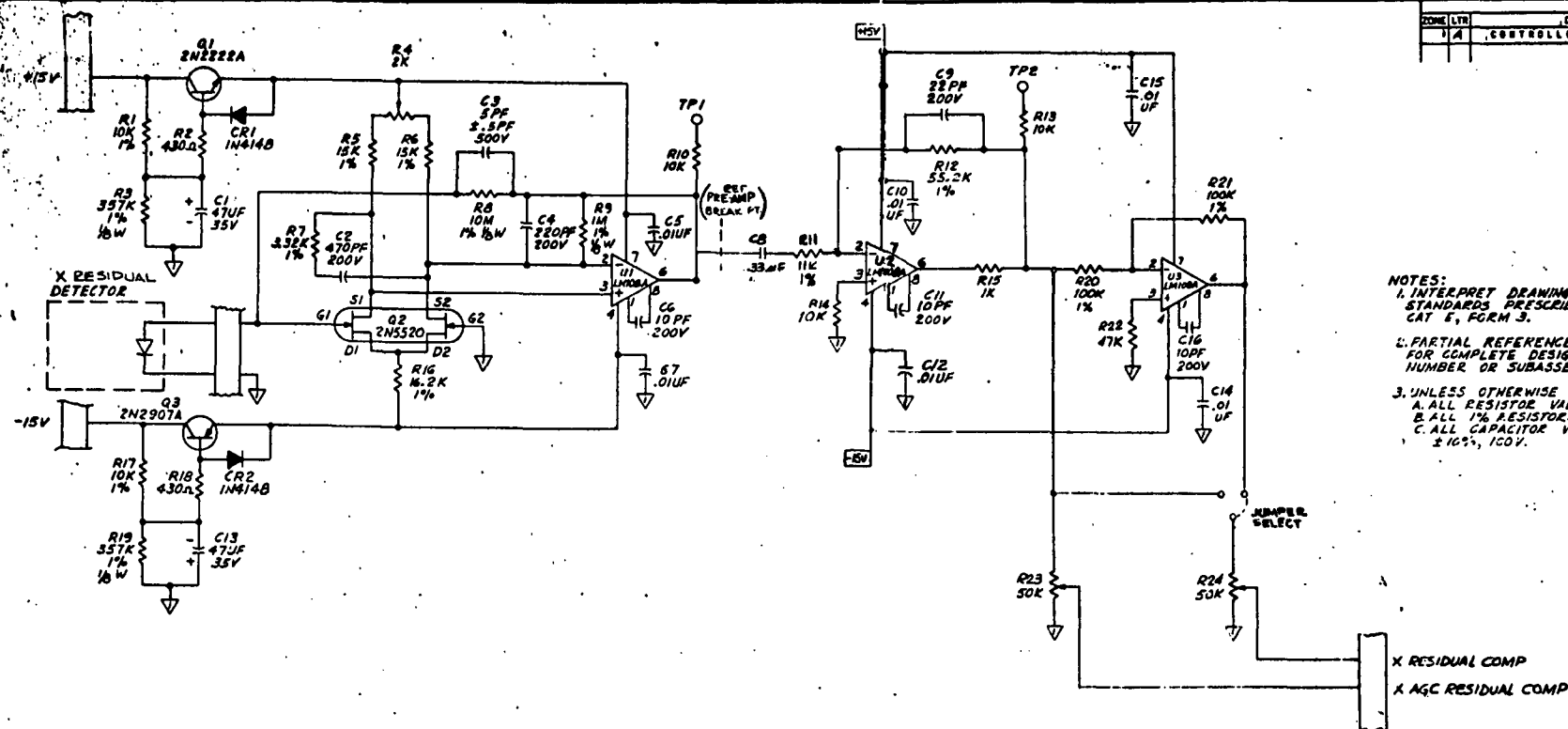
REVISIONS				
ZONE	LTR	DESCRIPTION	DATE	APPROVED



NOTES

- INTERPRET DRAWING IN ACCORDANCE WITH STANDARDS PRESCRIBED BY MIL-D-1000, CAT E, FORM 3.
- PARTIAL REFERENCE DESIGNATIONS ARE SHOWN. FOR COMPLETE DESIGNATION PREFIX WITH UNIT NUMBER OR SUBASSY DESIGNATIONS.
- UNLESS OTHERWISE SPECIFIED:-
 - ALL RESISTOR VALUES ARE IN OHMS $\pm 5\%$, $\frac{1}{10}W$
 - ALL 1% RESISTORS ARE $\frac{1}{10}W$.
 - ALL CAPACITOR VALUES ARE IN FARADS, $\pm 10\%$, 100V.

MATERIAL			UNLESS OTHERWISE SPECIFIED:			SIGNATURE		DATE		BARNES ENGINEERING COMPANY STAMFORD, CONNECTICUT SCHEMATIC, ELECTRICAL Z COMPARATORS (MAGSAT-ATA)	
FINISH			DIMENSIONS ARE IN INCHES AND INCLUDE CHEMICALLY APPLIED OR PLATED FINISHES TOLERANCES: FRACTIONS DECIMALS ANGLES ± 1/64 ± .01 ± .005 ± 1/2°			DRAWN	BMJ/dallis	18 Aug 76			
						CHECKED	W. V. ...	10-5-76			
						APPRO	EC Demand	5 Oct 76			
QTY	NEXT ASSY	USED ON	APPLICATION			BEC APPROVAL			DWS C		
EXCEPT AS MAY BE OTHERWISE PROVIDED BY CONTRACT, THESE DRAWINGS AND SPECIFICATIONS ARE THE PROPERTY OF BARNES ENGINEERING COMPANY, ARE ISSUED IN STRICT CONFIDENCE, AND SHALL NOT BE REPRODUCED, OR COPIED, OR USED AS THE BASIS FOR THE MANUFACTURE OR SALE OF APPARATUS WITHOUT PERMISSION.			ALL MACHINED SURFACES			✓ RMS			CODE IDENT NO. 00430		
			ALL MACHINED DIAMETERS			CONCENTRIC WITHIN			SCALE SHEET 10		
			BREAK SHARP EDGES .003 MAX RAD			TIR			208101-3504-1		



- NOTES:
1. INTERPRET DRAWING IN ACCORDANCE WITH STANDARDS PRESCRIBED BY MIL-D-1000, CAT E, FORM 3.
 2. PARTIAL REFERENCE DESIGNATIONS ARE SHOWN FOR COMPLETE DESIGNATION PREFIX WITH UNIT NUMBER OR SUBASSEMBLY DESIGNATIONS.
 3. UNLESS OTHERWISE SPECIFIED:
 - A. ALL RESISTOR VALUES ARE IN OHMS $\pm 5\%$, $\frac{1}{10}$ W
 - B. ALL 1% RESISTORS ARE $\frac{1}{10}$ W
 - C. ALL CAPACITOR VALUES ARE IN FARADS, $\pm 10\%$, 100V.

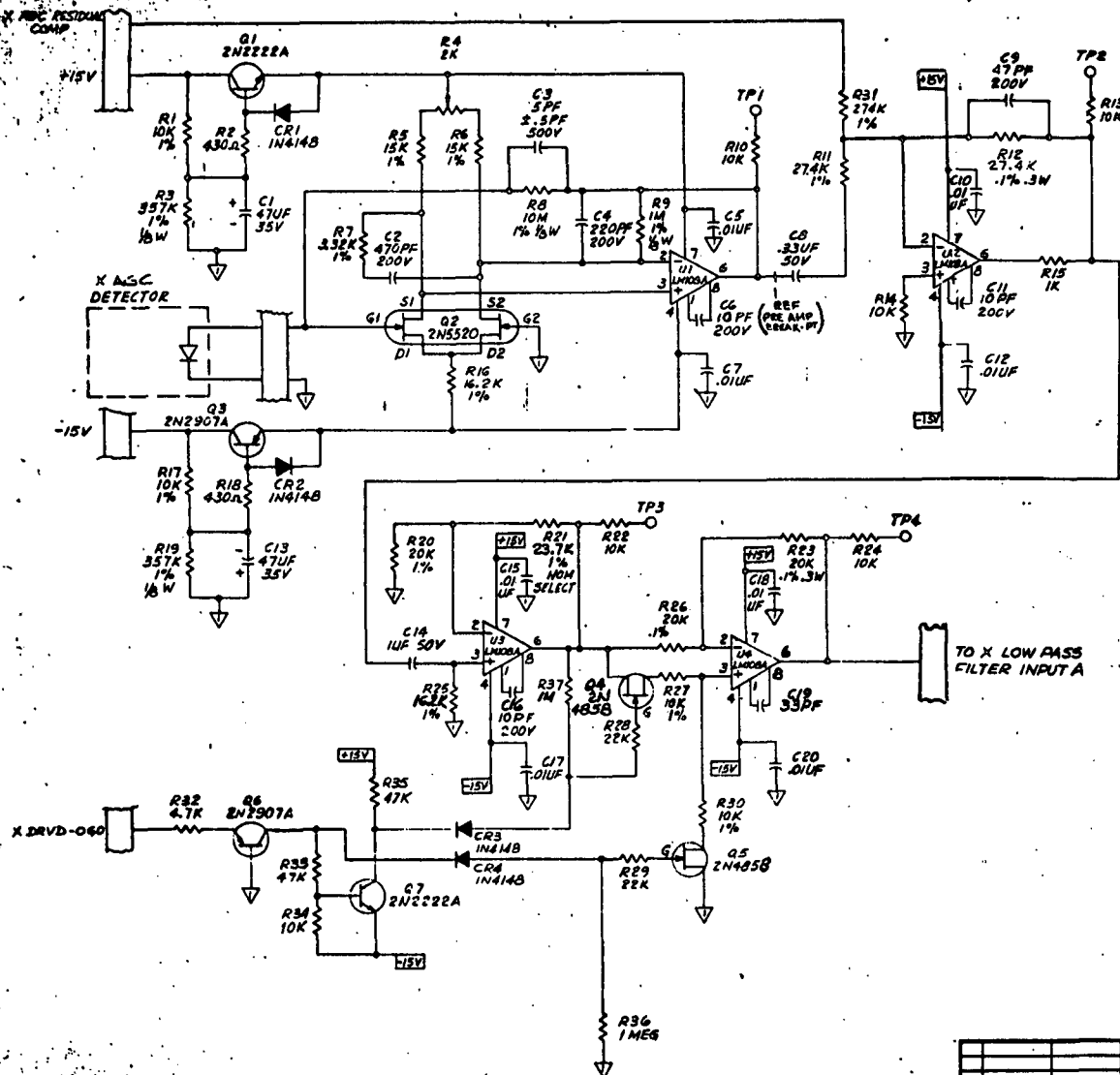
MATERIAL		UNLESS OTHERWISE SPECIFIED:		DIMENSIONS		DATE	
DIMENSIONS ARE IN INCHES AND INCLUDE CRITICAL APPLIED OR PLATED FINISHES		DRAWN		CHECKED		APPROVED	
TOLERANCES		FRACTIONS		DECIMALS		ANGLES	
PLACE PLACE		PLACE PLACE		PLACE PLACE		PLACE PLACE	
QTY		NEXT ASSY		USED ON		APPLICATION	
EXCEPT AS MAY BE OTHERWISE PROVIDED BY CONTRACT, THESE DRAWINGS AND SPECIFICATIONS ARE THE PROPERTY OF BARNES ENGINEERING COMPANY, AND SHALL NOT BE REPRODUCED, COPIED, OR USED AS THE BASIS FOR THE MANUFACTURE OR SALE OF APPARATUS WITHOUT PERMISSION.							
ALL MACHINED SURFACES				ALL MACHINED SURFACES			
CONCENTRIC WITHIN				CONCENTRIC WITHIN			
BREAK SHARP EDGES AND RAS RAS				BREAK SHARP EDGES AND RAS RAS			
REC APPROVAL				OTHER APPROVAL			
D 00430				208101-3506-1			
SCALE				SHEET 1 OF 1			

BARNES ENGINEERING COMPANY
STAMFORD, CONNECTICUT

SCHEMATIC, ELECTRICAL
X RESIDUAL CHANNEL
(MAGSAT-ATA)

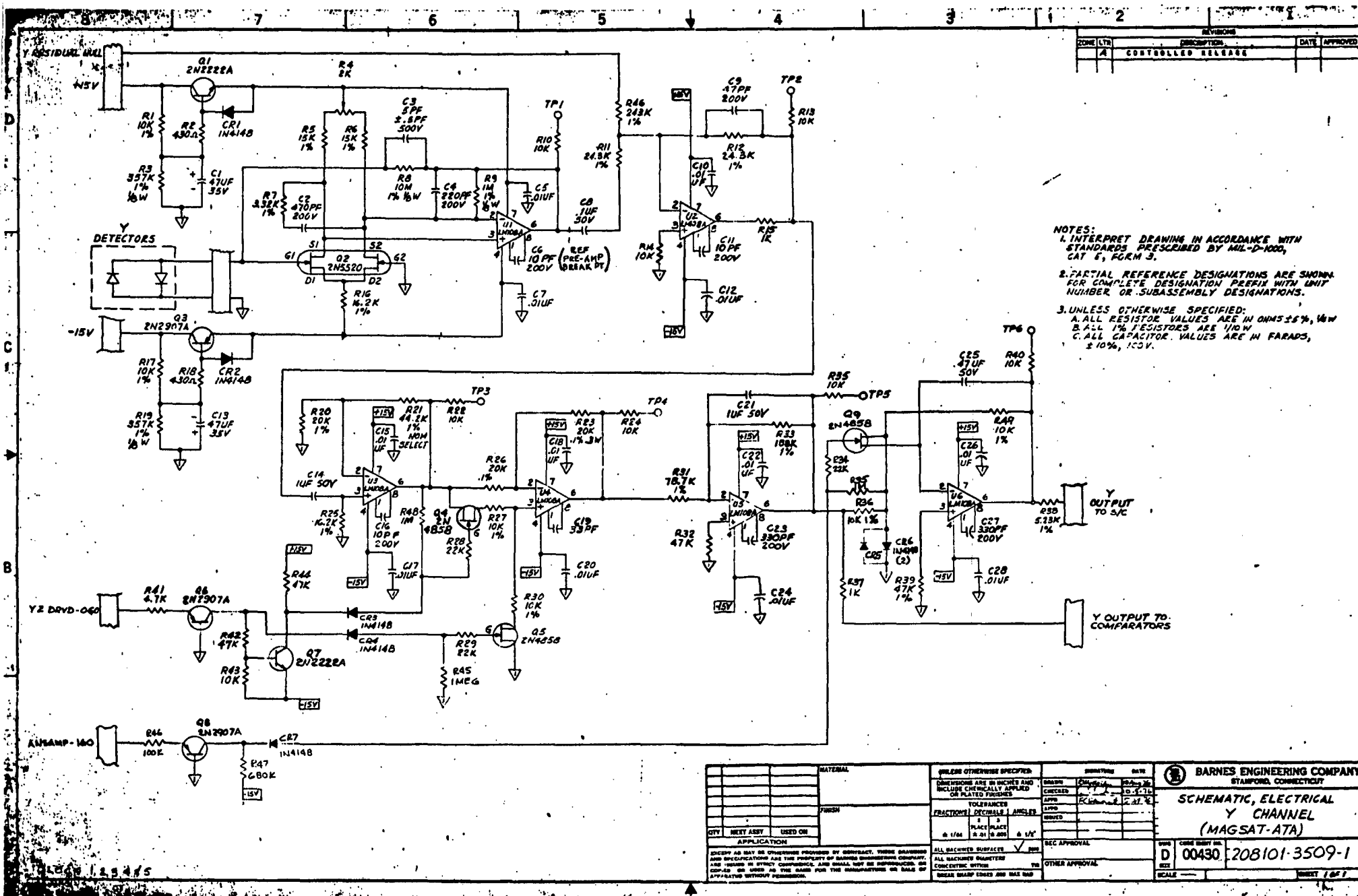
D 00430 208101-3506-1

SCALE SHEET 1 OF 1



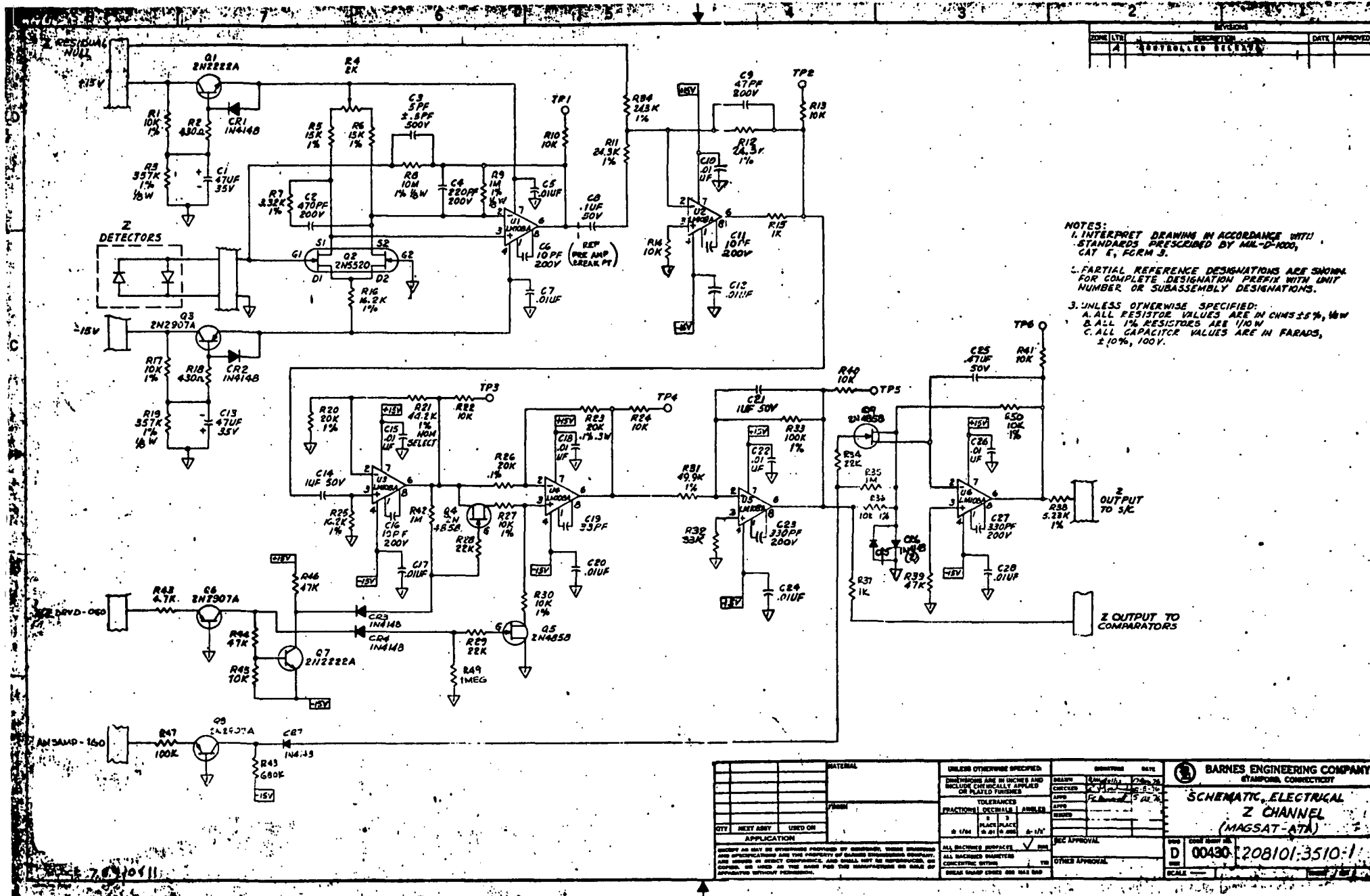
- NOTES:
1. INTERPRET DRAWING IN ACCORDANCE WITH STANDARDS PRESCRIBED BY MIL-D-1000, CAT E, FORM 3.
 2. PARTIAL REFERENCE DESIGNATIONS ARE SHOWN FOR COMPLETE DESIGNATION PREFIX WITH UNIT NUMBER OR SUBASSEMBLY DESIGNATIONS.
 3. UNLESS OTHERWISE SPECIFIED:
 - A. ALL RESISTOR VALUES ARE IN OHMS $\pm 5\%$, $\frac{1}{8}$ W
 - B. ALL 1% RESISTORS ARE $\frac{1}{10}$ W
 - C. ALL CAPACITOR VALUES ARE IN FARADS, $\pm 10\%$, 100V.

MATERIAL		UNLESS OTHERWISE SPECIFIED:		DRAWING NO. DATE		BARNES ENGINEERING COMPANY STAMFORD, CONNECTICUT
FINISH		DIMENSIONS ARE IN INCHES AND INCLUDE CHEMICALLY APPLIED OR PLATED FINISHES		CHECKED BY: 17-1-76		
CITY NEXT ASSY USED ON		TOLERANCES		APPROVED BY: 17-1-76		SCHEMATIC, ELECTRICAL X AGC CHANNEL (MAGSAT-ATA)
		FRACTIONS DECIMALS ANGLES		DRAWN BY: 17-1-76		
		1/16 1/32 1/64 1/8 1/4 1/2 1		DATE: 17-1-76		D 00430 208101-3507-1
		ALL DIMENSIONS UNLESS OTHERWISE SPECIFIED		SCALE: 1/16"		
APPLICATION		ALL DIMENSIONS UNLESS OTHERWISE SPECIFIED		REC APPROVAL		OTHER APPROVAL
COPYRIGHT AS MAY BE OTHERWISE PROVIDED BY CONTRACT, THESE DRAWINGS AND SPECIFICATIONS ARE THE PROPERTY OF BARNES ENGINEERING COMPANY, AND ARE NOT TO BE REPRODUCED, COPIED, OR USED AS THE BASIS FOR THE MANUFACTURE OR SALE OF APPARATUS WITHOUT PERMISSION.		ALL DIMENSIONS UNLESS OTHERWISE SPECIFIED		DATE: 17-1-76		



- NOTES:
1. INTERPRET DRAWING IN ACCORDANCE WITH STANDARDS PRESCRIBED BY MIL-D-1000, CAT. 6, FORM 3.
 2. PARTIAL REFERENCE DESIGNATIONS ARE SHOWN FOR COMPLETE DESIGNATION PREFIX WITH UNIT NUMBER OR SUBASSEMBLY DESIGNATIONS.
 3. UNLESS OTHERWISE SPECIFIED:
 A. ALL RESISTOR VALUES ARE IN OHMS ± 5%, 1/4W
 B. ALL 1% RESISTORS ARE 1/10W
 C. ALL CAPACITOR VALUES ARE IN FARADS, ± 10%, 100V.

MATERIAL FINISH CITY NEXT ASSY USED ON APPLICATION		DIMENSIONS DIMENSIONS ARE IN INCHES AND INCLUDE UNLESS OTHERWISE SPECIFIED TOLERANCES FRACTIONS DECIMALS ANGLES 1 1/4 PLACE PLACE 1/64 0.01 0.001 0.1°	DRAWN CHECKED APPROVED DATE 10-1-76 10-1-76 10-1-76	BARNES ENGINEERING COMPANY STAMFORD, CONNECTICUT SCHEMATIC, ELECTRICAL Y CHANNEL (MAGSAT-ATA)
ALL DIMENSIONS SURFACES ALL DIMENSIONS SURFACES CONCENTRIC WITHIN BREAK SHARP EDGES AND RADIUS		REC APPROVAL OTHER APPROVAL	D 00430 208101-3509-1	SCALE SHEET 1 OF 1




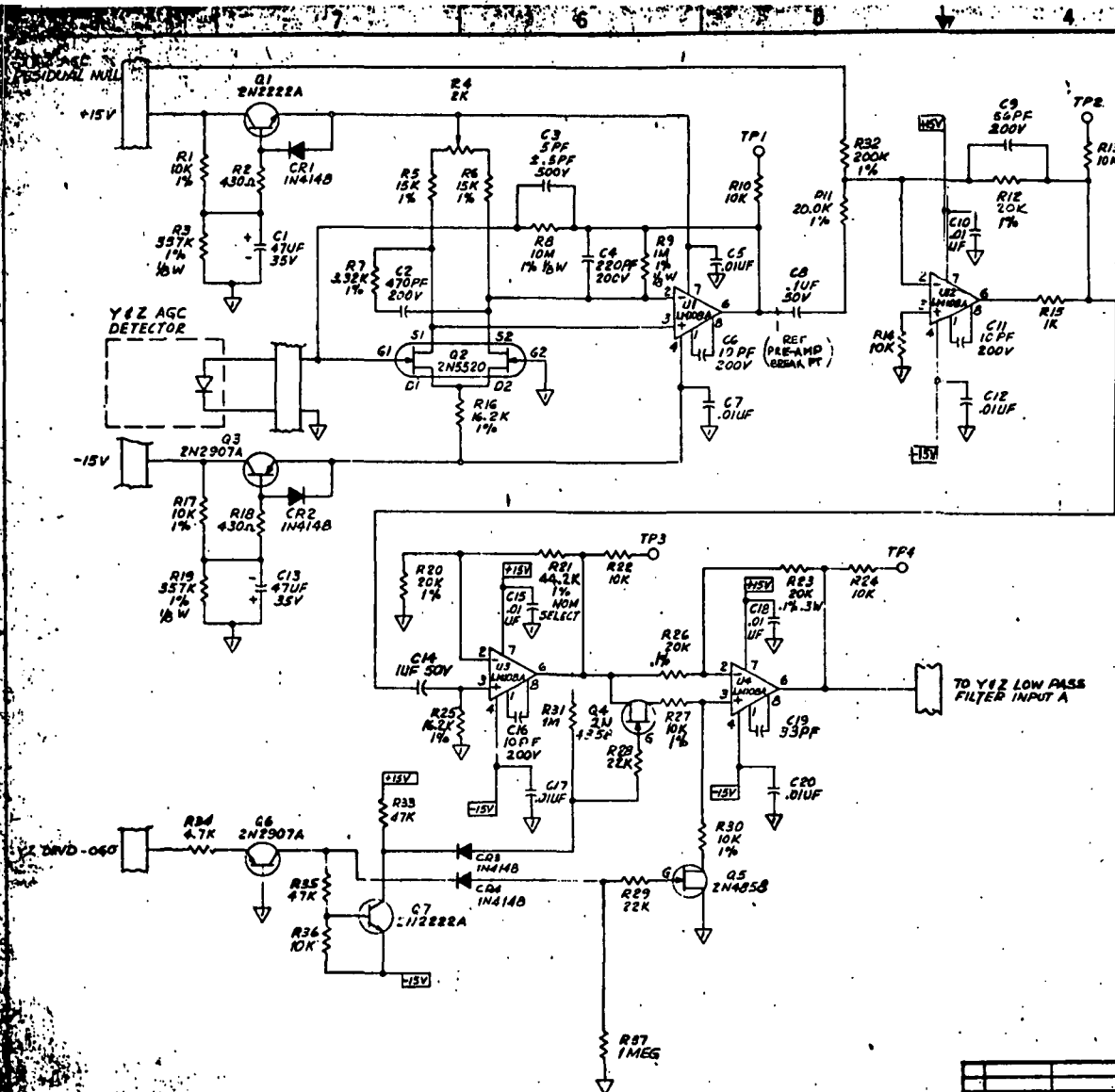
REVISION		DATE		APPROVED	
1	INITIALS	2	DATE	3	DATE
4	INITIALS	5	DATE	6	DATE
7	INITIALS	8	DATE	9	DATE
10	INITIALS	11	DATE	12	DATE
13	INITIALS	14	DATE	15	DATE
16	INITIALS	17	DATE	18	DATE
19	INITIALS	20	DATE	21	DATE
22	INITIALS	23	DATE	24	DATE
25	INITIALS	26	DATE	27	DATE
28	INITIALS	29	DATE	30	DATE
31	INITIALS	32	DATE	33	DATE
34	INITIALS	35	DATE	36	DATE
37	INITIALS	38	DATE	39	DATE
40	INITIALS	41	DATE	42	DATE
43	INITIALS	44	DATE	45	DATE
46	INITIALS	47	DATE	48	DATE
49	INITIALS	50	DATE	51	DATE
52	INITIALS	53	DATE	54	DATE
55	INITIALS	56	DATE	57	DATE
58	INITIALS	59	DATE	60	DATE
61	INITIALS	62	DATE	63	DATE
64	INITIALS	65	DATE	66	DATE
67	INITIALS	68	DATE	69	DATE
70	INITIALS	71	DATE	72	DATE
73	INITIALS	74	DATE	75	DATE
76	INITIALS	77	DATE	78	DATE
79	INITIALS	80	DATE	81	DATE
82	INITIALS	83	DATE	84	DATE
85	INITIALS	86	DATE	87	DATE
88	INITIALS	89	DATE	90	DATE
91	INITIALS	92	DATE	93	DATE
94	INITIALS	95	DATE	96	DATE
97	INITIALS	98	DATE	99	DATE
100	INITIALS	101	DATE	102	DATE

BARNES ENGINEERING COMPANY
 STAMFORD, CONNECTICUT

SCHEMATIC ELECTRICAL
Z CHANNEL
(MAGSAT-ATA)

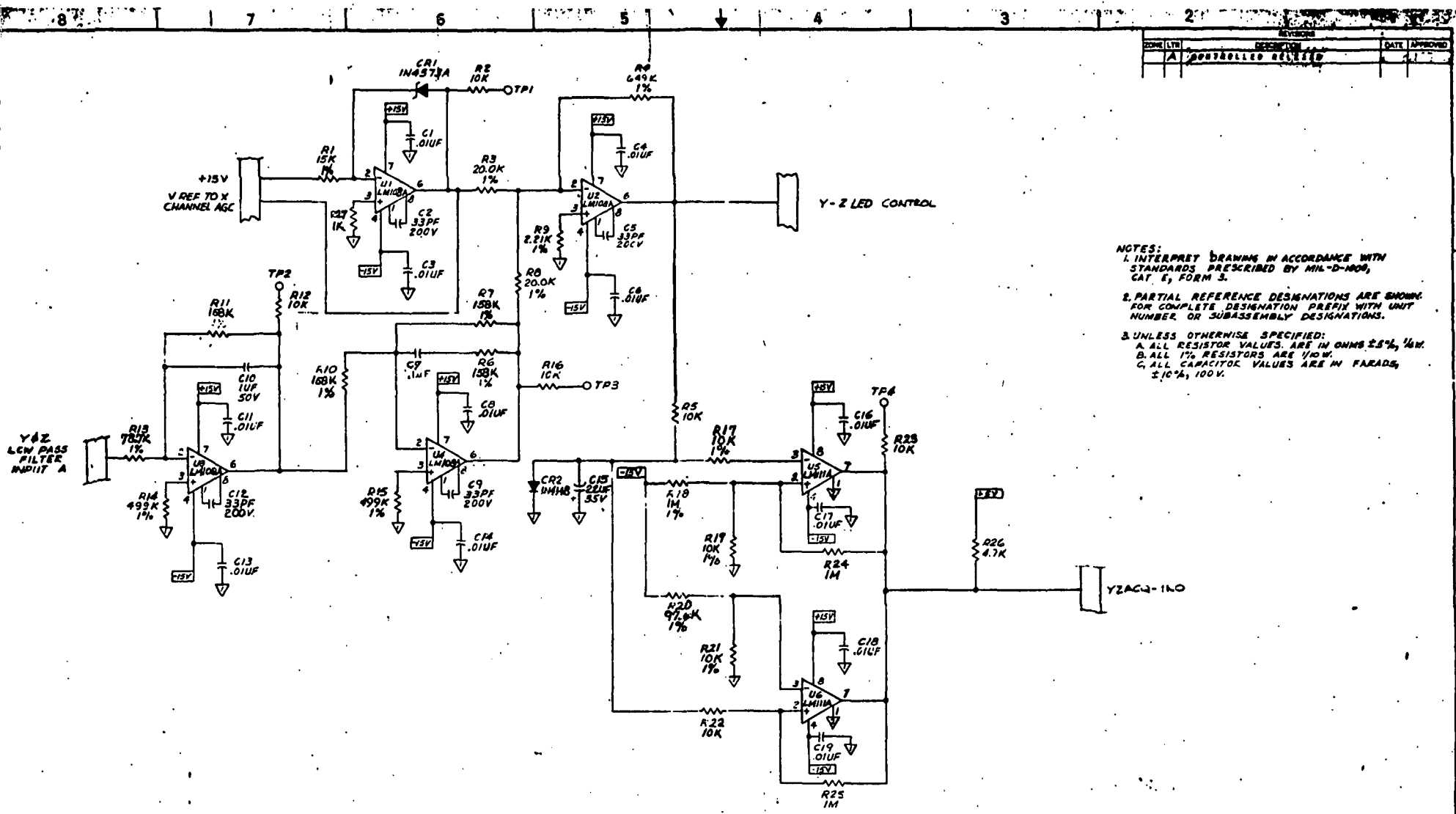
DATE: 00430-208101-3510-1
 SCALE: 1/1

			MATERIAL		UNLESS OTHERWISE SPECIFIED:		SIGNATURE		DATE		 BARNES ENGINEERING COMPANY STAMFORD, CONNECTICUT	
					(DIMENSIONS ARE IN INCHES AND INCLUDE CRITICALALLY APPLIED OR PLATED FINISHES)		DRAWS <i>P. H. H.</i> CHECKED <i>P. H. H.</i> APP'D <i>P. H. H.</i> ISSUED		<i>10-13-70</i> <i>10-13-70</i> <i>10-13-70</i>		SCHEMATIC, ELECTRICAL Y-Z RESIDUAL CHANNEL (MAGSAT-ATA)	
			FINISH		TOLERANCES							
					FRACTIONS DECIMALS ANGLES 1 2 1/16 0.001 1/32 1/2°							
CITY _____ STATE _____ ASSIST _____ USED ON _____ APPLICATION _____					ALL DIMENSIONS SURFACE <input checked="" type="checkbox"/> ALL DIMENSIONS HOLE <input type="checkbox"/> CONCEPT BY _____ YES _____ DESIGN REVIEW BY _____ AND DATE _____		SEC APPROVAL _____ OTHER APPROVAL _____		DDD CORR SHEET NO. D 00430 DESG 208/01-3511-1 SCALE _____			



- NOTES:
1. INTERPRET DRAWING IN ACCORDANCE WITH STANDARDS PRESCRIBED BY MIL-D-1000, CAT 6, FORM 3.
 2. PARTIAL REFERENCE DESIGNATIONS ARE SHOWN FOR COMPLETE DESIGNATION PREFIX WITH UNIT NUMBER OR SUBASSEMBLY DESIGNATIONS.
 3. UNLESS OTHERWISE SPECIFIED:
 - A. ALL RESISTOR VALUES ARE IN OHMS $\pm 5\%$, $\frac{1}{10}$ W
 - B. ALL 1% RESISTORS ARE $\frac{1}{10}$ W
 - C. ALL CAPACITOR VALUES ARE IN FARADS, $\pm 10\%$, 100V.

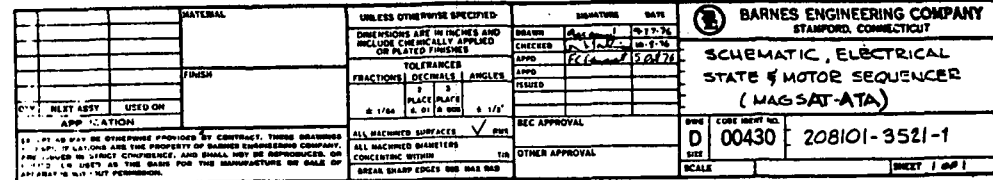
MATERIAL PARTS QTY UNIT USED BY APPLICATION		UNLESS OTHERWISE SPECIFIED: DIMENSIONS ARE IN INCHES AND INCLUDE CRITICAL APPLIED OR PLATED FINISHES TOLERANCES FRACTIONS DECIMALS ANGLES 1/16 1/32 1/64 1/8 1/4 1/2 3/4 1 1 1/2 2 3 4 5 6 7 8 9 10 11 12 13 14 15 16 17 18 19 20 21 22 23 24 25 26 27 28 29 30 31 32 33 34 35 36 37 38 39 40 41 42 43 44 45 46 47 48 49 50 51 52 53 54 55 56 57 58 59 60 61 62 63 64 65 66 67 68 69 70 71 72 73 74 75 76 77 78 79 80 81 82 83 84 85 86 87 88 89 90 91 92 93 94 95 96 97 98 99 100 101 102 103 104 105 106 107 108 109 110 111 112 113 114 115 116 117 118 119 120 121 122 123 124 125 126 127 128 129 130 131 132 133 134 135 136 137 138 139 140 141 142 143 144 145 146 147 148 149 150 151 152 153 154 155 156 157 158 159 160 161 162 163 164 165 166 167 168 169 170 171 172 173 174 175 176 177 178 179 180 181 182 183 184 185 186 187 188 189 190 191 192 193 194 195 196 197 198 199 200 201 202 203 204 205 206 207 208 209 210 211 212 213 214 215 216 217 218 219 220 221 222 223 224 225 226 227 228 229 230 231 232 233 234 235 236 237 238 239 240 241 242 243 244 245 246 247 248 249 250 251 252 253 254 255 256 257 258 259 260 261 262 263 264 265 266 267 268 269 270 271 272 273 274 275 276 277 278 279 280 281 282 283 284 285 286 287 288 289 290 291 292 293 294 295 296 297 298 299 300 301 302 303 304 305 306 307 308 309 310 311 312 313 314 315 316 317 318 319 320 321 322 323 324 325 326 327 328 329 330 331 332 333 334 335 336 337 338 339 340 341 342 343 344 345 346 347 348 349 350 351 352 353 354 355 356 357 358 359 360 361 362 363 364 365 366 367 368 369 370 371 372 373 374 375 376 377 378 379 380 381 382 383 384 385 386 387 388 389 390 391 392 393 394 395 396 397 398 399 400 401 402 403 404 405 406 407 408 409 410 411 412 413 414 415 416 417 418 419 420 421 422 423 424 425 426 427 428 429 430 431 432 433 434 435 436 437 438 439 440 441 442 443 444 445 446 447 448 449 450 451 452 453 454 455 456 457 458 459 460 461 462 463 464 465 466 467 468 469 470 471 472 473 474 475 476 477 478 479 480 481 482 483 484 485 486 487 488 489 490 491 492 493 494 495 496 497 498 499 500 501 502 503 504 505 506 507 508 509 510 511 512 513 514 515 516 517 518 519 520 521 522 523 524 525 526 527 528 529 530 531 532 533 534 535 536 537 538 539 540 541 542 543 544 545 546 547 548 549 550 551 552 553 554 555 556 557 558 559 560 561 562 563 564 565 566 567 568 569 570 571 572 573 574 575 576 577 578 579 580 581 582 583 584 585 586 587 588 589 590 591 592 593 594 595 596 597 598 599 600 601 602 603 604 605 606 607 608 609 610 611 612 613 614 615 616 617 618 619 620 621 622 623 624 625 626 627 628 629 630 631 632 633 634 635 636 637 638 639 640 641 642 643 644 645 646 647 648 649 650 651 652 653 654 655 656 657 658 659 660 661 662 663 664 665 666 667 668 669 670 671 672 673 674 675 676 677 678 679 680 681 682 683 684 685 686 687 688 689 690 691 692 693 694 695 696 697 698 699 700 701 702 703 704 705 706 707 708 709 710 711 712 713 714 715 716 717 718 719 720 721 722 723 724 725 726 727 728 729 730 731 732 733 734 735 736 737 738 739 740 741 742 743 744 745 746 747 748 749 750 751 752 753 754 755 756 757 758 759 760 761 762 763 764 765 766 767 768 769 770 771 772 773 774 775 776 777 778 779 780 781 782 783 784 785 786 787 788 789 790 791 792 793 794 795 796 797 798 799 800 801 802 803 804 805 806 807 808 809 810 811 812 813 814 815 816 817 818 819 820 821 822 823 824 825 826 827 828 829 830 831 832 833 834 835 836 837 838 839 840 841 842 843 844 845 846 847 848 849 850 851 852 853 854 855 856 857 858 859 860 861 862 863 864 865 866 867 868 869 870 871 872 873 874 875 876 877 878 879 880 881 882 883 884 885 886 887 888 889 890 891 892 893 894 895 896 897 898 899 900 901 902 903 904 905 906 907 908 909 910 911 912 913 914 915 916 917 918 919 920 921 922 923 924 925 926 927 928 929 930 931 932 933 934 935 936 937 938 939 940 941 942 943 944 945 946 947 948 949 950 951 952 953 954 955 956 957 958 959 960 961 962 963 964 965 966 967 968 969 970 971 972 973 974 975 976 977 978 979 980 981 982 983 984 985 986 987 988 989 990 991 992 993 994 995 996 997 998 999 1000 1001 1002 1003 1004 1005 1006 1007 1008 1009 1010 1011 1012 1013 1014 1015 1016 1017 1018 1019 1020 1021 1022 1023 1024 1025 1026 1027 1028 1029 1030 1031 1032 1033 1034 1035 1036 1037 1038 1039 1040 1041 1042 1043 1044 1045 1046 1047 1048 1049 1050 1051 1052 1053 1054 1055 1056 1057 1058 1059 1060 1061 1062 1063 1064 1065 1066 1067 1068 1069 1070 1071 1072 1073 1074 1075 1076 1077 1078 1079 1080 1081 1082 1083 1084 1085 1086 1087 1088 1089 1090 1091 1092 1093 1094 1095 1096 1097 1098 1099 1100 1101 1102 1103 1104 1105 1106 1107 1108 1109 1110 1111 1112 1113 1114 1115 1116 1117 1118 1119 1120 1121 1122 1123 1124 1125 1126 1127 1128 1129 1130 1131 1132 1133 1134 1135 1136 1137 1138 1139 1140 1141 1142 1143 1144 1145 1146 1147 1148 1149 1150 1151 1152 1153 1154 1155 1156 1157 1158 1159 1160 1161 1162 1163 1164 1165 1166 1167 1168 1169 1170 1171 1172 1173 1174 1175 1176 1177 1178 1179 1180 1181 1182 1183 1184 1185 1186 1187 1188 1189 1190 1191 1192 1193 1194 1195 1196 1197 1198 1199 1200 1201 1202 1203 1204 1205 1206 1207 1208 1209 1210 1211 1212 1213 1214 1215 1216 1217 1218 1219 1220 1221 1222 1223 1224 1225 1226 1227 1228 1229 1230 1231 1232 1233 1234 1235 1236 1237 1238 1239 1240 1241 1242 1243 1244 1245 1246 1247 1248 1249 1250 1251 1252 1253 1254 1255 1256 1257 1258 1259 1260 1261 1262 1263 1264 1265 1266 1267 1268 1269 1270 1271 1272 1273 1274 1275 1276 1277 1278 1279 1280 1281 1282 1283 1284 1285 1286 1287 1288 1289 1290 1291 1292 1293 1294 1295 1296 1297 1298 1299 1300 1301 1302 1303 1304 1305 1306 1307 1308 1309 1310 1311 1312 1313 1314 1315 1316 1317 1318 1319 1320 1321 1322 1323 1324 1325 1326 1327 1328 1329 1330 1331 1332 1333 1334 1335 1336 1337 1338 1339 1340 1341 1342 1343 1344 1345 1346 1347 1348 1349 1350 1351 1352 1353 1354 1355 1356 1357 1358 1359 1360 1361 1362 1363 1364 1365 1366 1367 1368 1369 1370 1371 1372 1373 1374 1375 1376 1377 1378 1379 1380 1381 1382 1383 1384 1385 1386 1387 1388 1389 1390 1391 1392 1393 1394 1395 1396 1397 1398 1399 1400 1401 1402 1403 1404 1405 1406 1407 1408 1409 1410 1411 1412 1413 1414 1415 1416 1417 1418 1419 1420 1421 1422 1423 1424 1425 1426 1427 1428 1429 1430 1431 1432 1433 1434 1435 1436 1437 1438 1439 1440 1441 1442 1443 1444 1445 1446 1447 1448 1449 1450 1451 1452 1453 1454 1455 1456 1457 1458 1459 1460 1461 1462 1463 1464 1465 1466 1467 1468 1469 1470 1471 1472 1473 1474 1475 1476 1477 1478 1479 1480 1481 1482 1483 1484 1485 1486 1487 1488 1489 1490 1491 1492 1493 1494 1495 1496 1497 1498 1499 1500 1501 1502 1503 1504 1505 1506 1507 1508 1509 1510 1511 1512 1513 1514 1515 1516 1517 1518 1519 1520 1521 1522 1523 1524 1525 1526 1527 1528 1529 1530 1531 1532 1533 1534 1535 1536 1537 1538 1539 1540 1541 1542 1543 1544 1545 1546 1547 1548 1549 1550 1551 1552 1553 1554 1555 1556 1557 1558 1559 1560 1561 1562 1563 1564 1565 1566 1567 1568 1569 1570 1571 1572 1573 1574 1575 1576 1577 1578 1579 1580 1581 1582 1583 1584 1585 1586 1587 1588 1589 1590 1591 1592 1593 1594 1595 1596 1597 1598 1599 1600 1601 1602 1603 1604 1605 1606 1607 1608 1609 1610 1611 1612 1613 1614 1615 1616 1617 1618 1619 1620 1621 1622 1623 1624 1625 1626 1627 1628 1629 1630 1631 1632 1633 1634 1635 1636 1637 1638 1639 1640 1641 1642 1643 1644 1645 1646 1647 1648 1649 1650 1651 1652 1653 1654 1655 1656 1657 1658 1659 1660 1661 1662 1663 1664 1665 1666 1667 1668 1669 1670 1671 1672 1673 1674 1675 1676 1677 1678 1679 1680 1681 1682 1683 1684 1685 1686 1687 1688 1689 1690 1691 1692 1693 1694 1695 1696 1697 1698 1699 1700 1701 1702 1703 1704 1705 1706 1707 1708 1709 1710 1711 1712 1713 1714 1715 1716 1717 1718 1719 1720 1721 1722 1723 1724 1725 1726 1727 1728 1729 1730 1731 1732 1733 1734 1735 1736 1737 1738 1739 1740 1741 1742 1743 1744 1745 1746 1747 1748 1749 1750 1751 1752 1753 1754 1755 1756 1757 1758 1759 1760 1761 1762 1763 1764 1765 1766 1767 1768 1769 1770 1771 1772 1773 1774 1775 1776 1777 1778 1779 1780 1781 1782 1783 1784 1785 1786 1787 1788 1789 1790 1791 1792 1793 1794 1795 1796 1797 1798 1799 1800 1801 1802 1803 1804 1805 1806 1807 1808 1809 1810 1811 1812 1813 1814 1815 1816 1817 1818 1819 1820 1821 1822 1823 1824 1825 1826 1827 1828 1829 1830 1831 1832 1833 1834 1835 1836 1837 1838 1839 1840 1841 1842 1843 1844 1845 1846 1847 1848 1849 1850 1851 1852 1853 1854 1855 1856 1857 1858 1859 1860 1861 1862 1863 1864 1865 1866 1867 1868 1869 1870 1871 1872 1873 1874 1875 1876 1877 1878 1879 1880 1881 1882 1883 1884 1885 1886 1887 1888 1889 1890 1891 1892 1893 1894 1895 1896 1897 1898 1899 1900 1901 1902 1903 1904 1905 1906 1907 1908 1909 1910 1911 1912 1913 1914 1915 1916 1917 1918 1919 1920 1921 1922 1923 1924 1925 1926 1927 1928 1929 1930 1931 1932 1933 1934 1935 1936 1937 1938 1939 1940 1941 1942 1943 1944 1945 1946 1947 1948 1949 1950 1951 1952 1953 1954 1955 1956 1957 1958 1959 1960 1961 1962 1963 1964 1965 1966 1967 1968 1969 1970 1971 1972 1973 1974 1975 1976 1977 1978 1979 1980 1981 1982 1983 1984 1985 1986 1987 1988 1989 1990 1991 1992 1993 1994 1995 1996 1997 1998 1999 2000 2001 2002 2003 2004 2005 2006 2007 2008 2009 2010 2011 2012 2013 2014 2015 2016 2017 2018 2019 2020 2021 2022 2023 2024 2025 2026 2027 2028 2029 2030 2031 2032 2033 2034 2035 2036 2037 2038 2039 2040 2041 2042 2043 2044 2045 2046 2047 2048 2049 2050 2051 2052 2053 2054 2055 2056 2057 2058 2059 2060 2061 2062 2063 2064 2065 2066 2067 2068 2069 2070 2071 2072 2073 2074 2075 2076 2077 2078 2079 2080 2081 2082 2083 2084 2085 2086 2087 2088 2089 2090 2091 2092 2093 2094 2095 2096 2097 2098 2099 2100 2101 2102 2103 2104 2105 2106 2107 2108 2109 2110 2111 2112 2113 2114 2115 2116 2117 2118 2119 2120 2121 2122 2123 2124 2125 2126 2127 2128 2129 2130 2131 2132 2133 2134 2135 2136 2137 2138 2139 2140 2141 2142 2143 2144 2145 2146 2147 2148 2149 2150 2151 2152 2153 2154 2155 2156 2157 2158 2159 2160 2161 2162 2163 2164 2165 2166 2167 2168 2169 2170 2171 2172 2173 2174 2175 2176 2177 2178 2179 2180 2181 2182 2183 2184 2185 2186 2187 2188 2189 2190 2191 2192 2193 2194 2195 2196 2197 2198 2199 2200 2201 2202 2203 2204 2205 2206 2207 2208 2209 2210 2211 2212 2213 2214 2215 2216 2217 2218 2219 2220 2221 2222 2223 2224 2225 2226 2227 2228 2229 2230 2231 2232 2233 2234 2235 2236 2237 2238 2239 2240 2241 2242 2243 2244 2245 2246 2247 2248 2249 2250 2251 2252 2253 2254 2255 2256 2257 2258 2259 2260 2261 2262 2263 2264 2265 2266 2267 2268 2269 2270 2271 2272 2273 2274 2275 2276 2277 2278 2279 2280 2281 2282 2283 2284 2285 2286 2287 2288 2289 2290 2291 2292 2293 2294 2295 2296 2297 2298 2299 2300 2301 2302 2303 2304 2305 2306 2307 2308 2309 2310 2311 2312 2313 2314 2315 2316 2317 2318 2319 2320 2321 2322 2323 2324 2325 2326 2327 2328 2329 2330 2331 2332 2333 2334 2335 2336 2337 2338 2339 2340 2341 2342 2343 2344 2345 2346 2347 2348 2349 2350 2351 2352 2353 2354 2355 2356 2357 2358 2359 2360 2361 2362 2363 2364 2365 2366 2367 2368 2369 2370 2371 2372 2373 2374 2375 2376 2377 2378 2379 2380 2381 2382 2383 2384 2385 2386 2387 2388 2389 2390 2391 2392 2393 2394 2395 2396 2397 2398 2399 2400 2401 2402 2403 2404 2405 2406 2407 2408 2409 2410 2411 2412 2413 2414 2415 2416 2417 2418 2419 2420 2421 2422 2423 2424 2425 2426 2427 2428 2429 2430 2431 2432 2433 2434 2435 2436 2437 2438 2439 2440 2441 2442 2443 2444 2445 2446 2447 2448 2449 2450 2451 2452 2453 2454 2455 2456 2457 2458 2459 2460 2461 2462 2463 2464 2465 2466 2467 2468 2469 2470 2471 2472 2473 2474 2475 2476 2477 2478 2479 2480 2481 2482 2483 2484 2485 2486 2487 2488 2489 2490 2491 2492 2493 2494 2495 2496 2497 2498 2499 2500 2501 2502 2503 2504 2505 2506 2507 2508 2509 2510 2511 2512 2513 2514 2515 2516 2517 2518 2519 2520 2521 2522 2523 2524 2525 2526 2527 2528 2529 2530 2531 2532 2533 2534 2535 2536 2537 2538 2539 2540 2541 2542 2543 2544 2545 2546 2547 2548 2549 2550 2551 2552 2553 2554 2555 2556 2557 2558 2559 2560 2561 2562 2563 2564 2565 2566	
--	--	---	--



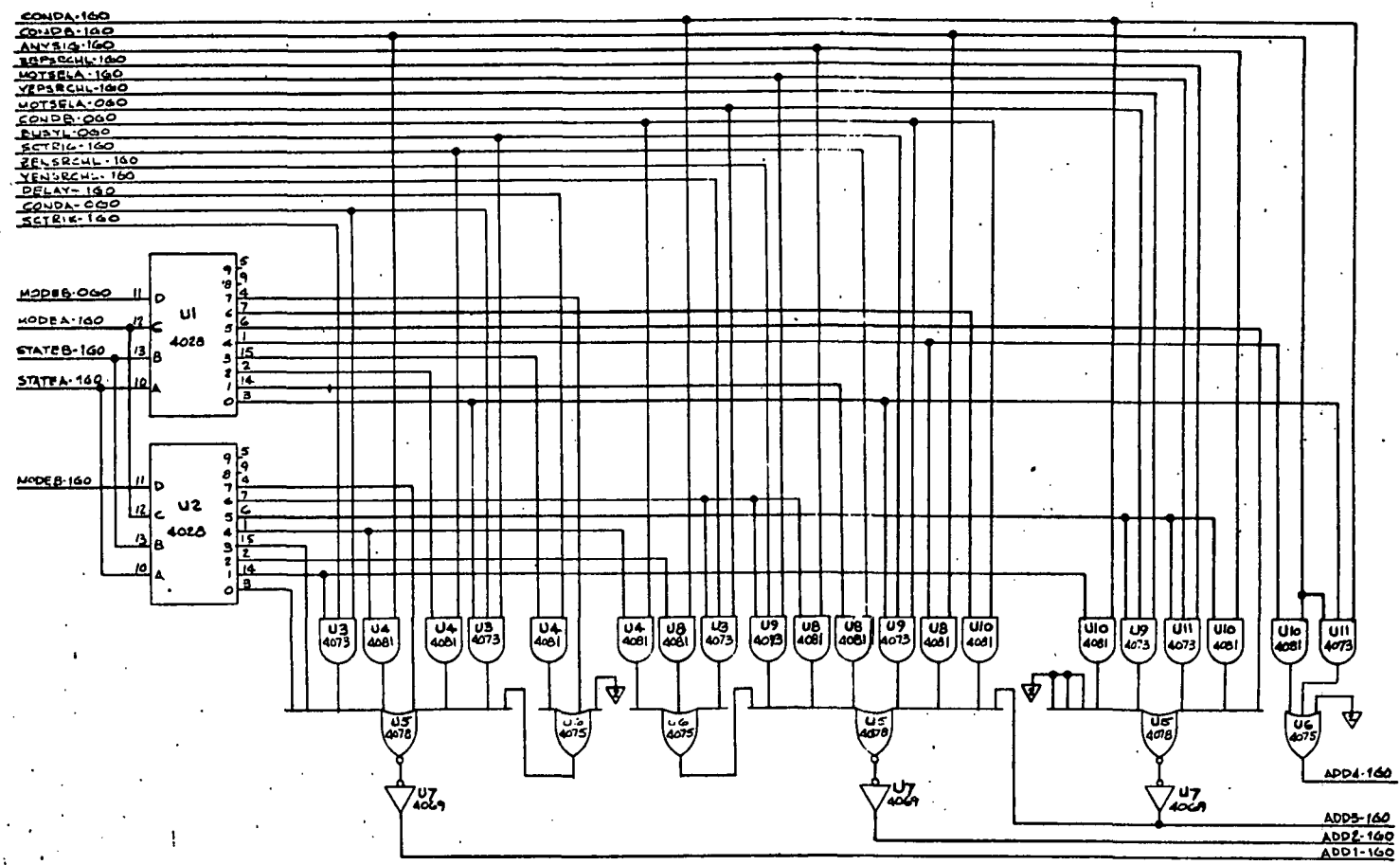
- NOTES:
1. INTERPRET DRAWINGS IN ACCORDANCE WITH STANDARDS PRESCRIBED BY MIL-D-1000, CAT. 1, FORM 3.
 2. PARTIAL REFERENCE DESIGNATIONS ARE SHOWN FOR COMPLETE DESIGNATION PREFIX WITH UNIT NUMBER OR SUBASSEMBLY DESIGNATIONS.
 3. UNLESS OTHERWISE SPECIFIED:
 - A. ALL RESISTOR VALUES ARE IN OHMS $\pm 5\%$, $\frac{1}{4}$ W.
 - B. ALL 1% RESISTORS ARE $\frac{1}{10}$ W.
 - C. ALL CAPACITOR VALUES ARE IN FARADS, $\pm 10\%$, 100V.

BLACK 16, 17, 18 & 19

MATERIAL		UNLESS OTHERWISE SPECIFIED:		DIMENSIONS ARE IN INCHES AND DECIMALS UNLESS OTHERWISE SPECIFIED	
FINISH		TOLERANCES		FRACTIONS DECIMALS ANGLES	
CITY		APPROVAL		DATE	
TEST ASBY		USED ON		SCALE	
APPLICATION		ALL MACHINED SURFACES		BEC APPROVAL	
BRIGHT & SHINY OR OTHERWISE PROVIDED BY CONTRACT, THESE DRAWINGS AND SPECIFICATIONS ARE THE PROPERTY OF BARNES ENGINEERING COMPANY, AND SHALL NOT BE REPRODUCED OR COPIED, OR USED IN THE MAKING OF THE MANUFACTURE OR SALE OF APPARATUS WITHOUT PERMISSION.		CONCENTRIC WITHIN		OTHER APPROVAL	
BARNES ENGINEERING COMPANY STAMFORD, CONNECTICUT		D 004330		208101-3513-1	



REVISIONS		
ZONE	LTN	DESCRIPTION



BLOCK 76

MATERIAL FINISH APPLICATION		UNLESS OTHERWISE SPECIFIED: DIMENSIONS ARE IN INCHES AND INCLUDE CHEMICALLY APPLIED OR PLATED FINISHES TOLERANCES FRACTIONS: DECIMALS: ANGLES: 1/64 3/64 1/32 1/16 1/8 1/4 1/2 3/4 1		DRAFTER: [Signature] CHECKER: [Signature] APPR: [Signature] ISSUED: [Signature]		BARNES ENGINEERING COMPANY STAMFORD, CONNECTICUT SCHEMATIC, ELECTRICAL LOGIC ARRAY (MAGSAT-ATA)	
QTY	NEXT ASSY	USED ON	ALL MACHINED SURFACES ALL BURNED SURFACES CONCENTRIC SURFACES BREAK SHARP EDGES AND RAS S&B		REC APPROVAL OTHER APPROVAL		CODE: 00430 DATE: 10-2-78 SCALE:

8

7

6

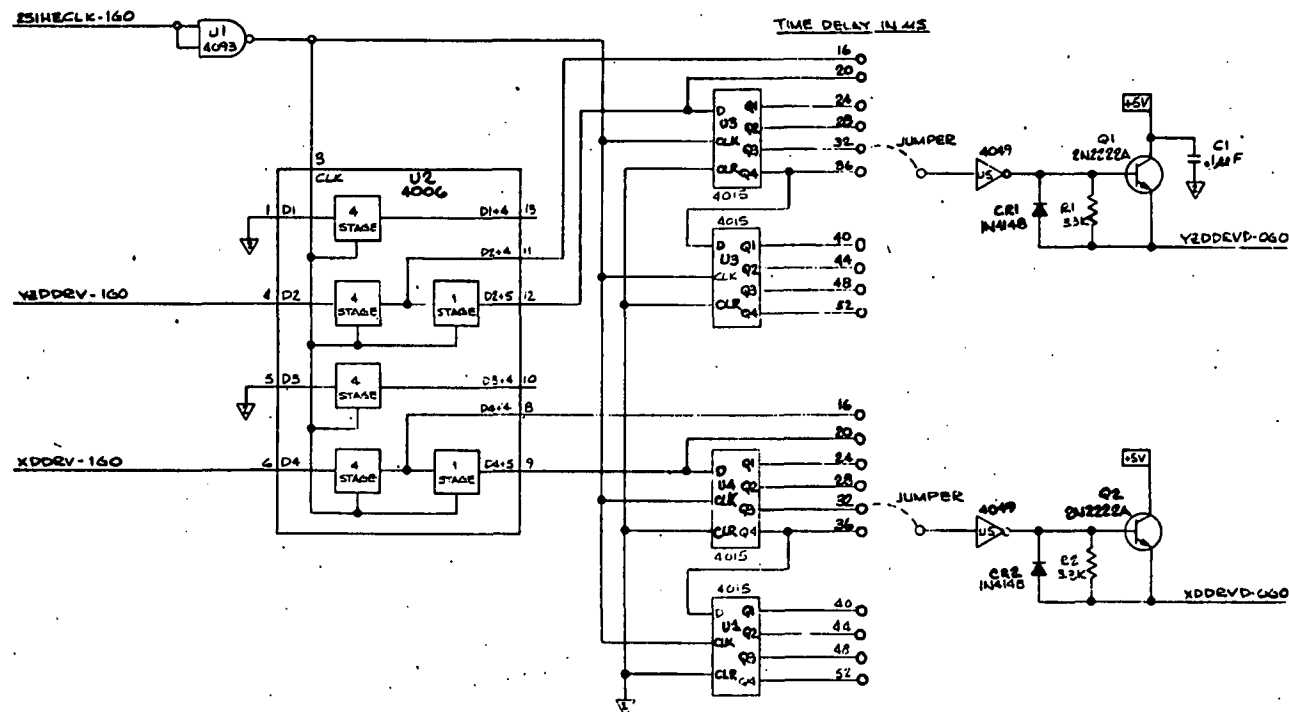
5

4

3

2

REV		DESCRIPTION		DATE	APPROVED
1	1				



Block 23 / 89

MATERIAL		UNLESS OTHERWISE SPECIFIED:		SIGNATURE		DATE	
FINISH		DIMENSIONS ARE IN INCHES AND INCLUDE CHEMICALLY APPLIED OR PLATED FINISHES		DRAWN		DATE	
QTY		TOLERANCES		CHECKED		DATE	
NEXT ASSY		FRACTIONS		APP'D		DATE	
USED ON		DECIMALS		ISSUED			
APPLICATION		ANGLES		REV		CODE	
EXCEPT AS MAY BE OTHERWISE PROVIDED BY CONTRACT, THESE DRAWINGS AND SPECIFICATIONS ARE THE PROPERTY OF BARNES ENGINEERING COMPANY. ANY REUSE IN STRICT CONFIDENCE, AND SHALL NOT BE REPRODUCED OR COPIED OR USED AS THE BASIS FOR THE MANUFACTURE OR SALE OF EQUIPMENT WITHOUT PERMISSION.		ALL MACHINED SURFACES		BEC APPROVAL		D	
		ALL PACHED DIAMETERS		OTHER APPROVAL		00430	
		BREATHE SHARP EDGES BUT MAX PAD				208101-3525-1	
						SCALE	
						SHEET 1 of 1	

BARNES ENGINEERING COMPANY
STAMFORD, CONNECTICUTSCHEMATIC, ELECTRICAL
DIGITAL PHASE SHIFTER
(MAGSAT-4A)

D 00430 208101-3525-1

APPENDIX G

RELIABILITY CONSIDERATIONS

BARNES ENGINEERING COMPANY

• 30 Commerce Road • Stamford, Connecticut

BEC REL 2081-01
10-11-1976

PRELIMINARY

RELIABILITY PREDICTION

(By Part Type/Part Count)

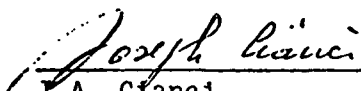
FOR

MAGSAT-ATA SYSTEM

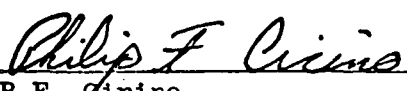
FOR


NASA/GSFC

Prepared By:


J.A. Cianci
Reliability Engineer

Approved By:


P.F. Cirino
Manager
Reliability Engineering


S.S. Pellingra
Director
Product Assurance


P.W. Collyer

1.0 PURPOSE

This report has been prepared for the purpose of reporting the reliability assessment of the BEC designed MAGSAT-ATA system based on a Part Type/Part Count analysis, and for evaluating this assessment against the specified contractual requirements.

2.0 REFERENCES

- 2.1 MILHDBK-217B Reliability Stress and
20 September 1974 Failure Rate Data for
Electronic Equipment

3.0 RELIABILITY ANALYSIS

3.1 Part Failure Rate

The base failure rates for all components were obtained by using the failure rates listed in Section 3.0 of MIL-HDBK-217B.

All Resistor's and Capacitor's quality factors were assumed to be those with failure rate level "R".

All Semiconductor Diodes and Transistors were assumed to be "JANTX" types. For any semiconductors which are not standard parts, their screening level was assumed to be "JANTX" equivalent as a minimum.

All Integrated Circuits have been chosen so that their screening level is to MIL-M-38510, Class "A" or equivalent.

All other components, such as Inductors, Transformers, Relays, etc., have been chosen such that their reliability screening level is comparable to the specific Military Specification applicable.

The failure rates for solder connections have been chosen from MIL-HDBK-217B to be the lowest failure rate possible since BEC has experienced a very high reliability for this kind of operation during past and present related space programs.

4.0

RELIABILITY PREDICTION

4.1

Reliability Analysis

Figure I shows the reliability model for the MAGSAT-ATA system. Table I lists the MAGSAT-ATA's component failure rates by module. Tables II through XXVI list the modules' circuit elements and their associated failure rates.

The results of this analysis indicate that the failure rate of the BEC designed MAGSAT-ATA system is:

$$\lambda \text{ Total} = 9,719.18 \times 10^{-9} \text{ Failures/hours}$$

$$\text{MTBF} = \frac{1}{\lambda \text{ Total}} = 102,889.34 \text{ Hours}$$

where:

$\lambda \text{ Total}$ = overall failure rate for the MAGSAT-ATA

MTBF = Mean time between failures for the MAGSAT-ATA system

The probability of success for a mission time of 5,760 hours is as follows:

$$P_s = e^{(-\lambda \text{ Total}) \times (t)}$$

where P_s = probability of success

$\lambda \text{ Total}$ = overall failure rate for the MAGSAT-ATA

t = mission time in hours = 8 month = 5,760 hrs.

$$P_s = e^{(-9,719.18 \times 10^{-9} \text{ f/hr}) \times (5,760 \text{ hours})}$$

$$P_s = 0.9456$$

For a mission time t of 4 months (or 2,880 hours)

$$P_s = .9724$$

FIGURE 1
RELIABILITY MODEL

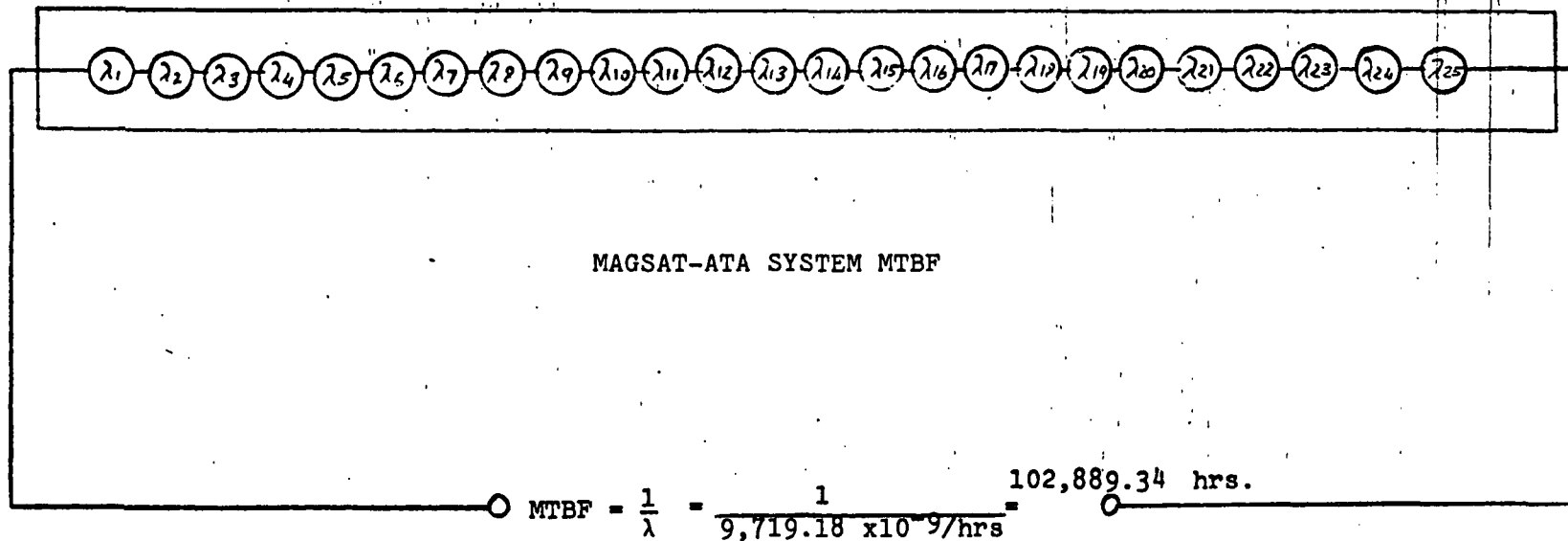


TABLE I
MAGSAT-ATA SYSTEM
SUMMARY OF COMPONENT FAILURE RATES BY MODULE

MODULE	MODULE FAILURE RATES (Fr $\times 10^{-9}$ /hour)
λ_1 : LED Driver	163.21
λ_2 : X-Comparators	130.67
λ_3 : Y-Comparators	130.67
λ_4 : Z-Comparators	130.67
λ_5 : X-Channel	706.39
λ_6 : X Residual Channel	159.31
λ_7 : X AGC Channel	447.78
λ_8 : X Channel AGC & Acquisition Detector	338.745
λ_9 : Y Channel	641.639
λ_{10} : Z Channel	639.16
λ_{11} : Y-Z Residual Channel	439.99
λ_{12} : Y & Z AGC Channel	446.865
λ_{13} : Y & Z AGC & Acquisition Detector	410.72
λ_{14} : Power Supply	506.235
λ_{15} : X Encoder Counter and Reg.	436.56
λ_{16} : Z_1 & Z_2 Encoder Counter & Reg.	540.64
λ_{17} : Encoder Counter	540.64
λ_{18} : Motor Drive I	263.77
λ_{19} : Motor Drive II	849.415
λ_{20} : S/C Command Interface	284.52
λ_{21} : State and Motor Sequencer	333.84
λ_{22} : Logic Array	308.16
λ_{23} : Mode and Conditional Latches	359.52
λ_{24} : Data Interrace Cont. & Clks	353.175
λ_{25} : Digital Phase Shifter	156.89

PRELIMINARY PARTS COUNT/PARTS TYPE

CIRCUIT RELIABILITY ESTIMATE

Table II

λ_1 : LED Driver

Component	Base Failure Rate (fr x 10 ⁻⁹ /hr.)	Quantity	Total Failure Rate (fr x 10 ⁻⁹ /hr.)
Resistor, Fixed, Film	0.28	14	3.92
Resistor, Fixed- Carbon	0.045	26	1.17
Capacitor, Fixed, Ceramic	1.0	10	10.0
Capacitor, Fixed, Solid Tantalum	1.1	2	2.2
Diode, Silicon, Gen. Purp.	3.4	6	20.4
Transistor, Silicon, PNP	8.4	2	16.8
Transistor, Silicon, NPN	5.6	10	56.0
Diode, Light Emitting	17	2	34.0
Solder Connections	0.12	156	18.72

$$\lambda_1 = 163.21$$

PRELIMINARY PARTS COUNT/PARTS TYPE

CIRCUIT RELIABILITY ESTIMATE

TABLE III

λ_2 : X-Comparators

Component	Base Failure Rate (fr x 10 ⁻⁹ /hr.)	Quantity	Total Failure Rate (fr x 10 ⁻⁹ /hr.)
Resistor, Fixed, Film	0.28	4	1.12
Resistor, Fixed Carbon	0.045	6	0.27
Capacitor, Fixed, Ceramic	1.0	4	4.0
Integrated Circuit, Linear	60	2	120
Solder Connections	0.12	44	5.28

$\lambda_2 = 130.67$

PRELIMINARY PARTS COUNT/PARTS TYPE
CIRCUIT RELIABILITY ESTIMATE
TABLE IV

λ_3 : Y-Comparators

Component	Base Failure Rate (fr x 10 ⁻⁹ /hr.)	Quantity	Total Failure Rate (fr x 10 ⁻⁹ /hr.)
Resistor, Fixed, Film	0.28	4	1.12
Resistor, Fixed, Carbon	0.045	6	0.27
Capacitor, Fixed, Ceramic	1.0	4	4.0
Integrated Circuit, Linear	60	2	120.0
Solder Connections	0.12	44	5.28

$$\lambda_3 = 130.67$$

PRELIMINARY PARTS COUNT/PARTS TYPE

CIRCUIT RELIABILITY ESTIMATE

TABLE V

λ_4 : Z Comparators

Component	Base Failure Rate (fr x 10 ⁻⁹ /hr.)	Quantity	Total Failure Rate (fr x 10 ⁻⁹ /hr.)
Resistor, Fixed, Film	0.28	4	1.12
Resistor, Fixed, Carbon	0.045	6	0.27
Capacitor, Fixed, Ceramic	1.0	4	4.0
Integrated Circuit, Linear	60	2	120.0
Solder Connections	0.12	44	5.28

$$\lambda_4 = 130.67$$

PRELIMINARY PARTS COUNT/PARTS TYPE
CIRCUIT RELIABILITY ESTIMATE
TABLE VI

λ_5 : X-Channel

Component	Base Failure Rate (fr x 10 ⁻⁹ /hr.)	Quantity	Total Failure Rate (fr x 10 ⁻⁹ /hr.)
Resistor, Fixed, Film	0.28	29	8.12
Resistor, Fixed, Carbon	0.045	20	0.9
Capacitor, Fixed, Ceramic	1.0	28	28.0
Capacitor, Fixed, Solid Tantalum	1.1	3	3.3
Capacitor, Fixed, Mica	0.3	1	0.3
Diode, Silicon, Gen. Purp.	3.4	4	13.6
Transistor, Silicon, PNP	8.4	2	16.8
Transistor, Silicon, NPN	5.6	2	11.2
Transistor, N-Channel, FET	15.2	4	60.8
Integrated Circuit, Linear	60	7	120.0
Detector, Silicon	57	2	114.0
Solder Connections	0.18	254	30.48

$$\lambda_5 = 706.39$$

PRELIMINARY PARTS COUNT/PARTS TYPE

CIRCUIT RELIABILITY ESTIMATE

TABLE VII

λ_6 : X Residual Channel

Component	Base Failure Rate (fr x 10^{-9} /hr.)	Quantity	Total Failure Rate (fr x 10^{-9} /hr.)
Resistor, Fixed, Film	0.28	14	3.92
Resistor, Fixed, Carbon	0.045	10	0.45
Capacitor, Fixed, Ceramic	1.0	12	12.0
Capacitor, Fixed, Solid Tantalum	1.1	2	2.2
Capacitor, Fixed, Mica	0.3	1	0.3
Diode, Silicon, Gen.Purp.	3.4	2	6.8
Transistor, Silicon, PNP	8.4	1	8.4
Transistor, Silicon, NPN	5.6	1	5.6
Transistor, N-Channel, FET	15.2	2	30.4
Relay, Latching	120	1	120.0
Detector, Silicon	57	1	57.0
Solder Connections	0.12	102	12.24

$$\lambda_6 = 159.31$$

PRELIMINARY PARTS COUNT/PARTS TYPE

CIRCUIT RELIABILITY ESTIMATE
TABLE VIII

λ_7 : X AGC Channel

Component	Base Failure Rate (fr x 10 ⁻⁹ /hr.)	Quantity	Total Failure Rate (fr x 10 ⁻⁹ /hr.)
Resistor, Fixed, Film	0.28	20	5.6
Resistor, Fixed, Carbon	0.045	16	0.72
Capacitor, Fixed, Ceramic	1.0	17	17.0
Capacitor, Fixed, Solid Tantalum	1.1	2	2.2
Capacitor, Fixed, Mica	0.3	1	0.3
Diode, Silicon, Gen. Purps.	3.4	4	13.6
Transistor, Silicon, PNP	8.4	2	16.8
Transistor, Silicon, NPN	5.6	2	11.2
Transistor, Silicon, FET	15.2	4	60.8
Integrated Circuit, Linear	60	4	240.0
Detector, Silicon	57	1	57
Solder Connections	0.12	188	22.56

$$\lambda_7 = 447.78$$

PRELIMINARY PARTS COUNT/PARTS TYPE

CIRCUIT RELIABILITY ESTIMATE

TABLE IX

λ_8 : X Channel AGC & Acquisition Detector

Component	Base Failure Rate (fr x 10 ⁻⁹ /hr.)	Quantity	Total Failure Rate (fr x 10 ⁻⁹ /hr.)
Resistor, Fixed, Film	0.28	15	4.2
Resistor, Fixed, Carbon	0.045	9	0.405
Capacitor, Fixed, Ceramic	1.0	15	15.0
Capacitor, Fixed, Solid Tantalum	1.1	1	1.1
Diode, Silicon, Gen. Purps	3.4	1	3.4
Integrated Circuit, Linear	60	5	300.0
Solder Connections	0.12	122	14.64

$$\lambda_8 = 338.745$$

PRELIMINARY PARTS COUNT/PARTS TYPE

CIRCUIT RELIABILITY ESTIMATE

TABLE X

λ_9 : Y Channel

Component	Base Failure Rate (fr x 10 ⁻⁹ /hr.)	Quantity	Total Failure Rate (fr x 10 ⁻⁹ /hr.)
Resistor, Fixed, Film	0.28	26	7.28
Resistor, Fixed, Carbon	0.045	19	0.855
Capacitor, Fixed, Ceramic	1.0	25	25.0
Capacitor, Fixed, Solid Tantalum	1.1	2	2.2
Capacitor, Fixed Mica	0.3	1	0.3
Diode, Silicon, Gen. Purps.	3.4	4	13.6
Transistor, Silicon, PNP	8.4	2	16.8
Transistor, Silicon, NPN	5.6	2	11.2
Transistor, Silicon, FET	15.2	4	60.8
Integrated Circuit, Linear	60	6	360.0
Detector, Silicon	57	2	114.0
Solder Connections	0.12	230	27.6

$$\lambda_9 = 641.639$$

PRELIMINARY PARTS COUNT/PARTS TYPE
CIRCUIT RELIABILITY ESTIMATE

TABLE XI

λ_{10} : Z Channel

Component	Base Failure Rate (fr x 10 ⁻⁹ /hr.)	Quantity	Total Failure Rate (fr x 10 ⁻⁹ /hr.)
Resistor, Fixed, Film	0.28	25	7.0
Resistor, Fixed, Carbon	0.045	20	0.9
Capacitor, Fixed, Ceramic	1.0	24	24.0
Capacitor, Fixed, Solid Tantalum	1.1	2	2.2
Capacitor, Fixed, Mica	0.3	1	0.3
Diode, Silicon, Gen. Purps	3.4	4	13.6
Transistor, Silicon, PNP	8.4	2	16.8
Transistor, Silicon, NPN	5.6	2	11.2
Transistor, Silicon, FET	15.2	4	60.8
Integrated Circuit, Linear	60	6	360.0
Detector, Silicon	57	2	114.0
Solder Connections	0.12	228	27.36

$$\lambda_{10} = 639.16$$

PRELIMINARY PARTS COUNT/PARTS TYPE

CIRCUIT RELIABILITY ESTIMATE

CIRCUIT TABLE XII

λ_{11} : Y-Z Residual Channel

Component	Base Failure Rate (fr x 10 ⁻⁹ /hr.)	Quantity	Total Failure Rate (fr x 10 ⁻⁹ /hr.)
Resistor, Fixed, Film	0.28	15	4.2
Resistor, Fixed, Carbon	0.045	10	0.45
Capacitor, Fixed, Ceramic	1.0	10	10.0
Capacitor, Fixed, Solid Tantalum	1.1	2	2.2
Diode, Silicon, Gen. Purps	3.4	2	6.8
Transistor, Silicon, PNP	8.4	1	8.4
Transistor, Silicon, NPN	5.6	1	5.6
Transistor, Silicon, FET	15.2	2	30.4
Integrated Circuit, Linear	60	3	180.0
Relay, Latching	120	1	120.0
Detector, Silicon	57	1	37.0
Solder Connections	0.12	122	14.64

$$\lambda_{11} = 439.99$$

PRELIMINARY PARTS COUNT/PARTS TYPE

CIRCUIT RELIABILITY ESTIMATE

TABLE XIII

λ_{12} : Y & Z AGC Channel

Component	Base Failure Rate (fr x 10 ⁻⁹ /hr.)	Quantity	Total Failure Rate (fr x 10 ⁻⁹ /hr.)
Resistor, Fixed, Film	0.28	20	5.6
Resistor, Fixed, Carbon	0.045	17	0.765
Capacitor, Fixed, Ceramic	1.0	17	17.0
Capacitor, Fixed, Solid Tantalum	1.1	2	2.2
Capacitor, Fixed, Mica	0.3	1	0.3
Diode, Silicon, Gen. Purps	3.4	4	13.6
Transistor, Silicon, PNP	8.4	2	16.8
Transistor, Silicon, NPN	5.6	2	11.2
Transistor, Silicon, FET	15.2	4	60.8
Integrated Circuit, Linear	60	4	240.0
Detector, Silicon	57	1	57.0
Solder Connections	0.12	180	21.6

$$\lambda_{12} = 446.865$$

PRELIMINARY PARTS COUNT/PARTS TYPE

CIRCUIT RELIABILITY ESTIMATE

TABLE XIV

λ_{13} : Y & Z AGC & Acquisition Detector

Component	Base Failure Rate (fr x 10 ⁻⁹ /hr.)	Quantity	Total Failure Rate (fr x 10 ⁻⁹ /hr.)
Resistor, Fixed, Film	0.28	15	4.2
Resistor, Fixed, Carbon	0.045	12	0.54
Resistor, Variable, Wire- wound	1.8	1	1.8
Capacitor, Fixed, Ceramic	1.0	17	17.0
Capacitor, Fixed, Solid Tantalum	1.1	1	1.1
Diode, Silicon, Zener	5.4	1	5.4
Diode, Silicon, Gen. Purps	3.4	1	3.4
Integrated Circuit, Linear	60	6	360.0
Solder Connections	0.12	144	17.28

$$\lambda_{13} = 410.72$$

PRELIMINARY PARTS COUNT/PARTS TYPE

CIRCUIT RELIABILITY ESTIMATE

TABLE XV

 λ_{14} : Power Supply

Component	Base Failure Rate (fr x 10 ⁻⁹ /hr.)	Quantity	Total Failure Rate (fr x 10 ⁻⁹ /hr.)
Resistor, Fixed, Film	0.28	11	3.08
Resistor, Fixed, Carbon	0.045	19	0.855
Resistor, Fixed, Wirewound	1.8	6	10.8
Capacitor, Fixed, Ceramic	1.0	13	13.0
Capacitor, Fixed, Solid Tantalum	1.1	9	9.9
Diode, Silicon, Gen. Purps	3.4	31	105.4
Diode, Silicon, Zener	5.4	2	10.8
Transistor, Silicon, NPN	5.6	6	33.6
Transistor, Silicon, PNP	8.4	4	33.6
Integrated Circuit, Voltage Reg.	60	3	180.0
Transformer	7.5	2	15.0
Inductor	7.5	6	45.0
Solder Connections	0.12	260	31.2

$$\lambda_{14} = 506.235$$

PRELIMINARY PARTS COUNT/PARTS TYPE
CIRCUIT RELIABILITY ESTIMATE
TABLE XVI

λ_{15} : X Encoder Counter and Reg.

Component	Base Failure Rate (fr x 10 ⁻⁹ /hr.)	Quantity	Total Failure Rate (fr x 10 ⁻⁹ /hr.)
Integrated Circuit, Digital CMOS	24	17	408.0
Solder Connections	0.12	238	28.56

$$\lambda_{15} = 436.56$$

PRELIMINARY PARTS COUNT/PARTS TYPE

CIRCUIT RELIABILITY ESTIMATE

TABLE XVII

λ_{16} : Z₁ & Z₂ Encoder Counter & Reg.

Component	Base Failure Rate (fr x 10 ⁻⁹ /hr.)	Quantity	Total Failure Rate (fr x 10 ⁻⁹ /hr.)
Integrated Circuit, Digital CMOS	24	23	502.0
Solder Connections	0.12	322	38.64

$$\lambda_{16} = 540.64$$

PRELIMINARY PARTS COUNT/PARTS TYPE
CIRCUIT RELIABILITY ESTIMATE
TABLE XVIII

λ₁₇: Encoder-Counter

Component	Base Failure Rate (fr x 10 ⁻⁹ /hr.)	Quantity	Total Failure Rate (fr x 10 ⁻⁹ /hr.)
Integrated Circuit, Digital CMOS	24	23	502.0
Solder Connections	0.12	322	38.64

$$\lambda_{17} = 540.64$$

PRELIMINARY PARTS COUNT/PARTS TYPE

CIRCUIT RELIABILITY ESTIMATE

TABLE XIX

λ_{18} : Motor Drive I

Component	Base Failure Rate (fr x 10 ⁻⁹ /hr.)	Quantity	Total Failure Rate (fr x 10 ⁻⁹ /hr.)
Resistor, Fixed, Carbon	0.045	10	0.45
Transistor, Silicon NPN	5.6	5	28.0
Integrated Circuit, Digital CMOS	24	9	216.0
Solder Connections	0.12	161	19.32

$$\lambda_{18} = 263.77$$

PRELIMINARY PARTS COUNT/PARTS TYPE

CIRCUIT RELIABILITY ESTIMATE

TABLE XX

λ_{19} : Motor Drive II

Component	Base Failure Rate (fr x 10 ⁻⁹ /hr.)	Quantity	Total Failure Rate (fr x 10 ⁻⁹ /hr.)
Resistor, Fixed, Carbon	0.045	11	0.495
Capacitor, Fixed, Ceramic	1.0	2	2.0
Diode, Silicon, Gen. Purps	3.4	7	23.8
Diode, Silicon, Zener	5.4	1	5.4
Diode, Light Emitting	17	5	85.0
Transistor, Photo	5.6	5	28.0
Transistor, Silicon, NPN	5.6	4	22.4
Integrated, Circuit, Digital CMOS	24	4	96.0
Motor	190	3	570.0
Solder Connections	0.12	136	16.32

$$\lambda_{19} = 849.415$$

PRELIMINARY PARTS COUNT/PARTS TYPE

CIRCUIT RELIABILITY ESTIMATE

TABLE XXI

λ_{20} : S/C Command Interface

Component	Base Failure Rate (fr x 10 ⁻⁹ /hr.)	Quantity	Total Failure Rate (fr x 10 ⁻⁹ /hr.)
Resistor, Fixed, Film	0.28	8	2.04
Integrated Circuit, Digital CMOS	24	11	264.0
Solder Connections	0.12	154	18.48

$$\lambda_{20} = 284.52$$

PRELIMINARY PARTS COUNT/PARTS TYPE

CIRCUIT RELIABILITY ESTIMATE

TABLE XXII

— λ_{21} : State and Motor Sequencer

Component	Base Failure Rate (fr x 10 ⁻⁹ /hr.)	Quantity	Total Failure Rate (fr x 10 ⁻⁹ /hr.)
Integrated Circuit, Digital CMOS	24	13	312.0
Solder Connections	0.12	182	21.84

$$\lambda_{21} = 333.84$$

PRELIMINARY PARTS COUNT/PARTS TYPE

CIRCUIT RELIABILITY ESTIMATE

TABLE XXIII

λ_{22} : Logic Array

Component	Base Failure Rate (fr x 10 ⁻⁹ /hr.)	Quantity	Total Failure Rate (fr x 10 ⁻⁹ /hr.)
Integrated Circuit, Digital CMOS	24	12	188.0
Solder Connections	0.12	168	20.16

$$\lambda_{22} = 308.16$$

PRELIMINARY PARTS COUNT/PARTS TYPE
CIRCUIT RELIABILITY ESTIMATE
TABLE XXIV

λ_{23} : Mode and Conditional Latches

Component	Base Failure Rate (fr x 10 ⁻⁹ /hr.)	Quantity	Total Failure Rate (fr x 10 ⁻⁹ /hr.)
Integrated Circuit, Digital CMOS	24	14	336.0
Solder Connections	0.12	196	23.52

$$\lambda_{23} = 359.52$$

PRELIMINARY PARTS COUNT/PARTS TYPE

CIRCUIT RELIABILITY ESTIMATE

TABLE XXV

λ_{24} : Data Interface Cont. and Clks.

Component	Base Failure Rate (fr x 10 ⁻⁹ /hr.)	Quantity	Total Failure Rate (fr x 10 ⁻⁹ /hr.)
Resistor, Fixed, Film	0.28	5	1.4
Resistor, Fixed, Carbon	0.045	7	0.315
Capacitor, Fixed, Ceramic	1.0	2	2.0
Capacitor, Fixed, Tantalum	1.1	1	1.1
Diode, Silicon, Gen. Purps	3.4	3	10.2
Integrated Circuit, Digital CMOS	24	13	312.0
Solder Connections	0.12	218	26.16

$$\lambda_{24} = 353.175$$

PRELIMINARY PARTS COUNT/PARTS TYPE

CIRCUIT RELIABILITY ESTIMATE

TABLE XXVI

λ_{25} : Digital Phase Shifter

Component	Base Failure Rate (fr x 10 ⁻⁹ /hr.)	Quantity	Total Failure Rate (fr x 10 ⁻⁹ /hr.)
Resistor, Fixed, Carbon	0.045	2	0.09
Diode, Silicon, Gen. Purps	3.4	2	6.8
Transistor, Silicon, NPN	5.6	2	11.2
Integrated Circuit, Digital CMOS	24	5	120.0
Solder Connections	0.12	90	10.8

λ_{25} = 156.89